

Lecture Notes in Civil Engineering

Nikolai I. Vatin · Ashot G. Tamrazyan ·  
Alexey N. Plotnikov ·  
Sergei N. Leonovich ·  
Leonids Pakrastins ·  
Ahmadjon Rakhmonzoda *Editors*

# Advances in Construction and Development

Proceedings of CDLC 2020

 Springer

# Lecture Notes in Civil Engineering

Volume 197

## Series Editors

Marco di Prisco, Politecnico di Milano, Milano, Italy

Sheng-Hong Chen, School of Water Resources and Hydropower Engineering,  
Wuhan University, Wuhan, China

Ioannis Vayas, Institute of Steel Structures, National Technical University of  
Athens, Athens, Greece

Sanjay Kumar Shukla, School of Engineering, Edith Cowan University, Joondalup,  
WA, Australia

Anuj Sharma, Iowa State University, Ames, IA, USA

Nagesh Kumar, Department of Civil Engineering, Indian Institute of Science  
Bangalore, Bengaluru, Karnataka, India

Chien Ming Wang, School of Civil Engineering, The University of Queensland,  
Brisbane, QLD, Australia

**Lecture Notes in Civil Engineering (LNCE)** publishes the latest developments in Civil Engineering—quickly, informally and in top quality. Though original research reported in proceedings and post-proceedings represents the core of LNCE, edited volumes of exceptionally high quality and interest may also be considered for publication. Volumes published in LNCE embrace all aspects and subfields of, as well as new challenges in, Civil Engineering. Topics in the series include:

- Construction and Structural Mechanics
- Building Materials
- Concrete, Steel and Timber Structures
- Geotechnical Engineering
- Earthquake Engineering
- Coastal Engineering
- Ocean and Offshore Engineering; Ships and Floating Structures
- Hydraulics, Hydrology and Water Resources Engineering
- Environmental Engineering and Sustainability
- Structural Health and Monitoring
- Surveying and Geographical Information Systems
- Indoor Environments
- Transportation and Traffic
- Risk Analysis
- Safety and Security

To submit a proposal or request further information, please contact the appropriate Springer Editor:

- Pierpaolo Riva at [pierpaolo.riva@springer.com](mailto:pierpaolo.riva@springer.com) (Europe and Americas);
- Swati Meherishi at [swati.meherishi@springer.com](mailto:swati.meherishi@springer.com) (Asia - except China, and Australia, New Zealand);
- Wayne Hu at [wayne.hu@springer.com](mailto:wayne.hu@springer.com) (China).

**All books in the series now indexed by Scopus and EI Compendex database!**

More information about this series at <https://link.springer.com/bookseries/15087>

Nikolai I. Vatin · Ashot G. Tamrazyan ·  
Alexey N. Plotnikov · Sergei N. Leonovich ·  
Leonids Pakrastins · Ahmadjon Rakhmonzoda  
Editors

# Advances in Construction and Development

Proceedings of CDLC 2020

 Springer

*Editors*

Nikolai I. Vatin  
Civil Engineering  
Peter the Great St. Petersburg Polytechnic  
University  
Saint Petersburg, Russia

Alexey N. Plotnikov  
Civil Engineering  
Chuvash State University  
Cheboksary, Russia

Leonids Pakrastins  
Faculty of Civil Engineering  
Riga Technical University  
Riga, Latvia

Ashot G. Tamrazyan  
Civil Engineering  
Moscow State University  
Moscow, Russia

Sergei N. Leonovich  
Department of Civil Engineering  
Belarusian National Technical University  
Minsk, Belarus

Ahmadjon Rakhmonzoda  
Department of Science and Innovation  
Tajik Technical University  
Dushanbe, Tajikistan

ISSN 2366-2557

ISSN 2366-2565 (electronic)

Lecture Notes in Civil Engineering

ISBN 978-981-16-6592-9

ISBN 978-981-16-6593-6 (eBook)

<https://doi.org/10.1007/978-981-16-6593-6>

© The Editor(s) (if applicable) and The Author(s), under exclusive license to Springer Nature Singapore Pte Ltd. 2022

This work is subject to copyright. All rights are solely and exclusively licensed by the Publisher, whether the whole or part of the material is concerned, specifically the rights of translation, reprinting, reuse of illustrations, recitation, broadcasting, reproduction on microfilms or in any other physical way, and transmission or information storage and retrieval, electronic adaptation, computer software, or by similar or dissimilar methodology now known or hereafter developed.

The use of general descriptive names, registered names, trademarks, service marks, etc. in this publication does not imply, even in the absence of a specific statement, that such names are exempt from the relevant protective laws and regulations and therefore free for general use.

The publisher, the authors and the editors are safe to assume that the advice and information in this book are believed to be true and accurate at the date of publication. Neither the publisher nor the authors or the editors give a warranty, expressed or implied, with respect to the material contained herein or for any errors or omissions that may have been made. The publisher remains neutral with regard to jurisdictional claims in published maps and institutional affiliations.

This Springer imprint is published by the registered company Springer Nature Singapore Pte Ltd. The registered company address is: 152 Beach Road, #21-01/04 Gateway East, Singapore 189721, Singapore

# Synopsis

The conference “Construction and Development: Life Cycle,” as a continuation of the conference “New in architecture, design, construction and renovation” dates back to 1997, the 11th conference was held in 2020. The result of the conference was a collection of articles presented by the results of research by more than a hundred scientists.

The conference is held by the Faculty of Civil Engineering of the Chuvash State University.

The collection is presented by topics devoted to the preservation of the urban historical environment, improving methods for calculating building structures, strengthening them and assessing their suitability for use, improving construction technology, geotechnics, energy efficiency of enclosing structures and energy systems, introducing new structures and materials, and economic evaluation of construction.

The collection contains a number of articles on the development in geotechnical engineering of pile structures obtained by the discharge-pulse technology, as well as their new type—piles with multiple extensions. The results of this work are being tested by researchers from the Faculty of Civil Engineering in collaboration with a geotechnical firm on construction sites in many cities.

Particular attention is paid to monitoring unique buildings and structures. Researchers of the Faculty of Civil Engineering of the Chuvash State University are implementing their developments at many famous sites in Russia.

The conference participants represent several cities in Russia and foreign countries. The publication is popular with researchers, graduate students, and undergraduates.

# Contents

## Architecture and Urbanism

<b>To the Question of the Development of Construction of High-Rise Buildings in Russia</b> .....	3
E. M. Mikryukova and I. A. Nikolaev	

## Calculation and Design of Building Structures

<b>Analysis of the Ultimate Loading on Concrete Beams in FEMAP NX Nastran</b> .....	13
A. V. Alekseytsev and M. D. Antonov	

<b>Nonlinear Analysis of Damaged Reinforced Concrete Columns, Restored with Carbon Fiber Jacket Using ABAQUS</b> .....	21
Gamal Algnde and Alexander Topilin	

<b>Spherical Domes of Paired Arches of the Same Radius</b> .....	35
Vasilij D. Antoshkin and Maria V. Gorina	

<b>On the Question of Protection from Progressive Collapse</b> .....	43
S. D. Bartenev and V. V. Bobrov	

<b>Development, Strength Check, Calculation of the Wind Load of a Multi-layer Guarding Structure</b> .....	49
M. A. Bakhmisova, Alexey N. Plotnikov, L. A. Sakmarova, and M. V. Petrov	

<b>Strength and Deformation of Caisson-Type Floor Plates. Experimental Research and Calculation</b> .....	55
Arkady Vulfovich Granovsky and Kirill Alekseevich Prusov	

<b>To the Calculation of Reinforced Concrete Beams According to the Deformation Model</b> .....	63
Dmitry Zamelin and Ivan Manaenkov	

<b>Anchorage Strength of Post-installed Reinforcement</b> .....	71
S. I. Ivanov	
<b>Distribution of Vertical Stresses in Multi-storey Buildings Under Influence of Nonlinear Shear Bonds Deformation</b> .....	79
V. A. Lyublinskiy, K. Alzaibak, and Kh. Alwaz	
<b>Erection of Flat Shells of Positive Gaussian Curvature Made from High-Strength Sand Concrete and Its Economic Efficiency</b> .....	87
Nikolay Palagin, Georgy Nikitin, and Aisyly Sadrutdinova	
<b>Relationship of Shear Force and Punching Analysis of Reinforced Concrete Slabs</b> .....	101
D. A. Pekin	
<b>Modeling the Bearing Capacity of Tank Trucks Filled with Bulk Material in Bending</b> .....	113
M. V. Petrov and E. G. Gonik	
<b>Rearing Capacity of Reinforced Masonry Under Central Compression Based on the Deformation Parameters of Its Components</b> .....	121
Alexey N. Plotnikov, Tatyana Vyacheslavovna Romanova, Boris Vasilievich Mikhailov, Olga Stanislavovna Yakovleva, and Mikhail Yurievich Ivanov	
<b>Criteria for Special Limiting State of Eccentrically Compressed Members of RC Frames</b> .....	135
Sergey Savin	
<b>Problems of Accounting for External Reinforcement in the Nonlinear Calculation of Normal Cross Sections of Bent Reinforced Concrete Elements</b> .....	147
O. A. Simakov and D. V. Fuchizhi	
<b>Traditional Measurements in Experiments on Determination of Mechanical Properties Materials and Nuances for Composites</b> .....	155
Alexander Anatolyevich Treshchev	
<b>Numerical Study of Crack Formation and Strains Distribution During the Punching of Reinforced Concrete Slabs</b> .....	169
Valery Borisovich Filatov and Zulfat Shavkatovich Galyautdinov	
<b>Reliability, Inspection and Monitoring of Buildings and Structures</b>	
<b>Forecast Durability for Protective Penetrating Waterproof Coating</b> .....	181
A. I. Bedov, A. I. Gabitov, I. G. Terekhov, and A. S. Salov	



<b>The Use of Carbon Fiber Tapes as One of the Ways to Increase the Seismic Resistance of Gas-Silicate Walls</b> .....	187
B. K. Dzhamuev and E. S. Erizhokova	
<b>Migrating Corrosion Inhibitor (MCI) for Concrete Rebar and Its Inhibitory Efficiency</b> .....	195
Sergei N. Leonovich, L. S. Karpushenkava, and S. A. Karpushenkov	
<b>Energy Efficiency and Sustainability of High-Rise Buildings and Structures</b> .....	205
Lydia Ivanovna Malyanova and Maria Alekseevna Sergeeva	
<b>Energy Survey of the Cogeneration Plant</b> .....	211
A. S. Mozgova and T. V. Shchennikova	
<b>Analysis of Correlation of Monitoring Parameters of a Multi-storey Building for Determining Its Deformed State</b> .....	219
Alexey N. Plotnikov, Sergey Andreevich Levin, Irina Sergeevna Gorbunova, Anastasia Georgievna Nikolaeva, and Nadezhda Nikolaevna Arinina	
<b>Rigidity of Supporting Sections of High Building Bars and the Possibility of Its Monitoring by Inclinometers</b> .....	233
Alexey N. Plotnikov and Mikhail Yurievich Ivanov	
<b>The Issues of Reliability of Microclimate Creation Systems</b> .....	247
N. G. Rusinova and N. A. Fedorov	
<b>Geotechnics, Foundations, Construction Technology, Innovations in Construction Education</b>	
<b>Tamped Slotted Foundations</b> .....	257
Alexey Glushkov, Vyacheslav Glushkov, and Ilya Glushkov	
<b>More About the Possibilities of the ERT Injection Piles</b> .....	265
N. S. Sokolov	
<b>Optimum Type of Depth Constructions in Insulated Soils</b> .....	271
N. S. Sokolov	
<b>Optimum Type of Depth Reinforced Concrete Structures When Strengthening the Foundation of Industrial Buildings</b> .....	281
Nikolay Sergeevich Sokolov, Svetlana Stanislavovna Viktorova, Galina Nikolaevna Alekseeva, Olga Pavlovna Terekhova, Lydia Ivanovna Malyanova, and Victor Vladimirovich Maguskin	
<b>Deep Earth Anchor ERT</b> .....	289
N. S. Sokolov and P. Yu. Fedorov	

<b>Fibre-Reinforced Bored Electric Discharge Technology Pile as a Buried Reinforced Concrete Structure</b> .....	299
P. Yu. Fedorov	
<b>Designing the Organization of Buildings and Structures Construction in Special Natural and Climatic Conditions</b> .....	305
Vasily Filippovich Bogdanov, Alina Iosifovna Sokolova, and Irina Vladimirovna Petrova	
<b>Overcoming Problems with Waste Water Treatment from Dense Emulsions in the Oil Refining Industry</b> .....	311
E. M. Mikryukova and E. V. Suvorova	

## About the Editors

**Nikolai I. Vatin** received his Ph.D. in Technical Sciences in 1986, and was awarded Ph.D. in Technical Sciences, and in 2001 was awarded an academic degree, Doctor of Science (Engineering). He is currently a Professor at Peter the Great Saint-Petersburg Polytechnic University. He has held positions such as Deputy Head of Department, Assistant Professor, Head of Department of Economy, Professor, Head of Department (since 2000), Dean, Director of the Institute of Civil Engineering (since 2013 up to 2018), and Professor (since 2018). His research interests include durability and safety of concrete and mortars, reliability of building structures, fiber-reinforced concrete. He is the editor-in-chief of three journals, and his papers have been published in proceedings of national and international prominence.

**Ashot G. Tamrazyan** qualified as a civil engineer in 1974 from the Yerevan Polytechnic University, Armenia. He received his Ph.D. in Engineering Sciences in 1983 from the National Research Moscow State University of Civil Engineering (NRU MGSU), Russia, and in 1998 he defended his doctoral dissertation at the same university. He has been a professor since 1999. Head of the Department of Reinforced Concrete and Stone Structures, NRU MGSU. He also has been an academician of the Russian Academy of Engineering since 2005, and an advisor to the Russian Academy of Architecture and Construction Sciences since 2004. He was awarded as a laureate of the Government of the Russian Federation Prize in Science and Technology in 2017. His research interests include building structures, buildings and structures, ensuring the reliability and safety of reinforced concrete structures under extreme natural and man-made impacts, etc.

**Alexey N. Plotnikov** graduated from the Chuvash State University with a degree in Industrial and Civil Engineering in 1983. He received his Ph.D. in 2013 from the National Research Moscow State University of Civil Engineering. From 2014 to 2018, he headed the department of building structures at the Chuvash State University and Dean of the Faculty of Civil Engineering of the Chuvash State University. Research interests: research in the field of automatic monitoring of buildings (SHM), non-linear work of reinforced concrete, resistance of masonry. Member of

the board of the Ministry of Construction, Architecture and Housing and Communal Services of the Chuvash Republic. Head of the conference “New in architecture, design of building structures and reconstruction”; “Construction and development: life cycle (CDLC).” Awarded with the Certificate of Honor of the Ministry of Education and Science of the Russian Federation, the Certificate of Honor of the Ministry of Construction of the Chuvash Republic, the Ministry of Transport of the Chuvash Republic.

**Sergei N. Leonovich** received his Ph.D. degree in 1989 from the Belarusian Polytechnic University. He received his Doctor of Science degree in 2000. He is currently the Dean of the Faculty of Civil Engineering of the Belarusian National Technical University, Professor of the Department of Building Materials and Construction Technology. He also is involved as a foreign academician of the Russian Academy of Architecture and Construction Sciences, co-chairman of the working group of the RILEM Technical Committee, and member of the Belarusian Academy of Architecture and Engineering Academy. His research interests include strength and crack resistance of structural building materials under a complex stress state, strength, crack resistance, and durability of structural concrete under temperature and humidity influences, predicting the durability of structural concrete under aggressive influences. He has been awarded with state awards of Belarus, Man of the Year, American Bibliographical Institute—2010.

**Leonids Pakrastins** received his Ph.D. in Structural Engineering from the Faculty of Civil Engineering, Riga Technical University, Latvia in 2005. He is currently the director of the Structural Engineering and Reconstruction Institute, Faculty of Civil Engineering, and Head of the Department of Structural Engineering of Riga Technical University, Latvia. His research interests include long-term thermal deformation of cement compositions, high performance fiber-reinforced concrete, numerical modeling of building structures, including those reinforced during reconstruction. He is a member of the RTU Promotion Council “RTU P—06” Civil Engineering; Transport and Traffic Science and other scientific committees. He also heads the Latvian standardization technical committee LVS/STK30 “Construction” and is the co-founder of the Latvian Association of Structural Designers. In 2013, he was awarded the title “Excellence in Teaching and Research” at Riga Technical University.

**Ahmadjon Rakhmonzoda** graduated from the Tajik Technical University with a degree in Industrial and Civil Engineering in 2010. He received his Ph.D. in Architecture and Civil Engineering from Kazan State University in 2015. His research interests include monitoring of buildings and structures, non-linear work of reinforced concrete, use of composite reinforcement, research on the loss of pre-stressed elements among others. Since 2016, he is responsible for the scientific research and

science of TTU, aimed to solving the complex of tasks for creating and supporting the activities of the system of effective use of the scientific potential of the university. He is the corresponding member of the Engineering Academy of the Republic of Tajikistan, 2017. He was also awarded the Ismoil Somoni State Prize in the field of technical sciences, 2018.

# **Architecture and Urbanism**

# To the Question of the Development of Construction of High-Rise Buildings in Russia



E. M. Mikryukova  and I. A. Nikolaev

## 1 Introduction

Today high-rise buildings have become the main focus of construction. The first thing that catches your eye when you come to a modern city is the skyscrapers, striking in their grandeur. And you wonder, really, this is the creation of human hands, and modern construction technologies have reached such heights.

The first high-rise buildings in Russia were the Ivan the Great Bell Tower, built in 1508, 60 m high and completed in 1600 to 81 m. In 1707, the Church of the Archangel Gabriel (Menshikov Tower) was built on Chistye Prudy; the height of the tower was 84.3 m. In 1723, the bell tower of the Peter and Paul Cathedral in St. Petersburg was built, the height of which was 122.5 m.

The first skyscrapers in the Soviet Union are considered to be the post-war Stalinist skyscrapers, which were built in the style of “Soviet art deco” and were named “seven sisters”. The tallest building in Moscow and Europe until 1990 was the main building of Moscow State University on Sparrow Hills, which is the center of the huge Moscow University complex. The height of the Moscow State University building is 240 m; the central part of the building is 36 floors.

In 1960 construction began on the Ostankino TV tower (formerly the All-Union Radio and Television Transmitting Station named after the 50th Anniversary of October), the tower is 540 m high. This is the tallest structure in Russia and Europe. The tower building has a conical base, in the form of a flower, an inverted lily, with strong petals and a thick stem. 149 tensioned cables prevent deformation and collapse of the concrete frame from individual round blocks.

Historically, it so happened that in Russia, in the capital Moscow, structures were also laid that were supposed to become the tallest skyscrapers in Russia and Europe—the 100-storey, 495-m Palace of the Soviets (considered the tallest in the world) in the

---

E. M. Mikryukova (✉) · I. A. Nikolaev  
Kalashnikov Izhevsk State Technical University, Izhevsk, Russia

1940s and the 612-m 118-storey Tower of Russia in the 2000s, but their construction was canceled for various reasons.

The tallest in Russia and Europe is the 462-m 88-storey skyscraper Lakhta Center in St. Petersburg, built in 2018. The Lakhta Center Tower is one of the northernmost skyscrapers in the world and one of the five most environmentally friendly high-rise buildings. Due to the proximity to the Gulf of Finland and weak soils, all foundations of the complex, including the central Lakhtinskaya skyscraper, stand on piles. The number of piles in this complex is 3480, their diameter varies from 0.6 to two m.

The city of Yekaterinburg, located on the eastern slope of the Middle Urals, on the banks of the Iset River, is famous for its skyscrapers. The Iset Tower is a 52-storey skyscraper on the territory of the future Yekaterinburg-City complex, built in 2016. The second largest skyscraper in the city—Vysotsky House—54 floors, 188.3 m high, built in 2015. When creating the skyscraper, special attention was paid to fire safety. The building has an addressable fire alarm, six thousand smoke detectors and two security zones, where neither smoke nor fire can enter. One of these areas is hidden on the technical floor.

To this day, the rise of skyscrapers continues to accelerate. In the past five years alone, more than half of all the tallest buildings in the world have been built, and the total number of skyscrapers has tripled over the past decade.

In our country, the capital is a leader in the construction of skyscrapers. This is due to the financial and material capabilities of Moscow. The concept of MIBC “Moscow City” was proposed in 1991, and in 1995 preparations began for the construction of the first skyscrapers of this center. Today “Moscow City” consists of 13 high-rise buildings, where a business activity zone is being created, uniting business, apartments, accommodation, and recreation. The North Tower is one of the lowest buildings in the business center, built in 2008. The tower is completed by significant iron trusses that serve as a decorative function. The 27-storey building, 108 m high, has an 18-storey atrium that culminates in a dome, which contributes to additional lighting of the office space. Evolution Tower is a symbol of the business center, 255 m high, 54 floors, the building was built in 2015. The tower has a spiral shape, embodying the union of two principles. The building turned out to be curved by more than 150 degrees. The main supporting structures are eight columns located strictly vertically along the entire height of the building, and only four corner supports follow the spiral geometry of the building. In 2011, the construction of the Imperia shopping center, symbolizing the cities of Moscow and St. Petersburg, was completed. The “City of Capitals” consists of two towers—the 76-storey “Moscow” 302 m high and the 65-storey “St. Petersburg”, 257 m high. The entire complex is located on a single podium and combines two buildings with a 17-storey stylobate and a 17-storey domed building with a atrium. The towers consist of individual rectangular blocks, which alternately move around their axis at the level of technical floors. The building has a very unusual geometry, a complex structural solution with a space frame, and stiffening rods. The Imperia shopping complex is a monolithic reinforced concrete skyscraper. In 2014, the Eurasia skyscraper was built with a height of 309 m. As conceived by the architects, the tower has a classic look combined with modernism, the only steel tower in Moscow City. In 2016, the construction of



the unique Federation complex was completed, consisting of two triangular towers of different heights located on the stylobate. The height of the 63-storey West Tower is 242 m, the 100-storey East Tower-374 m. During the construction of the Federation Tower complex, the most stringent building standards in the world were applied. The foundation of the Federation complex is a foundation that rests on a massive concrete slab. It took 14,000 cubic meters of concrete to fill it. The stability of the two buildings is ensured by a strong concrete core, which has 1.4 m at the base of the wall, as well as 25 columns along the perimeter, which intersects the two towers from the basement to the top floor. Each column at the base is  $2 \times 1.4$  m in size. Every 25–30 floors in the skyscrapers of the “Federation” complex there are outrigger floors, which are made of high-strength steel structures, which make the building more rigid and resistant to wind loads. The latest glazing systems have been applied. The glass surface reflects solar radiation while maintaining the optimal temperature in the building. In terms of density, glass approaches the thermal resistance parameters of a brick wall. At the time this technology began to be used in the tower, it was not used in any skyscraper in the world. At the level of 67–68 floors of the building, a media facade is installed, assembled from two million LEDs. This is the tallest media facade in Europe. Mercury Tower (Mercury Tower, Golden Tower) is a multifunctional business complex that is part of the Moscow International Business Center. The height of the tower is 338 m. Initially, it was planned to build the tower “Russia”, 612 m high, on this site. The Mercury Tower was supposed to be the first truly “eco-friendly” building in Moscow. The skyscraper was designed to provide daylight to 75% of offices with natural daylight and included a rainwater collection system for later use. For greater reliability, two independent reinforced concrete frames are provided, which made the “Mercury” resistant to earthquakes up to six points. This skyscraper includes a unified automated building management system (BMS), an integrated security system, a sprinkler fire extinguishing system, a water supply for fire extinguishing, a four-pipe air conditioning system, twenty-six high-speed ultra-modern elevators, and other advanced technologies.

## 2 Materials and Research Methods

For the classification of buildings, the criterion of height in meters, and not number of storeys, was adopted, since the height of the floor is taken differently depending on the purpose of the building and the requirements of national design standards [1–5]. “Terms and definitions” the following definition is given: “Multifunctional multi-storey building”—a building with a height of more than 75 m, which includes, in addition to residential premises, hotel rooms and premises for other functional purposes” [6].

The Russian construction industry does not have the experience of high-rise construction, as in other developed countries. Most often, problems arise due to the climate, the location of the building in the existing urban development, the lack

of construction technologies and equipment suitable for the construction of multi-storey buildings. Also, there are no correct requirements for proper documentation and control, for compliance with existing requirements for land use planning and zoning in the city, construction, and maintenance of a building, requirements for fire and evacuation safety of people in high-rise buildings.

One of the disadvantages of “skyscrapers” can be identified—the problem of transport. With dense development, the emergence of a transport crisis can be observed not only in the construction zone, but also in the territories and nearby streets. To avoid such a problem, for example, in Paris, office buildings are moved from the city center to the outskirts, as a result of which the situation on the streets is normalized during working hours, since people did not want to go there. High-rise construction infrastructure is more relevant for Russia. Among them are the modernization of engineering systems, transport accessibility, improvement of the adjacent territory, the use of modern building maintenance systems.

In the construction of high-rise buildings and low-rise buildings, concrete and steel are used as materials. The wind loads acting on the building are retained due to the rigidity of the “frame” of the structure, and due to the flexibility, resistance to seismic vibrations is achieved. Most often, facades are finished with steel profiles and light panels made of transparent glass, aluminum, or polymers.

Engineering systems and elevators are carefully selected by specialists during construction. The main thing for them is high quality and a long warranty period.

A special place in the analysis is occupied by the profitability of high-rise construction, because many experts often raise the question of the expediency of high-rise construction in our country, since they do not see the point in erecting these buildings, and focus on the vast territories of our country, where urban development has already formed.

The life support complex of the skyscraper includes about thirty systems: sewerage and water supply, microclimate, power supply, smoke removal, fire extinguishing, automation, etc.

Safety problems in the construction of “high rise” are important, because the organization of evacuation routes requires compliance with the mass of regulatory sources due to the complexity and length of paths providing access to the exits from the building [1, 7–9].

Experts say that the use of only non-combustible materials in the construction of skyscrapers is impossible, despite the high development of technologies in construction. Therefore, even in new homes, fire is a real threat. The risk of fire for people in multi-storey buildings is aggravated by the fact that, unlike low-rise buildings, evacuation of people is very difficult, and the complexity of extinguishing fires increases [9].

For high-rise buildings, an Automated Building Management System (BMS) is required, which provides centralized monitoring, dispatching, and management of engineering systems equipment. The main functions of automated complexes, communication, and information systems with which high-rise buildings are equipped are safety, maintenance of the building’s service life, and ensuring the

manufacturability of functional blocks and people's comfort. To eliminate redundancy and ensure consistency of work, technical systems should be combined into complexes that ensure the exchange of information between systems. It is necessary to organize a flexible and freely programmable distribution system for a building control center with a workstation, where only highly qualified specialists can work. In multi-storey buildings, it is necessary to provide premises for the placement of technological equipment of citywide service services: operational radio communication systems and state fire protection of the Ministry of Emergencies of the Russian Federation; a stationary observation post for the bearing structures of the building; for the central control room of the building security system. The short and incomplete list of design and construction works given above shows that the construction of high-rise buildings is an excessively expensive process [10].

For high-rise construction in modern Russia, the list of regulatory documents has not yet been fully approved. It is impossible to build high-quality facilities that meet modern safety and comfort standards using outdated technologies. For sustainable development of multi-storey construction, new rules are needed, simplification of the procedure for approving documents, GOSTs, and technical regulations.

### 3 Results and Challenges

In contrast to multi-storey buildings, the engineering systems of high-rise buildings have a number of characteristics. Let's consider them on the example of a multi-storey building of the multifunctional complex "University" on the street. Peace in the Kirov district of Yekaterinburg.

The building is designed with two inputs of the utility and drinking water supply. The drinking water supply system is divided into zones: water supply of built-in premises (offices) from pressure in the city water supply system, water supply of residential premises of the first zone, water supply of residential premises of the second zone. The lower distribution of the drinking water supply system for the built-in premises and the first zone with the laying of main pipelines under the ceiling of the technical underground was adopted. For the second zone, the distribution of the utility and drinking water supply system is provided in a warm attic. The drinking water supply networks are designed as dead ends. To equalize the pressures in the hot and cold water pipelines and to reduce the pressure on the branches in the apartments, pressure regulators are installed. The hot water supply system is designed to supply water to sanitary appliances in residential apartments and offices. A separate hot water supply system is provided for the offices—from the residential part. Circulation of hot water supply for the residential part and offices was carried out. In the project, the lower distribution of hot water and circulation for offices and the first zone with the laying of main pipelines along the technical underground is designed. For the second zone, hot water distribution is provided in the warm attic. For the needs of fire extinguishing, two transit pipelines were made from the input, bypassing the water meter unit and two zones of internal fire extinguishing. A pumping station for

a drinking water supply system, a water treatment station, and a fire extinguishing pumping station are designed for the building [10–16].

To drain wastewater from sanitary appliances of the residential part, a gravity system of domestic sewage was made with a release into the projected external network. In the same section, a separate sewerage system was designed for office bathrooms with independent release to the external network. To drain rain and melt water from the roof of the building, an internal drainage system was designed with the release of rainwater to the blind area and then along reinforced concrete trays to the roadway. For the autumn–winter period, it is planned to bypass wastewater into the household sewage system of the residential part. The sewerage system for ordinary waste water is designed to divert ordinary and emergency waste water from the OV and VK premises. In the OV and VK rooms there are recesses with automated submersible pumps with a built-in float switch and a check valve. These effluents are conditionally clean and are discharged into a wet well with subsequent removal [10–12, 16–18].

To provide general ventilation of apartments, the project provides for a mechanical ventilation system. Air exhaust and air flow into the apartments is carried out by two units with recuperators installed on the roof. Ventilation of office and MOS premises is carried out by separate systems with mechanical induction and natural ventilation. Exhaust air is discharged above the roof level. To reduce the noise characteristics in the ventilation systems of residential apartments and offices, sound attenuators are provided. To limit the spread of combustion products, the project provides for the removal of smoke. Axial roof fans are designed for the smoke exhaust system. The release of combustion products is carried out at a height of two meters from the level of the roof. The project provides for air pressurization systems by evacuation, lift shafts, tambour gateways [10, 19–21].

To maintain a comfortable air temperature in the office premises, the project provides for air conditioning systems. Outdoor units of air conditioners are located on the facade of the building. A system of channels is used to remove condensate. Condensate is removed by the sewerage system [10, 19–21].

Water, steel, panel radiators with bottom connection are provided as heating devices for apartments and offices. Convectors with side connection are provided for heating the auxiliary rooms of the MOS. To distribute the heating medium to apartments and offices, heating collectors are provided on the serviced floor. To account for the heat consumed by apartments and offices, the project provides for heat meters installed on floor heating collectors. In apartments and offices, heating pipelines are laid in the floor screed along the perimeter of the premises in a protective corrugated casing [10, 19–21].

Heat supply of the residential building is provided from the existing boiler house on the street. Cherry. The heat supply scheme is adopted as a two-pipe one with the heating system connected according to an independent scheme. According to the dependent scheme—ventilation systems and a closed circuit of the DHW system [10, 19–22].

Exits from the elevators on the intermediate floors are made through the elevator halls, which are separated from the adjoining corridors by fire-prevention partitions with self-closing doors. Elevator cabins are made of non-combustible materials [1, 7].

## 4 Conclusion

It is impossible to make an unambiguous conclusion about the necessity or inadmissibility of high-rise construction in Russian realities. The introduction of high-rise complexes in the largest cities of Russia seems to be justified. High-rise buildings avoid the expansion of the city's territory, creating a "compact" urban environment in the absence of territories. A compromise is needed between the advantages of multi-storey construction and the cost of their construction. As a result of the analysis, it can be concluded that in the future the pace of construction of high-rise buildings in cities will only increase and develop.

## References

1. SP RK 3.02-02-2008. Design of high-rise buildings and multifunctional complexes
2. SP 42.13330.2016. Urban planning. Planning and development of urban and rural settlements. Updated edition of SNiP 2.07.01-89 \* (with Amendments N 1, 2)
3. SP 14.13330.2018. Construction in seismic areas. Updated edition of SNiP II-7-81 \* (with Amendment No. 1)
4. SP 118.13330.2012. Public buildings and structures. Updated edition of SNiP 31-06-2009 (with Amendments N 1-4)
5. SP 55.13330.2016. Single-family residential houses. Updated edition of SNiP 31-02-2001 (with Amendment No. 1)
6. MGSN 4.19-2005. Design of multifunctional high-rise buildings and construction complexes in the city of Moscow
7. SP 267.1325800.2016. High-rise buildings and complexes. Registration rules
8. SP 394.1325800.2018. High-rise buildings and complexes. Operating rules
9. SP 1.13130.2009. Fire protection systems. Escape routes and exits (as amended No. 1)
10. SP 253.1325800.2016. Engineering systems of high-rise buildings
11. SP 30.13330.2012. Internal water supply and drainage of buildings
12. SP 73.13330.2012. Internal sanitary systems of buildings
13. SP 31.13330.2012. Water supply. Networks and external installations
14. SP 10.13130.2009. Fire protection systems. Internal water supply for the fire extinguisher
15. SP 8.13130.2009. Fire protection systems. Sources of water supply for fire fighting
16. Working documentation for the construction of a residential building on the street. Mira-Bibliotechnaya-Komsomolskaya in Kirovsky district of Yekaterinburg, 2nd stage of construction. Stage 5. Adjustment 4. Water supply and sanitation. Internal networks. 1272/2014-11.3a-VK (2019)
17. SP 32.13330.2012. Sanitation. Networks and external installations
18. Korolev, A.A., Sabiryanova, A.R., Mikryukova, E.M.: The feasibility of using soundproof sewer pipes in apartment buildings. In the collection: energy saving, information technology and sustainable development: electronic scientific publication: collection of documents of the international scientific and practical Internet conference. FSBEI HPE "Izhevsk State Technical University named after M.T. Kalashnikov", pp 140–142 (2014)

19. SP 60.13330.2016. Heating, ventilation, air conditioning. Updated edition of SNiP 41-01-2003 (with amendment No. 1)
20. SP 7.13130.2013. Heating, ventilation, air conditioning. Fire safety requirements (with amendments N 1, 2)
21. Working documentation for the construction of a residential building on the street. Mira-Bibliotechnaya-Komsomolskaya in Kirovsky district of Yekaterinburg, 2nd stage of construction. Stage 5. Adjustment 4. Heating, ventilation and air conditioning. 1272/2014-11.3a-OB1 (2019)
22. Working documentation for the construction of a residential building on the street. Mira-Bibliotechnaya-Komsomolskaya in Kirovsky district of Yekaterinburg, 2nd stage of construction. Stage 5. Correction 4. Piping for electrical communications. 1272/2014-11.3a-EL.KZh (2019)
23. STO 01422789-001-2009. Design of high-rise buildings

# **Calculation and Design of Building Structures**

# Analysis of the Ultimate Loading on Concrete Beams in FEMAP NX Nastran



A. V. Alekseytsev and M. D. Antonov

## 1 Introduction

Current software and methods in regulations led to make a nonlinear static analysis of Reinforced Concrete (RC) structure. At the same time regular service conditions provide restrictions on crack resistance and stiffness, that structure has sufficient load-bearing capacity before the beginning of structural failure. Analysis of stress–strain behavior at structure in such level of stress begins actual for emergencies that had not provided for normal service condition. Reserve of load-bearing capacity can be used for assessment stability and analysis risk in loss of property, and for optimization, when main criterion is provision required level of mechanical safety. There are many models for describing deformation of concrete in Ansys Mechanical 2020, NX Nastran, and other softwares. It is based on the yield surface shown in Fig. 1. At the same time, the main dependencies for comparison with design tensile and compressive resistance of concrete  $R_{bt}$  and compressive  $R_b$  in terms of principal stresses  $\sigma_1 - \sigma_3$  in concrete are:

$$\sqrt{\frac{1}{6}[(\sigma_1 - \sigma_2)^2 + (\sigma_2 - \sigma_3)^2 + (\sigma_1 - \sigma_3)^2]} = A + B(\sigma_1 + \sigma_2 + \sigma_3),$$
$$A = \frac{2}{\sqrt{3}} \left( \frac{R_b R_{bt}}{R_b + R_{bt}} \right), \quad B = \frac{2}{\sqrt{3}} \left( \frac{R_{bt} - R_b}{R_b + R_{bt}} \right). \quad (1)$$

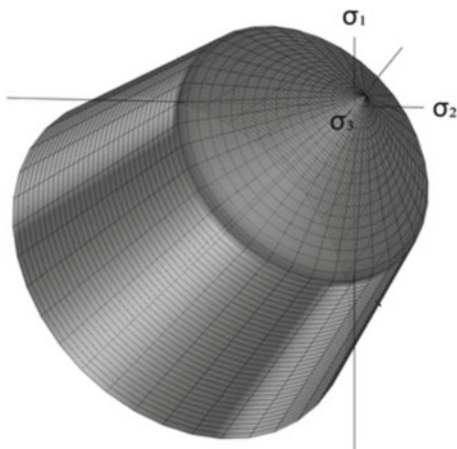
where  $R_b$ ,  $R_{bt}$ —design resistance of concrete to compression and tension, respectively. Let's complete the implementation of a model of reinforced concrete structures in Femap NX Nastran.

---

A. V. Alekseytsev (✉) · M. D. Antonov  
Moscow State University of Civil Engineering, Moscow 129337, Russia



**Fig. 1** Drucker-Prager yield surface for heavy concrete



## 2 Material and Research Methods

The Drucker-Prager (DP) model is used for concrete. Crack formation in concrete in DP model is described with considering opportunity of quasi-plastic material softening after reaching the level of stress close to limit of ultimate strength. This opportunity is represented by functions of hardening and softening in materials. More information about the property of this models for concrete are described in articles [1, 2]. Let's complete the realization of this model in pre-processor Femap. Here, one of the main parameters is the cohesion stress during biaxial compression. A number of articles by both domestic and foreign researchers are devoted to the estimation of this value. In this case, the calculation formulas and experimental data differ significantly. We calculate this stress based on the expression:

$$C = \frac{\sqrt{3}(3 - \varphi_B)}{6 \cos \varphi_B} R_{bt}, \quad (2)$$

where  $\varphi_B$ —is the angle of internal friction (taken 25–32 degrees),  $R_{bt}$ —tensile design resistance of concrete to tension.

The table of main constants for materials [Pa] is shown in Fig. 2.

Reinforcement is determined in accordance with SP 63.13330 and responded due to Prandtl diagram. The Mises strength criterion is used for reinforcement. Benchmark data for accounting nonlinear behavior of concrete and reinforcement are shown in Fig. 3. Model helps to take into account the level of propagation micro crack for compression using the angle of dilation and stress ratio. Finite Element model is formed with solid elements for concrete and rod elements for reinforcement.

ID 1 Title Beton Color 55 Palette... Layer 1 Type...

General Function References Nonlinear Ply/Bond Failure Creep Electrical/Optical Phase

Stiffness

Youngs Modulus, E 2,7E+10

Shear Modulus, G 1,125E+10

Poisson's Ratio, nu 0,2

Limit Stress

Tension 9000000,

Compression 11500000,

Shear 575000,

Thermal

Expansion Coeff, a 0,

Conductivity, k 0,

Specific Heat, Cp 0,

Heat Generation Factor 0,|

Mass Density 2500,

Damping, 2C/Co 0,

Reference Temp 0,

a)

ID 2 Title Reinforcement Color 104 Palette... Layer 1 Type...

General Function References Nonlinear Ply/Bond Failure Creep Electrical/Optical Phase

Stiffness

Youngs Modulus, E 2,E+11

Shear Modulus, G 0,77E+11

Poisson's Ratio, nu 0,3

Limit Stress

Tension 0,

Compression 0,

Shear 0,

Thermal

Expansion Coeff, a 0,

Conductivity, k 0,

Specific Heat, Cp 0,

Heat Generation Factor 0,

Mass Density 7850,

Damping, 2C/Co 0,

Reference Temp 0,

b)

Fig. 2 Constant of materials: concrete (a), reinforcement (b)

### 3 Results and Problems

The deformation of cantilever beam with length of 3 m,  $0,5 \times 0,5$  m in section is reviewed as test example. At the end of beam is applied vertical force of 500 kN, which has been distributed at extreme square. This load is exceeded to ultimate load, that beam can withstand. Searching of ultimate load is performed in consistent loading in 100 steps iteration process. Two schemes of beams are reviewed: (1) beam with reinforcement in top (two rebars with diameter of 12 mm; the grade of reinforcement is A400) the loss of adhesion between concrete and reinforcement has not taken into account. (2) concrete beam without reinforcement. Results of calculations for first scheme are performed at Figs. 4 and 5.

Figure 4 is performed distribution of discrete crack zone, which are involved by tension in concrete. This level approximately corresponds to load for normal service

ID 1 Title Beton Color 55 Palette... Layer 1 Type...  
 General Function References Nonlinear Ply/Bond Failure Creep Electrical/Optical Phase  
 Nonlinearity Type  
 None  Nonlinear Elastic  
 Elasto-Plastic (Bi-Linear)  Plastic  
 Nonlinear Properties  
 Plasticity Modulus, H 0,  
 Compute From Tangent Modulus, Et...  
 Hardening Rule 0..Isotropic  
 Function Dependence 0..None  
 Yield Function  
 Yield Criterion 3..Drucker-Prager  
 2 \* Cohesion 1200000,  
 Friction Angle 30,  
 Extended Material Model...

a)

ID 2 Title Reinforcement Color 104 Palette... Layer 1 Type...  
 General Function References Nonlinear Ply/Bond Failure Creep Electrical/Optical Phase  
 Nonlinearity Type  
 None  Nonlinear Elastic  
 Elasto-Plastic (Bi-Linear)  Plastic  
 Nonlinear Properties  
 Plasticity Modulus, H 0,  
 Compute From Tangent Modulus, Et...  
 Hardening Rule 0..Isotropic  
 Function Dependence 0..None  
 Yield Function  
 Yield Criterion 0..von Mises  
 Initial Yield Stress 365000000,  
 Friction Angle 0,  
 Extended Material Model...

b)

**Fig. 3** Initial data for nonlinear calculation of materials: concrete (a), reinforcement (b)

condition beam. Because the calculation was done taking into account geometrical nonlinearity for level of maximum ultimate load, crack zone is moved away from embedment. It should be noted that the considered DP model was developed for continuous body and it can't give a presentation of the quantitative character of the distribution of cracks, however it can be assessed by an ultimate deep of their distribution and development of plastic deformation in compression zone of concrete. Figure 5 shows that stress in reinforcement has reached yield point in the support zone for the load of  $0.34P$ . The character of development plastic deformation in tension zone for different steps of load is shown in Fig. 6. Failure of the sample occurs at a load exceeding the level of  $0.214P$ , while the section height is switched off from work to 0.6, where vertical and inclined cracks are formed. The order of development of plastic deformations at various stages of loading is presented by schemes a, b, c.

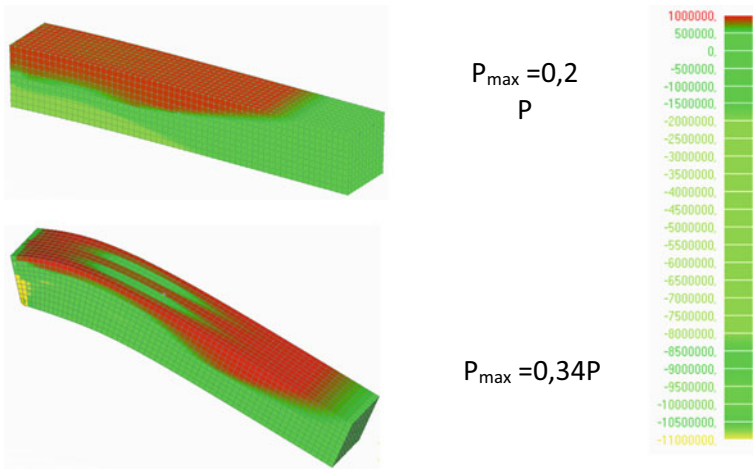


Fig. 4 Compression and tension zone of concrete for different level of load

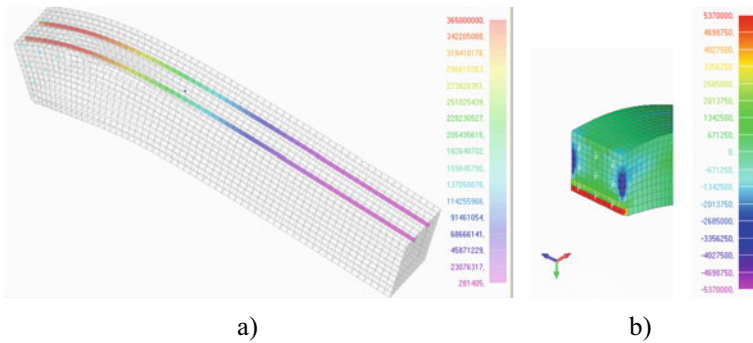
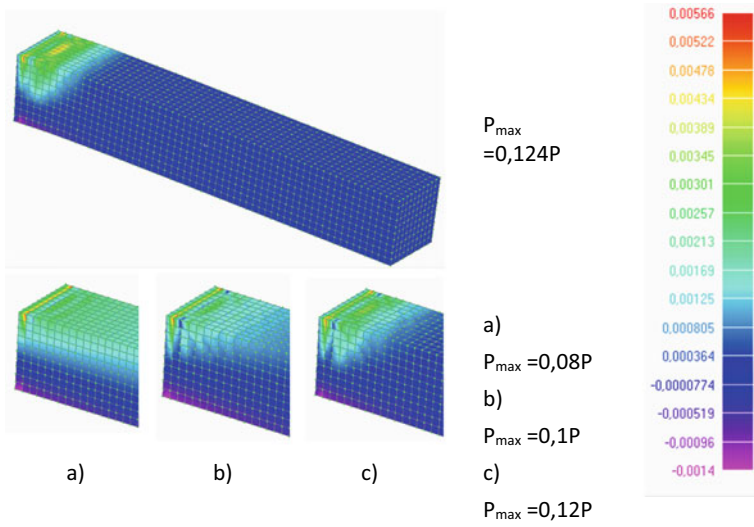


Fig. 5 Stress–strain behavior of beam for load close to ultimate load: Mises stress in rebars (a), shear crack stress at support (b)

Figure 7 shows the distribution of axial compressive and tensile stresses in a concrete specimen, depending on the level of its loading. The distribution of tensile stresses at the maximum load level shows the zone in which it is necessary to perform reinforcement, while in the state of pre-fracture, plastic deformations occur during both tension and compression. Data on ultimate loads are presented in summary Table 1.

The practice of software implementation has shown that the use of Femap and NX Nastran allows you to integrate calculation procedures into optimization algorithms based on evolutionary modeling [3–7], as well as to design structures with the required level of mechanical safety [6, 8–14].

In this case, the most promising for implementation are algorithms that have the ability to both parametric [15–18] and structural [19, 20] synthesis.



**Fig. 6** Results of calculating the ultimate load a-c deformation stages

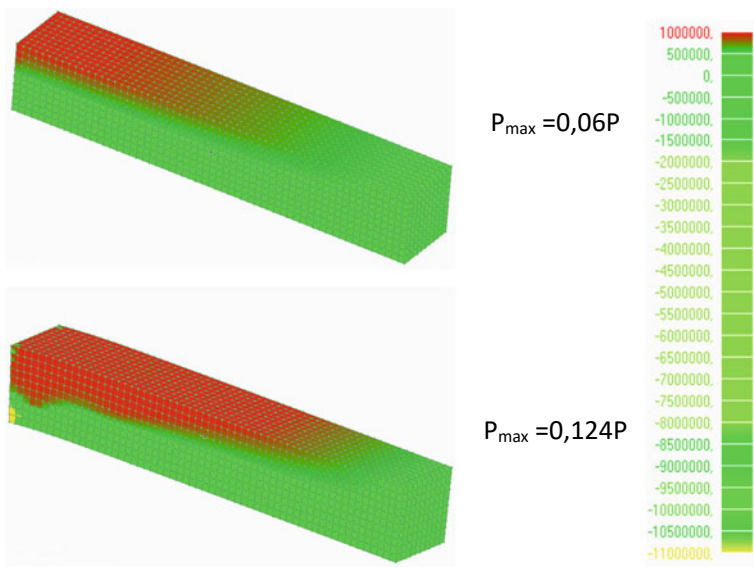


**Fig. 7** Data about stress in concrete in different steps of loading

**Table 1** Calculation results

Object	Ultimate load	Load level at beginning a crack formation
Reinforced concrete beam	170 kN	48 kN
Concrete beam	62 kN	30 kN
Effect of increasing load-bearing capacity	in 2.74 times	in 1.6 times

## 4 Conclusion

The presented approach to modeling the stress–strain state of concrete and reinforced concrete structures makes it possible to determine the ultimate bearing capacity and obtain detailed information on plastic deformations in the tensioned and compressed zone of reinforced and unreinforced concrete.

## References

1. Alejano, L.R., Bobet, A.: Drucker-Prager criterion. *Rock Mech. Rock Eng.* (2012). <https://doi.org/10.1007/s00603-012-0278-2>
2. Drucker, D.C., Prager, W.: Soil mechanics and plastic analysis or limit design. *Q. Appl. Math.* (1952). <https://doi.org/10.1090/qam/48291>
3. Alekseytsev, A.V., Akhremenko, S.A.: Evolutionary optimization of prestressed steel frames. *Mag. Civ. Eng.* (2018). <https://doi.org/10.18720/MCE.81.4>
4. Tamrazyan, A., Filimonova, E.: Searching method of optimization of bending reinforced concrete slabs with simultaneous assessment of criterion function and the boundary conditions. *Appl. Mech. Mater.* 404–409 (2014). <https://doi.org/10.4028/www.scientific.net/AMM.467.404>
5. Alekseytsev, A.V.: Frame structures optimization based on evolutionary modeling in active overall stability constraints. *J. Phys. Conf. Ser.* (2020). <https://doi.org/10.1088/1742-6596/1425/1/012036>
6. Prokurov, M., Indykin, A., Alekseytsev, A.: Increasing the reliability of the soil slopes design using evolutionary modelling. *MATEC Web Conf* (2018). <https://doi.org/10.1051/mateconf/201825104017>
7. Aoues, Y., Chateauneuf, A.: Reliability-based optimization of structural systems by adaptive target safety—application to RC frames. *Struct. Saf.* **30**, 144–161 (2008). <https://doi.org/10.1016/j.strusafe.2006.10.002>
8. Alekseytsev, A., Botagovsky, M., Kurchenko, N.: Cost minimization for safety enhancing of timber beam structures in historical buildings. *E3S Web Conf.* (2019). <https://doi.org/10.1051/e3sconf/20199703002>
9. Navarro, I.J., Yepes, V., Martí, J.V.: Life cycle cost assessment of preventive strategies applied to prestressed concrete bridges exposed to chlorides. *Sustain* **10** (2018). <https://doi.org/10.3390/su10030845>
10. Tamrazyan, A., Alekseytsev, A.: Multi-criteria optimization of reinforced concrete beams using genetic algorithms. *IOP Conf. Ser. Mater. Sci. Eng.* (2020). <https://doi.org/10.1088/1757-899X/869/5/052027>

11. Greiner, D., Periaux, J., Emperador, J.M., Galván, B., Winter, G.: Game theory based evolutionary algorithms: a review with nash applications in structural engineering optimization problems. *Arch. Comput. Methods Eng.* **24**, 703–750 (2017). <https://doi.org/10.1007/s11831-016-9187-y>
12. Alekseytsev, A.V., Al Ali, M.: Optimization of hybrid I-beams using modified particle swarm method. *Mag. Civ. Eng.* (2018). <https://doi.org/10.18720/MCE.83.16>
13. Tamrazyan, A.G., Alekseytsev, A.V.: Optimal structures design: accounting of costs and relative accidents risk. *Vestn. MGSU.* (2019). <https://doi.org/10.22227/1997-0935.2019.7.819-830>
14. Kaveh, A., Zakian, P.: Optimal seismic design of reinforced concrete shear wall-frame structures. *KSCE J. Civ. Eng.* **18**, 2181–2190 (2014). <https://doi.org/10.1007/s12205-014-0640-x>
15. Tamrazyan, A., Alekseytsev, A.: Evolutionary optimization of reinforced concrete beams, taking into account design reliability, safety and risks during the emergency loss of supports. *E3S Web Conf.* (2019). <https://doi.org/10.1051/e3sconf/20199704005>
16. Tamrazyan, A., Alekseytsev, A.: Strategy for the evolutionary optimization of reinforced concrete frames based on parallel populations evolving. *IOP Conf. Ser. Mater. Sci. Eng.* (2020). <https://doi.org/10.1088/1757-899X/869/5/052019>
17. Lee, C.K., Kim, S.K.: GA-based algorithm for selecting optimal repair and rehabilitation methods for reinforced concrete (RC) bridge decks. *Autom. Constr.* **16**, 153–164 (2007). <https://doi.org/10.1016/j.autcon.2006.03.001>
18. Esfandiari, M.J., Urgessa, G.S., Sheikholarefin, S., Manshadi, S.H.D.: Optimum design of 3D reinforced concrete frames using DMP SO algorithm. *Adv. Eng. Softw.* **115**, 149–160 (2018). <https://doi.org/10.1016/j.advengsoft.2017.09.007>
19. Xia, L., Fritzen, F., Breitkopf, P.: Evolutionary topology optimization of elastoplastic structures. *Struct. Multidiscip. Optim.* **55**, 569–581 (2017). <https://doi.org/10.1007/s00158-016-1523-1>
20. Luo, Y., Kang, Z.: Topology optimization of continuum structures with Drucker-Prager yield stress constraints. *Comput. Struct.* (2012). <https://doi.org/10.1016/j.compstruc.2011.10.008>

# Nonlinear Analysis of Damaged Reinforced Concrete Columns, Restored with Carbon Fiber Jacket Using ABAQUS



Gamal Algnde and Alexander Topilin

## 1 Introduction

Existing concrete structures are often in need of repair and/or restoration, mainly due to environmental damage, extreme events, or changes in design assumptions. Concrete columns are usually strengthened and restored with a concrete shell as this results in both increased ductility and strength. Currently, carbon fiber jacket (CFRP) is an interesting alternative to the latter due to its high strength-to-weight ratio, simple application procedure, and insignificant increase in geometry. This study presents a nonlinear analysis of damaged reinforced concrete columns restored with carbon fiber jacket (CFRP) using ABAQUS.

## 2 Structural Analysis Using the Finite Element Method FEM

Based on the main objectives of this study, 3D finite element models of reinforced concrete columns have been developed, and various issues related to modeling are addressed as follows:

1. Type of finite elements.
2. Properties of materials.
3. Assignment of cross-sections.
4. Definition of the step of application of the load.
5. Interaction between elements.
6. Specification of boundary conditions and loads.

---

G. Algnde (✉) · A. Topilin  
Moscow State University of Civil Engineering (National Research University) (MGSU), Moscow, Russia



**Table 1** System of units of measure

Length	Force	Mass	Time	Pressure	Density
mm	N	T	C	MPa	T\mm <sup>3</sup>

- 7. Creation of a mesh of finite elements FEM.
- 8. Assignment of job.
- 9. Evaluation of results.

Reinforced concrete column with a hole and a control column without holes were studied to calculate their residual strength.

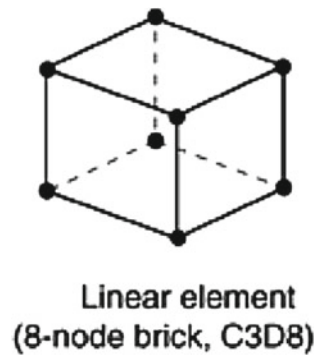
The following measurement system was adopted for modeling—SI (Table 1).

### 2.1 Type of Finite Elements

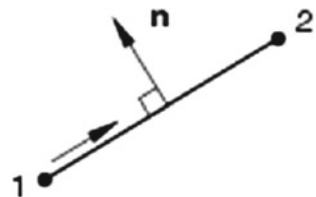
The concrete column element was modeled using a solid hexahedral element, which ABAQUS defines as C3D8 (Continuum three-dimensional (3D), 8 nodes), also using a deformable body. The solid element has eight nodes with six degrees of freedom at each node, as shown in Fig. 1.

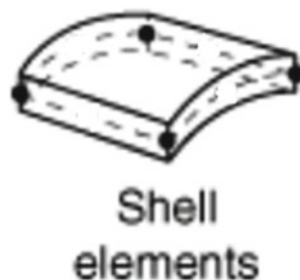
Steel reinforcement is modeled using bars in ABAQUS program defined as T3D2 element (2-node linear 3-D bar) (Fig. 2).

**Fig. 1** Three-dimensional deformable body



**Fig. 2** Three-dimensional truss



**Fig. 3** Shell element

Since the thickness of CFRP sheets (carbon fiber reinforced plastic) are much thinner than other sizes, CFRP acts like a shell, so 4-node shell elements (S4) were adopted to model them, as shown in Fig. 3.

## 2.2 Material Properties and Cross-Section Definition

### 2.2.1 Modeling Concrete Properties

Two types of properties are used to describe the nonlinear properties of concrete:

- Elastic properties.
- Plastic properties (Table 2).

**Table 2** Properties of concrete

Density of concrete	2.5E-9 t/mm <sup>3</sup>		
Cross-section of concrete	300 * 300 * 2000 mm	Hole dimensions	75 * 400 * 300 mm
Compressive strength of reference samples ( <i>fck</i> )	20 MPa		
Characteristic compressive strength of a concrete sample in the form of a cube ( <i>fck</i> , cube)	25 MPa		
Average compressive strength of concrete ( <i>fcm</i> )	$f_{cm} = f_{ck} + 8 = 28$ MPa		
Average tensile strength of concrete ( <i>fctm</i> )	$f_{ctm} = 0.3 * f_{ck}^{2/3} = 2.21$ MPa		
Elastic properties	Modulus of elasticity of concrete ( <i>Ecm</i> )	$E_{cm} = 22 * (f_{cm}/10)^{0.3} * 10^3 = 29962$ MPa	
	Poisson's ratio ( <i>v</i> )	0.2	

**Table 3** Parameters of the concrete damage plasticity model

Dilation angle ( $\psi$ )	Eccentricity ( $\epsilon$ )	$f_{b0}/f_{c0}$	$k_c$	Viscosity parameter
31	0.1	1.16	0.67	0.0001

Plastic properties: In the calculations of this work, a model of concrete with plastic failure (concrete damage plasticity model) was used. The parameters of the concrete damage plasticity model are presented in Table 3.

Dilation Angle ( $\psi$ ): Dilation angle that determines the ratio of volume and shear deformation.

Eccentricity ( $\epsilon$ ): A parameter that controls the rate at which a material transitions to the plastic state.

$f_{b0}/f_{c0}$ : Ratio of biaxial compressive strength of concrete to uniaxial compressive strength of concrete.

$k_c$ : The surface shape parameter for concrete (Table 4).

### 2.2.2 Modeling Properties of Steel Reinforcement

Two types of properties are used to describe the nonlinear properties of reinforcing steel:

- Elastic properties.
- Plastic properties (Fig. 4 and Table 5).

### 2.2.3 Modeling the Properties of CFRP (Carbon Fiber Reinforced Plastic)

CFRP (CFRP) was modeled with linear elastic behavior to break. In this study, CFRP is considered as an orthotropic element. Therefore, it is necessary to consider the properties of the element in each direction separately. The modulus of elasticity in the main direction is set at 138 GPa, and the CFRP thickness is 0.3 \* 3 mm. A standard composite shell was adopted in which each CFRP sheet was modeled as a separate layer (see Fig. 5). For an orthotropic material model, engineering constants in the ABAQUS software are shown in Table 6.

**Table 4** Dependences of stresses and damage coefficients on nonlinear deformations in compression and dependence of stresses and damage coefficients on nonlinear deformations in tension

Dependence of stresses and strains in compression		The coefficient of concrete damage in compression	
Stresses $\sigma_c$ (MPa)	Nonlinear strains $\epsilon_c^{in}$	Damage coefficient $d_c$	Nonlinear strains $\epsilon_c^{in}$
11.2	0	0	0
18.45395	0.000156	0	0.000156
23.91742	0.000372	0	0.000372
27.01647	0.000667	0	0.000667
28	0.001032	0	0.001032
27.4519	0.001357	0.019575059	0.001357
25.8638	0.001717	0.076292715	0.001717
23.31371	0.002109	0.167367512	0.002109
19.872	0.00253	0.290285726	0.00253
15.60236	0.002979	0.442773012	0.002979
8.30701	0.005873	0.703321077	0.005873
Dependence of stresses and strains in tension		The coefficient of concrete damage in tension	
Stresses $\sigma_t$ (MPa)	Crack strains $u_t^{ck}$ (mm)	damage coefficient $d_t$	Crack strains $u_t^{ck}$ (mm)
2.210419	0	0	0
1.129164	0.030924	0.17537	0.030924
0.660059	0.061849	0.35075	0.061849
0.459779	0.092773	0.52612	0.092773
0.352886	0.123697	0.7015	0.123697
0.272163	0.154621	0.87687	0.154621
0.199853	0.185546	0.9015	0.185546
0.135008	0.21647	0.92612	0.21647

**Fig. 4** Column cross-section

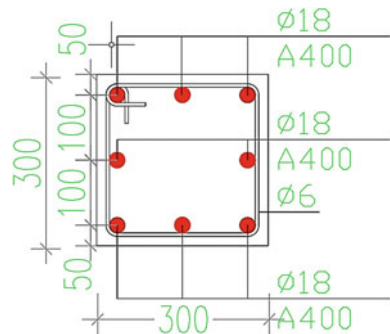


**Table 5** Properties of reinforcing steel

Density of steel reinforcement	7.85E-9 t/mm <sup>3</sup>		
Cross section of steel reinforcement	Longitudinal reinforcement (main)	8Ø18 mm	
	Transverse reinforcement	Ø6 mm	
Elastic properties	Modulus of elasticity of steel reinforcement ( <i>Ea</i> )	<i>Ea</i> = 200000 MPa	
	Poisson's ratio ( <i>ν</i> )	0.3	
Plastic properties	Stresses (MPa)—(A400)	400	400
	Nonlinear strains	0	0.1

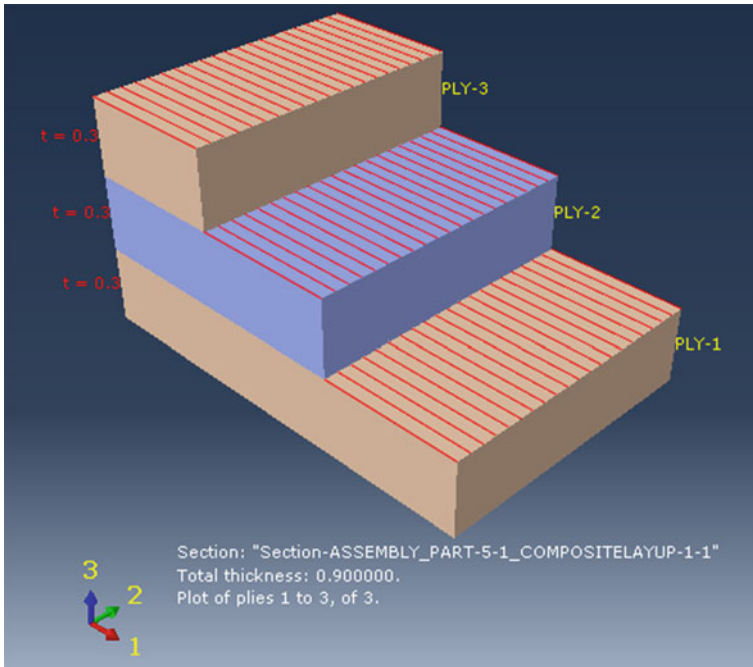


**Fig. 5** Standard composite shell

**Table 6** Orthotropic properties of the material in each direction

Elastic modulus (MPa)		Shear modulus (MPa)		Poisson's ratio	
<i>E</i> <sub>1</sub>	138,000	<i>G</i> <sub>12</sub>	5200	<i>Nu</i> <sub>12</sub>	0.28
<i>E</i> <sub>2</sub>	9500	<i>G</i> <sub>13</sub>	5200	<i>Nu</i> <sub>13</sub>	0.28
<i>E</i> <sub>3</sub>	9500	<i>G</i> <sub>23</sub>	1450	<i>Nu</i> <sub>23</sub>	0.4

## **2.3 Interaction Between Elements**

### **2.3.1 Assignment of Contact Properties of Reinforcement and Concrete**

The steel bars were assumed to be perfectly bonded to the adjacent concrete by embedding the steel bars elements into the concrete elements using the embedded region option in ABAQUS.

### **2.3.2 Assignment of Contact Properties of Concrete and CFRP**

In CFRP-reinforced concrete elements, there are two possible failure modes for CFRP sheets, namely CFRP rupture and CFRP debonding or delamination. The former mainly occurs in compression members such as CFRP columns, while the latter occurs in bending members such as CFRP beams. Thus, due to the dominance of CFRP rupture mode in CFRP-confined concrete columns, the bond between concrete and CFRP does not significantly affect the behavior of structures. Therefore, ABAQUS uses a tie constraint model between concrete and CFRP over the surface of the contacts.

### **2.3.3 Assignment of Contact Properties of Concrete and Rigid Plate**

For each rigid plate at the top and bottom of the columns, one reference point RP is defined in its center. Rigid plates have been constrained to the corresponding reference points. This is done using a rigid body constraint. A rigid body is a set of nodes, elements and/or surfaces whose movement is controlled by the movement of one reference point. In other words, when using this option, plates behave rigidly and boundary conditions can be applied to the corresponding reference points instead of using a rigid plate body. ABAQUS uses a tie constraint model between concrete and a rigid plate over the surface of the contacts.

## **2.4 Hole Restoration**

The hole is filled with concrete, and reinforcement of the same diameter as the reinforcement used in the column is used. The old reinforcement is connected to the new reinforcement using a shear bolt/wedge coupling sleeve.

Shear bolt/wedge coupling sleeve: designed primarily for splicing smaller diameter bars from (12–20 mm), the connecting sleeve has an oval cross-section, which allows two reinforcing bars of the same diameter to be overlapped in the sleeve, as shown in Fig. 6.



**Fig. 6** Coupling sleeve with shear bolt/wedge

ABAQUS uses a tie constraint model between old and new concrete, as well as old and new reinforcement over the surface of the contacts.

### 2.5 Assignment of Boundary Conditions and Loads

A compressive load is applied to the RP of the upper rigid plate in the U3 direction using the displacement control method. The solution strategy is based on a static general method that is simple and has an enough short analysis time. The boundary conditions and load application are shown in Fig. 7.

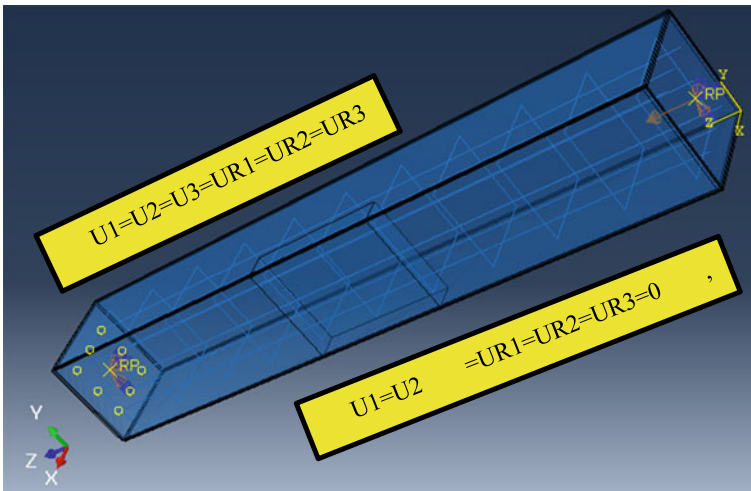


**Fig. 7** Boundary conditions and loads

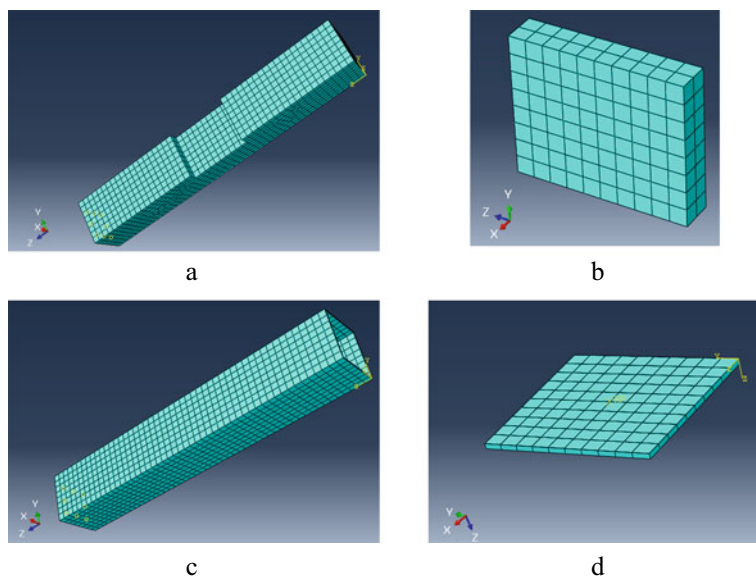


**Fig. 8** Finite element model: **a** column, **b** concrete in the hole, **c** CFRP, **d** rigid plate

## ***2.6 Creation of a Mesh of Finite Elements***

See Fig. 8.

## ***2.7 Results of Calculation by the Finite Element Method***

### **2.7.1 Influence of CFRP Shell Thickness on the Load-Bearing Capacity of a Restored Reinforced Concrete Column**

Based on the results of the analysis, we found that the appropriate thickness of the CFRP shell can be selected depending on the goal: either restore only the previous bearing capacity of the column with a slight increase in the bearing capacity, or significantly increase its bearing capacity in case of additional loads. Figure 9 shows the bearing capacity-displacement curves of a reinforced concrete column restored with a CFRP shell with variable shell thickness.



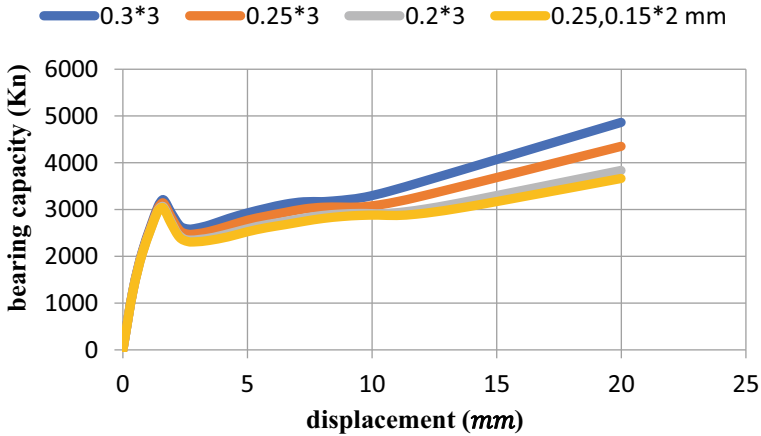


**Fig. 9** Bearing capacity-displacement curves of a reinforced concrete column restored with carbon fiber jacket (CFRP) with variable shell thickness

### 2.7.2 Comparison of the Load-Bearing Capacity of a Damaged Column and a Restored Column with Carbon Fiber Jacket (CFRP)

If we want to restore only the previous bearing capacity of the column with a slight increase in bearing capacity, we use a carbon fiber reinforced plastic (CFRP) shell with a thickness of (0.2; 15 \* 2 mm), in this case the bearing capacity has increased by 82%. And if we want to significantly increase the bearing capacity of the column in case of additional loads, we use a carbon fiber reinforced plastic (CFRP) shell with a thickness of (0.3 \* 3 mm), in this case the bearing capacity has increased by 142%. Figure 10 shows the bearing capacity-displacement curves of a reinforced concrete column restored with a CFRP shell and a reinforced concrete column with a hole.

### 2.7.3 Efficiency of CFRP When the Column is Subjected to an Eccentric Compressive Load

Figure 11 shows the efficiency of CFRP in restoring a column with a change in eccentricity of load application.

1. Pure axial compression (point A). This is the largest axial compressed load that a column can support.
2. Compression with slight bending (point B). This is a case of high axial load acting at low eccentricity. The stress distribution becomes inclined, but the section is still in compression. Failure occurs due to concrete crushing.
3. Compression control (point C). There is both a compression zone and a tension zone for concrete. The steel is subjected to tension. Failure occurs due to

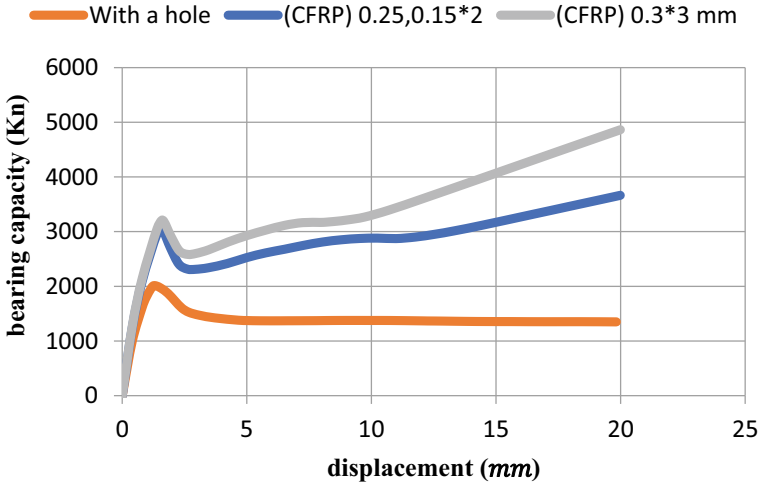


Fig. 10 Bearing capacity-displacement curves of a reinforced concrete column restored with a CFRP shell and a reinforced concrete column with a hole

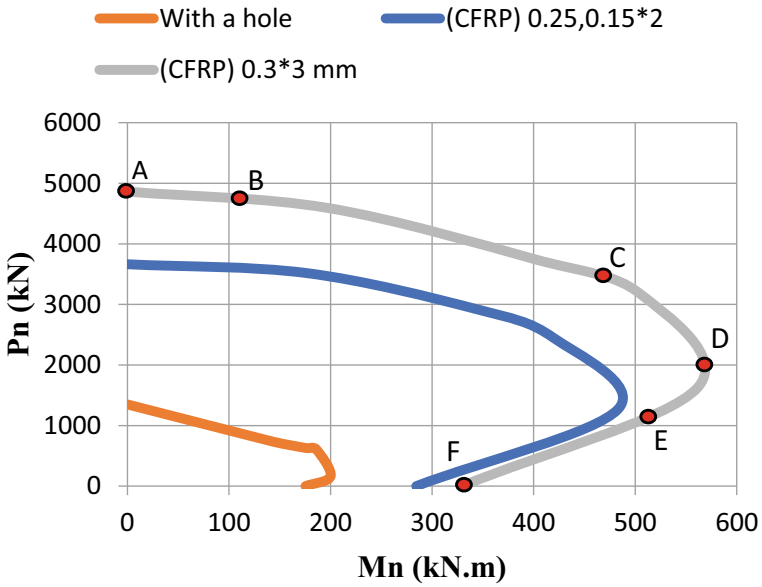
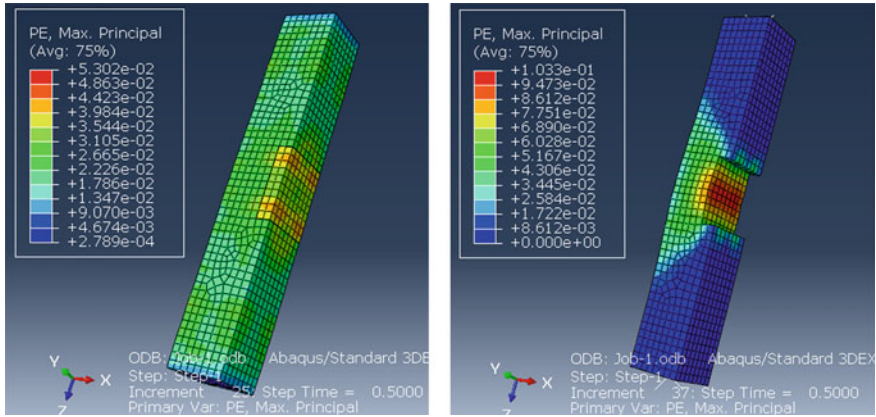


Fig. 11 Interaction curve of CFRP—reinforced concrete column



**Fig. 12** Principal plastic deformations of a reinforced concrete column

crushing of the concrete on the compression side, whereas the stress in steel ( $f_s$ ) is less than the yield stress ( $f_y$ ).

4. Balanced condition (point *D*). Equilibrium is reached when the compressive strain in the concrete reaches its limit and the tensile reinforcement simultaneously reaches yield. The Failure of concrete occurs simultaneously with the yields of the steel.
5. Tension control (point *E*). This is a case of low axial load with high eccentricity, that is, a large moment. In case of failure, the strain in tensile steel is greater than the yield strain.
6. Pure flexure (point *F*). In this case, a bending moment  $M$  acts on the section, while the axial load is  $P = 0$ . Failure occurs in the same way as in a beam subject only to a bending moment.

### 2.7.4 Principal Plastic Deformations

The principal plastic deformations of a reinforced concrete column restored with a CFRP shell and a reinforced concrete column with a hole at maximum load are shown in Fig. 12. Here we notice the huge role of CFRP in reducing these plastic deformations.

## 3 Conclusion

In this work, calculations and studies of nonlinear analysis of damaged reinforced concrete columns, restored with a carbon fiber reinforced plastic (CFRP) shell, were carried out. The ABAQUS software system was chosen as the flagship system due to its objective advantages over analogues.

Realistic modeling of nonlinear properties of reinforced concrete in numerical calculations is a complex multi-component problem.

During the study, a model of deformation and strength of reinforced concrete, reinforcement, and carbon fiber reinforced plastic shell (CFRP) was studied. When comparing the bearing capacity of a damaged column and a restored column with a carbon fiber reinforced plastic (CFRP) shell, two cases were considered: in the first, a carbon fiber reinforced plastic (CFRP) shell with a thickness of (0.2; 15 \* 2 mm) was used, in this case the bearing capacity has increased by 82%; the second used a carbon fiber reinforced plastic (CFRP) shell with a thickness of (0.3 \* 3 mm), in this case the bearing capacity has increased by 142%. It has also been shown that CFRP is highly effective in restoring a column when the eccentricity of the load is changed, and the huge role of CFRP in reducing plastic deformations.

## References

1. Alfarah, B., López-Almansa, F., Oller, S.: New methodology for calculating damage variables evolution in plastic damage model for RC structures. *Eng. Struct.* **132**, 70–86 (2017)
2. ABAQUS—Применение комплекса в инженерных задачах
3. Daniel, I.M., Ishai, O.: *Engineering mechanics of composite materials*. New York, Oxford (2006)
4. Mechanical Rebar Splicing Systems
5. Hafezolghorani, M., Hejazi, F., Vaghei, R., Jaafar, M.S.B., Karimzade, K.: Simplified damage plasticity model for concrete. *Struct. Eng. Int.* **1** (2017)
6. Tao, Y., Chen, J.F.: Concrete damage plasticity model for modeling FRP-to-concrete bond behavior. *J. Compos. Constr.* **19**(1), 04014026 (2015)
7. Martinez, J., Zareh, H.: *Abaqus/CAE Vibrations Tutorial*. Portland State University, Mechanical Engineering
8. EN234: *Computational methods in Structural and Solid Mechanics*, EN234 ABAQUS TUTORIAL, School of Engineering, Brown University
9. C.-D. 200/2004, *Guide for the Design and Construction of Externally Bonded FRP Systems for Strengthening Existing Structures*, National Research Council, Rome (2004)
10. Mander, J.B., Priestley, M.J.N., Park, R.: Theoretical stress-strain model for confined concrete. *J. Struct. Eng. ASCE* **114**(8), 1804–1826 (1988)
11. Wang, W., Dai, Y., Zhang, C., Gao, X., Zhao, M.: Micromechanical modeling of fiber-reinforced composites with statistically equivalent random fiber distribution. *Materials* **9**, 624 (2016). <https://doi.org/10.3390/ma9080624>
12. Demin, W., Fukang, H.: Investigation for plastic damage constitutive models of the concrete material. *Science Direct. Procedia Eng.* **210**, 71–78 (2017)
13. ABAQUS.: *User's manual*. Standard, Simulia, Rhode Island, USA (2010)

# Spherical Domes of Paired Arches of the Same Radius



Vasilij D. Antoshkin and Maria V. Gorina

The disadvantage of most of the known solutions of geodesic and mesh domes is a large number of different types of nodes for connecting shell elements, sharp angles of connections, different types, and complexity of performing support nodes, due to the fact that these support nodes are located at different levels, as well as the complexity and complexity of performing enclosing structures and roofing.

To increase the reliability of the dome cover frame, simplify the manufacture of frame components, as well as the manufacture of enclosing structures and roofs, it is necessary to solve problems related to reducing the number of connected mounting elements, reducing the material consumption of nodal joints, and forming, by optimizing the geometry of the cutting of the sphere (excluding sharp corners), the location of supports at the same level of the sphere.

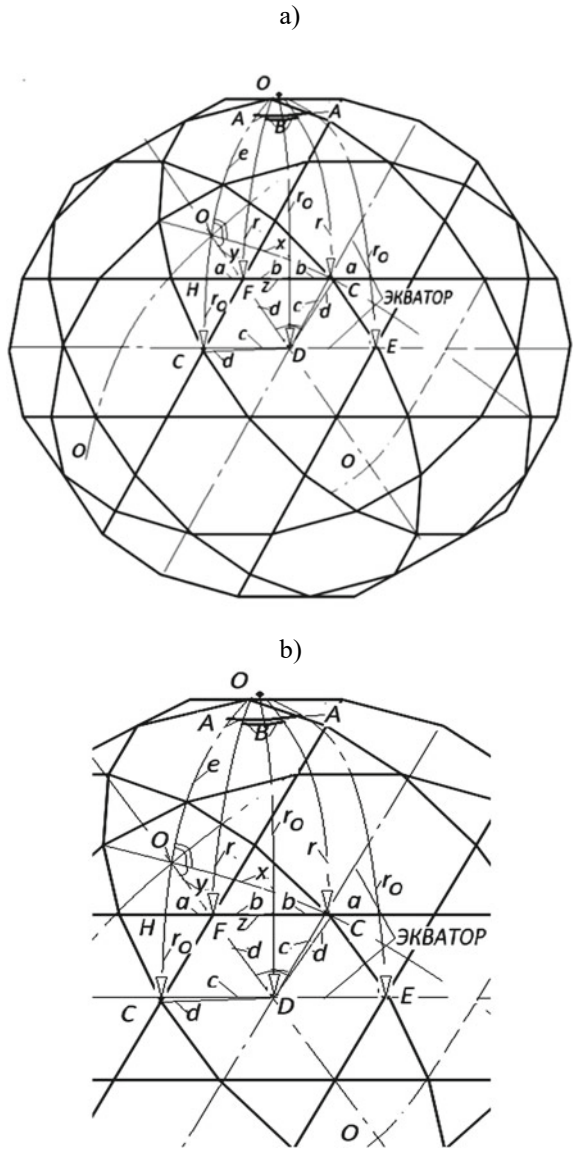
As a result of this work, geodesic domes with a specific coating are proposed, which is made by dividing the faces with large circles along the midpoints of the edges and the centers of the faces of a regular spherical polyhedron, for example, an icosahedron, etc. [1–9]. To do this, several “cuts” of the spherical shell frame are performed sequentially. The first “cut” of the shell frame is obtained by dividing into spherical elements and shapes, for example, arched arcs, polygons, triangles, etc., paired circles of the same radius, parallel to the specified large circles passing through the midpoints of adjacent edges. The second “cut” of the frame is formed by paired circles of the same radius, parallel to the specified large circles passing through the midpoints of the edges, through one edge. The third “cut” is formed by paired circles parallel to the large circles passing through the vertices of the faces of the corresponding regular spherical polyhedron.

Thus, in a geodesic dome based on a regular spherical polyhedron (icosahedron), it is possible to form a framework in the form of a network with minimal arch segments and nodes of intersecting paired arches in different directions [10–17]. The framework is created on the basis of regular spherical polyhedra, while maintaining a

---

V. D. Antoshkin (✉) · M. V. Gorina  
Mordovia State University, Saransk, Russia

**Fig. 1** Diagram of a geometric network of circles of one radius based on a regular spherical twenthedron: a—a general view of the scheme; b—a fragment of the cutting scheme; O—a pole on the vertex of the adjacent face of the icosahedron on the sphere and the vertices of the faces;  $r$ —the radius of the circles of paired arches;  $r_o$ —the radius of the equator



minimum number of standard sizes, and provides an effective location of the support nodes significantly below or above the equator and at one, well-defined level (Fig. 1). It is these forms of domes, broken and flat, that are most in demand by modern architecture.

There can be at least three independent variants of the arrangement of paired circles (and, accordingly, the arches of the frame) (according to the number of independent axes of symmetry of regular polyhedra). In the studied regular spherical polyhedron

based on the icosahedron, the vertices of the faces are denoted as  $O$ , and the radius of the circles parallel to the equator is denoted as  $r$ . If we analyze the possibility of forming the first one. the most obvious variant of the geometric network on the sphere, we conclude that the poles for the construction should be chosen by the vertices of the faces  $O$  of a regular spherical twenthedron (icosahedron), and solve the problem for the geometric network (Fig. 1).

We show a fragment of the circle construction scheme in Fig. 1b, where the arcs are cut off at the edges and bisectors of the faces of the arc  $x$  and the arc  $y$ , which determine the position of the main figures of this network. On circles of the same radius, the arc  $z$  is cut off, which contracts the arcs  $x$  and  $y$ . The radius of the equator is shown for clarity and is denoted as  $r_0$ .

We give the known parameters of the spherical face  $O O O$  of a regular twenty-sided rectangle inscribed in the sphere as a spherical triangle. According to the problem, when paired circles consist of repeated arcs of length  $2A$  and  $2b$ , it appears that the interior angle at the Zenith of the considered triangle  $O_b = 36^\circ$  (Fig. 1b), a total arc  $z$  pulls arcs triangles in the polar angles. An arc representing half the edge of a spherical icosahedron,  $d + y = 0.5e = 31.71748^\circ$ . The polar angles dividing the equator into equal segments give  $2c = 36^\circ$ .

Also, to simplify the problem, we denote the internal angles  $FDO = ODC$  as  $D_b$ . They divide the circles parallel to the equator into equal arcs  $b$ . The angle  $\angle DCO$  is denoted as  $C_{yd}$ . The internal angles at the zenith will be  $A = 18^\circ - B$ .

Учитывая данные упрощения, найдём неизвестные параметры треугольников, образованных большими окружностями осей граней правильного двадцатигранника непосредственно из формул сферической тригонометрии [16. 17]

$$\sin D_b = \frac{\sin 18^\circ \sin e}{\sin(d + y)}. \quad (1)$$

Подставляя значения, получим  $D_b = 31,71747^\circ$ ,

$$\cos C_{yd} = -\cos 2D_b \cos 36^\circ + \sin 2D_b \sin 36^\circ \cos(d + y). \quad (2)$$

$$C_{yd} = 85,10039675^\circ,$$

$$\sin x = \frac{\sin(d + y)}{\sin C_{yd}} \sin 2D_b, \quad (3)$$

тогда  $x = 28,611377^\circ$ .

Определяем радиус парных окружностей, принимая  $O_r = 108^\circ$

$$\cos r = \cos e \cos x + \sin e \sin x \cos 108^\circ, \quad (4)$$

$$r = 74,70259296^\circ.$$

Given these simplifications, we find the unknown parameters of the triangles formed by the large circles of the axes of the faces of a regular twenty-sided square directly from the formulas of spherical trigonometry [16. 17].

$$\sin D_b = \frac{\sin 18^\circ \sin e}{\sin(d + y)} \quad (5)$$

Substituting the values, we get  $D_b = 31.71747^\circ$ ,

$$\cos C_{yd} = -\cos 2D_b \cos 36^\circ + \sin 2D_b \sin 36^\circ \cos(d + y). \quad (6)$$

$$C_{yd} = 85,10039675^\circ,$$

then  $x = 28,1611377^\circ$ .

Determine the radius of the pair of circles, taking  $O_r = 108^\circ$

$$\cos r = \cos e \cos x + \sin e \sin x \cos 108^\circ, \quad (7)$$

$$r = 74,70259296^\circ.$$

To construct the cut, we need arcs of parallel circles on the sphere, which are defined by the internal angles  $A$  and  $B$

$$\sin(A + 2B) = \frac{\sin 108^\circ}{\sin r} \sin x, \quad (8)$$

then  $A = 36^\circ - A + 2B = 8,26769323^\circ$

$$\sin x = \frac{\sin(d + y)}{\sin C_{yd}} \sin 2D_b, \quad (9)$$

Using a method similar to the obtained cut of the circle 20 ( $a + b$ ), the parameters of another cut 10 ( $a + 3b$ ), also consisting of arcs of 2 standard sizes, can be found.

The elements of the formed paired arches of each direction of one of the frames, cut through one node, can be connected in nodes with the arches of the other direction by detachable connections, for example, on bolts; or rigidly, on welding and on glue through one node. Thus, no more than four elements are connected in a node, and elements of the same direction can be uncut in the node.

A spherical dome (Fig. 2) can be made of wooden jambs in the form of parts of arches of the same radius and with fractures along the length and at the intersections with the formation of straight sections, the parts are connected along the length of each broken arch on straight sections and nodes using spikes (S. I. Peselnik node),



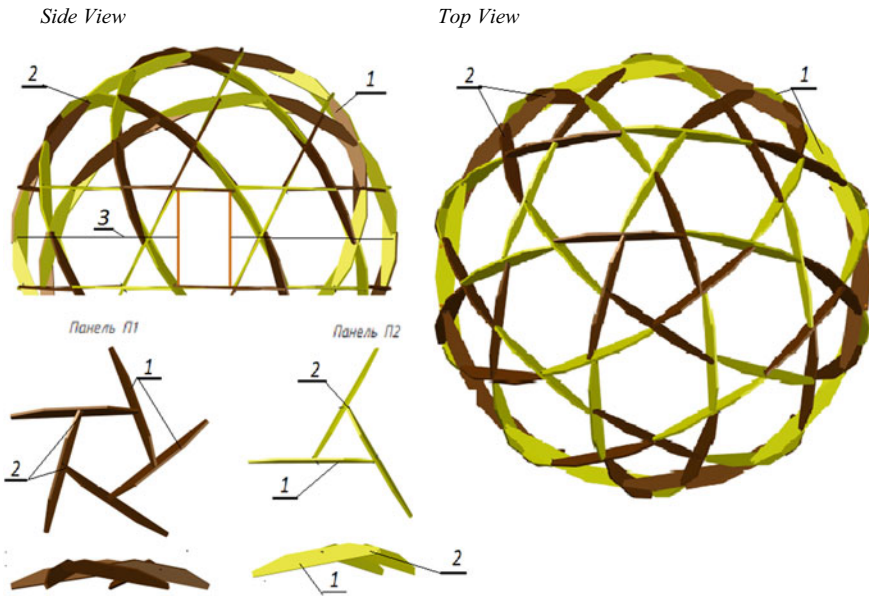


**Fig. 2** The frame of a spherical dome made of wooden circles in the form of frame pentagonal and triangular panels: 1—wooden circles; 2—Zöllinger node; 3—steel tightening along the equator of the dome

or with bolts (F. I. Peselnik node). Zöllinger, providing a connection angle of up to 70°.

To ensure the rigidity of the collapsed dome along the equator line, for the perception of the strut and for filling polygons and triangles in the frames, tightening rods and struts can be installed.

The geodesic dome of such an effective cutting can include the rods of one of the specified frames, which can be made of pipes in the form of parts of arches of the same radius and bent at the intersection points to form straight sections (Fig. 3). The parts can be connected along the length of each polyline arch on straight sections and nodes by welding and joined cylindrical inserts that provide any angle of connection (Figs. 3 and 4).

Such parts and nodes of intersecting arches of this design should be located alternately from the bottom and from the top. To ensure the rigidity of such a broken dome along the equator line for the perception of the strut and for filling polygons and triangles in the frames, the rods of the puffs and struts can also be installed.

A spherical dome can be complicated and made of four parallel arches already two radii of one of the specified frames on the basis of an icosahedron (Fig. 5), which can be made of pipes in the form of parts of arches, docked at the nodes on welding.

The diagram of Fig. 6 shows such an arrangement of circles of the same radius, which makes it possible to create an effective design of the dome from two independent systems of frames in the form of paired arches [11–18].

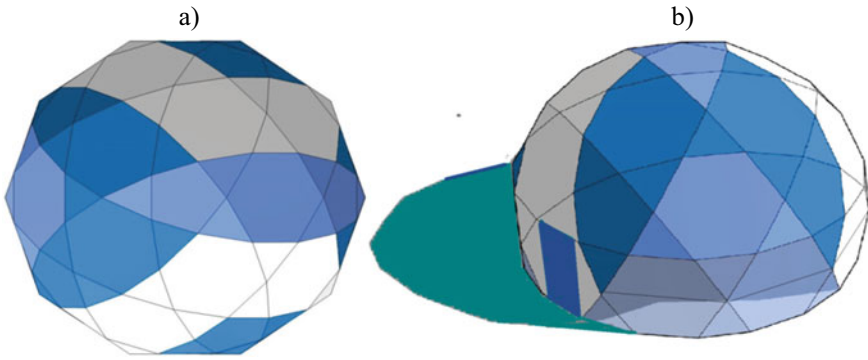


**Fig. 3** Tent dome made of paired broken arches: **a** top view; **b** isometry

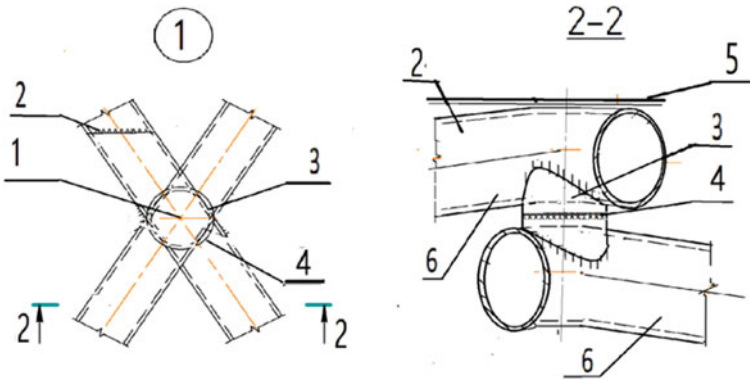


**Fig. 4** Node of intersecting polyline arches; 1—the center of the node; 2—joints on straight sections of arches; 3—tubular insert in the nodes of arches; 4—mounting joint of arches in the nodes of arches; 5—awning cover; 6—straight section of arches

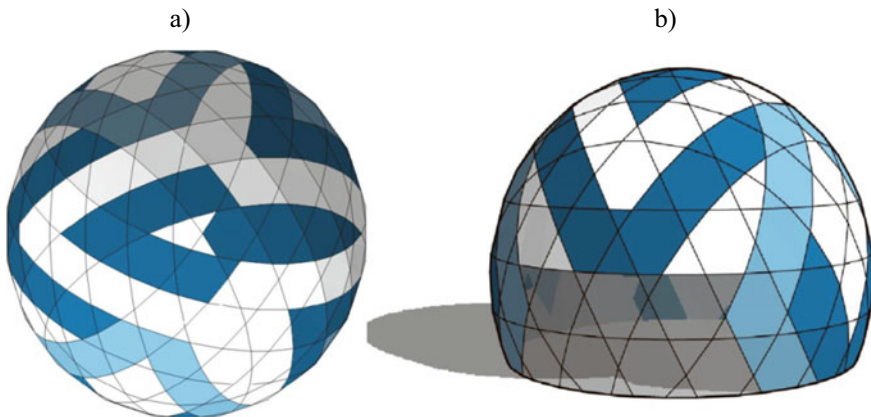


**Fig. 5** Tent dome of arches of two radii: **a** top view; **b** isometry

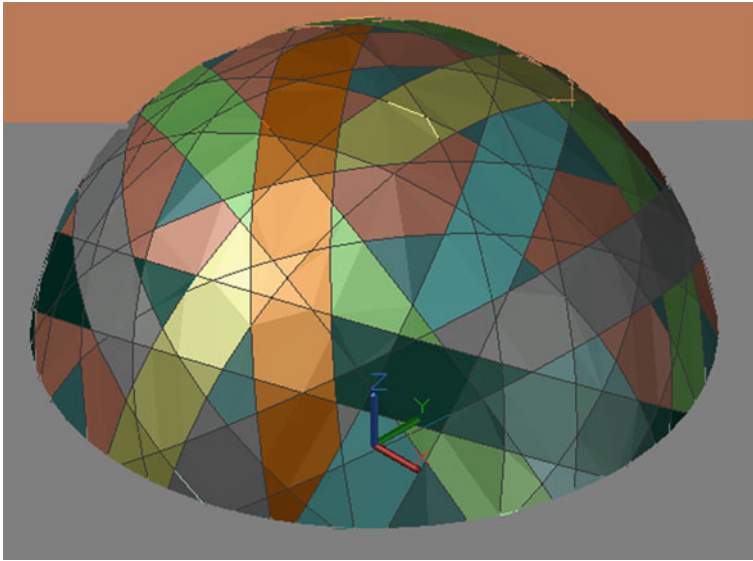


**Fig. 6** Tent dome of paired arches of the same radius combined from two independent frames

The elements of the arches of the combined frames are arranged in such a way that no more than four rods converge at the nodes, that is, two arches each.

The coating can be made from a roll of material, for example, profiled sheets, taking into account the parallelism of the arches, or fabric awning, or paintings made of double membranes with the formation of the inflatable structure.

The chaotic arrangement of the arches in Fig. 6 of the combined two frames actually contains two regular simple frames of paired arches.

### Conclusions

The proposed cutting solution is the geometric basis of a geodesic dome formed by paired circles of the same radius. It significantly simplifies the solution to all nodes of the frame body, including reference nodes, as the nodes on the same level, and apply technology pre-Assembly of the elements of the dome. Technological solutions such as domes give certainty to play geometry of this complex shape, simplify manufacturing of the frame units, and offer shell device for covering and roof.

### References

1. Antoshkin, V.D.: The problem of emplacement of triangular geometric net on the sphere with nodes on the same level. *Int. J. Comput. Civ. Struct. Eng.* **13**(2), 154–160 (2017)
2. Antoshkin, V.D.: Effective constructively-technological solutions prefabricated spherical domes. *J. Reg. Architect. Constr.* **3**(24), 112–121 (2015)

3. Antoshkin, V.D., Gudozhnikov, S.S., Perfilieva, O.I., Erofeeva, I.V.: Advanced technological solutions prefabricated spherical shells. In: CONFERENCE 2014, actual problems of architecture and construction/proceedings of the thirteenth international scientific and technical conference: in 2 parts. vol. 17, pp. 4–15 (2014)
4. Antoshkin, V.D., Kononov, A.G.: Prefabricated spherical shell of hexagonal panels. *Ogarev-Online* **13**(54), 6 P (2015)
5. Antoshkin, V.D., Kurbakov, G.V., Bochkin, V.S.: Method of installation of curved design *tredoevropsky Vestnik pro Vedu a Vyzkum* **83**, 1 P (2015)
6. Antoshkin, V.D., Kurganski, V.G.: A.S.No.1661316 (USSR) joint connection of wooden elements/publ. 09.11.1988
7. Travush, V.I., Antoshkin, V.D., Yerofeev V.T.: Team spherical shell. Patent for useful model RUS 129534–/27.07.2013
8. Travush, V.I., Antoshkin, V.D., Yerofeev V.T.: Team spherical shell. Patent for invention RUS No 2520192—06.27.2013
9. Travush, V.I., Antoshkin, V.D., Erofeeva I.V.: Antoshkin Team spherical shell. Patent for invention RUS 2564545—28.07.2014
10. Travush, V.I., Antoshkin, V.D., Yerofeev, V.T., Gudoshnikov, S.S.: Modern constructive and technological solutions of spherical shells. *J. Constr. Reconstr.* **6**(44), 45–55 (2012)
11. Travush, V.I., Antoshkin, V.D., Yerofeev, V.T., Gudoshnikov, S.: Constructive-technological capabilities of teams spherical shells. *J. Constr. Reconstr.* **6**(50), 36–48 (2013)
12. Travush, V.I., Antoshkin, V.D.: The problem 7 forming triangular geometric line field. *MATEC Web Conf.* **86**, 010 (2016). <https://doi.org/10.1051/mateconf/20168601032>
13. Travush, V.I., Antoshkin, V.D.: The problem 4 of placement triangular geometric line field. *MATEC Web Conf.* **86**, 010 (2016). <https://doi.org/10.1051/mateconf/20168601031>
14. Travush, V.I., Antoshkin, V.D.: To the problem 5 of emplacement of triangular geometric net on the sphere. *MATEC Web Conf.* **106**, 02003 (2017). <https://doi.org/10.1051/mateconf/201710602011>
15. Travush, V.I., Antoshkin, V.D.: To the problem 6 of emplacement of triangular geometric net on the sphere. *MATEC Web Conf.* **106**, 02012 (2017). <https://doi.org/10.1051/mateconf/201710602012>
16. Travush, V.I., Antoshkin, V.D., Svyatkina, A.Y.: The task of forming a network on the sphere from the circles of the same radius. *TPACEE 2018 E3S Web Conf.* **91**, 02011 (2018)
17. Travush, V.I., Antoshkin, V.D., Chorina, M.V., et al.: The task 3 of forming a network on the sphere from the circles of the same radius. *E3S Web of Conf.* **175**, 11029 (2020). <https://doi.org/10.1051/e3sconf/202017511029/>
18. Antoshkin, V.D.: Constructive and technological solutions of prefabricated spherical shells: autoref. dis.... dok. tehn. nauk. YuZGU. - Kursk: 36 P (2018)

# On the Question of Protection from Progressive Collapse



S. D. Bartenev  and V. V. Bobrov 

## 1 Introduction

The problem of protecting buildings and structures from progressive collapse is very relevant all over the world. In recent years, a large number of building collapses caused by emergency impacts, such as household explosions, mechanical removal of supports, have been recorded. The perception of such loads was not previously taken into account in the design. In connection with the increase in such cases and in order to improve the mechanical safety of buildings and ensure the safety of people, in accordance with [1], such loads have become necessary to take into account. Until recently, such loads and impacts, as well as the methodology for accounting for them, did not have the required regulatory framework for calculating them.

To implement this requirement, SP 296.1325800.2017 [1] and SP 385.1325800.2018 [2] were developed.

According to [1], progressive collapse means the successive destruction of load-bearing building structures with the collapse of the entire building or parts of it due to local damage. In an emergency, the destruction of individual load-bearing structural elements is allowed, but these destructions should not lead to a progressive collapse.

On January 6, 2019, SP 385 [2] entered into force, establishing provisions for the design of buildings and structures of normal and increased levels of responsibility of classes KS-2 and KS-3 of various structural systems in order to ensure their protection from progressive collapse.

---

S. D. Bartenev (✉) · V. V. Bobrov

National Research Moscow State University of Civil Engineering (NIU MGSU), Moscow, Russia

## 2 Research Materials and Methods

The article analyzes the technical literature and scientific research on the issue of progressive collapse, as well as the current regulatory framework.

The design of protection against progressive collapse is carried out in the event of an emergency design situation due to the expected initial local destruction in any place of the building or structure.

Under the assumed initial local destruction (hereinafter referred to as local destruction), it is understood that one load-bearing structural element is excluded from operation, simulating the loss of its load-bearing capacity and (or) stability, which in turn leads to a change in the structural system of a building or structure.

## 3 Results and Issues

A large number of scientific papers and publications are devoted to the study of progressive collapse [3–12], which indicates that there are many aspects that require attention and further serious study.

When designing structures, scenarios for the implementation of the most dangerous emergency design situations should be developed and strategies should be developed to prevent the progressive collapse of the structure in the event of local structural failure. Each scenario corresponds to a separate special combination of loads and, in accordance with the instructions of SP 20.13330 [13], must include one of the normalized (design) special impacts or one variant of local destruction of load-bearing structures for emergency special impacts.

In [3] calculation of the analysis of the survivability of statically indeterminate reinforced concrete beam and truss structural systems of buildings and structures under accidental impacts, the article formulates the problem of the calculation analysis of the survivability of such structural systems and an algorithm for determining the parameter of vitality, with special effects in the form of sudden shutdown of one of the structures.

Given the authors the analysis of the survivability of excess beam structural systems under accidental impact and the criteria for an emergency limit state for redundant systems allow to define a minimum load level of the structural system (option survivability  $\lambda$ ), in which the structural system in case of sudden removal of one bearing structural element (tie) begins destruction, leading to local or progressive destruction of the structure.

The article proposes criteria for the load-bearing capacity at a special limit state of various structural systems that arise under impacts, the excess of which can cause a progressive collapse of the structural system.

As a rule, the strength indicators serve as the criteria for such an assessment [14]. The authors come to the conclusion that structural systems of high-strength materials at small dimensions of the cross-sections of the elements, as well as for structural systems working in harsh environments, when the reduced cross-section or the estimated length as a criterion of resistance to progressive collapse must be considered, and the buckling bearing element of the structural system. The article presents proposals for normalizing the survivability parameters of reinforced concrete structural systems under extreme conditions caused by the sudden loss of stability of the load-bearing element from the accumulation of corrosion damage.

The most common form of protection for operational buildings and structures is the calculation of adaptive adaptability with the imaginary removal of each load-bearing element. In this case, the calculation checks all dangerous variants of local damage. The question arises as to how to perform the calculation, so that when providing protection against progressive collapse, an economically acceptable solution is obtained. To do this, it is necessary to analyze the behavior of the structural system when removing key load-bearing elements.

In the event of a sudden failure of one of the load-bearing elements of the system, there is a need to study the dynamic increase in stresses in the elements of the system. In [5], a definition of the dynamic increase in stresses arising from the reinforcement of two-component composite rod elements during local brittle destruction of concrete is given. When a brittle fracture of the concrete matrix occurs, the stresses acting in the stretched concrete are transferred to the reinforcement. Due to the instantaneous transmission of these stresses, longitudinal vibrations occur in the reinforcing bar, and the magnitude of the dynamic stresses may exceed the calculated tensile strength of the steel.

In [15], constructive proposals for the protection of buildings and structures of an increased level of responsibility from progressive destruction are considered. The authors consider the following active protection methods: the method of creating alternative paths of force resistance, which ensures the preservation of the load-bearing capacity of the structural system after switching off one of the structural elements and the destruction is localized; the method of creating local zones of increased resistance, when the entire building or part of it has increased resistance to beyond-design impacts in the event of accidents; a method of structural synthesis of a constructive system with the creation of predefined requirements.

In the monograph [6] and articles [7, 8], the solution to the problem of ensuring stability to a progressive collapse was obtained in a quasi-static formulation based on the energy principles proposed by Geniev et al. [9]. At the moment, there is no solution to such problems in a dynamic formulation, although this can be a test for approximate solutions to a wide class of practically important problems.

The authors of [16] consider the issues of determining the dynamic characteristics of multi-storey frame buildings with local damage and note that taking into account the time of column removal in a building in comparison with “instantaneous” has a number of specific features that directly affect the value of its natural frequencies, periods, and forms of vibrations. The article presents the results of the calculation of a 45-storey frame building for progressive collapse. The analysis carried out by the

authors shows that with the growth of the number of floors, the periods of fluctuations of the building increase, and the frequency of fluctuations decreases. The article considers a building with transition floors, the presence of which reduces the periods of fluctuations due to increased rigidity. The coefficient of dynamism, taking into account the time of failure of the column for such buildings, can be reduced by more than 15%.

It is impossible not to mention the works [17, 18]. In [17], the author notes that the most effective solution to protect buildings and structures from progressive collapse is a probabilistic approach to design. The introduction of such a technique significantly increases the reliability and durability of buildings. The method is based on the method of optimal design of building structures. A deterministic approach to the calculation of building structures leads to overspending of materials due to overstating loads and underestimating the strength characteristics of structures.

SP 385.1325800.2018 [2] sets out the requirements for calculation models. When calculating, a spatial calculation model should be used, which takes into account the interaction with the ground base according to SP 22.13330 [19]. It is necessary to consider the inclusion of items that in normal use are curtains, and when a local destruction of the structures actively involved in the work and participate in the redistribution efforts in the elements of the structural system.

The calculation of structures for stability against progressive collapse should be performed for each of the considered local destructions separately and independently of other possible local destructions.

In the analysis model structures should take into account the real diagram of the material structures and their joints (bundle masonry work under construction on the stretch; non-perception in the platform joint tensile stresses; the brittle fracture of structures and components of their conjugation, etc.) and the possibility of a particular limit state.

To perform calculations, it is necessary to use modern calculation programs that work according to the finite element method. Such programs include SACAD, LIRA-SOFT, LIRA-CAD, and STARKES.

The SCAD software package implements calculation modes for progressive collapse in accordance with SP 385.1325800.2018 [2] and in accordance with section II.6 manuals [20].

According to [20], it is advisable to use the dynamic calculation method when calculating for a progressive collapse, if the object is experiencing technological dynamic effects.

The method of dynamic calculation of extra-centrally compressed reinforced concrete elements in time and the features of calculating buildings and structures for progressive destruction in the entire range of combinations of force and temperature loads are considered in [10, 11].



## 4 Conclusion

In the course of the study, a review of the literature on the topic of progressive collapse was conducted, during which studies of reinforced concrete structures with a sudden shutdown (removal) of one of the load-bearing structural elements were considered.

It is revealed that as a criterion for assessing the resistance to progressive collapse, in addition to the strength indicators prescribed by the norms, it is necessary to consider the loss of stability of the bearing element of the structural system under dynamic stress increases or other physical influences.

The current regulatory documents do not cover the entire variety of specific situations for buildings and structures that differ in their design features, but contain basic principles of protection against progressive collapse. In order to provide protection against the progressive collapse of buildings and structures with different design solutions, it is advisable to further study this issue in order to specify the provisions of existing regulatory documents, by developing manuals or new sets of rules.

## References

1. SP 296.1325800.2017. Buildings and structures. Special effects
2. SP 385.1325800.2018. Protection of buildings and structures from progressive collapse. Design rules. Basic provisions
3. Travush, V.I., Fedorova, N.V.: Survivability of structural systems under special effects. *Eng. Constr. Mag.* **5**(81), 73–80 (2018)
4. Tamrazyan, A.G.: Scientific bases of risk assessment and safety assurance of reinforced concrete structures, buildings and structures under combined special impacts. *Bull. SIC Constr.* **1**(16), 106–114 (2018)
5. Kolchunov, V.I., Savin, S.Y.: Dynamic effects in a composite two-component rods which appear when local fracture of the matrix is occurred. *J. Appl. Eng. Sci.* **15**(3), 325–331 (2017)
6. Kolchunov, V.I., Andrososva, N.B., Klyueva, N.V., Bukhtiyarova, A.S.: Survivability of buildings and structures under beyond design impacts. DIA, Moscow (2014)
7. Fedorova, N.V., Khalina, T.A.: Investigation of dynamic reloading in reinforced concrete structural systems under sudden structural changes. *Ind. Civ. Constr.* **5**, 45–49 (2017)
8. Demyanov, A.I., Kolchunov, V.I., Senchenko, D.S., Terskikh, A.B.: Computational model of static-dynamic deformation in a reinforced concrete centrally stretched structure at the moment of destruction of the concrete matrix. *Constr. Reconstr.* **2**(70), 3–9 (2017)
9. Geniev, G.A., Kolchunov, V.I., Klyueva, N.V.: Strength and deformability of reinforced concrete structures under beyond design impacts. DIA, Moscow (2004)
10. Tamrazyan, A.G.: Calculation of extra-centrally compressed reinforced concrete elements under dynamic loading under fire conditions. *Ind. Civ. Eng.* **3**, 29–35 (2015)
11. Tamrazyan, A.G.: Unaccounted effects in the calculation of reinforced concrete structures for combined special effects. In: *Construction materials, equipment, technologies of the XXI century*, vol. 11–12(250–251), pp. 42–46 (2019)
12. Klyueva, N.V., Tamrazyan, A.G.: Fundamental properties of structural systems that reduce the risk of failure of building elements. *Izvestiya Yugo-Zapadnogo gosudarstvennogo universiteta* **5–2**(44), 126–131 (2012)
13. SP 20.13330.2016. “SNiP 2.01.07–85” Loads and impacts. Updated version
14. Kolchunov, V.I., Savin, S.Y.: Criteria for the survivability of a reinforced concrete frame with loss of stability. *Eng. Constr. Mag.* **4**(80), 73–80 (2018)

15. Klyueva, N.V., Androsova, N.B.: Some proposals for the structural protection of buildings and structures from progressive destruction. *Constr. Reconstr.* **4**, 72–78 (2015)
16. Tamrazyan, A.G., Mehralizadeh, A.: Features of the influence of the time of local damage in the calculation of buildings on the progressive collapse. *Bull. Civ. Eng.* **6**(41), 42–46 (2013)
17. Kodysh, E.N.: Design of protection of buildings and structures from progressive collapse, taking into account the occurrence of a special limit state. *Ind. Civ. Eng.* **10**, 95–101 (2018)
18. Kodysh, E.N., Trekin, N.N., Chesnokov, D.A.: Protection of buildings and structures from progressive collapse. *Ind. Civ. Eng.* **6**, 8–13 (2016)
19. SP 22.13330.2016. “SNIIP 2.02.01–83\*” Foundations of buildings and structures. Updated version
20. Manual for the design of measures to protect buildings and structures from progressive collapse. FAA FTS, Moscow (2018)

# Development, Strength Check, Calculation of the Wind Load of a Multi-layer Guarding Structure



M. A. Bakhmisova , Alexey N. Plotnikov , L. A. Sakmarova ,  
and M. V. Petrov 

## 1 Introduction

The problem of external influences on the enclosing structure is relevant today. Until the mid-1990s, the enclosing structures were made of brick, as a rule, from single-layer massive masonry. Products were used as masonry materials—bricks, reinforced concrete, and stones. The use of hollow products—hollow ceramic bricks as masonry materials can be attributed to the end of the nineteenth century, during the beginning of mass construction, in the middle of the twentieth century. The widespread use of silicate bricks began. Since the beginning of the 2000s, due to the introduction of strict requirements for energy efficiency and energy saving, the structures of external brick walls have changed. Multi-layer enclosing structures with effective insulation began to be actively introduced.

With the introduction into the practice of construction of non-bearing external walls, hollow products in their composition, effective insulation, lightweight concrete products, the front layer of brick in wall structures ceased to be connected to the inner layer (base) by a rigid connection (cushion rows), due to various deformative characteristics, when in this case, the connection of layers is carried out using flexible connections. In most cases, a three-layer (or two-layer) construction was adopted, consisting of:—a front outer layer of brickwork;—a layer of effective heat-insulating material (mineral wool boards, expanded polystyrene boards, etc.);—the inner structural layer of their lightweight concrete, aerated concrete stones, monolithic reinforced concrete, precast concrete panels and an air gap (according to the requirements of vapor permeability).

The reliability and strength of the structure against temperature effects, due to temperature drops of the outside air and heating of the cladding surface when exposed to solar radiation, should be ensured by arranging a system of temperature expansion joints in the cladding layer. So in [1] materials are indicated that can be used as a facing

---

M. A. Bakhmisova (✉) · A. N. Plotnikov · L. A. Sakmarova · M. V. Petrov  
Chuvash State University Named I.N. Ulyanova, Cheboksary, Chuvash Republic, Russia

layer and their possible deformations. In [2] are possible solutions to reinforce the covering layer with a thermal conductivity of inclusions and additional armatures depending on the composition of the wall, and on the recommendations of the calculation was performed by placing the anchor in the structure.

## 2 Materials and Methods

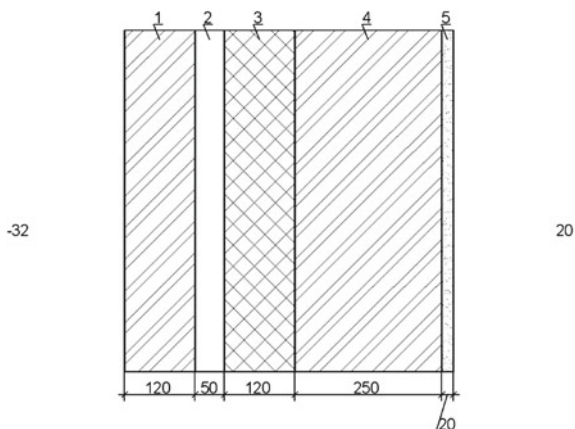
Currently, this design is popular among designers because of the convenience in calculations and operation. But there is also a negative feature—the appearance of cracks, and other deformation on the face layer in “half a brick”. The reliability and strength of the structure against temperature effects, due to changes in the outside air temperature and heating of the cladding surface when exposed to solar radiation should be ensured by means of a system of expansion joints in the cladding layer. The choice of the optimal technical solutions for the “pie” of the enclosing structure, the materials, and products used must be ensured by the correct calculation of the structure layers. In accordance with the requirements of EN 771, DIN 105, the following ceramic bricks and stones can be used as part of the facing layer: solid ceramic facing brick; facade hollow brick with vertical voids; silicate brick; clinker brick; concrete blocks and stones. The design of the facing layer (taking into account the geometrical parameters of the facing structures) contains in its design the following main prefabricated products: various types of flexible ties, clamps; bearing brackets, which must be taken into account when calculating, since they are heat-conducting inclusions [3].

A three-layer wall with KNAUF Therm Wall expanded polystyrene insulation and flexible connections was chosen as the enclosing structure. The heat engineering calculation was carried out taking into account heat-conducting inclusions. The presence of heat-conducting inclusions in the form of fastening parts completely changes the picture of the temperature field of the outer fence. Taking into account the coefficient of heat engineering heterogeneity in the design will improve the heat-shielding properties of the fence.

Resistance to heat transfer of the enclosing structure in Cheboksary Ronorm =  $0.00035 \cdot 5403.3 + 1.4 = 3.29_{\text{M}^2\text{C}/\text{BT}}$  (Fig. 1).

The degree of thermal effects on building structures depends on local climatic conditions, total mass, thermal insulation, finishing properties of the enclosing structure, and the shape of the building. As a result of temperature and humidity deformations in the masonry of the face layer, 120 mm thick, the formation of vertical and oblique cracks is possible. The horizontal tensile stresses in the face layer near the corners caused by its out-of-plane bending are comparable in magnitude with the stresses from axial forces. The moments causing bending of the facing layer masonry from its plane are concentrated mainly near the  $n$  and  $z$ -shaped corners. In these areas, the influence of bending of the face layer from its plane increases, since there is a shift of two walls relative to each other. The normative document EN 846-5:

**Fig. 1** Scheme of a three-layer enclosing structure



2000h. 5 contains data on permissible tensile and compressive loads and deformation characteristics under load for a given structure and its members and flexible ties [1].

The main parameters that must be taken into account when designing and calculating the fastening structures of the facing layer made of brick and stone structures are quality (strength, type), composition, thickness, completeness of products, nodes for supporting the masonry on the console, connection nodes for connections, their number and placement, expansion joints, cladding thickness, brick overhang, accounting for ledges (bay windows and slopes).

### 3 Experimental and Results

In accordance with SP 20.13330.2016 “Loads and Impacts”. Cheboksary—2 wind region, 4 snow region. Private—a building area. I—ice-covered area of the construction region. Determination of the wind load on the enclosing structures is one of the main tasks in their design. A lot of works by domestic and foreign authors have been written on this topic. As a result of wind influences, a variable distribution of external pressure along the facade cladding is formed. In turn, under the influence of external pressure gradients, an internal flow arises in the air gap of hinged structures and an internal pressure distribution different from the external one is generated.  $Y = 1.1$ —load safety factor for facing. The height of the building is assumed to be 75 m, which corresponds to an approximate height of 25 floors. The building itself is rectangular with dimensions in the axes of 18 m  $\times$  36 m. Distances:  $b_1 = 3600$  mm,  $b_2 = 18,000$  mm,  $b = 36,000$  mm,  $d = 18,000$  mm, distance  $h-d = 57,000$  mm.

The form for calculating the main average wind load for SP 20.13330.2016 [4]:

$$W_m = W_o \cdot k \cdot c, \quad (1)$$

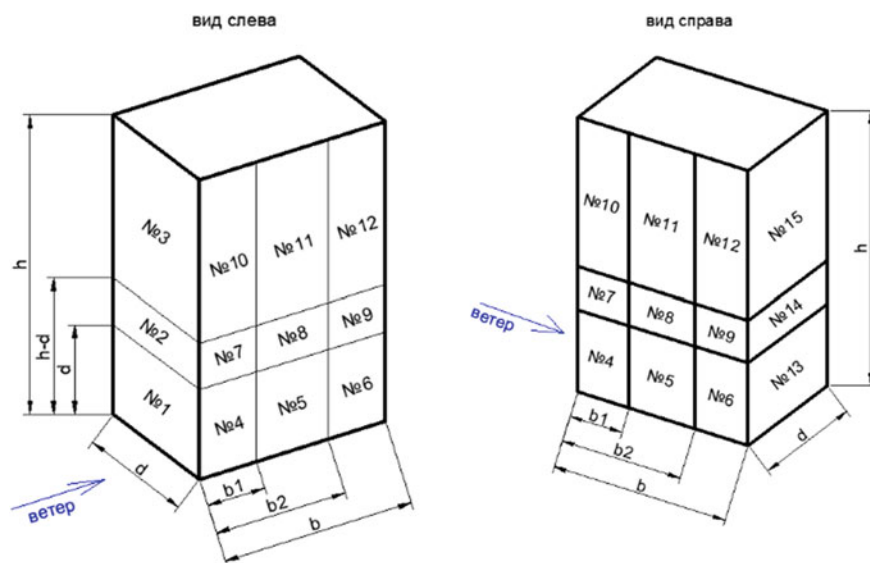


Fig. 2 Building scheme for calculation

$W_m$ —is the standard value of the main average wind load,  $\text{kg/m}^2$ ;

$W_o$ —is the standard value of wind pressure,  $\text{kg/m}^2$ , in our region it is  $30 \text{ kg/m}^2$ ,

$k$ —is a coefficient that takes into account the influence of height on wind pressure,  $c$  is the aerodynamic coefficient. For the calculation of the type of terrain,

$C$ —urban areas with dense development of buildings with a height of more than 25 m were selected and sections of the building were determined (Fig. 2 and Table 1).

The wind load safety factor is 1.4. After calculating the strength and wind load, it is necessary to check the structure for temperature effects, taking into account the amplitude of the cold and warm months and the maximum, minimum air temperatures in Cheboksary according to table in [4–6].

Thus, the developed design meets the requirements.

## 4 Conclusions

Thus, the article calculates the enclosing structure and its ability to withstand wind load. A three-layer wall with 120 mm expanded polystyrene insulation KNAUF Therm Wall was chosen as the enclosing structure, a brick on the inside of 250 mm, with an outside 120 mm and flexible connections.

Also, as a result of the analysis of wind and temperature effects, it was identified that at negative temperatures, the front layer of the building warps inward, which is prevented by the inner layer of the facade structure. As a result, significant shear

**Table 1** Determination of the design wind pressure for sections of the building

Area	Koef. $k$	Koef. $c$	Design wind pressure, $\text{kg/m}^2$
1.	0.54	0.8	18.14
2.	0.95	0.8	28.92
3.	1.1	0.8	29.96
4.	0.54	-1	-22.68
5.	0.54	-0.8	-18.14
6.	0.54	-0.5	-11.34
7.	0.95	-1	-39.9
8.	0.95	-0.8	-29.92
9.	0.95	-0.5	-19.95
10.	1.1	-1	-29.2
11.	1.1	-0.8	-29.96
12.	1.1	-0.5	-23.1
13.	0.54	-0.5	-11.34
14.	0.95	-0.5	-19.95
15.	1.1	-0.5	-23.1

stresses appear in the face layer in the horizontal joints, perpendicular to the plane of the wall, which, together with normal stresses from bending moments, lead to the opening of horizontal mortar joints. When the face layer is made of hollow ceramic materials, rainwater enters through the formed horizontal cracks into the voids of the bricks, which at negative temperatures can contribute to their destruction. Also, most of the deformations are located in the lower zone, where the masonry adheres to the floor slab, as well as above the lintels of the door and window openings. Large-scale digitalization and the introduction of new materials and technologies in the construction industry will progress—this is a market demand, where efficiency and time reduction, costs are now a priority. Therefore, construction becomes smart not only in computer design, but also in the process of checking the strength, and further creating an object, using sensors, materials, and technologies. New technologies are aimed at optimizing and efficiently at all stages of the project, from engineering surveys to operation.

It is not easy to introduce the latest technologies in construction, since the main requirements for facilities are compliance with safety, quality, thermal protection, that is, each technology must have a regulatory framework, standardization, and self-sufficiency. Any technology requires appropriate design, knowledge, calculations for verification, and a whole range of works.

## References

1. Guidelines for the selection of facing products for external walls (general provisions. Nomenclature of indicators. Basic requirements)
2. Galen Technical Solutions Album (2015)
3. Bakhmisova, M., Sakmarova, L.: Multilayer enclosing structures and their properties under temperature effects (NASKR-2018), pp. 88–96 (2018)
4. SP 20.13330.2016. Loads and impacts
5. SP 131.13330.2018. Construction climatology
6. SP 50.13330.2012. Thermal protection of buildings



# Strength and Deformation of Caisson-Type Floor Plates. Experimental Research and Calculation



Arkady Vulfovich Granovsky and Kirill Alekseevich Prusov

## 1 Introduction

One of the main trends in modern construction is to increase the comfort of residential and industrial premises by increasing the spans of overlapped premises, enlarging the grid of supporting structures (spacing of columns, bearing walls) with a simultaneous increase in the bearing capacity of the floors [1–21]. Caisson-type ceilings fully meet these requirements. The use of modern technologies, including formwork systems, makes it possible to eliminate a significant drawback of coffered ceilings—this is busyness, leading to increased labor intensity. Monolithic reinforced concrete floors with a system of cross beams (ribs) are classic structures that, since the 1920s, have been widely used in construction practice. In the 60 s, overlapping of precast-monolithic constructive solutions was most widespread in Russia. With spans from 187 to 30 m and a rib step of 3 m, the height of the ribs, according to the data given in [1], is from 0.75 to 2.0 m. According to the specialists of the company PKB KATRIEL, the will: reduce concrete consumption by 40–70% and save reinforcement by 2.5–3.5 times compared to girder and non-girder monolithic reinforced concrete floors; the possibility of constructing floors with a grid of vertical bearing elements (walls, columns) from  $12 \times 12$  m to  $34 \times 34$  m. With a comparable consumption of materials with beam (flat) monolithic ceilings, the bearing capacity of coffered ceilings is 2–3 times higher. At the same time, the floor thickness is 1.5–2.2 times less than when using the traditional beam scheme. The structure of the coffered floor is more resistant to seismic loads, and also has advantages over beam structures in conditions of progressive collapse.

Specialists of the Italian company “GEOPLAST S.p.A” [2] have proposed a new type of formwork “Skydom” with rib spacing up to 0.9 m and rib height up to the flange 0.4 m. The experience of using this formwork has shown its high efficiency.

---

A. V. Granovsky · K. A. Prusov (✉)

National Research Moscow State University of Civil Engineering, Moscow, Russia

The work [3] presents the results of experimental and theoretical studies of large-size reinforced concrete models of cross-ribbed shells. An approach to the design assessment of the strength and stiffness of the floor is proposed. In the Standards [4], in multi-storey buildings with large spans, it is recommended to use caisson floors, the calculation of which should be carried out as spatial structures. It should be noted that, as noted in [1], at the present time there is no proven methodology for calculating cross structures. In practice, continuous (solid plate with “smeared” stiffness) and discrete (rod system) models are used. At the same time, the existing methods do not take into account the peculiarities of the operation of slabs as a ribbed spatial reinforced concrete structure with cracks. In works [5–10], studies of hollow-core slabs using, mainly, a single-span beam system are given and recommendations are given for the design of hollow-core slabs, including the caisson type, under the action of a static load.

### *1.1 Description of Experimental Samples*

Experts from TechEnergAlliance LLC made an experimental sample of a caisson-type floor slab with the following basic geometric parameters:— dimensions in plan— $6.0 \times 6.0$  m; column section— $0.3 \times 0.3 \times 0.6$  (N) m; slab height along the edge— $0.25$  m; plate shelf thickness— $50$  mm; plate rib thickness— $125$  mm. Volume, taking into account solid monolithic reinforced concrete sections:  $V_S = V_{\text{tot.}} - V_{\text{low}} = 6 \times 6 \times 0.25 - 2.92 = 6.08 \text{ m}^3$ . Mass and weight of the slab:  $P = 6.08 \times 2500 = 15\,200$  kg;  $q = 15\,200/36 = 420 \text{ kg/m}^2$ ; slab concrete class (according to the project)—B25. Figures 1, 2 and 3 show the process of installing a monolithic reinforced concrete slab of a caisson type. At the 1st stage (Fig. 1), a diagram of the installation of void former is shown. Figure 2 shows the layout of the reinforcing cage in the sections of internal and contour ribs. Figure 3 shows general view of the sample after concreting.

*Experimental research.* The tests were carried out in the laboratory building of TsNIISK named after V.A. Kucherenko. In the course of the experiment, two schemes of loading a prototype were considered in order to control various limiting states of the product: in the 2nd test scheme, loading of the prototype was carried out over the entire area of the plate until the actual value of the breaking load was reached, based on the strength of the product (1st group limit states), and the actual value of the deflections and crack opening width (2nd group of limit states) under the control load established in the design documentation for the product. Figure 4 shows a diagram of stage 2 of plate loading.

In accordance with the requirements of GOST 8829, during the test, the following controlled parameters were recorded: the values of the load on the plate from the loads installed on it and the corresponding deflection; crack opening width, incl. upon reaching the control values of the loads; the values of the breaking load, the corresponding deflection, and the nature of the destruction of the product.



**Fig. 1** General view of the formwork under the slab before installing the reinforcement cages



**Fig. 2** Reinforcement of slab sections (internal and contour edges)



Fig. 3 General view of the prototype after concreting

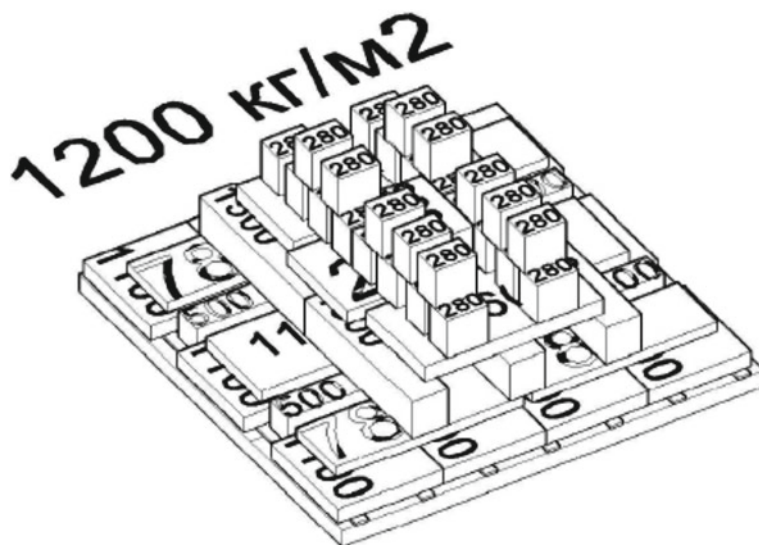
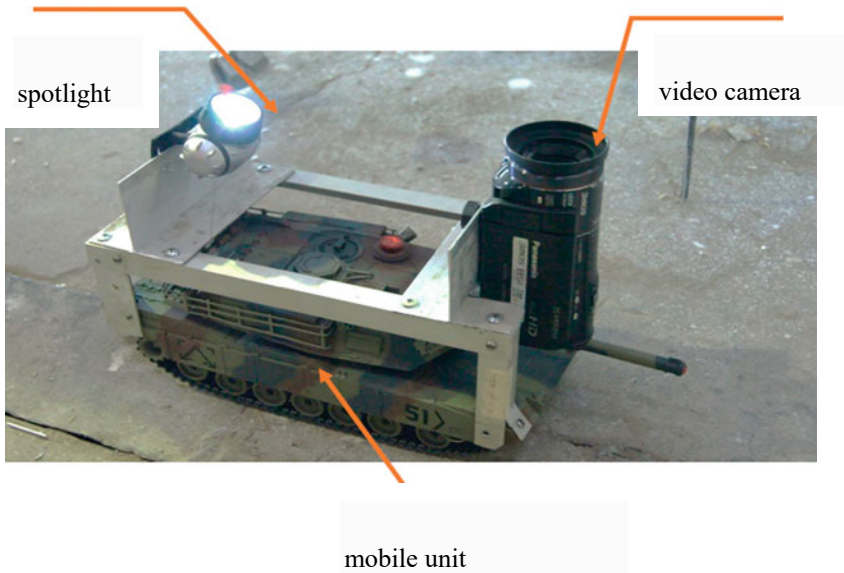


Fig. 4 Loading of the floor slab according to the 2nd test scheme



**Fig. 5** Installation for fixing and photographing cracks

To assess the moment of appearance of cracks in the edges of the slab and the width of their opening, a special mobile unit was used, on which a video camera was fixed (Fig. 5). From the video camera, the image was transmitted to a special monitor. When comprehending the values of the calculated (design) loads on the product, the sample was unloaded with the fixation of the values of residual deflections and the nature of the cracks (the state of the cracks was recorded: closure of cracks or the residual value of the width of their opening). At the moment when the values of deflections at different points of the slab increased under constant load, the tests were stopped and the value of the ultimate breaking load was recorded.

Analysis of the results of experimental studies of the strength and deformability of a caisson-type floor slab when the load is located over its entire area allows us to note the following.

1. With the permissible standard of the slab deflection  $1/200 \times L = 3$  cm, the actual deflection of the slab under a load of  $1220 \text{ kg/m}^2$  ( $800 \text{ kg/m}^2 +$  own weight of the slab  $420 \text{ kg/m}^2$ ) was: in the center of the slab—33 mm, after unloading—24 mm. In the middle of the contour beam—15 mm, after unloading—12 mm.
2. Upon reaching the ultimate breaking load ( $1620 \text{ kg/m}^2$ , taking into account the slab's own weight of  $420 \text{ kg/m}^2$ ), the deflection in the middle of the slab was 60 mm.
3. Fig. 6 shows the nature of the cracks recorded at a load of  $1060 \text{ kg/m}^2$  ( $640 \text{ kg/m}^2$ —load on the slab from the weight +  $420 \text{ kg/m}^2$ —from the slab's own weight). The crack opening width was 0.08–0.15 mm. After removing the load, the cracks were completely closed.



**Fig. 6** The nature of cracks on supports at a load of  $10 \text{ kN/m}^2$

4. When the load on the slab reached  $1620 \text{ kg/m}^2$  (taking into account the slab's own weight— $420 \text{ kg/m}^2$ ), the support zones of the slab were destroyed with the formation of a hinge.
5. According to clauses 9.1.3 and B.1 (table B1 GOST 8829) for the 1st case of failure of a bent structure, characterized by the achievement in the working reinforcement of a normal or inclined section of stresses corresponding to the yield strength of steel or early fragmentation of compressed concrete, the calculated load-bearing capacity of the floor slab is determined by dividing the control value of the breaking load (at which the structure turned into a mechanism) by the coefficient  $C = 1.35$  (Table B.2 GOST 8829):

$$N_{\text{calc.}} = N_{\text{res.}}/1.35 = 1620/1.35 = 1200 \text{ kg/m}^2$$

Thus, the calculated load on the investigated structure of a coffered-type slab made of concrete of class B22.5 with the adopted reinforcement scheme and taking into account the slab's own weight of  $420 \text{ kg/m}^2$  should not exceed  $1200 \text{ kg/m}^2$  (Fig. 7).

When designing caisson-type floor slabs, the design load of the moment of formation of the 1st crack (calculated according to the Standards) multiplied by a coefficient 1.3 (clause B.11 of GOST 8829) should be taken as the control load for cracking.

The computational analysis was performed using the software package. The physical model of the tested structure was simulated using Autodesk Revit and Autodesk Robot Structural Analysis software.

According to the test results, it was recommended to install a reinforcing cage in the support zone of the slab, providing both the perception of the horizontal force and the joint work of the slab with the column.

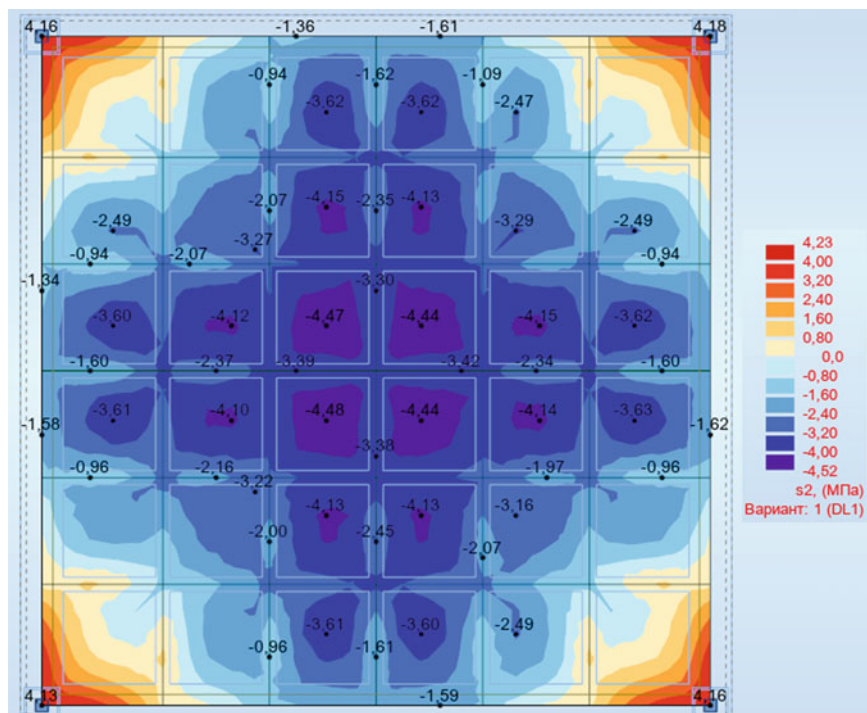


Fig. 7 Isofields of stresses along the upper layer of the slab

## References

1. Plotnikov, A.N.: Strength and deformability of the cross-ribbed overlap, taking into account the redistribution of efforts. Dissertation.... Cand. Tech. Sciences, MGSU, p. 268 (2013)
2. GEOPLAST S.p.A. Skydom. <https://www.geoplastglobal.com/ru/produkcija/perekrytija/skydome/>
3. Shugaev, V.V., Lyudkovsky, A.M.: Research of the deformative state of ribbed reinforced concrete shells under the action of a concentrated load. Sat. "Research and strength calculations of spatial structures." NIIZhB, M., Stroyizdat, pp. 28–47 (1980)
4. SP 52–103–2007 (to SNiP 52–01–2003). Reinforced concrete monolithic building structures
5. Malakhova, A.N.: Hollow caisson floor slabs of monolithic multi-storey buildings. MGSU Bull. **6**, 15–24 (2016)
6. Efimtseva, E.E.: Methods for modeling coffered ceilings. Actual Probl. Humanit. Nat. Sci. **11–5**, 14–20 (2015)
7. Kibkalo, A.V., Volkov, M.D.: Coffered ceilings as an effective type of ribbed slabs. Young Sci. **25**(129), 37–40 (2016)
8. Granovsky, A.V., Chupanov, M.R.: Experimental studies of the bearing capacity of coffered floor slabs. Ind. Civ. Constr. **5**, 43–48 (2015)
9. Malakhova, A.N.: Monolithic coffered ceilings of buildings. MGSU Bull. **1**, 79–86 (2013)
10. Zemlyansky, A.A., Zhukov, A.N., Bulavina, D.A.: Experience of full-scale testing of reinforced concrete ribbed slabs. Acad. Bull. UralNIIproekt RAASN. **4**(43), 79–82 (2019)

11. Navarro, I.J., Yepes, V., Martí, J.V.: Life cycle cost assessment of preventive strategies applied to prestressed concrete bridges exposed to chlorides. *Sustainability* **10** (2018). <https://doi.org/10.3390/su10030845>
12. Tamrazyan, A., Alekseytsev, A.: Multi-criteria optimization of reinforced concrete beams using genetic algorithms. In: *IOP Conference Series: Materials Science and Engineering* (2020). <https://doi.org/10.1088/1757-899X/869/5/052027>
13. Greiner, D., Periaux, J., Emperador, J.M., Galván, B., Winter, G.: Game theory based evolutionary algorithms: a review with nash applications in structural engineering optimization problems. *Arch. Comput. Methods Eng.* **24**, 703–750 (2017). <https://doi.org/10.1007/s11831-016-9187-y>
14. Alekseytsev, A.V., Al Ali, M.: Optimization of hybrid I-beams using modified particle swarm method. *Mag. Civ. Eng.* (2018). <https://doi.org/10.18720/MCE.83.16>
15. Tamrazyan, A.G., Alekseytsev, A.V.: Optimal structures design: accounting of costs and relative accidents risk. *Vestn. MGSU* (2019). <https://doi.org/10.22227/1997-0935.2019.7.819-830>
16. Kaveh, A., Zakian, P.: Optimal seismic design of reinforced concrete shear wall-frame structures. *KSCE J. Civ. Eng.* **18**, 2181–2190 (2014). <https://doi.org/10.1007/s12205-014-0640-x>
17. Tamrazyan, A., Alekseytsev, A.: Strategy for the evolutionary optimization of reinforced concrete frames based on parallel populations evolving. In: *IOP Conference Series: Materials Science and Engineering* (2020). <https://doi.org/10.1088/1757-899X/869/5/052019>
18. Lee, C.K., Kim, S.K.: GA-based algorithm for selecting optimal repair and rehabilitation methods for reinforced concrete (RC) bridge decks. *Autom. Constr.* **16**, 153–164 (2007). <https://doi.org/10.1016/j.autcon.2006.03.001>
19. Esfandiari, M.J., Urgessa, G.S., Sheikholarefin, S., Manshadi, S.H.D.: Optimum design of 3D reinforced concrete frames using DMPSO algorithm. *Adv. Eng. Softw.* **115**, 149–160 (2018). <https://doi.org/10.1016/j.advengsoft.2017.09.007>
20. Xia, L., Fritzen, F., Breitkopf, P.: Evolutionary topology optimization of elastoplastic structures. *Struct. Multidiscip. Optim.* **55**, 569–581 (2017). <https://doi.org/10.1007/s00158-016-1523-1>
21. Luo, Y., Kang, Z.: Topology optimization of continuum structures with Drucker-Prager yield stress constraints. *Comput. Struct.* (2012). <https://doi.org/10.1016/j.compstruc.2011.10.008>



# To the Calculation of Reinforced Concrete Beams According to the Deformation Model



Dmitry Zamelin and Ivan Manaenkov

## 1 Introduction

In the actual edition of the Russian Building Code [1] presented the procedure for calculating reinforced concrete structures in two ways: by limiting forces and by a nonlinear deformation model. The method of limiting forces has a field of application limited by the shape of the cross-section of the element and the location of the reinforcement and is applicable without modifications only in the case of elements with a fairly simple cross-sectional shape. Nonlinear deformation model is a method for calculating reinforced concrete elements based on the use of stress–strain curves [2–4]. The main provisions of the calculation method are set out in the works of Karpenko [5, 6]. A feature of the method is taking into account the stress distribution over the section that is close to the real one, depending on the deformations of the material. The calculation is performed by the iterative method based on stress–strain diagrams of concrete and reinforcement, taking into account the hypothesis of flat sections. The deformation model is a fairly convenient tool for designing reinforced concrete structures due to the fact that it does not restrict the cross-sectional shape and distribution of reinforcement, it allows taking into account the effect of specific operating conditions on the strength and deformation characteristics, and the presence of indirect, fiber and other types of reinforcement. In view of the foregoing, one of the most important stages of the calculation is the choice of the stress–strain diagram that most closely matches the actual nature of the material’s work in the structure.

To date, a large amount of experimental and theoretical research has been accumulated, offering various types of diagrams depending on design solutions, materials, and operating conditions of structures.

Studies [7–11] are devoted to the construction of a stress–strain diagram for concrete with indirect reinforcement in the form of welded mesh. A significant

---

D. Zamelin · I. Manaenkov (✉)

Moscow State University of Civil Engineering (National Research University), Yaroslavskoe shosse, 26, 129337 Moscow, Russian Federation

increase in the strength and deformation characteristics of concrete was noted when using such a constructive solution in compressed and bent elements. The correctness of the method is evidenced by the good agreement of the calculated results with experimental data.

Scientific publications [12, 13] propose methods for determining the parametric points of stress–strain diagrams for materials of pipe-concrete columns. An increase in the strength and deformation characteristics of concrete in a steel pipe under central and eccentric compression was recorded.

In works [14, 15], elements with indirect reinforcement with composite materials are considered. An increase in the strength and deformation characteristics of concrete in a steel pipe under central and eccentric compression has been established.

Articles [16–19] are devoted to the study of fiber reinforcement for the strength and deformation characteristics of concrete. Methods for constructing diagrams for the cases of using fibers from various materials are presented.

The works [20–22] consider the effect on the stress–strain diagram of various operating conditions, such as temperature effects, dynamic loading, etc.

Despite the spread of modern software systems for the design of structures taking into account physical and geometric nonlinearity based on the finite element method, there are a number of difficulties in their work: high complexity of assembly of finite element model; the problem of modeling the contact of different materials; good convergence usually requires high-quality experimental data to work out the finite element model. In comparison with this, the deformation model is a more accessible method for carrying out engineering calculations of reinforced concrete structures, at least at the stage of the initial assessment of the effectiveness of design solutions and the assignment of structural parameters.

When calculating, the cross-section is divided into relatively small sections of concrete and reinforcement, within which stresses and deformations are taken as averaged (see Fig. 1). The calculations are carried out by the iterative method until the required accuracy of solving the system of equations for the equilibrium of the section (1).

$$\left. \begin{aligned} M_x &= D_{11} \cdot \frac{1}{r_x} + D_{12} \cdot \frac{1}{r_y} + D_{12} \cdot \varepsilon_0; \\ M_y &= D_{12} \cdot \frac{1}{r_x} + D_{22} \cdot \frac{1}{r_y} + D_{23} \cdot \varepsilon_0; \\ N &= D_{13} \cdot \frac{1}{r_x} + D_{23} \cdot \frac{1}{r_y} + D_{23} \cdot \varepsilon_0 \end{aligned} \right\}, \quad (1)$$

where  $1/r_x$  и  $1/r_y$ —curvature in planes  $XOZ$  and  $YOZ$  respectively;  $\varepsilon_0$ —relative longitudinal deformation of the element;  $D_{ij}$ —stiffness.

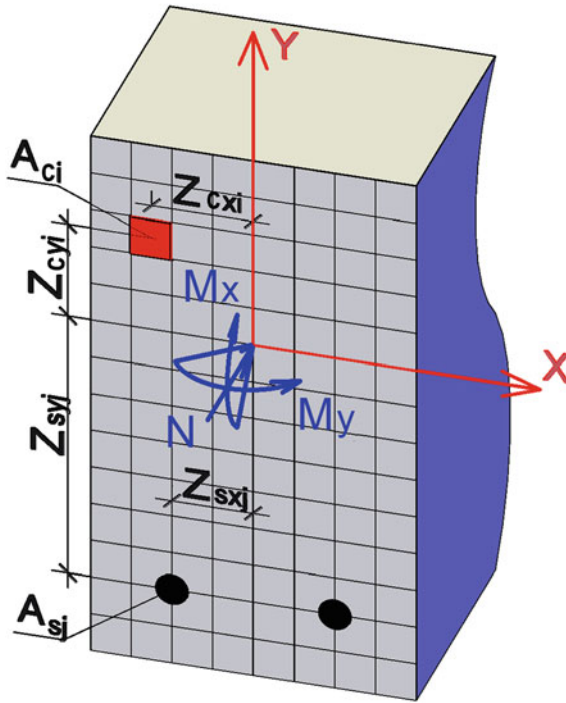


**Fig. 1** The scheme of dividing the cross-section of an element for the general case of calculation by the nonlinear deformation model in accordance with [1]

## 2 Materials and Methods

This article is devoted to the analysis of the stress–strain state of reinforced concrete beams. The dimensions of the cross-section of the beams are taken as  $300 \times 500$  ( $h$ ) mm from. Concrete strength class 25, reinforced with rods of class A500 with different reinforcement coefficient  $\mu = 100\% \cdot A_s / (b \cdot h_0)$ . The parameters of the cross-sections of the beams are shown in Fig. 2. Bending takes place in a vertical plane ( $M = M_x; M_y = 0; N = 0$ ).

For the calculation for concrete, a three-line stress–strain diagram was adopted, for reinforcement—a two-line diagram similar to the Prandtl diagram (see Fig. 3).

## 3 Results

The results of the calculations are shown in Tables 1, 2, 3 and 4 and in graphical form in Figs. 4, 5, 6 and 7, where — —  $M/M_{ult}$ ; — —  $\varepsilon_s/\varepsilon_{s,ult}$ ; — —  $\varepsilon_{c,max}/\varepsilon_{c,ult}$ .

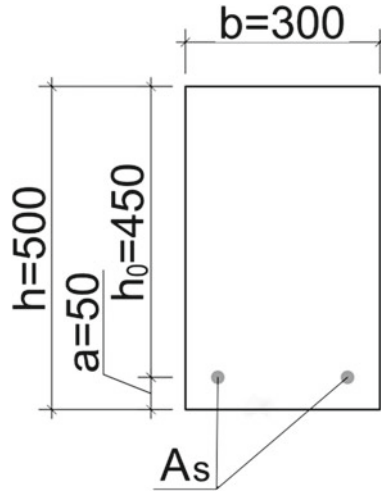


Fig. 2 Parameters of cross-sections of beams

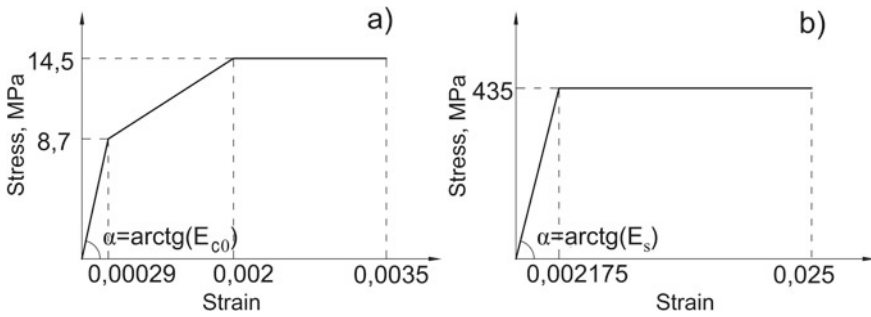


Fig. 3 Forms of accepted stress-strain diagrams of concrete (a) and steel reinforcement (b)

Table 1 Calculation results with a reinforcement coefficient  $\mu = 0.1\%$ ;  $A_s = 1.4 \text{ cm}^2$

N <sup>o</sup>	M (kN m)	M <sub>ult</sub> (kN m)	$\frac{M}{M_{ult}}$	$\epsilon_{b,max}$	$\frac{\epsilon_{b,max}}{\epsilon_{b,ult}}$	$\epsilon_s$	$\frac{\epsilon_s}{\epsilon_{s,ult}}$
1	6,61	26,44	0,25	0,000068	0,0195	0,000550	0,2188
2	13,22	26,44	0,5	0,000137	0,0391	0,001100	0,4380
3	19,83	26,44	0,75	0,000206	0,0589	0,001610	0,6440
4	26,44	26,44	1	0,000292	0,0834	0,002175	1

**Table 2** Calculation results with a reinforcement coefficient  $\mu = 1\%$ ;  $A_s = 13.9 \text{ cm}^2$

Nº	$M$ (kN m)	$M_{ult}$ (kN m)	$\frac{M}{M_{ult}}$	$\varepsilon_{b,max}$	$\frac{\varepsilon_{b,max}}{\varepsilon_{b,ult}}$	$\varepsilon_s$	$\frac{\varepsilon_s}{\varepsilon_{s,ult}}$
1	52,55	210,18	0,25	0,00022	0,0640	0,000512	0,2048
2	105,09	210,18	0,50	0,00051	0,1466	0,001049	0,4196
3	157,64	210,18	0,75	0,00105	0,3000	0,001658	0,6632
4	210,18	210,18	1,00	0,00192	0,5486	0,002175	1

**Table 3** Calculation results with a reinforcement coefficient  $\mu = 2\%$ ;  $A_s = 26.7 \text{ cm}^2$

Nº	$M$ (kN m)	$M_{ult}$ (kN m)	$\frac{M}{M_{ult}}$	$\varepsilon_{b,max}$	$\frac{\varepsilon_{b,max}}{\varepsilon_{b,ult}}$	$\varepsilon_s$	$\frac{\varepsilon_s}{\varepsilon_{s,ult}}$
1	76,10	304,40	0,25	0,00027	0,07714	0,000422	0,1688
2	152,20	304,40	0,5	0,00074	0,21114	0,000903	0,3612
3	228,30	304,40	0,75	0,00171	0,48857	0,001466	0,5864
4	304,40	304,40	1	0,00350	1	0,002126	0,8504

**Table 4** Calculation results with a reinforcement coefficient  $\mu = 3\%$ ;  $A_s = 39.3 \text{ cm}^2$

Nº	$M$ (kN m)	$M_{ult}$ (kN m)	$\frac{M}{M_{ult}}$	$\varepsilon_{b,max}$	$\frac{\varepsilon_{b,max}}{\varepsilon_{b,ult}}$	$\varepsilon_s$	$\frac{\varepsilon_s}{\varepsilon_{s,ult}}$
1	78,21	312,85	0,25	0,000254	0,072,571	0,000317	0,1268
2	156,43	312,85	0,5	0,000681	0,194,571	0,000682	0,2728
3	234,64	312,85	0,75	0,00164	0,468,571	0,001132	0,4528
4	312,85	312,85	1	0,00350	1	0,001678	0,6712

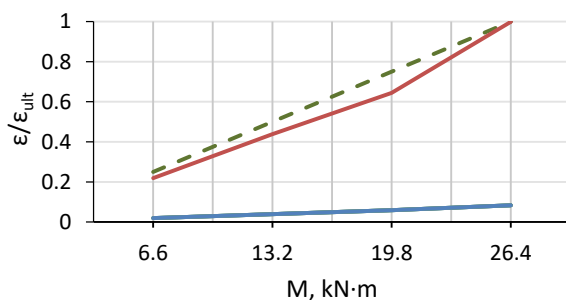


**Fig. 4** Relative deformation on loading level when  $\mu = 0.1\%$

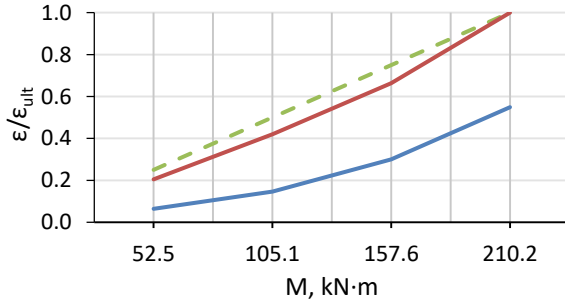


**Fig. 5** Relative deformation on loading level when  $\mu = 1\%$

**Fig. 6** Relative deformation on loading level when  $\mu = 2\%$

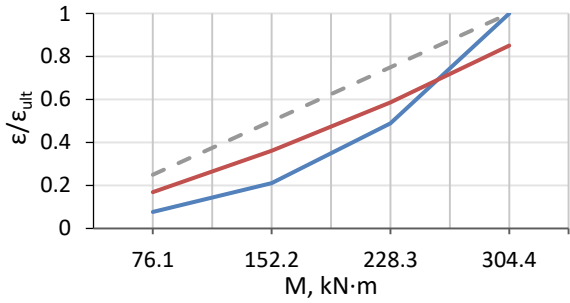
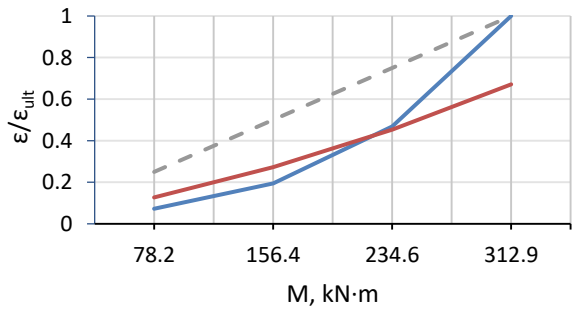


**Fig. 7** Relative deformation on loading level when  $\mu = 3\%$



## 4 Conclusions

Based on the calculation results, we can conclude:

- For the cases  $\mu = 0.1\%$  and  $\mu = 1\%$ , the loss of bearing capacity begins with the tensioned reinforcement; for the cases  $\mu = 2\%$  and  $\mu = 3\%$  the loss of bearing capacity begins from the concrete of the compressed zone;

- The dependence of tensile reinforcement stresses on the loading level is close to linear. Some deviations are associated with a change in the shoulder of the internal pair of forces due to the nonlinear work of the concrete in the compressed zone;
- Deformations of concrete in the compressed zone have a clearly pronounced nonlinear character of growth (which corresponds to the state diagram adopted for concrete) and the ratio  $\varepsilon_{c,\max}/\varepsilon_{c,\text{ult}}$  at intermediate stages of loading turns out to be significantly less than  $M/M_{\text{ult}}$ .

Nonlinear deformation model is a convenient tool for performing engineering calculations of reinforced concrete elements; allows you to apply a unified approach to the calculation of structures for stresses and deformations; allows you to obtain a sufficient amount of information about the stress–strain state of the cross-section and its individual zones at all stages of loading up to the exhaustion of the bearing capacity.

## References

1. Russian Building Code SP 63.13330.2018. Concrete and reinforced concrete structures. General provisions
2. Mkrtchyan, A.M., Aksenov, V.N.: Analytical description of the diagram of high-strength concrete deformations. Eng. J. Don **3**(26) (2013). <http://ivdon.ru/ru/magazine/archive/n3y2013/1818>
3. Trekin, N.N., Kodysh, E.N., Trekin, D.N.: Calculation for the formation of normal cracks on the basis of deformation model. Ind. Civ. Constr. **7**, 74–78 (2016)
4. Arleninov, P.D., Krylov, S.B.: The current state of nonlinear calculations of reinforced concrete structures. Earthquake engineering. Constr. Safety **3**, 50–53 (2017)
5. Karpenko, N.I., Karpenko, S.N.: On the diagrammatic method for calculating the deformations of bar elements and its special cases. Concr. Reinf. Concr. **6**, 20–27 (2012)
6. Karpenko, N.I.: General Models of Reinforced Concrete Mechanics. Strojizdat, Moscow (1996)
7. Manaenkov, I.K.: Perfection of the concrete compression diagram with indirect reinforcement. Build. Reconstr. **2**(76), 41–50 (2018)
8. Tamrazyan, A.G., Manaenkov, I.K., Koroteev, D.D.: Study of reinforced concrete beams with indirect reinforcement of compressed zone in the form of cross welded mesh. J. Mech. Cont. Math. Sci. **1S**, 621–631 (2019)
9. Manaenkov, I.K., Korenkov, P.A., Grezeva, A.S., Zinoveva, E.A.: Calculation of deformations of concrete with indirect reinforcement according to limit state design. IOP Conf. Ser. Mater. Sci. Eng. **869**, 052033 (2020)
10. Manaenkov, I.K., Savin, S.Y.: Numerical analysis of the ultimate compressibility of concrete with indirect reinforcement for plotting a stress-strain diagram. IOP Conf. Ser. Mater. Sci. Eng. **1030**, 012090 (2021)
11. Krishan, A.L., Rimshin, V.I., Troshkina, E.A.: Compressed and bending concrete elements with confinement reinforcement meshes. IOP Conf. Ser. Mater. Sci. Eng. **753**, 022052 (2020)
12. Krylov, S.B., Smirnov, P.P., Obozov, V.I., Savrasov, I.P.: Critical force for design the pipe-concrete structural strength. Earthquake engineering. Constr. Safety **1**, 9–12 (2017)
13. Krishan, A.L., Troshkina, E.A., Astafyeva, M.A.: Strength of compressed concrete filled steel tube elements of circular and square cross-section В сборнике. IOP Conf. Ser. Mater. Sci. Eng. **012053** (2018)
14. Krishan, A.L., Chernyshova, E.P., Astafieva, M.A.: Behavior of compressed concrete in a glass fiber-reinforced shell. IOP Conf. Ser. Mater. Sci. Eng. **687**, 033034 (2019)

15. Tamrazyan, A.G., Chernik, V.I.: Stress-strain model for concrete confined by a discrete frp-jackets. *Ind. Civ. Constr.* **8**, 43–53 (2020)
16. Folino, P., Ripani, M., Xargay, H., Rocca, N.: Comprehensive analysis of fiber reinforced concrete beams with conventional reinforcement. *Eng. Struct.* **202**, 109862 (2020)
17. Klyuev, S.V., Klyuev, A.V., Abakarov, A.D., Shorstova, E.S., Gafarova, N.G.: The effect of particulate reinforcement on strength and deformation characteristics of fine-grained concrete. *Mag. Civ. Eng.* **7(75)**, 66–75 (2017)
18. Plevkov, V.S., Belov, V.V., Baldin, I.V., Nevskij, A.V.: Models of nonlinear straining of carbon fiber reinforced concrete under static and short-term dynamic loads. *Bull. Civ. Eng.* **3(56)**, 72–82 (2016)
19. Korsun, V., Mashtaler, S., Vatin, N., Korsun, A., Franchi, A., Crespi, P.: The strength and strain of high-strength concrete elements with confinement and steel fiber reinforcement including the conditions of the effect of elevated temperatures. *Procedia Eng.* **117**, 970–979 (2015)
20. Karpenko, N.I., Jarmakovskij, V.N., Karpenko, S.N., Kadiev, D.Z.: About the diagram method of determination of parametric points of microcracking formation process in concrete elements under axial compression in conditions of low negative temperatures action. *Hous. Constr.* **6**, 3–9 (2019)
21. Tamrazyan, A.G., Alekseytsev, A.V.: Evolutionary optimization of reinforced concrete beams, taking into account design reliability, safety and risks during the emergency loss of supports. *E3S Web Conf.* **97**, 04005 (2019)
22. Kolchunov, V.I., Fedorova, N.V.: Deformation models of reinforced concrete under special impacts. *Ind. Civ. Constr.* **8**, 54–60 (2018)



# Anchorage Strength of Post-installed Reinforcement



S. I. Ivanov 

## 1 Introduction

Traditional [1] and new [2, 3] regulatory documents regulating the use of joints in reinforced concrete structures contain instructions for operational (in the manufacturing process) quality control, but do not contain instructions for strength control.

One of the types of control of the strength of anchorage of reinforcement is control according to the results of testing samples for the action of axial (along the reinforcement) pulling force.

This type of testing becomes most relevant when introducing new progressive solutions for embedding post-installed reinforcement in a finished concrete base (optimization of the diameter and shape of the hole for installing reinforcement, optimization of the hole making method), the use of new filling adhesives (cement-polymer and polymer), the use of new filling technologies (filling the hole after installation, by gravity or under pressure), the introduction of new care technologies in the process of curing (at negative temperatures, filling in water, etc.), when using new types of reinforcement (new section profiles, non-metallic reinforcement) and assessing the impact on the strength of possible violations of the design solution (the influence of atmospheric moisture in the hole, pressing the reinforcement against the wall of the hole, diagonal skew of the reinforcement, etc.).

In the domestic normative literature on testing reinforced concrete structures [4, 5], there are no requirements and guidelines for such tests.

There is an indication of clause 10.1.4 of GOST 8829 [4] that “products are recognized as meeting the strength requirements if ... for structures with prestressed reinforcement, the displacement of the free ends of the rods on the support ... does not exceed  $0.1 \div 0.2$  mm”, which cannot be used directly without adjustment for acceptance tests.

---

S. I. Ivanov (✉)

Laboratories No. 2 NIIZhB them. A.A. Gvozdeva, 2nd Institutskaya street, 6s5, 109428 Moscow, Russia

In this regard, the task arose to develop a test procedure for assessing the strength of post-installed reinforcement and a technique for assessing test results.

## 2 Materials and Research Methods

In foreign regulatory documents [6], a test procedure is given to determine the adhesion strength of reinforcement to concrete. However, it is based on the testing of concrete specimens of class B25 and does not provide guidance on the assessment of test results for the investigated design cases.

Bulletin No. 72 [7] presents the main results of studies of reinforcement anchoring in concrete and justification of the accepted design methods for calculating the required anchorage length. It is shown that the resistance of anchored reinforcement can be conditionally divided into two types: the resistance of the surrounding concrete to splitting and the resistance due to the stress state in the anchorage zone. For the problem under consideration, only the results of studies of resistance of the first type can be used.

Studies of anchors installed in concrete using adhesives were carried out at the University of Stuttgart [8, 9]. Based on the results of the work, a standard [10] was developed and put into effect for the calculation of fastenings to reinforced concrete, according to which the strength of concrete reinforcement and glued reinforcement is calculated using the same method.

In the early 2000s, studies were carried out [11] based on a comparison of the test results of reinforcement concreted in concrete with the test results of reinforcement glued into concrete at different embedment depths. The influence of the depth of embedment of reinforcement, the strength of the concrete of the base, the size of the aggregate, the size of the base, the temperature of hardening, etc. were investigated (see Fig. 1a–d).

Criteria for evaluating the test results were developed: a method was proposed for determining the breaking force, depending on the movement of the section of the bar on the concrete surface, for different embedding depths, as well as a method for determining the adhesion strength, taking into account the actual strength of the concrete base.

Based on the results of the work, a standard was developed to control the strength of reinforcement gluing into concrete [12, 13].

## 3 Results and Issues

In 2017–2019, in the laboratory of reinforced concrete structures and quality control of the N.I. A.A. Gvozdev carried out work on the development of a method for controlling the strength of reinforcement gluing into concrete and its approbation. The work was carried out on the basis of the data presented in [11, 13], processing

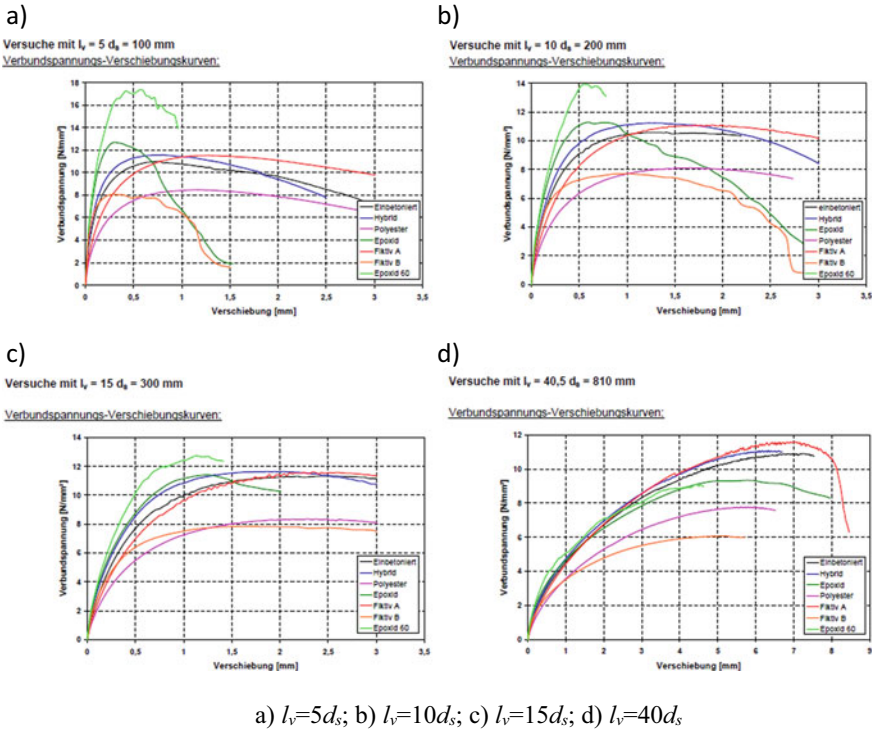


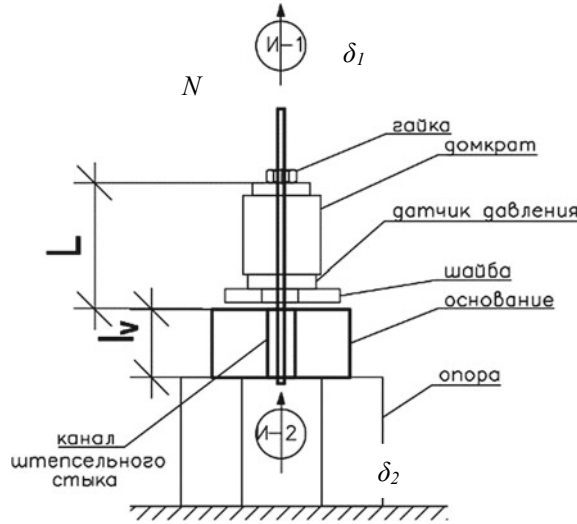
**Fig. 1** Results of “load–displacement” tests in the loaded section for different anchorage depths ( $l_v$ ) of reinforcement with a diameter of 20 mm in B25 concrete

the results of studies of the strength of adhesive anchors EDILSK ISA MGSU and the results of our own tests [14–19].

Based on the results of the work, the standard [20] was developed and put into effect, according to which the method for determining the adhesion strength includes:

- production of control samples from concrete of classes B25-B60 with a reinforcement embedment depth of  $10d_s$ ;
- testing to failure with the construction of a load–displacement graph for the loaded section of the bar (see Fig. 2, displacement  $\delta_1$  on the concrete surface, from the side of the loaded end of the reinforcement, without taking into account the deformations of the reinforcement at the free length  $L$ );
- determination of the force  $N_u$  corresponding to the displacement of the loaded section by 1.5 mm (with  $d_s < 20$  mm) ÷ 3.0 mm (with  $d_s > 40$  mm);
- correction of force taking into account the actual strength of the reinforcement embedding composition according to the formula:

$$N_{u,Rb} = N_u \left( \frac{R_b}{R_{b,test}} \right)^{0.3} \tag{1}$$



$N$  - longitudinal force;  $L$  is the free length of the reinforcing bar;  $l_v$  - anchoring length;  $\delta_1$  - displacement of the loaded section;  $\delta_2$  - displacement of the unloaded section.

Fig. 2 Scheme of testing and controlled parameters

where:  $R_b$  is the standard strength of concrete for the design class, equal to 25 MPa for the design class B25 and 60 MPa for the class B60;

$R_{b, \text{test}}$  is the average concrete strength of the channel filling composition in the control sample.

- determination of the average value of  $R_{bm}$  in a series of tests according to the formula:

$$R_{bm} = \frac{N_{u, Rb, m}}{\pi \cdot d \cdot l_v} \left( \frac{0,08}{f_R} \right)^{0,4} \tag{2}$$

where

$l_v$ —the length of the embedment of reinforcement in concrete;

$f_R = 0.056$  for fittings of class A500;

$d$  is the diameter of the reinforcement.

- the obtained value of the average resistance is compared with the value of the required strength  $R_{bm, rqd}$ , determined depending on the design class of concrete filling the hole according to table. 9.2. GOST 58429 [20]; if condition (3) is fulfilled, the adhesion strength of the reinforcement with the hole filling composition is equivalent to the strength of the concreted bar:

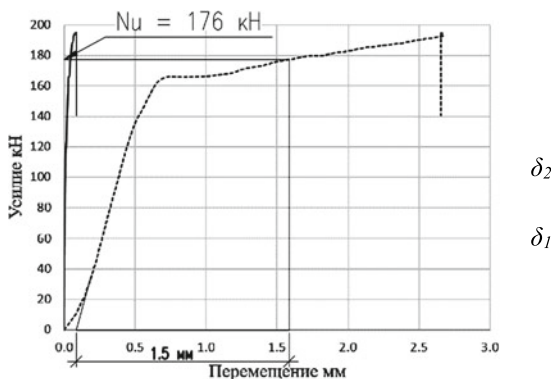
$$R_{bm} \geq R_{bm, rqd} \tag{3}$$

A preliminary analysis showed that the test methodology and evaluation of test results presented in the standard [20] are suitable for the task at hand. In order to take into account the provisions of the current regulatory documents [4], the methodology was supplemented by the requirement of paragraphs. 10.1.4 GOST 8829 on limiting the value of displacement of free ends of rods.

Thus, the following were proposed: Test procedure, including design and requirements for the production of control samples and testing in accordance with GOST 58,429 with additional measurement of displacements  $\delta_2$  in the unloaded section (see Fig. 2); Methodology for evaluating test results, including determining the breaking force taking into account displacements in the loaded section  $\delta_1$  and displacements in the unloaded section  $\delta_2$ , determining the bond strength taking into account the actual compressive strength of the sealant composition and assessing the bond strength of the reinforcement with the hole filling composition.

For approbation of the proposed method, pilot tests of a control sample were performed, in which a rod made of A500 reinforcement with a diameter of 20 mm for a length of  $10 d_s$  was embedded using fine-grained concrete of design class B30 (actual strength 66 MPa).

The test result in the form of a graph of displacements as well as the main stages of processing are shown in Fig. 3. Failure of the sample occurred due to rupture of the reinforcement. The required failure pattern due to anchorage failure was not implemented.

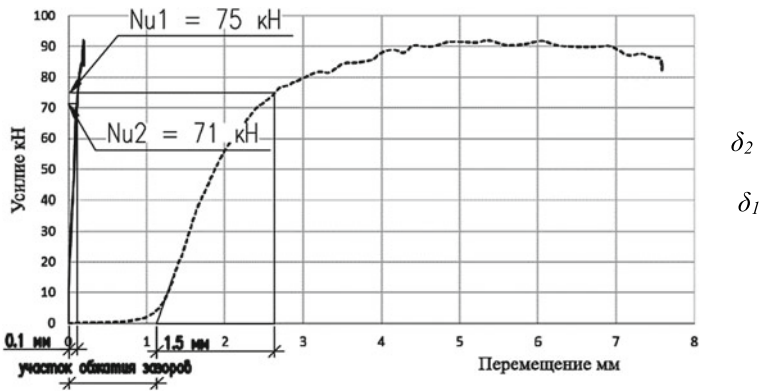


$$N_{u,Rb} = N_{ub} \cdot \left( \frac{R_{b,30}}{R_{b,test}} \right)^{0.3} = 176 \cdot \left( \frac{30}{66} \right)^{0.3} = 139 \text{ kN}$$

$$R_{bm} = \frac{N_{u,Rb}}{\pi \cdot d \cdot l_v} \cdot \left( \frac{0.08}{f_R} \right)^{0.4} = \frac{0.139}{3.14 \cdot 0.02 \cdot 0.2} \cdot \left( \frac{0.08}{0.056} \right)^{0.4} = 12.8 \frac{H}{MM^2}$$

$$R_{bm} = 12.8 \frac{H}{MM^2} \geq R_{bm,reqd} = 12.7 \frac{H}{MM^2}$$

**Fig. 3** Dependence “load–displacement” for reinforcement  $d_s = 20$  mm with an anchorage length  $l_v = 10d_s$



$$N_{u,Rb} = N_{ub} \cdot \left( \frac{R_{b,30}}{R_{b,test}} \right)^{0.3} = 71 \cdot \left( \frac{30}{66} \right)^{0.3} = 56 \text{ kN}$$

$$R_{bm} = \frac{0.056}{3.14 \cdot 0.02 \cdot 0.08} \cdot \left( \frac{0.08}{0.056} \right)^{0.4} = 12.9 \frac{H}{\text{MM}^2} \quad R_{bm} = 12.9 \frac{H}{\text{MM}^2} \geq R_{bm,req} = 12.7 \frac{H}{\text{MM}^2}$$

**Fig. 4** Dependence “load–displacement” for reinforcement  $d_s = 20$  mm with an anchorage length  $l_v = 4d_s$

However, the maximum permissible displacement of the loaded section  $\delta_1 = 1.5$  mm was achieved with a force  $N_u = 176$  kN.

Therefore, in order to achieve the required fracture pattern by the contact of the reinforcement and the composition of the hole filling, the anchorage length was reduced to  $l_v = 4d_s$ . The test results are shown in Fig. 4.

At the embedment depth  $l_v = 4d_s$ , the destruction occurred due to the violation of the anchoring and the stretching of the reinforcement. The maximum permissible displacement of the loaded section  $\delta_1 = 1.5$  mm was achieved with a force of  $N_u = 75$  kN. However, the maximum allowable displacement of the unloaded section  $\delta_2 = 0.1$  mm was achieved with a force  $N_{u2} = 71$  kN. Therefore, the processing of the results was carried out for the smallest force  $N_u = 71$  kN.

## 4 Conclusion

1. A test procedure is proposed to control the adhesion strength of post-installed reinforcement in a finished concrete base, based on the results of foreign and domestic studies of reinforcement anchoring.
2. The technique has been tested on control samples. Its applicability is shown to control the adhesion of reinforcement with the composition of filling the hole and the concrete of the base.

3. The technique can be recommended to control the adhesion strength of the reinforcement with the composition of the filling of the plug joint channel.

**Acknowledgements** The author is grateful to Prof. Walter Berger, without whose active assistance the work could not have taken place and the team of the laboratory of reinforced concrete structures and quality control of the N.I. A.A. Gvozdev.

## References

1. Recommendations for the Design and Implementation of Contact Joints with Breakage of Reinforcement in Reinforced Concrete Columns of Multi-storey Buildings. NIIZhB (1985)
2. Bolgov, A.N., Stepanova, V.F., Ivanov, S.I.D.V., Kuzevanov Shilin, A.A.: On the Development of a new set of rules “Concrete and reinforced concrete structures. Rules for repair and reinforcement.” *Ind. Civ. Constr.* **2**, 16–22 (2018)
3. Sokolov, B.S.: Theoretical foundations of the methodology for calculating plug joints of reinforced concrete structures of buildings and structures. *Large Panel Hous. Constr.* **3**, 60–63 (2016)
4. GOST 8829–2018. Prefabricated Reinforced Concrete and Concrete Building Products. Loading Test Methods. Rules for Assessing Strength, Stiffness and Crack Resistance
5. Recommendations for Testing and Assessing the Strength, Stiffness and Crack Resistance of Prototypes of Reinforced Concrete Structures. Moscow, NIIZhB, p. 36 (1987)
6. RILEM. Recommendations for the Testing and Use of Constructions Materials. RILEM, p. 618 (1994)
7. Bond and anchorage of embedded reinforcement. Background to the fib model code for concrete structures 2010/technical report (170 pages, ISBN 978–2–88394–112–0, May 2014)
8. Eligehausen, R., Malleé, R., Silva, J.F.: *Anchorage in Concrete Construction*, First edn. Ernst & Sohn GmbH & Co. KG (2006). Print ISBN: 9783433011430. Online ISBN: 9783433601358. <https://doi.org/10.1002/9783433601358>
9. Appl, V.: *Tragverhalten von Verbunddübeln unter Zugbelastung*. Stuttgart (2009). <https://doi.org/10.18419/opus-321>
10. EN 1992–4:2018. Eurocode 2—Design of Concrete Structures. Part 4: Design of Fastenings for Use in Concrete—CEN, Brussels (2018)
11. Spieth, H.A.: *Tragverhalten und Bemessung von eingemörtelten Bewehrungsstäben (Behavior and Design of Post-installed Bonded Rebar Connections)*, Dissertation, Universität Stuttgart, 2002 (in German)
12. EOTA Technical Report TR 048. Details of tests for post-installed fasteners in concrete, Version 2015
13. EOTA EAD DP 14-33-0087-06.01. Systems for Post-installed Rebar Connections with Mortar, EOTA, p. 36 (2016)
14. Ivanov, S.I., Smotrov, V.A.: The experience of laboratory tests of anchoring in concrete. *Concr. Technol.* **5–6**, 27–29 (2016)
15. Ivanov, S.I.: Determination of the Bearing Capacity of Anchors Based on the Results of Field Tests. Collection of the Conference “New in Architecture, Design of Building Structures and Reconstruction” (NASKR-2016). Cheboksary, ChGU Publishing House, pp. 244–249, 23–24 Nov 2016
16. Ivanov, S.I.: Laboratory tests of anchoring in concrete. *Ind. Civ. Eng.* **1**, 29–34 (2017)
17. Ivanov, S.I.D.V., Kuzevanov Bolgov, A.N.: To the calculation of anchors installed in a finished base. *Ind. Civ. Constr.* **6**, 45–49 (2018)

18. Kuzevanov, D.V., Ivanov, S.I., Bolgov, A.N.: Calculation of fastenings to concrete using mechanical and adhesive anchors. *Ind. Civ. Constr.* **4**, 25–30 (2019)
19. Ivanov, S.I.D.V., Kuzevanov Bolgov, A.N.: About a new methodological guide for the design of embedded parts of reinforced concrete structures. *Bull. Sci. Res. Cent. Constr. (Moscow)* 28–34 (2020)
20. GOST 58429–2019. Reinforcement Bars Glued into Concrete. Test Methods



# Distribution of Vertical Stresses in Multi-storey Buildings Under Influence of Nonlinear Shear Bonds Deformation



V. A. Lyublinskiy , K. Alzaibak , and Kh. Alwaz

## 1 Introduction

Bearing structures with one vertical seam and, therefore, one row of transverse connecting elements is called simply connected, two rows of bonds—doubly connected, etc. [1]. If the connection is hinged, each vertical supporting structure would deform by itself, and the joints rotating without support would remain horizontal [1]. Real connection will resist bending and shear, then vertical structures in the system receive additional forces and deform. Local moments and shear forces occur at the contact levels of the bond with vertical structures. The shear forces  $Q_{ij}$  from the ties accumulate along the length of the vertical structure and create a normal force  $N_i$  (Fig. 1).

The quantity  $N_i$  depends on the type and rigidity of the shear bonds, rigidity, geometry and load of the entire supporting system. Connections have greater deformability compared to rigid vertical structures and as a result, have a significant impact on stress–strain state formation of the entire building load-bearing system [2–4].

Nonlinear deformation of shear bonds leads to stresses and strains redistribution in structural elements, especially in areas where significant stresses and large deformations occur, and shear bonds are in the plastic region or close to it [5–7].

## 2 Materials and Methods in Research

*Multi-storey Building Study was conducted*—Fig. 2.

A building consists of 12 floors, basement and attic premises.

Parameters:

---

V. A. Lyublinskiy · K. Alzaibak (✉) · Kh. Alwaz  
Moscow State University of Civil Engineering, Yaroslavskoye shosse, 26, Moscow 129337, Russia

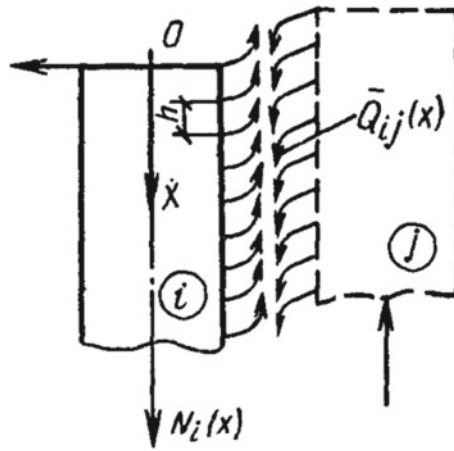


Fig. 1 Relationship between  $N_i$  and  $Q_{ij}$  in a simply connected structure

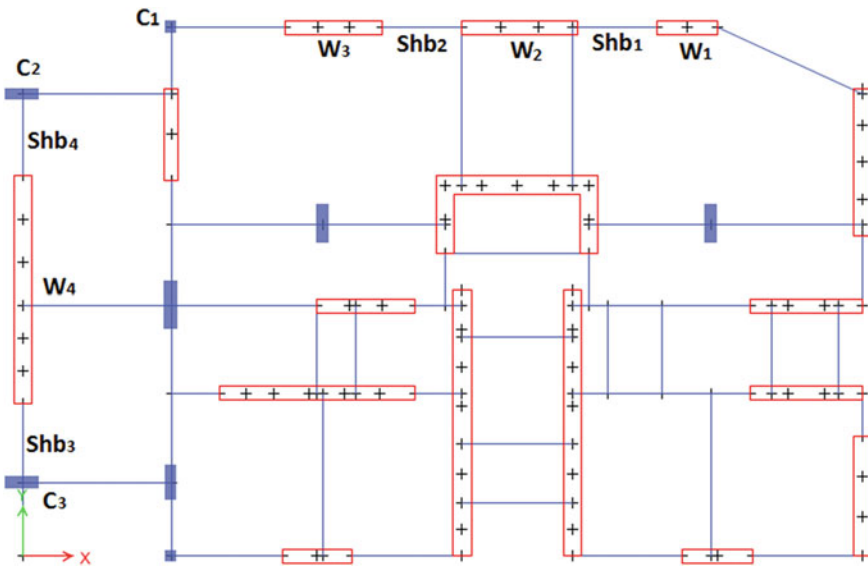


Fig. 2 Building scheme design (communication)

- Walls 30 cm thick connected by lintels with a cross-sectional size 20 by 40 cm
- Length of 2 m
- Columns 40 by 40 cm
- Concrete grade B25 used

A 12 stories building was subjected to permanent, temporary and wind loads. The calculation was carried out by using the ETABS software package based on the finite

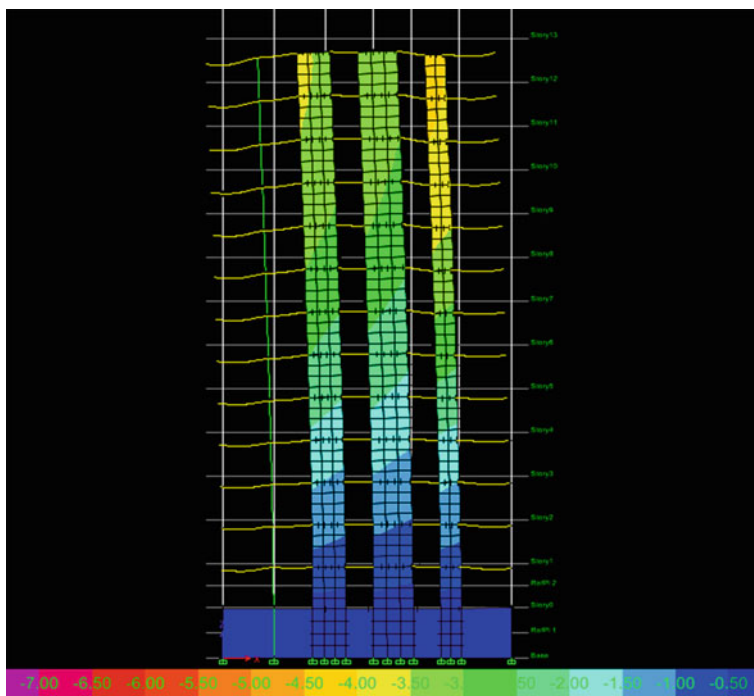


Fig. 3 Vertical deformations in walls (1, 2, 3) as a result of linear calculation

element method. The finite element of the shell type was adopted for walls, an elastic element—for ties; the rigidity of which was refined at each stage of the calculation. The base of the building was assumed to be non-deformable.

Consider the walls  $w_1$ ,  $w_2$  and  $w_3$  (Fig. 2). Vertical deformations and stresses developed in the elements as a result of calculation of the building with constant elements rigidity in the supporting system (Figs. 3 and 4).

To correct the shear modulus value, the experimental deformation diagram « $Q$ - $\Delta$ » [8] was used. A secant module was used to determine the rigidity  $K$  for bonds of the lintel type. The loading was carried out by the stepwise method (Fig. 5) with practically zero compliance until the moment a plastic hinge appeared in one of the shear bonds.

### 3 Results and Discussions

Structural behavior of the building was considered, taking into account the nonlinear change in the rigidity of shear bonds under sequential loading. Shearing forces and corresponding deformations were recorded during loading. The final floor state of the

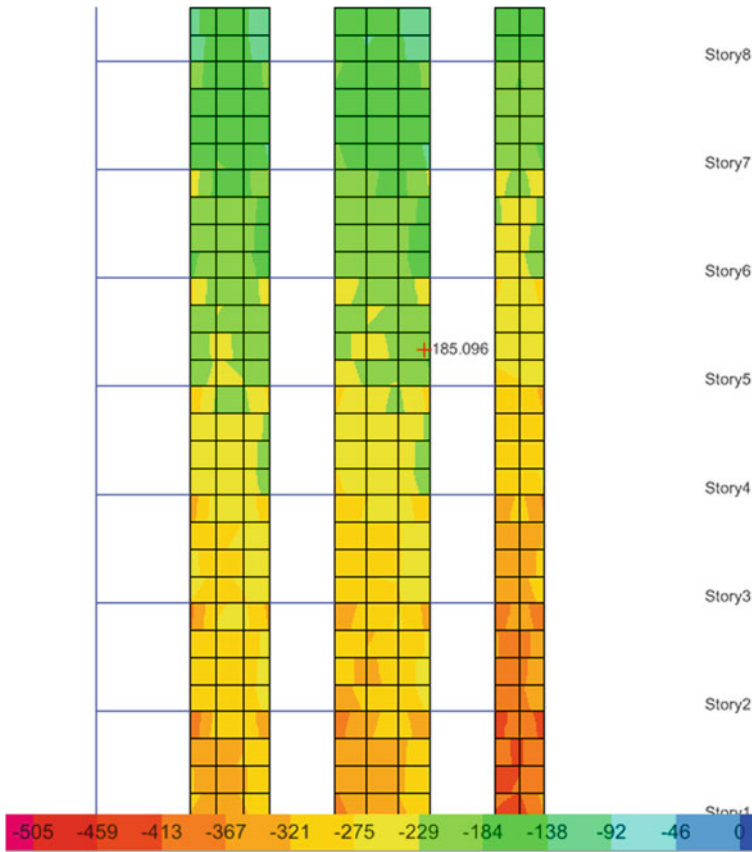


**Fig. 4** Vertical stresses in walls (1, 2, 3) as a result of **linear** calculation

shear bonds, indicated in the diagram Shb1, Shb2, Shb3, in the form of deformation diagrams is shown in Figs. 6, 7 and 8.

It is clearly seen from the diagram for Shb1 (Fig. 6) that shear bonds on the fifth and higher floors work in the plastic region, and nonlinear deformation of the bridges leads to an intensive redistribution of forces to adjacent vertical structures. The number of ties in the upper part of the building that are in the plastic stage is a consequence of shear forces intense redistribution along the height of the tie. Shb2 and Shb3 bonds work in an elastic field. Further loading was stopped.

An increase in shear forces results in additional compressive forces and tensile stresses in the building walls (in addition to stresses from external loading). Figure 9 shows a diagram fragment of normal stresses with a rigidity  $k_3 = 1.67E^6$  kH/M at the level of the first floor.

Figure 10 shows the same plot with initial rigidity  $K_1 = 5.0E^6$  kN/m. For wall  $W_1$ , the voltage drops at the first-floor level increased by 20% compared that to rigidity  $K_3$  and for  $W_2$  the stresses increased.

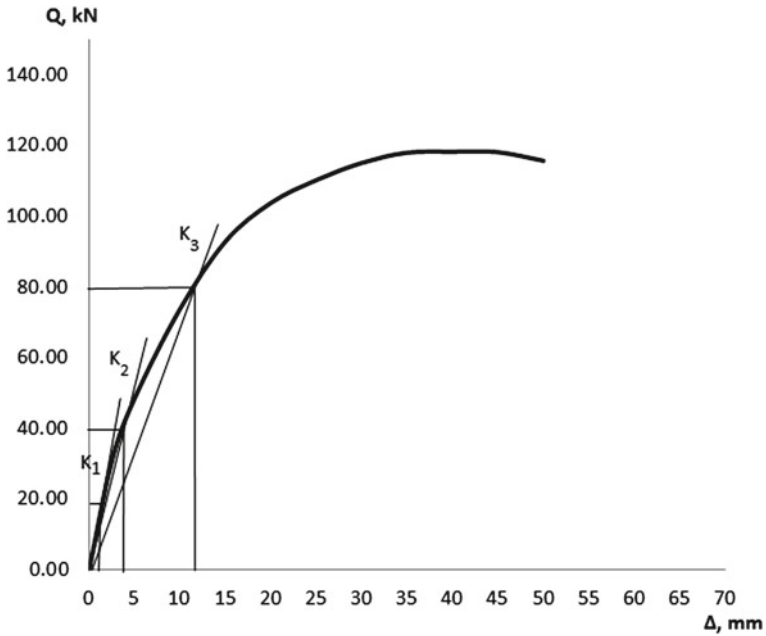


Fig. 5 Experimental strain diagram deformation “ $Q-\Delta$ ” for shear connector

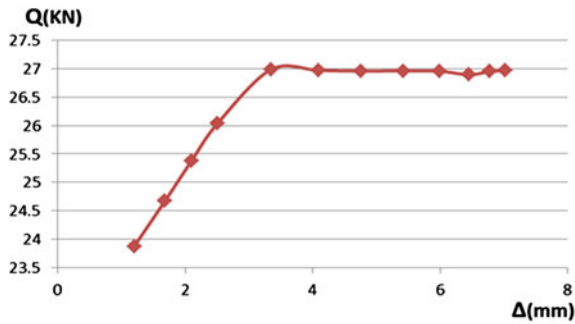


Fig. 6 Strain/shear force diagram of shear bond (Shb1)

Thus, we can note the following: stresses increased in wall  $W_1$  while decreasing in wall  $W_2$ , wall and  $W_3$  for nonlinear analysis.

Increase in compressive stresses due to work of the shear bonds in the bearing system and its general distribution over the building height is given in Fig. 11.

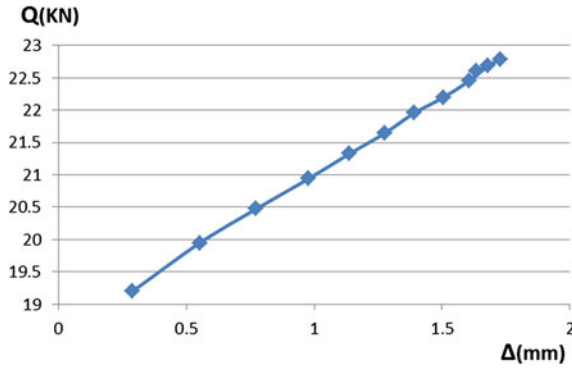


Fig. 7 Strain/shear force diagram of shear bond (Shb2)

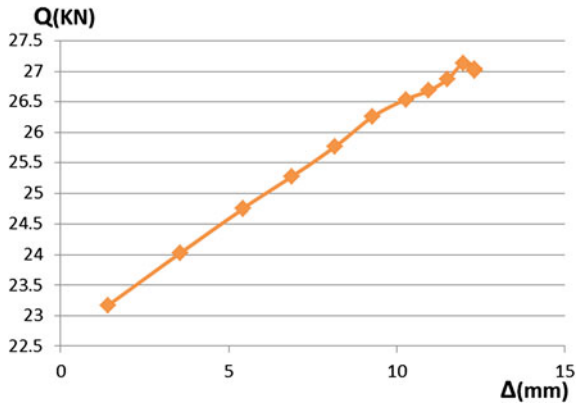


Fig. 8 Strain/shear force diagram of shear bond (Shb3)

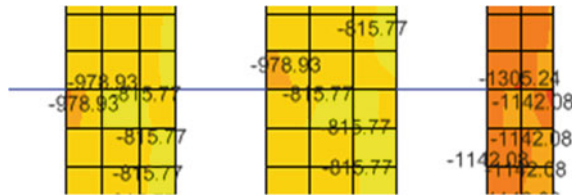


Fig. 9 Stresses of walls  $W_1, W_2, W_3$  for  $K_3$

### 4 Conclusion

Higher number of stores in the building will lead to external load increase and, therefore, shear deformations in shear bonds increase. The spatial work of shear bonds is a mechanism for the spatial redistribution of stresses in vertical structures.

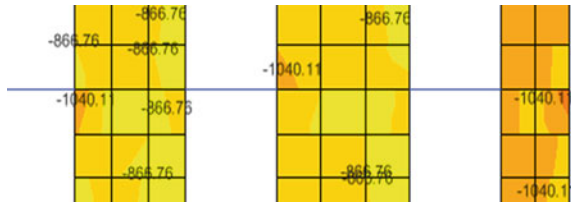


Fig. 10 Stresses of walls  $W_1, W_2, W_3$  for  $K_1$

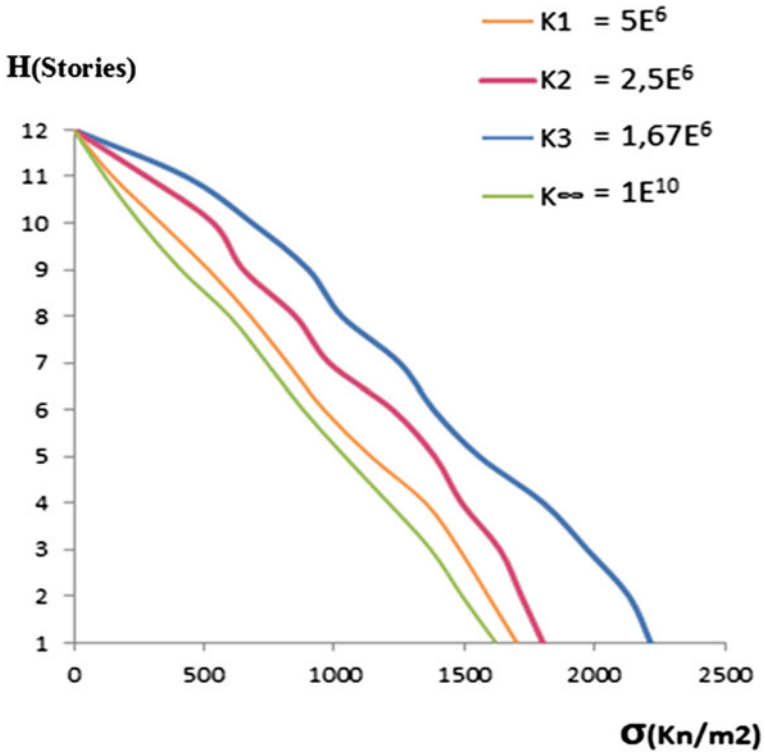


Fig. 11 Diagram of changing vertical stresses in wall ( $W_1$ ) according to the change of rigidity of the shear bonds ( $K$ )

The nonlinear behavior of the tie elements is a key factor in the determination of deformations and stresses in vertical supporting structures.

Magnitude of the change in vertical stresses in load-bearing structures reaches 6–9% in the zones of maximum stress.

## References

1. Drozdov, P.: Design and calculation of load-bearing systems of multi-storey buildings and their elements (Stroyizdat, Moscow), p. 223 (1977)
2. Sokolov, B., Mironova, Y.: Strength and flexibility of vertical joints of wall panels using flexible hinges. *Hous. Constr.* **5**, 60–62 (2014)
3. Blazhko, V.: On the determination of the ductility of connections in the formation of design models of panel buildings. *Hous. Constr.* **3**, 17–21 (2017)
4. Todut, C., Dan, D., Stoian, V.: Theoretical and experimental study on precast reinforced concrete wall panels subjected to shear force. *Eng. Struct.* **80**, 323–338 (2014)
5. Lyublinskiy, V., Tomina, M.: Influence of non-linear deformation of bridges on the process of distribution of forces in the bearing elements of the diaphragm. *Syst. Technol. Met.* **2**(38), 153–158 (2018)
6. Tamrazian, A.G., Manaienkov, I.K.: On the calculation of flat ferroconcrete floors with the consideration of the actual rigidity of section. *Sci. Rev.* **8**, 87–92 (2015)
7. Lyublinskiy, V.A.: The deformability of shear bonds in the load-bearing systems of panel buildings. *J. Phys. Conf. Ser.* **1425**, 012159 (2020)
8. Hola Musa.: Non-linear Deformations and Ultimate Bearing Capacity of Vertical Diaphragms of Monolithic Multi-storey Buildings. PhD dissertation, Moscow State University of Civil Engineering, Moscow, p. 163 (1985)



# Erection of Flat Shells of Positive Gaussian Curvature Made from High-Strength Sand Concrete and Its Economic Efficiency



Nikolay Palagin , Georgy Nikitin, and Aisylu Sadrutdinova

## 1 Introduction

One of the promising areas in construction is the production of high-strength crushed stone and sand (fine-grained) concretes in reinforced concrete structures and economic efficiency of its use.

In [1] the question of the use of blast furnace sludge with carbonate-containing additives in the composition of sand concrete was studied. It was found that their presence promotes the formation of calcium hydro silicates, which contain carbonate groups similar in composition to hydro silicate phases. This leads to an increase in concrete strength by 11.2%, density by 14% and a decrease in water absorption by 5%.

In [2], the issues of density, strength and water absorption of sand concrete made by the zone injection method were studied. We used fractionated sand with a fineness module of 2.5 and Portland cement grade PC500 D0. Varying the water-cement and cement-sand ratio determined the optimal compositions of sand concrete for road use with strength from 40.8 to 72.3 MPa.

In [3], using the Maple 13 program, second-order regression equations were obtained that adequately assess the dependence of the compressive strength of sand concrete at the age of 28 days.

In [4], the influence of contaminants in the sand, the dispersion of additives and the concentration of diopside on the strength and deformation properties of sand concrete was studied.

In [5], the effect of additives based on pickling solutions of steel rolling plants on the structure and strength of sand concrete was experimentally studied. It has been found that these additives compact and strengthen the concrete structure.

---

N. Palagin (✉) · G. Nikitin  
Kazan State University of Architecture and Engineering, Kazan, Russia

A. Sadrutdinova  
LLC «Reshenie», Kazan, Russia

Their optimal content has been determined, which ensures the maximum increase in concrete strength.

In [6], the dependence of the strength of a sand concrete mixture on the shape and relief of the particle surface, as well as the content of dusty and clay particles and impurities enveloping the sand grains, was investigated.

The Moscow State University of Civil Engineering developed the sand concrete modified with a micro dispersed additive obtained by joint grinding of quartz sand, super plasticizer C-3 and calcium stearate [7]. At the same time, sand concrete has a compressive strength of up to 50 MPa, bending strength of up to 8.3 MPa, water absorption of 1.4% and frost resistance of more than F75.

Researchers from the USA and Vietnam have developed ultra-high-strength concrete with a strength of 155 MPa at the age of 90 days using local building materials [8]. This strength was achieved with a natural set of strength with the content of silica particles of 5%. The highest strength is obtained by hardening for 2 days at 60 °C and then 3 days at 90 °C.

The article [9] studies the effect of the composition of sands of natural origin on the strength of concrete. Studies have shown that samples on sands with smectite clays had lower strength compared to samples on other sands. And vice versa, the samples containing sands with Na<sub>2</sub>O had the best strength characteristics.

The work [10] is devoted to an experimental study of the strength, water absorption and water resistance of sand concrete modified with the waterproofing composition «Hydropen Plug». It was revealed that this new type of concrete has high strength and water resistance characteristics.

In [11], a new method for calculating the composition of ultra-strong concrete is proposed. It has been established that concretes made using sandstone have higher strength compared to concrete on river sand.

Based on a review of research in [12], it was found that concrete made from sea sand and seawater gains strength faster. However, the use of these materials, due to the presence of chlorides, causes rapid corrosion of steel reinforcement. It is proved that the use of polymer reinforcement with mineral additives solves this problem.

In [13], the effect of cement with mineral additives from ground natural sand (sand cement) and cement with mineral additives from granite screening on the properties of heavy concrete was experimentally studied. It was revealed that concrete on sand cement has increased shrinkage deformations and cracking. This is the reason for a decrease in compressive and tensile strength in bending, a decrease in waterproofing and frost resistance. Also, concrete on sand cement does not provide sufficient corrosion protection for steel reinforcement.

In the Voronezh State University of Architecture and Civil Engineering, when testing beams with dimensions 60 × 120 (h) × 1400 mm, the question of the magnitude of their deflection with the upper layer of high-strength concrete was investigated [14]. The upper compressed layer was made of high-strength concrete of B60-B90 classes with a height of 46 ... 51 mm, the lower tension layer was made of concrete of B20 ... B30 classes. It was found that the use of high-strength concrete in the compressed zone leads to a decrease in deflections. Recommendations for their calculation are given.

In [15], considered the work to implement the parameters of mechanical safety of the high-rise residential complex “One Tower” with a height of 403.9 m in the Moscow International Business Center “Moscow-City”. “Moscow-City” is a complex object in the plan, consisting of an underground part measuring  $186.9 \times 37.2$  m with 4 underground floors, a stylobate part of 12 floors measuring  $166.95 \times 30.7$  m and a high-rise part of 92 floors measuring  $113.4 \times 27$  m. The high-rise part is built of monolithic reinforced concrete a frame with a stiffening core and supporting columns. The supporting structures are designed from ordinary concrete of B50 class and high-strength concrete of B60 and B80 classes. The calculation was performed by ANSYS Mechanical SP.

In [16], the physical, chemical and granulometric characteristics of screenings of crushed stone crushing from open pits of the Sverdlovsk and Chelyabinsk regions were studied. Efficient compositions of heavy concrete of B22.5-B40 classes have been developed and studied with the use of the specified screenings and additives MC-Power Flow and Centrament Air 202. The economic efficiency of using screenings in the composition of heavy concrete was revealed. The experimental batch of reinforced concrete trays was manufactured at one of the Tyumen region reinforced concrete products enterprises.

In [17], the influence of the introduction of basalt fiber into tensile concrete on its basic properties was considered. Tensile concrete was modified by an expanding sulfoaluminate type additive. It was found that this leads to an increase in the strength of the concrete. Also, due to the addition, the effect of simultaneous expansion and hardening is realized. This increases the impermeability and durability of this kind of concrete, which predetermines the prospects for their use for the repair of various kinds of buildings and structures.

In [18], the results of research aimed at studying the structural behavior of beams made of self-compacting concrete with the addition of nano silica (Nano-SiO<sub>2</sub>) and nano manganese ferrite (Nano-MnFe<sub>3</sub>O<sub>4</sub>) are presented. Experiments have shown that the use of nano additives and the replacement of 25% of the cement with fly ash improved the mechanical properties and increased the durability of self-compacting concrete. From the most optimal compositions, reinforced concrete beams were made and tested for bending.

In [19], the selection of compositions of refractory concretes obtained from a briquette based on forsterite concentrate from wastes of the Kovdor mining and processing plant and magnesium phosphate acting as a binder is considered. The grain composition of the batch mixture was selected, the ratio of aggregate and binder was determined to improve the structural properties of concrete, revealed the influence of the composition and temperature of heat treatment of the briquette on the physic-technical properties of the obtained materials.

In [20], the results of studies are given to determine the economic efficiency of the erection of prefabricated and monolithic long cylindrical shells from HSSC of B60 and B80 classes in comparison with heavy concrete of B20-B80 classes. Studies have shown that concerning Kazan the use of HSSC compared with the heavy one makes it possible to reduce the consumption of steel (up to 30.6% in prefabricated shells and up to 23.7% in monolithic), concrete (up to 15.9% in prefabricated shells and up

to 14.0% in monolithic) and the total cost of materials (up to 18.9% in prefabricated shells and up to 20.3% in monolithic).

The analysis of the works showed that only in [20] explored the question of the economic feasibility of designing building structures from high-strength sand concrete.

As you know, the properties of sand concrete are determined by the same factors as ordinary concrete, however, it has some features due, first of all, to the high content of cement stone. This type of concrete has several noticeable advantages: increased strength in compression and tension, high-quality structure and high manufacturability, the ability to obtain thin-walled structures, decorative concrete and fiber-reinforced concrete, as well as some other advantages [21–25].

Sand concrete also has disadvantages due to the large surface of the aggregates. This increases the cement consumption by 15–20% in comparison with equally strong heavy concrete. Therefore, when using sand concretes, along with plasticizing ones, mineral additives should also be added to the composition or composite cement or cement of low water demand should be used.

Also, sand concrete has increased air entrainment, which requires the use of effective thinners or defoamers. Air entrainment depends on the type of plasticizer. So, in [26] it was found that the additive Melflux 2651F underestimates the air entrainment rate by 33%, the other additives (C-3, Sika VC5-800) only increase this indicator.

Recently, sand concrete is increasingly used due to the widespread availability of a raw material base. More than 50 deposits and occurrences of sand and gravel material are known on the territory of the Republic of Tatarstan. The predicted resources of building sand in the republic are estimated at 1 billion m<sup>3</sup>, including real ones for processing—about 300 million m<sup>3</sup>, mainly in areas of the valleys of the Volga, Kama, Vyatka and Sviyaga rivers. According to the strategy of environmental safety of the Republic of Tatarstan and the development of the natural resource complex of the Republic for 2017–2021 and in the future until 2030, the building materials industry has been tasked with expanding the range of products manufactured from local mineral raw materials.

Because most of the European territory of Russia (Moscow, the Moscow region, the Volga region, Vologda, etc.) does not have deposits of coarse aggregate or has deposits of sedimentary rocks that are limited suitable for use in reinforced concrete, the use of sand concrete is an important task in its production. Besides, the extraction of stone and its processing into crushed stone require large amounts of electricity and very laborious. There is also an ecological aspect of the problem: in the production of crushed stone with a fraction of more than 5 mm, a large number of screenings of a fraction of less than 5 mm (up to 20–30%) is formed, which form large-tonnage dumps, thereby violating the ecological balance of nature. Only a small amount of such waste is used as raw material for the preparation of limestone flour and mineral powder for asphalt concrete. The destruction of mountains during its extraction leads to irreversible climatic changes in Karelia, the North Caucasus and the Ural. The use of sand as aggregate causes less damage to the environment than the use of crushed stone.

In the world practice of construction, high-strength and ultra-high-strength heavy concretes of a new generation are increasingly used. They can significantly reduce the dimensions of sections of elements, save concrete and reinforcement [27, 28]. The implementation of the special technical properties of these concretes has opened up almost endless possibilities for the construction of unique buildings and structures around the world. In Russia, the use of such concretes began much later than in Western European countries, the USA, Canada and Japan. Some of the most notable objects erected with the use of concrete of B80...B90 class are the buildings of the «Federation» complex of the «Moscow City» MIBC [29] and the Public and business complex «Lakhta-Center» in St. Petersburg [30].

An alternative to high-strength heavy concrete is high-strength sand concrete (HSSC) [31]. This concrete is a composite material that includes graded quartz sand, a highly active binder and effective modifiers. A decrease in the amount of binder in the composition of concrete is achieved by grinding part of the sand, using plasticizing additives, and products autoclaving. Plasticizers (C-3/2.5, Sika VC5-800/2.5, Metflux 2651/2.5) are mainly used as chemical additives, which can significantly reduce the water demand of the concrete mix and the consumption of cement [23].

The use of HSSC has the following advantages: higher initial and final strength; early demoulding; decrease in building thickness or increase in the bearing capacity of bending structures; higher density, water and gas impermeability due to the low content of capillary pores; higher wear resistance; increased corrosion protection of reinforcement due to the slow spread of carbonization; increased resistance to chemically active substances, etc.

The introduction of high-strength sand concretes with the use of river sands of the Republic of Tatarstan and chemical additives is an alternative to traditional concrete, which requires expensive high-strength crushed stone imported from the Ural.

Based on fractionated sands of local deposits of the Kama, Volga and Vyatka rivers, the TBMPs department of KSUAE developed compositions of high-grade sand concrete B60-B80 [32]. The project “High-strength sand concrete” was included in the list of innovative projects and developments in the field of building materials and technologies of the Ministry of Construction, Architecture and Housing of the Republic of Tatarstan. In 2017, on the instructions of the President of the Republic of Tatarstan, together with the State Housing Fund, the Department of TBMPs of KSUAE continued work on high-strength sand concrete. In particular, the scientists of this department, together with the specialists of Kazan Giproniaviaprom OJSC, completed an alternative design of the supporting frame of an 18-storey residential building in the “Salavat Coopere” complex of Kazan from high-strength sand concrete of B80 class instead of the initial project of heavy concrete of B25 class. As a result, savings in concrete amounted to 20%, for steel reinforcement—29% [33].

The article [34] presents the results of studies to determine the economic efficiency of the construction of solid columns of one-story industrial buildings with bridge cranes according to the series 1.424.1-5 “Reinforced concrete columns of rectangular cross-section for one-story industrial buildings with a height of 8.4 ... 14.4 m, equipped with bridge support cranes with lifting capacity up to 32 tons” from HSSC

of B60 and B80 classes in comparison with heavy concrete of B20...B80 classes. Studies have shown that concerning Kazan, the use of HSSC, in comparison with heavy concrete of B20...B40 classes, used in the standard series, makes it possible to reduce, depending on the size of the span, the pitch of the columns, the height of the floor and the lifting capacity of the cranes, the consumption of steel by 43.2 ... 71.5% and the total cost of materials by 18.2 ... 34.5%.

Despite the listed advantages, today in the Republic of Tatarstan and Russia there is the problem of widespread use of the HSSC of a new generation. It is in the insufficiently rapid development of methods for calculating the load-bearing structures made of it. So, the use of sand concrete is limited to the manufacture of small pieces and all kinds of decorative architectural and finishing products, as well as coatings for roads, airfields and floors of industrial buildings.

Following the above, it is necessary to continue the work on the design of various building structures from the HSSC. Economic feasibility should be the only criterion for the effectiveness of its application. In this regard, the topic considered in the article is relevant for the development of the construction industry both in the Republic of Tatarstan and in Russia as a whole.

The purpose of the studies, the results of which are presented in this article, was to identify the economic efficiency of the construction of prefabricated and monolithic flat shells of positive Gaussian curvature from HSSC of B60 and B80 classes in comparison with heavy concrete of B25-B80 classes.

## 2 Materials and Methods

### 2.1 General Information About Flat Shells of Positive Gaussian Curvature

For shells of positive Gaussian curvature (Fig. 1), the following conditions are valid:

$$\begin{cases} \rho = \rho_{\max}\rho_{\min} > 0; \\ \rho_{\min} > 0; \\ \rho_{\max} > 0, \end{cases} \tag{1}$$

where  $\rho$  is the Gaussian curvature;  $\rho_{\max}\rho_{\min}$ —the main curvatures at any point of the middle surface of the shell.

Flat shells that have a slight rise above the reference plane at

$$f_1 \leq a/5 \quad \text{and} \quad f_2 \leq b/5, \tag{2}$$

where  $a$  and  $b$  are half the dimensions of the sides of the shell in the plan;  $f_1$  and  $f_2$ —booms for lifting the shell on the contour (Fig. 1).

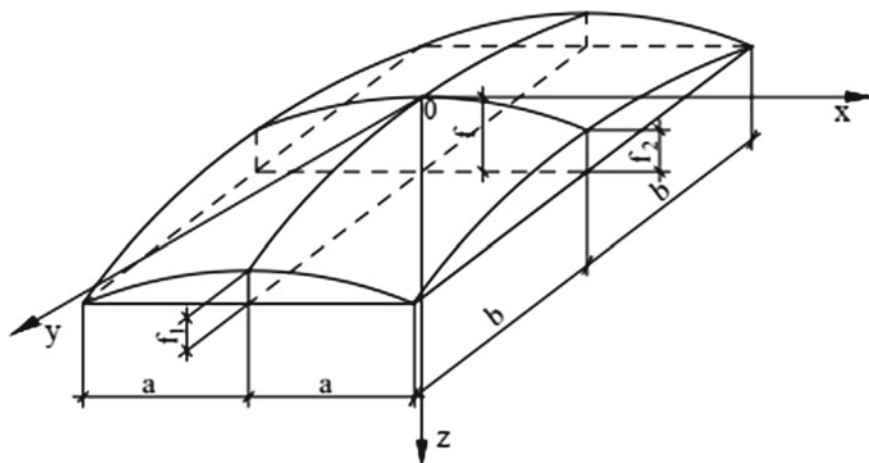


**Fig. 1** Scheme of a shell of positive Gaussian curvature

With equal dimensions of the sides of the shell  $2a = 2b = l$  and  $f_1 = f_2 = f_k$  conditions (2) have the form:

$$f_k \leq l/10 \quad (3)$$

The dimensions of the shells in the plan are 18 ... 36 m—for industrial buildings, up to 100 m and more—for public buildings.

From the loads distributed over the surface, these shells experience mainly compression, which is one of their main advantages. In terms of material consumption, they are more economical than cylindrical shells by 25 ... 30%.

Prefabricated shells can be designed as freestanding (single-wave) and multi-wave in one and two directions (Fig. 2).

Along the contour, they rest on diaphragms in the form of arches, trusses or beams, as well as curved beams laid on walls or supported by columns. Cylindrical ribbed panels have dimensions of  $3 \times 6$  m and  $3 \times 12$  m.

## 2.2 *Structural Solutions of the Investigated Shells, Applied Materials and Calculation Methods*

**Prefabricated Shells.** In the “Manual for the design of reinforced concrete spatial structures of pavements and floors (to SP 52-117-2008 \* “Reinforced concrete spatial structures of pavements and floors. Design rules”) for prefabricated shells, a method is given for determining efforts by an engineering method. However, it does not consider various schemes for applying snow load and does not consider the wind effect, as recommended by SP 20.13330 “Loads and Impacts”. To reflect the actual

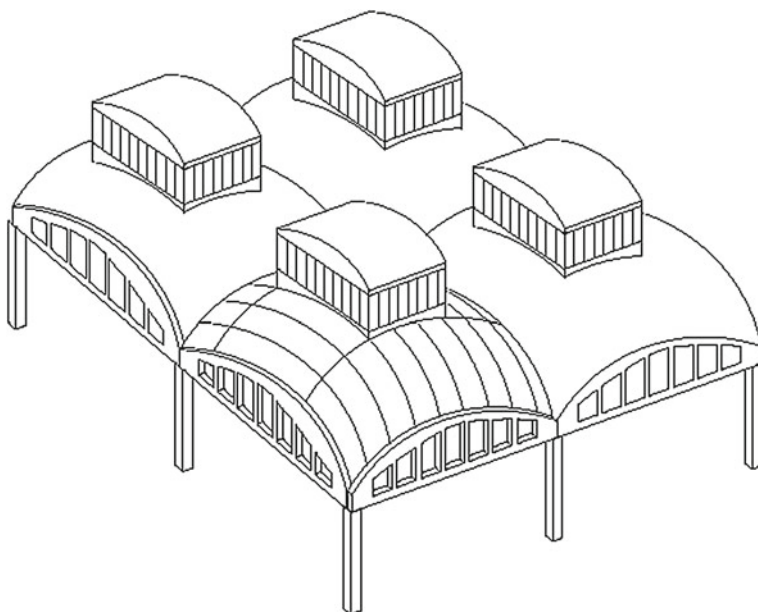


**Fig. 2** General view of multi-wave prefabricated reinforced concrete flat shells of positive Gaussian curvature

work of the shells, the indicated types and schemes of load application must be considered. This can be done least effortlessly using a SP. However, before using an SP, it was necessary to make sure that the calculation results for determining the efforts in the SP and the engineering method are comparable. So to perform the calculations LIRA-SAPR software package was chosen.

As prefabricated we considered freestanding shells square in plan. The slab consisted of ribbed cylindrical panels with a size of  $3 \times 6$  m with a shelf thickness of 40 mm, a section of longitudinal and transverse contour ribs— $100 \times 300$  (h) mm, a section of an intermediate transverse rib— $200 \times 300$  (h) mm. Along the perimeter of the shells, prefabricated monolithic contour beams with a length of 6 m, a cross-section width of 600 mm are installed, with reinforcement of the lower prefabricated part with rigid reinforcement of two rolled I-beams and flexible bar reinforcement, the upper monolithic part—flexible bar reinforcement; the support of the beams is carried out according to a continuous pattern on the columns installed with a step of 6 m; the joint of the beams to each other is rigid; the joint of columns with beams is articulated, with a foundation is rigid. The section of the columns (corner— $900 \times 700$  mm, ordinary— $800 \times 700$  mm) is taken from the condition that the beams are supported on them (Fig. 3). In the corner zones of the shell, a monolithic reinforced concrete block is laid on top of the precast panels.



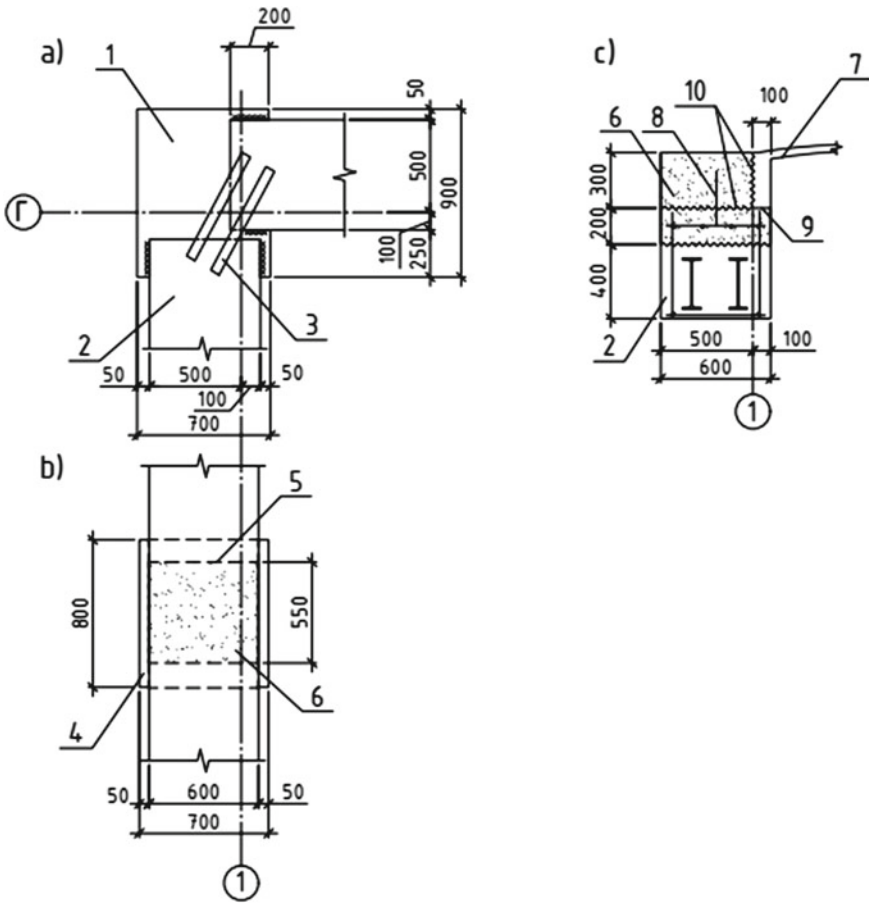


**Fig. 3** Supporting nodes for a prefabricated flat shell of positive Gaussian curvature: a—contour beams on the corner column; b—the same for an ordinary column; c—prefabricated panel on a contoured beam; 1—corner column; 2—contour beam; 3—steel plates on the top of the contour beams; 4—ordinary column; 5—end face of the contour beam; 6—monolithic concrete; 7—panel; 8—steel stop; 9—embedded parts of the panel and the contour beam; 10—dowels

The determination and comparison of efforts were carried out on the example of a shell designed in Kazan with a span of 42 m with the class of heavy concrete panels, contour beams and blocking—B25.

The forces (maximum shear forces along the edges  $S$ , normal forces at the center  $N_{x,y=0}$ , maximum normal forces  $N_{x;x=0}^{max}$ , the main tensile forces  $N_{pr,t}$  and compressive forces  $N_{pr,c}$  in the corner zones and the span) in the shell itself were determined and compared, as well as span  $M_1$  and support  $M_{sup}$  bending moments in contour beams. The analysis of the performed calculations showed that the values of the efforts determined by the engineering method and with the help of an SP differ from  $-18.3\%$  to  $+17.5\%$ , which indicates their comparability. Therefore, in the future, to

determine the efforts taking into account the effect of wind load, as well as various schemes for applying snow load, the LIRA-SAPR software package was used.

With the help of the SP, the forces in the slab and contour beams of freestanding shells with dimensions of  $18 \times 18$  m,  $24 \times 24$  m,  $42 \times 42$  m and  $66 \times 66$  m were determined. Variants of the application of the snow load were adopted according to SP 20.13330, and the wind effect was determined as the sum of the average and pulsation components.

For the efforts obtained, calculations and design of shell elements with dimensions in terms of  $18 \times 18$  m,  $24 \times 24$  m,  $42 \times 42$  m and  $66 \times 66$  m, made of heavy concrete of classes B25, B40, B60 and B80 and HSSC of classes B60 and B80, were performed.

The class of the flange meshes reinforcement and the panel ribs transverse reinforcement is B500C, the class of the longitudinal reinforcement of the panel ribs, the monolithic part of the contour beams, concrete footing and columns is A500C, the class of the transverse reinforcement of the columns is A240C. Fencing vertical structures are wall panels and glazing panels mounted on sheeting rails column.

Calculations were made for the 1st and 2nd groups of limiting states of the shell slab (stability check, strength calculation, including corner zones, deformation calculation), contour girders, including their joint (in the stages of operation and installation); cylindrical panel (at the stages of manufacturing, transportation and installation); columns (in operation). The purpose of the calculations was to determine the required amount of reinforcement in the shell elements. At the same time, in the case of using both heavy concrete and HSSC, if the design requirements allowed, the thickness of the flange of the panels, the height of their longitudinal and transverse ribs, as well as the thickness of the concrete footing were changed. The calculation of all elements, except columns, was carried out by an engineering method according to the methodology of the current standards. The density of heavy concrete, its strength and deformation characteristics were also taken according to the norms, and the strength and deformative characteristics of HSSC—according to the results of the experiments of the TBMPs department of KSUAE. The strength and deformation characteristics of the reinforcement were taken according to the standards. The reinforcement of the columns was taken according to the results of the calculation in the SP, taking into account the design requirements. Based on the results of the calculations, the design of the shell elements was carried out.

For each calculated shell, concerning Kazan, the consumption of materials (concrete and reinforcement) and their cost, including the total cost, were determined, and their comparison was made for the cases of manufacturing shells from heavy concrete and HSSC. The composition of heavy concrete and HSSC of various classes was adopted based on the results of developments in the TBMPs department of KSUAE.

**Monolithic Shells.** The calculation and design of freestanding monolithic shells with dimensions in terms of  $24 \times 24$  m,  $48 \times 48$  m,  $60 \times 60$  m,  $72 \times 72$  m,  $84 \times 84$  m from heavy concrete of B25, B40, B60, B80 classes and HSSC of B60 and B80 classes was performed.

The shells consisted of the shell itself (slab), contour beams and columns. The geometric parameters of the shells and their elements were taken in accordance with the recommendations of the standards and based on the experience of design practice. The column spacing was taken equal to 12 m. All longitudinal reinforcement is ordinary class A500C, the class of transverse and structural reinforcement is A240C.

The calculation, which consisted of determining the required amount of reinforcement, was carried out in the LIRA-SAPR software package with the application of wind and various snow load schemes. The scheme of reinforcement of the contour beams and columns, based on the analysis of the diagrams of the forces acting in them, was assumed to be symmetrical. The slab reinforcement scheme was assigned in accordance with general recommendations and consisted of 4 types of reinforcement.

In manufacturing the shell of heavy concrete, the reinforcement was taken according to the results of the calculation of the SP, “tuned” to SP 63.13330 “Concrete and reinforced concrete structures. Basic Provisions”, and in the manufacture of HSSC, their reinforcement was determined as follows. Since the deformative and strength characteristics of HSSC and heavy concrete of the same classes differ, they were set directly in the SP. This could be done only when the SP was “tuned” to the currently non-operating SNiP 2.03.01-84 \* “Concrete and reinforced concrete structures”, in which the method for calculating longitudinal reinforcement according to group 1 of limit states is identical to the method of SP 63.13330, and the method for calculating transverse reinforcement and the calculation of crack resistance is excellent. Also, the values of  $R_s$ ,  $R_{sc}$  and  $R_{sw}$  in SNiP 2.03.01-84 \* and SP 63.13330 are slightly different. Therefore, when defining the reinforcement directly in the slab and the contour beam, first, the required longitudinal reinforcement was adjusted according to the values of  $R_s$  and  $R_{sc}$ , then the crack resistance was manually calculated for the forces obtained in the SP. The design of transverse reinforcement was carried out manually according to the SP 63.13330 method. The selection of longitudinal and transverse reinforcement in the columns was carried out based on the results provided by LIRA-SAPR SP, taking into account the correction of the values of  $R_s$ ,  $R_{sc}$  and  $R_{sw}$ .

The design of the shell elements was carried out in accordance with the required amount of reinforcement and the design requirements of the standards.

### 3 Results

The studies allow us to conclude that the use of high-strength sand concrete (HSSC) of B60 and B80 classes, in comparison with the heavy one during the construction of the shells considered in the article, allows to obtain a significant economic effect; namely, to reduce the consumption of steel (up to 36.0% in prefabricated shells and up to 43.0% in monolithic ones), concrete (up to 11.3% in prefabricated shells and up to 12.9% in monolithic) and the total cost of materials (up to 27.0% in prefabricated shells and up to 29.4% in monolithic ones). The use of HSSC makes it possible

to reduce the mass of structural elements (by 13.0% in prefabricated shells and by 20.8% in monolithic shells), which, in turn, leads to a decrease in the load on the foundations.

## 4 Conclusion

In the scientific and technical literature, it was possible to find only information about the economic efficiency of designing long cylindrical shells, an 18-story residential building and solid columns of one-story industrial buildings with bridge cranes from HSSC (see the section “Introduction”).

The use of high-strength sand concrete (HSSC) is an alternative to crushed stone. In the scientific and technical literature, there is no information on the design of flat shells of positive Gaussian curvature from it.

The performed studies have shown that the use of HSSC of B60 and B80 classes, in comparison with the heavy one in the design of the shells considered in the article, allows to obtain a significant economic effect; namely, to reduce the consumption of steel (up to 36.0% in prefabricated shells and up to 43.0% in monolithic shells), concrete (up to 11.3% in precast shells and up to 12.9% in monolithic shells) and the total cost of materials (up to 27.0% in prefabricated shells and up to 29.4% in monolithic ones). The use of HSSC allows to reduce the mass of structural elements (by 13.0% in prefabricated shells and by 20.8% in monolithic shells), which leads to a decrease in the load on the foundations.

In this regard, it can be concluded that the results obtained are novel, and the results of the studies carried out can be recommended for use in construction practice.

## References

1. Skripnikova, N.K., Shekhovtsov, V.V., Grigorevskaya, D.K., Semenovych, M.A., Yur'ev, I.Yu.: Small-grain concrete based on metallurgy waste. *J. Constr. Archit.* **21**(2), 185–191 (2019)
2. Borovskikh, I.V., Morozov, N.M., Iskandarova, A.F.: Fine concrete for concrete paving. *Int. Sci. J. (Symbol of Science)* **8**, 39–41 (2016)
3. Van Lam, T., Bulgakov, B.I., Alexandrova, O.V.: Mathematical modeling of the impact of raw material composition on compressive strength of high performance fine-grained concrete. In: *Proceedings of the Moscow State University of Civil Engineering*, vol. 12, issue 9(108), pp. 999–1009 (2017)
4. Ilyina, L.V., Khakimullina, S.A., Kadorkin, D.A.: Influence of dispersed mineral additives strength fine concrete. *Fundam. Res.* **4**, 34–38 (2017)
5. Lukutsova, N.P., Pashayan, A.A., Khomyakova, E.N.: Study of the effect of additives based on etching solutions containing iron salts on the structure and strength of fine-grained concrete. *Proc. Moscow State Univ. Civil Eng.* **1**, 94–104 (2016)
6. Andreeva, A.V., Burenina, O.N., Davydova, N.N., Davaasenge, S.S., Savvinova, M.E.: Fine concrete in winter concreting. *Volga Sci. Bull.* **12–1**(52), 19–23 (2015)
7. Bazhenov, Yu.M., Lukutsova, N.P., Karpikov, E.G.: Thin concrete modified with a complex micro dispersed additive. *Proc. Moscow State Univ. Civil Eng.* **2**, 94–100 (2013)

8. Alsalman, A., Dang, C., Micah Hale, W.: Development of ultra-high performance concrete with locally available materials. *Constr. Build. Mater.* **133**, 135–145 (2017)
9. Hasdemir, S., Turul, A., Yilmaz, M.: The effect of natural sand composition on concrete strength. *Constr. Build. Mater.* **112**, 940–948 (2016)
10. Musafirova, G.Ya., Musafirov, E.V.: Performance assessment of the developed fine-grained concrete modified with a waterproofing compound “HYDROPEN PLAG”. In: *Materials of the XX International Scientific and Methodological Seminar*, pp. 279–281 (2016)
11. Shen, W., Liu, Y., Cao, L., Huo, X., Yang, Z., Zhou, C., He, P., Lu, Z.: Mixing design and microstructure of ultra-high strength concrete with manufactured sand. *Constr. Build. Mater.* **143**, 312–321 (2017)
12. Xiao, J., Qiang, C., Nanni, A., Zhang, K.: Use of sea sand and seawater in concrete construction: current status and future opportunities. *Constr. Build. Mater.* **155**, 1101–1111 (2017)
13. Smolyakov, A.: Influence in cement of mineral additives from milked natural sand and granite balance on the properties of heavy concrete. In: *Contemporary Issues of Concrete and Reinforced Concrete: Collected Research Papers*, vol. 11, pp. 271–287. Minsk. Institute BelNIIS (2019)
14. Potapov, Yu.B., Barabash, D.E., Rogatnev, Yu.F., Panfilov, D.V., Mehdi, J.M.: Deflection calculation of reinforced concrete flexural elements with the top layer made of high quality concrete. *Proc. Moscow State Univ. Civil Eng.* **3**, 26–36 (2016)
15. Belostotskii, A.M., Akimov, P.A.: Analysis of parameters of mechanical safety of high-rise (404-meter) residential building (One Tower) in the Moscow international business center. *Int. J. Comput. Civ. Struct. Eng.* **12**(1), 8–45 (2016)
16. Akhtyamov, V.F., Khafzova, E.N.: Influence of technological non-metallic production wastes on heavy weight concrete properties, vol. 15, № 2, Continuous issue **60**, 261–268 (2018)
17. Paulava, I., Belamesava, K.: Dependence of concrete strength on different methods of basalt fibre adding. In: *Contemporary Issues of Concrete and Reinforced Concrete: Collected Research Papers*, Institute BelNIIS, vol. 11, pp. 63–75 (2019) (Minsk, 2019)
18. Hamdy, G.A., Ahmed, H.E.H., Barakat, A.Y.Y., Mostafa, M.A.: Experimental investigation of self-compacting concrete beams with nano materials additives. *Intellekt. Sist. Proizv.* **17**(3), 20 (2019)
19. Belogurova, O.A., Savarina, M.A., Sharay, T.V.: Refractory concrete from waste from the Kovdorsky GOK on a magnesium phosphate binder. In: *Proceedings of the Fersman Scientific Session of the Scientific Center of the Russian Academy of Sciences*, vol. 16, pp. 18–22 (2019)
20. Palagin, N., Dul'miyeva, A.: Cost-effective design of long cylindrical shells of high-strength sand concrete. *IOP Conf. Ser. Mater. Sci. Angl.* **890**, 012078 (2020)
21. Bazhenov, Yu.M., Demyanova, V.S., Kalashnikov, V.I.: *Modified High-Quality Concrete*. DIA, Moscow (2006)
22. Lvovich, K.I.: *Sand Concrete and Its Use in Construction*. Stroy-Beton, St. Petersburg (2007)
23. Morozov, N.M., Khozin, V.G., Muginov, H.G.: Features of the formation of the structure of modified sand concrete. *Build. Mater. J.* **9**, 72–73 (2010)
24. Kalashnikov, V.I.: Evolution of the development of compositions and changes in the strength of concrete. *Concretions of the present and future*. *Build. Mater. J.* **1–2**, 96–103 (2016)
25. Nizina, T.A., Ponomarev, A.N., Balykov, A.S.: Fine-grained dispersed reinforced concrete based on complex modifying additives. *Build. Mater. Mag.* **9**, 68–72 (2016)
26. Morozov, N.M., Muginov, N.G., Khozin, V.G., Antakov, A.B.: High-strength sand concrete for monolithic construction. *Izvestiya KGASU* **2**, 183–188 (2012)
27. Aitchin, P.C., Neville, A.: High: performance concrete demystified. *Cons. Internet.* **15**(1), 21–26 (1993)
28. Edward, G., Navy, P.: *Fundamentals of High Performance Concrete*, 2nd edn. Wiley (2001)
29. Kaprielov, S.S., Travush, V.I., Karpenko, N.I., Sheinfeld, A.V., Kardumyan, G.S., Kiseleva, Yu.A., Prigozhenko, O.V.: Modified high-strength concrete of classes B80 and B90 in monolithic structures. *Build. Mater. Mag.* **3**, 9–13 (2008)
30. Ilyukhina, E.A., Lakhman, S.I., Miller, A.B., Travush, V.I.: Constructive solutions of the high-rise building (Lakhta Center) in St. Petersburg. *J. (Constr. Sci.)* **3**, 110–121 (2019)

31. Kapriellov, S.S., Sheinfield, A.V., Kardumyan, G.S., Dondukov, V.G.: Modified high-strength fine-grained concrete with improved deformation characteristics. *Concr. Reinf. Concr.* **2**, 2–7 (2006)
32. Khozin, V.G., Khanifov, F.M.: Strategy for the innovative development of concrete construction in the Republic of Tatarstan. In: International Scientific and Technical Conference “High-Strength Concrete: Technology, Construction, Economics (HSC–2016)”, pp. 10–12. KSUAE. Kazan (2016)
33. Mirsayapov, I.L., Nikitin, G.P., Simakov, V.D.: The use of high-strength concrete of B80 class for the supporting system of an 18-storey residential building in the “Salavat Coopere” complex. *Izvestiya KGASU* **3**(45), 145–152 (2018)
34. Palagin, N.G., Trunov, A.N.: Production of solid columns of one-story industrial buildings with overhead cranes from high-strength sand concrete and its economic efficiency. Engineering staff—the future of the innovative economy of Russia: materials of the VI All-Russian. student conf (Yoshkar-Ola, November 10–13, 2020): at 8 o'clock. Part 5: Innovations in construction, environmental management and technosphere safety. Yoshkar-Ola: LLC “Vertola”, pp. 78–81 (2020)

# Relationship of Shear Force and Punching Analysis of Reinforced Concrete Slabs



D. A. Pekin 

## 1 Introduction

The calculation of reinforced concrete slabs for shear forces and punching was dealt with by leading Russian specialists both in the Soviet period and at the present time. Taking into account the actual sequence of the development of the theory of reinforced concrete, methods of calculation and implementation of structural solutions, the initial attention was mainly paid to the rod elements. In this regard, and also due to the relatively small volume of construction from monolithic reinforced concrete until the beginning of the 90s of the last century, for the calculation of slabs for the action of shear forces, assumptions and a methodology based on the rod analogy were used or only the calculation for punching was performed [1].

## 2 Relationship of Shear Force and Punching Failure

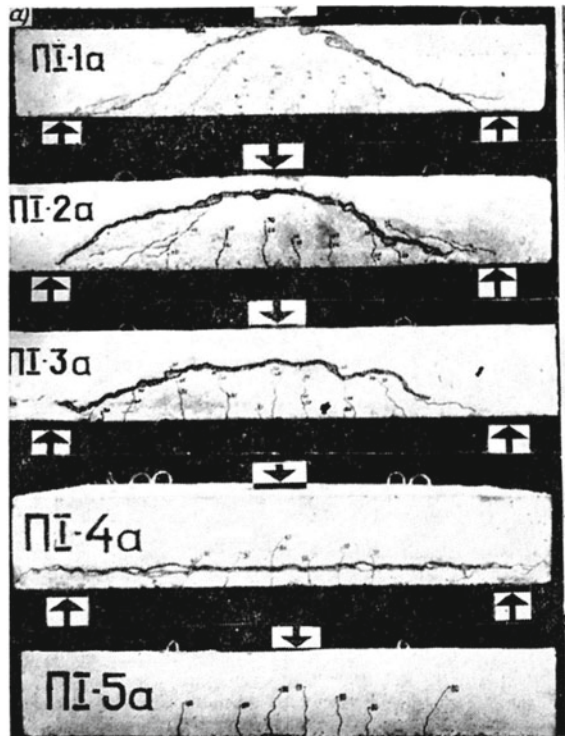
At Russian Research, Design and Technological Institute of Concrete and Reinforced Concrete, special experimental studies were carried out [2] to compare the mechanisms of failure along a sloping section and from punching, as well as to search for transitional forms that allow developing criteria for applying the calculation method for the action of shear forces or punching. The prototypes were tested, supported on two sides on a span of 1.4 m, 300 mm high, with a loading platform of 200 × 200 mm in the middle of the span (i.e., the sloping section span was 0.6 m), while varying their width in multiples of the size of the loading platform—200 (III-1a), 3 × 200 (III-2a), 5 × 200 (III-3a) and 7 × 200 (III-4a) mm, as well as control prototype with dimensions 1.4 × 1.4 × 0.3 (h) m (III-5a), supported on 4 sides, to implement

---

D. A. Pekin (✉)

Moscow State University of Civil Engineering, Moscow, Russia

**Fig. 1** Features of prototypes failure



standard punching mechanism (the marking of the prototypes, indicated in brackets, is shown in the photographs in Fig. 1).

Based on the results of this research work, the important issue of the similarity of fracture mechanisms in shear force and from punching was not considered, despite the results obtained during the experiments:

1. The formation and development of main sloping cracks was ignored in prototypes with dimensions close to square in plan, in which the punching mechanism was realized;
2. There were no proposals to improve the punching shear design method, which then and now does not take into account the formation and development of the main sloping cracks;
3. The effect of bending of the prototypes and the change in the height of the compressed zone of concrete both on the lateral faces of the prototypes and along the width of the cross section with an increase in its width were not taken into account (the height of the compressed zone of concrete along the width of the prototypes changes, increasing from the middle of the cross section to the lateral edges).

The following figure shows photographs of prototypes after failure, demonstrating the features of the formation and development of normal and sloping cracks on the





**Fig. 2** Prototype in [7] after punching failure. Side view

free lateral faces of elements, with the exception of sample III-5a, which had a support.

A contradiction in the picture of the formation and development of cracks on the lateral face for prototype III-5a, shown in Fig. 1, which in the description [2] is indicated as supported on four sides, but at the same time having developed normal cracks on the lateral surface, characteristic of the support of the prototype only on two sides (when supported along the contour, such normal cracks on the lateral faces cannot form, especially along mid-span, see Fig. 2). It is possible that the prototype was also tested with support on both sides, or another photograph was inserted, or this could be due to other reasons related to the test bench.

### 3 Shear Force Analysis of Reinforced Concrete Slabs

In Russian modern building codes, the method of calculating slabs for the action of shear forces appeared relatively recently and immediately caused many questions from designers and developers of programs for calculating building structures, since the results of the calculation significantly increased the required amount of shear reinforcement. The calculation of plates for the action of shear forces in accordance with clause 8.1.55 of SP 63.13330 should be performed according to the formula:

$$\frac{Q_x}{Q_{x,ult}} + \frac{Q_y}{Q_{y,ult}} \leq 1 \quad (1)$$

where  $Q_x$  and  $Q_y$  are shear forces acting on the lateral sides of the flat selected element;  $Q_{x,ult}$  and  $Q_{y,ult}$  are the ultimate shear forces perceived by a flat selected element and calculated by the formula:

$$Q_{ult} = Q_b + Q_{sw} \quad (2)$$

where  $Q_b$  and  $Q_{sw}$  are the ultimate shear forces perceived, respectively, by concrete and shear reinforcement and determined by the formulas:

$$Q_b = 0,5R_{bt}bh_0 \quad (3)$$

$$Q_{sw} = \frac{R_{sw}A_{sw}}{s_w}h_0 \quad (4)$$

where  $b$  and  $h_0$  the width and effective depth of the section, respectively;  $A_{sw}$  and  $s_w$  the area of the shear reinforcement located in one normal section and the step of these rows, respectively;  $R_{bt}$  and  $R_{sw}$  tensile strength of concrete and shear reinforcement, respectively.

Previously, without taking into account this requirement, the calculation for the action of shear forces was carried out by analogy with the rods and for each direction separately, i.e., each term on the left side of expression (1) should not exceed one. Before the standard requirements of SP 63.13330.2012 came into effect in our country, millions of square meters of monolithic reinforced concrete flat slabs and foundation plates were built, which, taking into account these requirements, may no longer satisfy the ULS, and if necessary, reconstruction of buildings or structures, even if related or insignificant changes for the slabs may require strengthening to meet this requirement of the codes.

If we analyze this formula on the basis of a special case with equality  $Q_{x,ult} = Q_{y,ult} = Q_{ult}$  and  $Q_x = Q_y = Q$  we get:

$$\frac{Q_x}{Q_{ult}} + \frac{Q_y}{Q_{ult}} = \frac{Q_x + Q_y}{Q_{ult}} = \frac{2Q}{Q_{ult}} \leq 1 \quad (5)$$

Consequently, in this case, the ultimate shear force perceived by a flat highlighted element must be greater than twice the shear force acting on the lateral side of the element in any direction, which leads to a two-fold reserve of bearing capacity relative to consideration in separate directions. Obviously, this requirement, together with the empirical approach in determining the ultimate force for concrete according to Formula (3), which is borrowed and is only allowed in the design of rods, leads to a discrepancy between the physical nature of the shear force failure mechanism and an unjustified reserve of bearing capacity that has passed the test of time.

Another proposal for the calculation of reinforced concrete slabs of monolithic frames of multi-storey civil buildings for the action of shear forces on page 24 [3] leads to a less significant reserve of bearing capacity:

$$\left(\frac{Q_x}{Q_{x,ult}}\right)^2 + \left(\frac{Q_y}{Q_{y,ult}}\right)^2 \leq 1, \quad (6)$$

since the ratios in brackets must be less than one, and squaring them decreases the value of the sum. After similar transformations of this formula to consider the particular case  $Q_{x,ult} = Q_{y,ult} = Q_{ult}$  and  $Q_x = Q_y = Q$  we get:

$$\left(\frac{Q_x}{Q_{ult}}\right)^2 + \left(\frac{Q_y}{Q_{ult}}\right)^2 = \frac{Q_x^2 + Q_y^2}{Q_{ult}^2} = \frac{2Q^2}{Q_{ult}^2} \leq 1 \quad (7)$$

Therefore, in this case, the square of the ultimate shear force perceived by a flat highlighted element must be greater than twice the square of the shear force acting on the lateral side of the element in any direction, which leads to a bearing capacity margin equal to 41% (the square root of 2 is  $\sim 1.41$ ) regarding consideration in separate directions.

In addition, it should be noted that the Formula (6) was previously used to calculate the action of the shear forces of double curvature bending (subject to bending in a plane not parallel to the axes of symmetry of the cross section) of rod reinforced concrete elements of rectangular section in accordance with clause 7.39 of SNiP II-B.1-62. And thus, when calculating one sloping section, horizontal and vertical shear bars (or stirrup segments) were taken into account to determine the ultimate shear forces along the reinforcement in two directions  $Q_{sw,x}$  and  $Q_{sw,y}$ ,  $y$ . In this case, the shear forces  $Q_x$  and  $Q_y$  act in the same section, in contrast to plates. And this nuance, obviously, contradicts the physical meaning and those test results, on the basis of which it was proposed to use this approach for calculating double curvature bent elements of rectangular section, which does not allow to unambiguously determine the possibility of using this formula for calculating reinforced concrete slabs.

In this regard, we can agree with the proposal [4] to take into account the resultant shear forces in the element and the need to consider the shear reinforcement distributed over the area of the calculated element (one amount of reinforcement for two directions), which leads to the following shape transformations of expression (1):

$$\frac{\sqrt{Q_x^2 + Q_y^2}}{Q_{ult,min}} \leq 1 \quad (8)$$

where  $Q_{ult,min}$  is the minimum of the ultimate shear forces perceived by a flat selected element and calculated from the Formula (2). Or taking into account the resulting concrete in two directions and the total amount of shear reinforcement:

$$\frac{\sqrt{Q_x^2 + Q_y^2}}{\sqrt{Q_{bx}^2 + Q_{by}^2 + Q_{sw}}} \leq 1 \quad (9)$$

where  $Q_{bx}$  and  $Q_{by}$  are the ultimate shear forces perceived by concrete in the  $x$  and  $y$  directions, respectively;  $Q_{sw}$  bearing capacity for forces reinforcement:

$$Q_{sw} = R_{sw} A_{sw} h_0 \quad (10)$$

where  $h_0$  is the effective depth of section;  $A_{sw}$  is the total area of the shear reinforcement located in the element.

It should be noted that in SNiP 2.03.01-84\* and Eurocode 2, there are no requirements and special calculation methods specifically for reinforced concrete slabs for the action of shear forces. And in accordance with clause 5.26 of SNiP 2.03.01-84\* in solid slabs, regardless of height, it is allowed not to install shear reinforcement, while ensuring the calculation requirements according to the instructions in clause 3.32 (calculation of reinforced concrete elements without shear reinforcement for the action of a shear force to ensure strength along an sloping crack), with the exception of areas where punching shear mechanism is possible. The situation is similar in Eurocode 2.

Modern theoretical studies and proposals for improving the method of punching shear [5, 6] also continue the traditional direction and use classical assumptions when calculating for punching in the form of the absence of main sloping cracks and the possibility of uniform distribution of shear forces along the sloping face of the punching pyramid, which leads to the following contradictions:

1. When determining the bearing capacity for punching, the addition of the bearing capacity for concrete at stage I of stress–strain behavior (in the absence of cracks) and the bearing capacity for shear reinforcement at stage III of SSB (with cracks) is performed;
2. The assumption of a uniform distribution of shear stresses along the sloping faces of the punching shear pyramid has some limitations, since the relative deformations of concrete elongation are extremely small, and do not allow in practice to develop such a uniform distribution of stresses.

The proposed approach, taking into account the accepted assumptions, can be valid only for certain cases, for example, for concrete structures, where bending stresses, due to their smallness, can be neglected, or in prestressed reinforced concrete structures in the absence of normal and sloping cracks.

## 4 Punching Experimental Analysis of Flat Slab

An analysis of the normative methods of punching shear design in accordance with SNiP 2.03.01-84\*, SP 63.13330.2012 and Eurocode 2, taking into account the experimental data obtained, and a proposal for the development of the method are published in article [7]. According to the test results, it was found that the sloping angle of the punching shear pyramid (main sloping crack) was about  $20^\circ$  and normal cracks on the lateral surfaces (in contrast to III-5a shown in Fig. 1) did not form, due to the impossibility of bending the element directly on the support contour.

For testing [7], a support contour with dimensions in plan of  $2.16 \times 2.16 \times 0.24$  (h) m was made from a paired channel No. 24 of a box-shaped cross section. The support contour was installed on 8 racks 1.2 m high, resting on the load-bearing floor. The slab prototype was installed on a sand-cement mortar with a support length of 100 mm along the supporting contour. The loading was carried out through a load plate by 4 hydraulic power exciters from a common collector, capable of creating

a force of 1000 kN each. The total mass of the tooling applied before the start of the experiment was 80 kN. Further, the load applied to the slab fragment through the column changed stepwise, increasing by 200 kN with an interval of 20 min, immediately until the moment of destruction.

In the manufacture of a slab fragment, heavy concrete of class B30 and reinforcement of class A500C 18Ø12 mm with a step of 100 mm in two directions in the lower zone at a distance from the center of 1 row of reinforcement to the edge of the slab equal to 25 mm were used. The overall dimensions of the slab fragment are  $2.0 \times 2.0 \times 0.24$  (h) m. The column head was made in the form of a cube with a side size of 0.5 m and structural reinforcement of longitudinal (4Ø16 mm) and shear reinforcement (5Ø8 mm with step 100 mm).

It is interesting to note the general regularity according to the test results of beams and slabs without shear reinforcement in [2, 7], associated with the formation of main sloping cracks from supports on stretched faces to column face on compressed faces of prototype with a slope angle significantly less than  $45^\circ$ . In addition, an important not previously noted nuance according to the results of observation of the destruction of the sample in [7] is Fig. 3—this is the exit of the main sloping cracks on a stretched horizontal surface at opposite supports in the direction of longitudinal reinforcement located with a smaller concrete cover, and the absence of similar cracks of such an development on the stretched surface in the perpendicular direction, which is associated with the operation of the hydraulic loading system and almost instantaneous zeroing pressure (external load) upon destruction of the sample.

In this case, after the transition to the plastic stage of the structure's operation, when most of the bars of two directions cease to resist external load and a significant increase in deflections is recorded, the factor of reinforcement placement in thickness begins to influence—the closer the longitudinal reinforcement is to the tensioned surface of the slab, the more it bends near the support and in the event of an inflection point in the reinforcement or a certain angle of rotation of the section, it begins to provoke concrete cleavage due to the occurrence of reactive pressure of the reinforcement and the exit of the main sloping cracks on the tensioned surface of the prototype, which, together with the destruction of the compressed zone of concrete around the head of the column (load area) by cut (not necessarily in the plane of the normal section) leads to the formation of a punching shear pyramid.

It should be noted that most of the tests of various conventional prototypes for punching without shear reinforcement were carried out with an almost equal ratio of the sloping section span (the length of the horizontal projection of an sloping crack) to the height of the elements, which led to the formation of a punching shear pyramid at an angle close to  $45^\circ$ . This is due to the limitation of the dimensions in terms of the tested images by the capabilities of laboratory equipment (4 rack presses). But if it was possible to test samples of large dimensions in plan [2, 7], then the angle of sloping reached  $20^\circ$ . It is also obvious that in the absence of bending of the specimens (at  $h_0/c > 2$ ) or sufficient resistance of concrete to tensile stresses without cracking and the ratio of the height of the elements to the sloping section span of more than one, the slope of the punching shear pyramid will exceed  $45^\circ$  and tend to  $90^\circ$  in the



**Fig. 3** Prototype in [7] after punching failure. Tensioned surface

limit:

$$\lim_{h_0/c \rightarrow \infty} \varphi = 90^\circ \quad (11)$$

where  $c$  and  $\varphi$  are the sloping section span and the angle of sloping, respectively.

At the same time, to obtain results close to the experimental data, it is necessary, instead of the tensile resistance  $R_{bt}$  of concrete, to use the concrete shear resistance  $R_{bs}$ , which reaches, according to various estimates, up to  $2.5R_{bt}$  without taking into account the lateral compression [8].

Another aspect is related to the options for loading reinforced concrete slabs and their support on vertical supporting structures. Obviously, in flat slabs with support on columns, pylons or walls under the action of loads uniformly distributed over the area (or close to them) and sufficient bearing capacity for the action of shear forces only on concrete, there is no need to calculate the slabs for the shear force

outside the support zones. And vice versa, in the case of a concentrated load acting on the overlap and a sufficient bearing capacity with respect to the shear force only on concrete at the place of its application, there is no need to check the strength on the supports. Similar statements apply to foundation slabs as well. Despite all its obviousness, this of course requires rigorous proof. Using the example of a flat slab, uniformly distributed load and the same dimensions of elements in the plan:

1. Given:

- $q$ —uniformly distributed load;
- $A_i$ —area of the  $i$ -th slab element;
- $R_j$ —reaction in the  $j$ -th vertical support;
- $n$ —number of elements of flat slabs;
- $m$ —number of supports.

2. Let's compose the equation of equilibrium of the acting support reactions and vertical forces on the vertical axis  $Z$ :

$$\sum Q_z = \sum_{i=1}^n q A_i + \sum_{j=1}^m R_j = 0 \quad (12)$$

3. Since in practice, the number of flat slab elements is always significantly greater than the number of supports:

$$n \gg m, \quad (13)$$

then, taking into account equality (12):

$$q A_i < R_j, \quad (14)$$

then, according to (14), while ensuring the bearing capacity for the action of shear forces on concrete on the support, the strength of any individual slab element will be ensured, which was required to be proved.

## 5 Punching Catastrophic Failure Analysis

It should also be noted that in real monolithic reinforced concrete flat slabs under the action of uniformly distributed loads, the main sloping cracks can form at an angle close to  $45^\circ$ . This is confirmed by the specific example shown in Fig. 4, catastrophic failure of the flat slab of the stylobate part of the building at the interface with the column at the facility in Moscow near the Paveletsky railway station in 2009. Then, at the stage of developing the detailed design documentation, the new design organization made changes to the initial project, which passed the examination, in



**Fig. 4** Flat slab after punching failure

the form of excluding capitals and reducing the cross section of columns, which led to the implementation of a punching mechanism.

This aspect was most likely known to the authors of the method for calculating reinforced concrete slabs for punching and therefore, taking into account other experimental studies, served as the basis for using the corresponding sloping angle of the pyramid in the codes. But nevertheless, such an approach, taking into account a wide variety of design solutions, is not universal, has a number of the above disadvantages and requires further development.

In the following publications, on the basis of experimental studies [2, 7, 8] and proposals for improving the method of calculating slabs for punching shear in [7], a comparative analysis of the calculations of the bearing capacity for the action of shear forces and punching shear will be carried out to develop a unified and universal approach to the calculation of reinforced concrete slabs.

## 6 Conclusions

1. Based on the analysis of the experimental data presented, it can be stated that the failure of plates under the action of shear forces and from punching has a related nature and a similar mechanism due to the formation and development of main sloping cracks.



2. The current normative calculation method in accordance with the requirements of clause 8.1.55 of SP 63.13330.2018 for the action of shear forces has a significant reserve for the bearing capacity and may lead to the need to strengthen reinforced concrete slabs not affected by the reconstruction of buildings and structures.
3. Against this background and the current volume of construction with the use of monolithic reinforced concrete, the creation of a unified and universal method for calculating reinforced concrete slabs for the action of shear forces and punching is an urgent task.

## References

1. Shtaerman, M., Ivyansky, A.: Flat Slabs. State Publishing House of Literature on Construction and Architecture, Moscow (1953)
2. Gvozdev, A., Zalesov, A., Ermukhanov, K.: Transitional forms between failure along a sloping section and punching. *Concr. Reinf. Concr.* **3**, 27–29 (1980)
3. Ivanov, A.: Development of theory and applied methods for assessing the force resistance of monolithic civil buildings, taking into account the nonlinearity of deformation. Abstract of the Dissertation of Doctor of Technical Sciences, Moscow (2008)
4. Karpenko, S.: On modern methods of calculating high-rise buildings from monolithic reinforced concrete. *High Rise Build.* **3**, 34–39 (2007)
5. Karpenko, N.: On the construction of a general method for calculating reinforced concrete slabs for punching, taking into account the influence of moments. *MGSU Bull.* **3**, 86–91 (2011)
6. Karpenko, N.: A practical method for calculating reinforced concrete slabs for punching according to various schemes. *Concr. Reinf. Concr.* **5**, 10–16 (2012)
7. Pekin, D.: Influence of bending on the punching mechanism of the support zone of a reinforced concrete slab. *Ind. Civ. Constr.* **10**, 20–28 (2019)
8. Petrov, A.: Experimental study of concrete under compression and shear loading. *Concr. Reinf. Concr.* **11**, 34–36 (1965)

# Modeling the Bearing Capacity of Tank Trucks Filled with Bulk Material in Bending



M. V. Petrov  and E. G. Gonik 

## 1 Introduction

Tank trucks are used for transportation of various bulk materials (cement, flour, grain, sugar, etc.) by vehicles. They are manufactured at various factories in Russia and abroad.

Such enterprises are OOO SeverMolMash (Vologda), OOO Gero (St. Petersburg), ZAO Cheboksary enterprise Sespel (Cheboksary), machine-building plants Bonum (Rostov-on-Don), “Betsema” (Krasnogorsk, Moscow region), “Alekseevka KhimMash” (Voronezh region), Tropper GmbH (Austria), MAISONNEUVE group (France), Hendricks Fahrzeugwerke GmbH., SPITZER SILO FAHRZEUGE GmbH, Feldbrze Speinder (Germany), etc.

Tank trucks (Fig. 1) are thin-walled cylindrical shells with diameters up to 2500 mm, length up to 16,000 mm, and wall thickness up to 10 mm.

The tank is attached to the vehicle on supports. Under the influence of the mass of the load, it bends between the supports. When lifted to unload the cargo, the tank bends and may become unstable.

The stability of empty cylindrical shells has been experimentally and theoretically investigated in many scientific works [1–17]. Loss of stability in bending of thin-walled shells filled with bulk material is considered in [18–24].

In order not to lose stability, experimental and theoretical studies, mathematical models are needed for correct calculations of the geometric dimensions of the tank that satisfy the conditions for bending stability. Therefore, such studies are relevant.

The load-bearing capacity of a tanker truck will be estimated by the loss of its stability in bending. The aim of the work is to model the bearing capacity of a tanker filled with bulk material during bending and its experimental substantiation.

---

M. V. Petrov · E. G. Gonik (✉)

Department of Building Structures, Faculty of Civil Engineering, Chuvash State University Named After I.N. Ulyanov, Moskovsky Avenue, 15, Chuvash Republic, Volga Federal District, 428015 Cheboksary, Russia



**Fig. 1** Tank truck for transportation of liquid and bulk materials

## 2 Experimental Research

First, let us study the behavior of model specimens under load. The experiments were carried out on model samples similar to full-scale tank trucks. The material and dimensions of the samples are shown in Table 1.

The samples were rigidly fixed at one end; the other end was free. There a lateral force  $F$  was applied, which gradually increased until stability was lost. The value of the force  $F$  and the corresponding deflection  $y$  were measured (Fig. 2). The experiments were carried out on empty samples and filled with iron powder to 90% of the volume. The results of experiments and calculations are presented in Table 2.

**Table 1** Dimensions of the tested samples

Series of samples	Radii $R$ (mm)	Wall thickness $h$ (mm)	Length $L$ (mm)	$h/R$	$L/R$	Sample material
1	31,8	0,1	135	0,003	4,12	Aluminum alloy 3004
2	41,6	0,12	165	0,0029	3,96	Aluminum alloy 3004
3	41,2	0,42	171	0,01	4,15	Alloy D16T
4	41,2	0,42	348	0,01	8,3	Alloy D16T

**Fig. 2** Deflection versus force plot. Graph (1) corresponds to samples without filler, and graph (2) corresponds to samples filled with bulk material for samples of the first series

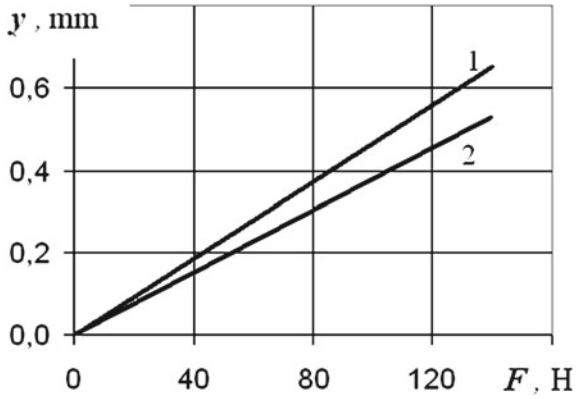


**Table 2** Comparison of experimental results and analytical solution

Series of samples	Percentage of sample filling (%)	Critical force, $F_{cr}$ (kN)		Difference $F_{cr}$ (%)	Increase in $F_{cr}$ for a filled sample, % in the experiment
		Experiment	Calculation		
1	0 (empty)	0,153	0,16	4,5	40,5
	90	0,215	0,18	16	
2	0	0,262	0,269	2,7	16,9
	90	0,341	0,265	22,3	
3	0	1,77	2,21	25	26,3
	90	2,235	2,07	7,5	
4	0	0,83	1,1	32,5	12,3
	90	0,932	1,15	23,4	

Experimental studies show that the loss of stability occurs in the elastic stage of material operation (Fig. 2). Therefore, for mathematical modeling, you can use the principle of superposition. The loss of stability of the samples is characterized by the formation of dents on the surface (Fig. 3) shows aluminum samples of two series after the experiments.

### 3 Design Ratios

For empty thin-walled shells, the critical stress  $\sigma_{cr}$  in bending is recommended in [1] to be calculated by the formula:

$$\sigma_{cr}^I = \kappa(l)E \frac{h}{R}, \tag{1}$$



**Fig. 3** Shape of shells after loss of stability

where  $E$  is the modulus of elasticity of the shell material;  $h$ -wall thickness;  $R$ -radius of the sample. The coefficient  $k(L)$  takes values 0,3 for medium-length shells, 0,22 for longer shells.

The flexural stability of thin-walled shells filled with bulk material is additionally influenced by the weight load and the resistance of bulk material to the formation of dents, similar to the action of internal pressure.

The weight load along the length of the shell is evenly distributed and the maximum compressive stress in the buckling zone is calculated from the relationship [20, 22]:

$$\sigma_u = \frac{M}{W}, \quad (2)$$

where  $M$  is the bending moment in the cross section at the point of buckling;  $W$  is the axial moment of resistance of the shell.

The value of the bending moment depends on the conditions for fastening the shell. For example, for a console-pinned shell,

$$M = \frac{ql^2}{2}, \quad (3)$$

where  $q$ —uniformly distributed weight load,  $l$ —distance from the free end of the shell to the point of buckling.

For a shell hinged at the ends:

$$M = \frac{ql^2}{8} \quad (4)$$

where  $l$  is the distance between the hinged supports.

Taking the material to be ideally free-flowing, the internal hydrostatic pressure is calculated by the formula [21]:

$$P = \rho g H, \quad (5)$$

where  $\rho$  is the bulk density of the bulk material,  $H$  is the height of the aggregate, and  $g = 9.8 \text{ m/s}^2$ .

Since the shell is in a momentless stressed state before loss of stability, the pressure of the bulk material creates an axial stress at the point of loss of stability equal to [1]:

$$\sigma_p = \frac{PD}{4h} = \frac{PR}{2h} = \frac{\rho g HR}{2h}. \quad (6)$$

Using the principle of superposition and relationship (1–6), the critical stress is

$$\sigma_{cr} = \sigma'_{cr} + \sigma_u + \sigma_{p'} = k(l)E \frac{h}{R} + \frac{M}{W} + \frac{\rho g HR}{2h}. \quad (7)$$

The critical bending moment  $M_{cr}$  at the point of buckling is equal to

$$M_{cr} = \sigma_{cr} \cdot W. \quad (8)$$

For a cantilevered tank, the lateral critical force is

$$Q_{cr} = \frac{M_{cr}}{l}. \quad (9)$$

If we take into account the weight load, then

$$Q_{cr} = F_{cr} + ql = \frac{M_{cr}}{l}, \quad (10)$$

where  $F_{cr}$  is the critical concentrated force.

From formula (10), the critical force is equal to

$$F_{cr} = \frac{M_{cr}}{l} - ql. \quad (11)$$

The permissible lateral force, taking into account the safety factor “ $n$ ”, is equal to

$$F = \frac{F_{cr}}{n}$$

Expression (11) allows you to calculate the critical length of the tank for the transportation of bulk material:

$$Fl_{cr} = M_{cr} - ql_{cr}^2.$$

From here,

$$l_{cr} = \frac{-F + \sqrt{F^2 + 4qM_{cr}}}{2q}. \quad (12)$$

If the tank is fixed on two end pivot bearings, then the critical bending moment is

$$M_{cr} = R \frac{l}{2} - q_{cr} \frac{l^2}{8} = q_{cr} \frac{l^2}{4} - q_{cr} \frac{l^2}{8} = q_{cr} \frac{l^2}{8} = \sigma_{cr} \cdot W, \quad (13)$$

where  $R$  is the reaction of the support.

From dependence (13), the critical weight load

$$q_{cr} = \frac{8\sigma_{cr}W}{l^2}. \quad (14)$$

Critical tank length:

$$l_{cr} = \sqrt{\frac{8\sigma_{cr}W}{q}}. \quad (15)$$

Let us calculate the critical forces  $F_{cr}$  for model samples using the proposed method and compare with the experimental results (Table 2). Table 2 shows that the critical forces obtained by calculations and experiments differ within 23.4%, which is quite satisfactory for factory conditions.

## 4 Conclusions

1. The method for calculating the bearing capacity is verified by experiments.
2. Using dependencies (8–15), you can calculate for the tank critical bending moment, shear load, length.

## References




1. Volmir, A.S., Nauka, M.: Stability of Deformable Systems, p. 984s (1967)
2. Darevsky, V.M.: Stability of a cantilever cylindrical shell under bending by a shear force with torsion and internal pressure. *Calculation Spat. Struct.* **5**, 431–449 (1959)
3. Ilgamov, M.A.: Experimental Study of the Stability of a Cantilevered Cylindrical Shell Under the Action of a Transverse Force and Internal Pressure. *Research on the Theory of Plates and Shells*, vol. 2. Publishing House of Kazan University, pp. 186–191 (1964)
4. Konoplev, Yu.G.: Experimental study of the stability of a cylindrical shell under the action of an arbitrary number of local axial forces. *Res. Theor. Plates Shells* **6–7**, 481–484 (1970)
5. Bazhenov, V.G., Kibets, A.I., Petrov, M.V., Shoshin, D.V.: Numerical analysis of deformation, loss of stability and supercritical behavior of large-sized containers for road transportation of bulk cargo. *Prob. Strength Plast.* **70**, 89–97 (2008)
6. Bazhenov, V.G., Gonik, E.G., Kibets, A.I., Petrov, M.V., Fedorova, T.G.: Stability and supercritical behavior of large-size tankers for transportation of loose goods. *J. Mach. Manuf. Reliab.* **44(5)**, 422–427 (2015)
7. Bazhenov, V.G., Gonik, E.G., Kibets, A.I., Petrov, M.V., Fedorova, T.G., Frolova, I.A.: Stability and supercritical behavior of thin-walled cylindrical shell with discrete aggregate in bending. *Mater. Phys. Mech.* **28**, 16–20 (2016)
8. Petrov, M.V.: Experimental study of the loss of stability of thin-walled shells in pure bending. In: Petrov, M.V., Fedorova, T.G., Gonik, E.G. (eds.) *Bulletin of the Chuvash State Pedagogical University (I. Yakovleva). Limit State Mechanics*, vol. 2, no. 24, pp. 119–125 (2015)
9. Gonik, E.G., Kibets, A.I., Petrov, M.V., Fedorova, T.G., Frolova, I.A.: Influence of approximation of the deformation diagram on critical loads during transverse bending of a cylindrical shell. *Probl. Strength Plast.* **79(2)**, 169–181 (2017)
10. Gonik, E.G.: Experimental study of the loss of stability of cantilevered cylindrical thin-walled shells during transverse bending (Gonik, E.G., Petrov, M.V., Fedorova, T.G. (eds.)) *Problems Strength Plast.* **78(2)**, 228–235 (2016)
11. Mossakovsky, V.I.: Modeling the bearing capacity of cylindrical shells. In: Mossakovsky, V.I., Manevich, L.I., Miltsyn, A.M. (eds.) *Kiev Naukova Dumka*, p. 141 (1977)
12. Konovalov, Yu.V.: Bending of an infinite cylindrical shell. *Priklad. Mat. Mehan.* **4(5–6)**, 35–54 (1940)
13. Manevich, A.I., Ponomarenko, E.A., Prokopalo, E.F.: Stability of orthotropic cylindrical shells under bending by shear force. *Communication 1. Theory Prob. Strength* **1**, 101–111 (2013)
14. Paimushin, V.N.: Torsion, bending and bending-torsional forms of buckling of a cylindrical shell under combined types of loading. *Izv. RAS. MTT.* **3**, 125–136 (2007)
15. Sharinov, I.L.: Strained state of a cylindrical cantilever shell under the action of a concentrated normal force applied to a free edge (Sharinov, I.L. (ed.)) *Eng. J.* **5(2)**, 284–292 (1965)
16. Altukher, G.M., Evlanov, V.V.: Nonaxisymmetrical longitudinal—transversebending of cylindrical shells under the combined influence of pure bending and pressure. *Strength Mater.* **13(10)**, 1277–1282 (1982)
17. Mallock, A.: Note on the instability of tubes subjected to end pressure and on the folds in a flexible material. *Proc. Roy. Soc.* **81(A-549)**, 388–393 (1908)
18. Bazhenov, V.G.: Experimental and theoretical study of elastoplastic buckling of cylindrical shells filled with bulk material under the action of transverse force (Bazhenov, V.G., Gonik, E.G., Kibets, A.I., Petrov, M.V., Fedorova, T.G., Frolova, I.A. (eds.)) *Scientific Notes of Kazan University. Physics and Mathematics*, vol. 159, no. 3, pp. 282–295 (2017)
19. Gonik, E.G.: Experimental study of elastoplastic deformation and loss of stability of reinforced cylindrical shells with filler during bending (Gonik, E.G., Kibets, A.I., Petrov, M.V., Fedorova, T.G. (eds.)) *Problems Strength Plast.* **75(3)**, 215–220 (2013)
20. Petrov, M.V.: Stability in bending of thin-walled shells filled with various loose materials. In: Petrov, M.V., Gonik, E.G., Fedorov, T.G. (eds.) *Bulletin of ChGPU im (AND I. Yakovleva). Limit State Mechanics*, vol. 4, no. 34, pp 52–58 (2017)



21. Petrov, M.V.: A method of approximate calculation of stability in transverse bending of thin-walled cylindrical shells of medium length, filled with loose material. In: Petrov, M.V., Fedorova, T.G., Gonik, E.G., Pfanenstil, N.G. (eds.) Bulletin of ChGPU im (I. Yakovleva). Limit State Mechanics, vol. 4, no. 38, pp. 120–128 (2018)
22. Gonik, E.G.: Calculation of the limiting state of thin-walled cylindrical shells during bending filled with loose filler. In: Gonik, E.G., Petrov, M.V. (eds.) Bulletin of ChGPU im (I. Yakovleva). Limit State Mechanics, vol. 2, no. 40, pp. 117–127 (2019)
23. Gonik, E.G.: Investigation of elastoplastic bending and loss of stability of shells of revolution taking into account contact interaction with a loose filler. In: Gonik, E.G., Kibets, A.I., Petrov, M.V., Fedorova, T.G., Frolov, I.A. (eds.) Dynamic and Technological Problems of Mechanics and Structures and Continuous Media. Proceedings of the XXIII International Symposium. A.G. Gorshkov, pp 57–59 (2017)
24. Petrov, M.V.: Influence of imperfections in the geometry of thin-walled cylindrical shells filled with bulk material on their stability in bending. In: Petrov, M.V., Fedorova, T.G., Mikhailov, B.V., Gonik, E.G., Pfanenstil, N.G. (eds.) NASKR-2018. Publishing House of Chuvash.un-ta, Cheboksary, pp. 148–156 (2018)

# Bearing Capacity of Reinforced Masonry Under Central Compression Based on the Deformation Parameters of Its Components



Alexey N. Plotnikov , Tatyana Vyacheslavovna Romanova, Boris Vasilievich Mikhailov , Olga Stanislavovna Yakovleva , and Mikhail Yurievich Ivanov 

## 1 Introduction

To increase the bearing capacity, reduce material consumption and, accordingly, the cost of construction, masonry reinforcement is traditionally used. Mesh reinforcement located in the horizontal joints of the masonry limits lateral deformations. As a result, the compressive efficiency of the brick increases, as well as crack resistance.

According to the design codes used in the calculation of reinforced masonry, the actual stress–strain state of the reinforced masonry components is not taken into account. New materials are emerging, such as porous bricks and composite rebar. They require taking into account their specific properties and mechanisms of operation and destruction of reinforced-masonry structures.

There are several approaches to modeling the work of masonry. They can be classified into two principal groups. In the first group, which forms the basis of the current SP15.13330.2012 “Stone and reinforced-stone structures”, the method of sections with homogenization is used. In both domestic and foreign (Eurocode 6) regulatory documents, masonry is considered as a homogeneous structure in which the physical and mechanical characteristics of its components (brick and mortar) are averaged. In the second group of calculation methods, masonry is represented by a material with a complex composite structure, multi-modular materials with radically different characteristics.

In the work of Antakov and Sokolov [1], diagrams of deformation of masonry of compressed structures were obtained on the basis of the theory of the resistance of anisotropic materials to compression, taking into account the values of the resistance of the material to tension and shear when determining the compressive strength. The authors, taking into account the analysis of a variety of experimental data on testing

---

A. N. Plotnikov (✉) · T. V. Romanova · B. V. Mikhailov · O. S. Yakovleva · M. Y. Ivanov  
Chuvash State University Named After I.N. Ulyanov (ChuvSU), 15 Moskovskiy Prospekt,  
Cheboksary, Russian Federation

prototypes, analytically described the stages of the stress state. When determining the magnitudes of the pull-off, shear, and crushing forces, they used the strength characteristics of the masonry: standard tensile strength  $R_t$ , shear  $R_{sh}$ , compression  $R$  and geometric parameters—the areas of the corresponding surfaces  $A_t, A_{sh}, A_{ef}$ .

In works [2–4] it is shown that in order to use the given deformation criteria in the calculation of elements and structures, appropriate deformation diagrams of the material are required—during tension, shear, and compression.

Modeling of the properties of masonry has recently been carried out by a number of researchers. In the work of Kashevarova [5], taking into account orthotropy, identified criteria that consider the structural destruction and deformation softening of the masonry. Possible values of the shear coefficient of the layers, which provide the minimum level of stress intensity, have been determined. Criteria for tensile and shear strength of brick and mortar are considered; parameters of the strength of the contact point between brick and mortar in a horizontal joint are applied. The tests have shown that the strength in a complex stress state depends on the angle of inclination of the load to the horizontal seams, the ratio of the nature of the load. Moreover, the deformation characteristics of the masonry components themselves are not specified.

Pangaeva [6] allows you to select the composition and system of ligation of masonry in a targeted manner, takes into account the different nature of deformation and destruction of typical elements of masonry—butt and spoon rows, vertical and horizontal mortar joints. He showed that a fragment of 510 mm in length from five spoonfuls of brick is sufficient to obtain reliable data on the stress–strain state of brick and mortar can be taken as a typical element of masonry.

Discrete model Kabantseva [7] considers masonry as a continuous (continuous) composite material, takes into account the processes of contact interaction of its main components—brick and mortar.

Masonry models as structures made of piecewise homogeneous physically nonlinear materials of different modules were considered by other authors for methods of structural modeling [8–10].

## 2 Material and Research Methods

Transverse reinforcement is performed to increase the compressive bearing capacity of the masonry walls, columns, and walls. According to current standards, the number of reinforcement in the masonry is determined by the percentage of reinforcement by volume

$$\mu = \frac{V_a}{V_k} 100, \quad (1)$$

where  $V_a$ —reinforcement volume:

$$V_a = (C_1 + C_2)A_{st}, \tag{2}$$

$V_k$ —the volume of the masonry, respectively:

$$V_k = C_1 C_2 S. \tag{3}$$

The minimum percentage of reinforcement is taken  $\mu_{\min} = 0.1\%$ ; maximum  $\mu_{\max} = 1\%$ , respectively.

The tensile strength of masonry with mesh reinforcement is determined by the formula:

$$R_{sku} = kR + \frac{2R_{sn}\mu}{100}, \tag{4}$$

where  $R_{sn}$  is the standard resistance of the reinforcement.

For reinforcement made of steel of class B500,  $R_{sn}$  should be taken with a reduction factor of 0.6.

The compressive strength of the brick in unreinforced masonry is used within 25 ... 30%. The formation of the first cracks occurs at the level of 0.4 ... 0.7 $R_u$  (from the ultimate strength) [11]. Tensile stresses build up in brick, while the mortar of vertical joints has a lower strength to their perception compared to brick. Cracks appear above the vertical seams, gradually merge in height and, as a result, divide the masonry into columns that are multiples of the half-brick section. Fracture occurs as a result of separation with the formation and development of vertical main cracks. In addition, the appearance of cracks in the masonry is facilitated by the uneven density and strength of the solution of horizontal joints, the uneven surface of the brick bed. The first cracks appear as a result of the bending and shear stresses of individual bricks, and their further development is due to the transverse expansion of the masonry.

The optimal way to increase the strength of the masonry is its transverse reinforcement with metal or composites [12]. Transverse reinforcement reduces cracking of the masonry by transferring part of the stresses to the reinforcement and restraining deformations. The first cracks in the reinforced masonry appear later. They are not merged vertically or divided into columns. Horizontal reinforced joints allow more even transfer of the compressive load from one row of masonry to another. The use of mesh reinforcement can increase the use of brick strength up to 39%, increase the strength of the masonry by 80%. Consequently, calculations of masonry reinforced with transverse metal meshes should be based on consideration of tensile forces in their rods.

Reinforced masonry is in a volumetric stress state (Fig. 1), for which Hooke’s law is given in the following interpretation:

$$\varepsilon_x = \frac{1}{E} [\sigma_x - \nu(\sigma_y + \sigma_z)]. \tag{5}$$

**Fig. 1** A masonry element with an axis arrangement. 1—the initial stage of cracking, 2—breaking cracks

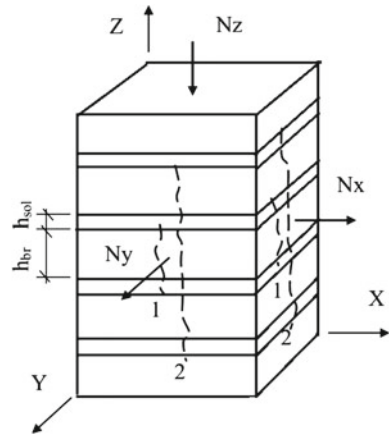
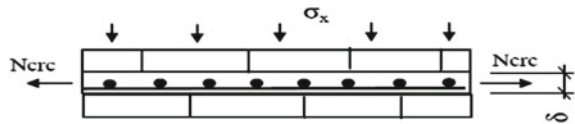


**Fig. 2** Diagram of efforts in the masonry layer



Considering the scheme of efforts (Fig. 2), we write down the equation of efforts for it:

$$N^I = N_{crc} - N_s. \tag{6}$$

As shown in [13–20], the force of cracking and the force  $N_s$  arising in the reinforcement is written through the mechanical parameters of the materials:

$$N^I = R_t A_j - \varepsilon_s E_s A_s, \tag{7}$$

where  $A_j$  is the cross-sectional area of four mortar joints in the vertical plane;  $\varepsilon_s$ —deformation of the reinforcement corresponding to the deformation of the formation of a crack in the mortar joint,  $A_s$ —the total cross-sectional area of the reinforcement of one direction within four rows of masonry,  $R_t$ —tensile strength of the masonry along the tied seam. In this case, the stress refers only to the sum of 4 layers of mortar joints, because the effect of transverse reinforcement is manifested when the mesh is located at least every 4 rows.

The derivation of the strength formula through deformation characteristics is based on the analysis of the structure of the formula SP 15.13330.2012 “Stone and reinforced masonry structures” to determine the design resistance of reinforced masonry under central compression (8) and the constraint imposed on it (9),

$$R_{sk} = R + \frac{p\mu R_s}{100}, \quad (8)$$

$$R_{sk} \leq 2R. \quad (9)$$

It should be taken into account that the strength of reinforced stone masonry should not abruptly break off after a linear increase, but increase asymptotically. It is also known that the stresses in the steel reinforcement of the cross meshes do not reach the yield point at the moment of cracking in the masonry, i.e., do not reach the yield point  $R_s$ . From the analysis (7), the effect of reinforcement according to the formulas can be infinite. This formula is modified by introducing the natural logarithm function to better match the physical model. The argument of the logarithm is  $(1 + x)$  to exclude negative and non-existent values of the function. In this case, the relative deformations are replaced by the ultimate deformations of the mortar joint under tension  $\varepsilon_u$ .

$$N^I = R_t A_j - \varepsilon_u E_s \ln(1 + A_s). \quad (10)$$

A formula was obtained for calculating the bearing capacity of masonry with transverse reinforcement with steel meshes, taking into account the increase in strength due to the elastic resistance of the reinforcement in the seams:

$$R_{sk} = R \left( \frac{R_t A_j}{R_t A_j - \varepsilon_u E_s \ln(1 + A_s)} \right). \quad (11)$$

Currently, practical methods for calculating masonry are based on empirical dependences obtained during testing of traditional materials. At the same time, modern lightweight, heat-efficient, hollow stones, high-strength mortars with thin seams are used in practice. The errors of using the normative approach are increasing. The need for physical substantiation of the theory of work of reinforced masonry is growing.

To illustrate the obtained analytical relationship, a test was carried out on a sample of masonry reinforced with steel meshes.

The sample had dimensions in section  $0.51 \times 0.51$  m, height  $h = 1.34$  m. It was laid out of ceramic bricks KR-r-by  $250 \times 120 \times 65/1NF/125/2.0/30/GOST 530-2012$  on a cement-sand mortar M100 brands; the reinforcement is made with meshes made of wire  $\varnothing 4$  Bp500 in accordance with GOST 6727-80 with a cell measuring  $50 \times 50$  mm, laid horizontally every 3 rows of bricks (Fig. 3).

For testing, a single, solid ceramic brick was used with a bending strength  $R_{ben} = 2.6$  MPa, in compression  $R_c = 13.4$  MPa, the weight of the brick was 3.7 kg. The cement-sand mortar of the M100 grade had a cubic strength  $R_m = 10$  MPa.

For reinforcing wire  $\varnothing 4$  Bp500 ( $A_s = 12.57 \text{ mm}^2$ ), the standard value of the tensile resistance is  $R_{sn} = 500$  MPa, and the calculated value is  $R_s = 415$  MPa.

To determine the physical and mechanical characteristics of the working reinforcement, tensile tests were carried out in accordance with GOST 12004-81. In

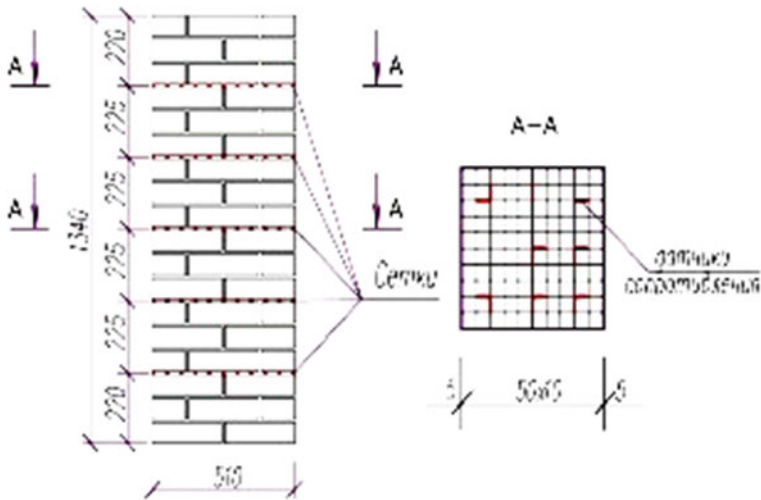


Fig. 3 Reinforcement mesh layout

order to carry out subsequent measurements, a calibration dependence was built using strain gauges.

For the subsequent measurement of deformations and stresses, strain gauges with a base of 20 mm and a resistance of 100 Ohm were glued to the mesh rods. The strain gauge glued to the mesh was coated with a transparent sealant in 1 layer, the wires were attached to the mesh with tape.

To determine the forces in the reinforcing bars of the masonry mesh, strain gauges (resistors) were installed on it at characteristic points. The sensors are located on two grids: above the 9th and 15th rows of the masonry (Fig. 4).

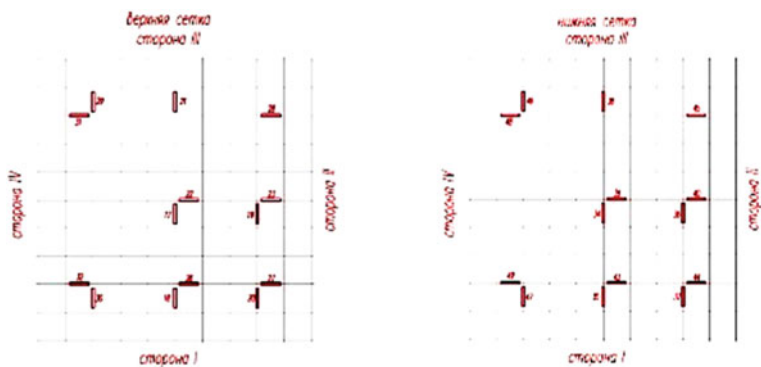
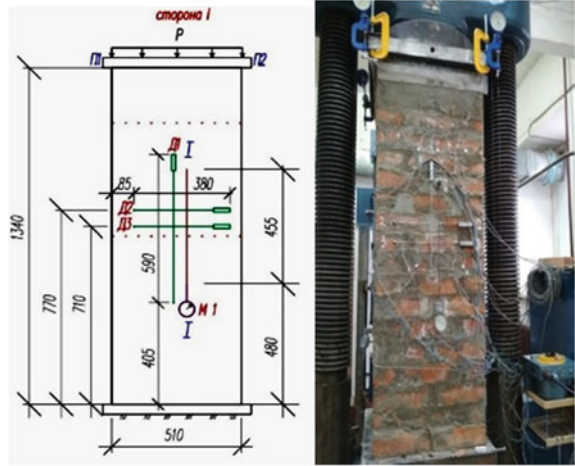


Fig. 4 Location of load cells on reinforcing masonry mesh

Fig. 5 Test stand



As you can see, the location of the strain gauges in both grids is the same in plan. The names of the grids “top” and “bottom” show their position relative to each other in height.

The following measuring instruments were used for testing:

- deflection meters Aistova 6-PAO (P1-P4) with an accuracy of 0.01 mm (Fig. 5) to assess the total vertical deformations of the masonry column;
- Messura based on dial indicators ICH-10 (M1-M4), with an accuracy of 0.01 mm for measuring longitudinal deformations of the masonry;
- electronic strain gauges DPL-10 with connection to the recorder “Terem—4.0” 0.001 mm for measuring surface deformations of masonry:
  - (a) D1, D4, D6, D9—for measuring longitudinal deformations of the masonry (duplicating M1-M4);
  - (b) D2, D3, D5, D7, D8, D10—to measure the transverse deformations of the masonry.

Roman numerals on the prototype indicate both the numbers of the sides of the masonry and mechanical deflection meters for measuring longitudinal deformations. Electrical tensometers of both transverse and longitudinal deformations of masonry are numbered in Arabic numerals. During testing, it was possible to compare deformation readings for different types of devices. The readings of the strain gauges from the reinforcing meshes were taken by the AID-5 device (Fig. 6).

The test was carried out in accordance with the requirements of large scale simulation. The dimensions of the cross-section of the base of the masonry (510 mm) allowed the strain gauges to be maximally spaced along the length and width of the mesh to record the differences in reinforcement deformations.

The specimen was tested by step loading under central compression on a hydraulic press with a capacity of 500 tf with hinged end faces and preliminary centering along



**Fig. 6** Placement of strain gauges on the sample surface



the physical axis. The sample was laid out on the press. The geometric axes of the sample and the distribution plates are aligned.

The sample was loaded in steps of 20 tf. At each stage, an exposure was carried out for 10 min, during which the instrument readings were recorded and the sample was examined. Measurement of reinforcement deformations was carried out by the electric strain gauge method using a strain gauge bridge with a communication unit for 28 sensors. The measurement of the longitudinal deformations of the prototype was carried out using measures with a graduation of 0.01 mm, installed on a 455 mm base on all four sides. Also, the measurement of longitudinal and transverse deformations was carried out by electric strain gauges with a base of 150 mm. The loading was carried out until the hydraulic cylinder's power reserve was exhausted (410 tf).

### 3 Results and Problems

According to the available data of strain gauges on reinforcing meshes using a calibration schedule (Fig. 7), the forces and stresses in the rods of the masonry mesh were determined.

The stresses in the central and peripheral parts of the reinforcement mesh are shown in Figs. 8 and 9.

As a result of data processing and analysis, the following patterns were determined:

- the values of stresses at the design loads in the reinforcing bars are far from the design resistances and are about 37% in the center of the masonry and 20% in the peripheral sections;
- stresses at different elevations along the height of the column are different. For meshes located above (or closer to the load source), the stress values at the center of the section are 1.36 times the values of the underlying mesh. For grids located on the periphery at the corners of the section, 1.33 times more;

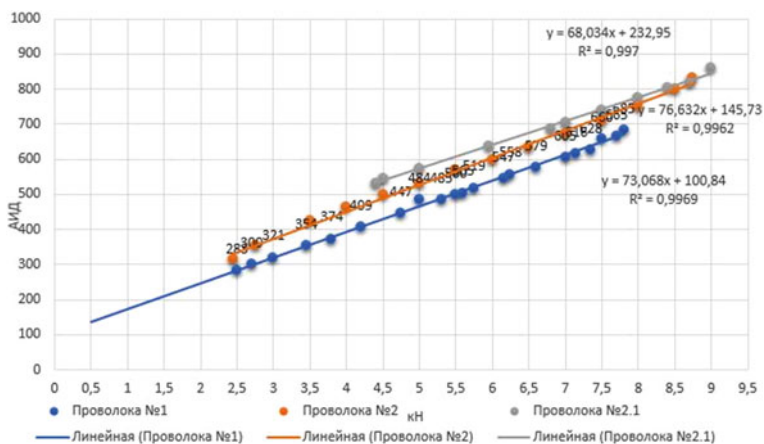


Fig. 7 Calibration graph of strain gauges on wire

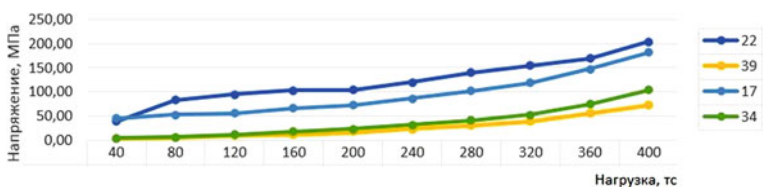


Fig. 8 Stresses in the central part of the mesh

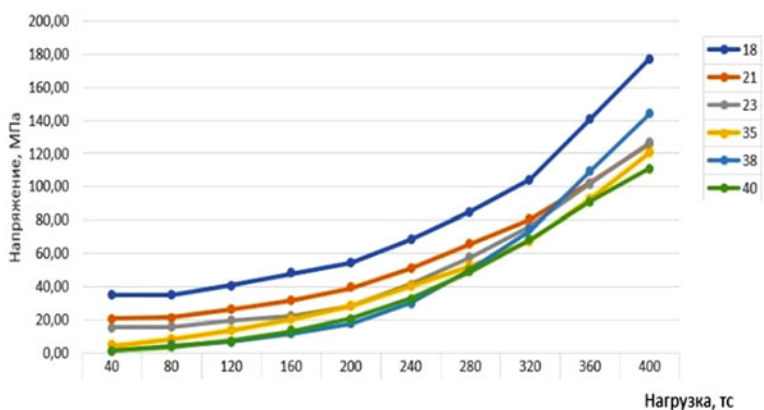


Fig. 9 Stresses in the peripheral part of the reinforcement mesh

- at the moment of the formation of initial cracks in the reinforced masonry, the stresses in the rods were about 92 MPa in general along the center of the section and 48 MPa at the peripheral points along the corners;
- up to a load of 200 tf, we can talk about a linear dependence of stresses, then a nonlinear increase in stresses occurs, while the initial cracks in the masonry have not yet been fixed.

The data presented show that in the calculations according to the standards for solid brick masonry, a large safety factor is laid. The use of the value of the design tensile strength of steel in the formulas is limited (reduced) by the introduction of operating conditions for various types of reinforcing steels. Most of all, the value is underestimated for the most often used in construction reinforcement of the class B500 and Bp500 and is 60% of the calculated value. Even so, the margin of safety remains 1.2 times. Consequently, there is a need to clarify the calculations and improve them.

During the tests, longitudinal deformations were measured on all four sides (Fig. 10).

In general, a similar picture is observed for longitudinal deformations according to the data of mechanical and electronic devices.

The transverse deformations of the masonry in the reinforced and unreinforced layers show nonlinear work, which indicates an increase in the intensity of cracks within the volume of the masonry (Fig. 11).

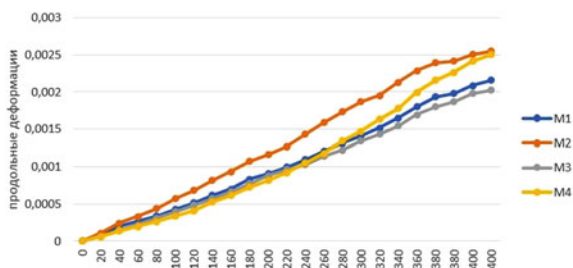
According to the presented graphs:

- there was a greater formation of cracks in the considered reinforced layer;
- transverse deformations in this layer are numerically greater than in the overlying one;
- nets located in the horizontal seam provide a deterrent.

The brick under the reinforced layer perceives the load more evenly. Probably due to the impossibility of stretching the lower edge of the brick, located above the reinforced horizontal seam, by the same values as the reinforcement, this layer collapsed first.

The bearing capacity of the unreinforced and reinforced pillar has been determined. The values, respectively,  $N_{ur} = 624$  kN,  $N_u = 973$  kN, the difference was 1.56. According to the ultimate strength of the reinforced masonry, the strength should be  $N_u = 1600$  kN.

**Fig. 10** Longitudinal deformations of the masonry on four sides



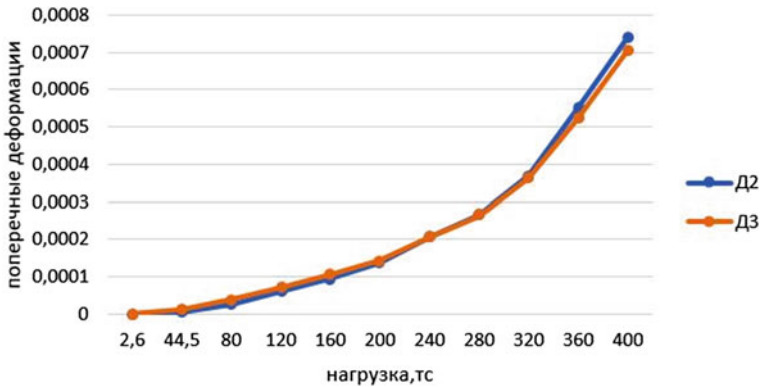


**Fig. 11** Transverse deformations of masonry. D3—closer to the reinforced layer, D2—to the layer without reinforcement

The maximum test load achieved was 4020 kN. The bearing capacity reserve is estimated at 2.5 times.

Let us make a calculation to determine the design resistance of the reinforced masonry according to the previously derived formula (11). Let us consider four rows of an experimental sample. The seams are assumed to be 1 cm thick. Eleven wire rods are located in one horizontal seam.

$$\begin{aligned}
 R_{sk} &= R \left( \frac{R_t A_j}{R_t A_j - \varepsilon_u E_s \ln(1 + A_s)} \right) \\
 &= 3.0 \left( \frac{16 * 204}{16 * 204 - 1.5 * 10^{-4} * 2000000 * \ln(1 + 1.3827)} \right) \\
 &= 3.0 \left( \frac{3264}{3264 - 2604.7} \right) = 14.85 \text{ МПа}, \tag{12}
 \end{aligned}$$

where  $\varepsilon_u = 1.5 * 10^{-4}$  is the deformation of the reinforcement, corresponding to the deformation of the formation of a crack in the mortar joint (ultimate deformation);

$A_j$ —cross-sectional area of four mortar joints in the vertical plane,  $A_j = 51 * 1 * 4 = 204 \text{ cm}^2$ ;

$A_s$ —the total cross-sectional area of the reinforcement of one direction within four rows of masonry,  $A_s = 12.57 * 10^{-2} * 11 = 1.3827 \text{ cm}^2$ ;

$R_t$ —is the tensile strength of the masonry along the tied seam,  $R_t = 0.16 \text{ МПа} = 16 \text{ N/cm}^2$  (according to table 11 SP15.13330.2012. Stone and reinforced-masonry structures).

$E_s = 200,000 \text{ МПа} = 2 * 10^7 \text{ N/cm}^2$ —modulus of elasticity of reinforcing steel.

In this case,  $N_u = 3862 \text{ kN}$ , which is close to the ultimate test load of 4020 kN.

The tests were carried out with a gradual, within two hours, loading of the sample, which made it possible to evaluate the deformation characteristics of this type of masonry. The relationship between stresses and strains appeared to be nonlinear.

The modulus of elasticity (or the initial modulus of deformation) of masonry with mesh reinforcement according to SP 15.13330.2012 (clause 6.21) is assumed to be the same as for unreinforced:

$$E_0 = \alpha R_u. \quad (13)$$

According to the results of the experiment, for a conditional material at  $\alpha = 1000$ , we can take  $E_0 = 15,450$  MPa. According to the measured deformations,  $E_0 = 10,666$  MPa.

Poisson's ratio was defined as the ratio of transverse to longitudinal deformation at a third of the breaking load

$$\nu = \frac{\varepsilon_x}{\varepsilon_y}, \quad (14)$$

where  $\varepsilon_x$  and  $\varepsilon_y$  are relative, respectively, transverse and longitudinal deformations.

At a maximum load of 4020 kN, the generalized modulus of deformation was  $E = 6925$  MPa. The fall of  $E$  occurs 1.6 times.

The value of Poisson's ratio for reinforced masonry increases slightly with increasing load. The average value was 0.2278, which differs from the norm  $\nu = 0.25$  by less than 10%.

The value of the absolute vertical deformation of the masonry column was  $\varepsilon_y = 4.17\text{--}4.58$  mm. Relative vertical deformations  $\varepsilon_y = 3.11 * 10^{-3} - 3.41 * 10^{-3}$ .

The peculiarities of the work of the reinforced masonry are in the layer-by-layer resistance of the reinforcement meshes laid in horizontal seams. Their effect changes the conditions for the occurrence and development of cracks. Cross meshes have a higher elastic modulus than masonry. They create lateral compression stresses and prevent the development of deformations in the transverse direction.

In similar experiments [15], at the last stages of loading, small pieces of masonry mortar peeled off along the surface of the brick and mortar joint, which separated and flew off at a distance of 10–20 mm from the massif with a characteristic crackling. With the destruction of unreinforced samples, this phenomenon was not recorded. This experimentally established fact confirms the assumption about the restraining effect of the cross-reinforcement mesh on the development of Poisson phenomena arising in horizontal seams.

However, the reinforcing bars do not fully utilize their strength. The forces in them do not reach the yield strength of the steel both during the formation of initial cracks and during the further increase in the load.

The development of main cracks was not recorded. Failure occurred brick by brick, with the first visible cracks appearing in the brick mainly above the reinforced joint layer. The cracks were of a mirror-like nature (they formed symmetrically along the opposite masonry faces).

## 4 Conclusion

Information about the deformations of the components that make up the masonry allows you to determine its bearing capacity. The results of the experiment carried out for reinforced masonry made of solid ceramic bricks showed the convergence of the strength characteristics of the masonry with an analytical calculation according to the developed method. The convergence is determined to be 4%. In comparison with the current standards, the safety margin was 2.5 times.

There were no main cracks in the sample, which is typical for pillars with indirect reinforcement. The destruction proceeded in two forms: the loss of the strength of the brick (its crushing-crushing) and the destruction of the mortar and the pouring out of its surface layers from the seams with the brick continuity still preserved.

The stress values in the reinforcement meshes were far from the yield point of the reinforcement and amounted to 37% of this value in the center of the masonry and 20% in the peripheral areas. At the moment of the formation of the first visible cracks, the stresses in the meshes were 92 MPa in the center of the section and 48 MPa in the corner points.

The generalized modulus of deformation of the reinforced masonry in the process of loading decreased by 1.6 times.

## References

1. Antakov, A.B., Sokolov, B.S.: Analytical assessment of the stress-strain state of masonry under compression based on the author's theory. *Build. Mater.* **9**, 51–55 (2019) (rus)
2. Sokolov, B.S.: Development of methods for calculating stone and reinforced stone structures. In: Sokolov, B.S., Antakov, A.B. (eds.) *New in Architecture, Design of Building Structures and Reconstruction: Materials of the IV International (X All-Russian) Conference NASKR-2018*, pp. 174–183. Publishing House of Chuvash, un-that, Cheboksary (2018) (rus)
3. Kaushik, H.B., Rai, D.C., Jain, S.K.: Uniaxial compressive stress-strain model for clay brick masonry. *Curr. Sci.* **92**(4), 497–501 (2007)
4. Nwofor, T.C.: Experimental determination of the mechanical properties of clay brick masonry. *Can. J. Environ. Constr. Civ. Eng.* **3**(3) (2012)
5. Kashevarova, G.G.: A model of a masonry wall for the study of schemes and mechanisms of destruction. In: Kashevarova, G.G., Vildeman, V.E., Akulova, A.N. (eds.) *Information, Innovations, Investments: Collection of Articles. Materials conference*, pp. 38–41. Scientific and Technical center Inform., Perm (2002) (rus)
6. Pangaev, V.V.: Development of computational and experimental methods for studying the strength of masonry of stone structures. In: Pangaev, V.V. (ed.) *Abstract for the Application. Art. Doctors of Those Sciences. Novosibirsk* (2009) (rus)
7. Kabantsev, O.V.: *Scientific Foundations of the Structural Theory of Masonry for Assessing the Limiting States of Stone Structures of Earthquake-Resistant Buildings*: dis. Doct. Tech. Sciences: 05.23.01, Moscow (2016) (rus)
8. Kapustin, S.A., Likhacheva, S.Yu.: *Modeling the Processes of Deformation and Destruction of Materials with a Periodically Repeating Structure. Monograph*, Nizhny Novgorod (2012) (rus)
9. Ivanov, V.A.: Numerical modeling of the dynamics of structures supported by a system of reinforcing rods. In: Ivanov, L.I., Vutsin, M.V. Skobeeva (eds.) *Modern Problems of Continuum Mechanics 2019: Collection of Articles. Art. Based on the Materials of the Conference from the*

- International Participation, pp. 119–124. Chuvash Publishing House University, Cheboksary (2019) (rus)
10. Akhaveissy, A.H.: The DSC Model for the nonlinear analysis of In-plane loaded masonry structures. *Open Civil Eng. J* **6**, 200–204 (2012)
  11. Ali, S.S., Page, A.W.: Finite element model for masonry subjected to concentrated loads. *Proc. Am. Soc. Civil Eng. J. Struct. Div.* **114**, 1761–1784 (1990)
  12. Sokolov, B.S., Antakov, A.B.: Research results of stone and reinforced stone masonry. *Bull. MGSU* **3**, 99–106 (2014) (rus)
  13. Plotnikov, A.N.: Strength calculation of reinforced masonry based on deformation parameters of its constituent materials. In: Plotnikov, A.N., Yakovleva, O.S., Romanova, T.V. (eds.) *Modern Problems of Continuum Mechanics—2019: Collection of Articles. Art. Based on the Materials of the Conference from the International Participation*, pp. 60–68. Publishing House “Wednesday”, Cheboksary (2019) (rus)
  14. Antakov, A.B., Plotnikov, A.N., Pozdeev, V.M.: Bearing capacity of masonry reinforced with grids made of basalt-plastic reinforcement. Modern problems of calculating reinforced concrete structures, buildings and structures for emergency impacts. In: Tamrazyan, A.G., Kopanitsa, D.G. (eds.) *M.: MGSU*, pp. 15–21 (2016) (rus)
  15. Onishchik, L.I.: *Stone Structures for Industrial and Civil Buildings* (Gosstroyizdat, M. (ed.)), p. 208 (1939) (rus)
  16. Plotnikov, A.N.: Mechanics of operation of transverse reinforcement in masonry. In: Plotnikov, A.N., Romanova, T.V. (eds.) *In the collection: Collection of Scientific Works of Young Scientists and Specialists. In 2 parts. otv. editor A.N. Zakharova, Cheboksary*, pp. 99–104 (2019) (rus)
  17. Derkach, V.N., Zhernosek, N.M.: Methods for Assessing the Strength of Masonry in Domestic and Foreign Practice of Inspection of Buildings and Structures, vol. 3. *Bulletin of the Belarusian-Russian University*, pp. 135–142 (2010) (rus)
  18. Donchenko, O.M., Degtev, I.A.: *Towards the Development of the Theory of Crack Resistance and Resistance of Masonry in Compression* (2000) (rus)
  19. Khatkevich, A.M.: The nature of destruction of stone and reinforced stone pillars at central loading. *Constr. Appl. Sci. Build. Constr.* **12** (2009) (rus)
  20. Guchkin, I.S., Artyushin, D.V.: Determination of the strength (mark) of ceramic bricks in structures by a non-destructive method. *Construction* **1**, 103–104 (2006) (rus)

# Criteria for Special Limiting State of Eccentrically Compressed Members of RC Frames



Sergey Savin 

## 1 Introduction

The problem of assessing the bearing capacity of eccentrically compressed rod elements of reinforced concrete frames of buildings under special influences caused by a sudden failure of an individual element of the bearing system is related to the factors of long-term power and environmental resistance (physical nonlinearity, creep, corrosion) [1–6] and subsequent dynamic loading. In cases where the eccentrically compressed elements of the structural system overloaded as a result of an emergency have a slender section, or have acquired environmental (corrosion) or mechanical (chips, death) damage during installation and operation, then a possible scenario for the exhaustion of their bearing capacity may become buckling.

Kolchunov and Prasolov [7] performed experimental studies on scale models of flat reinforced concrete frames, which demonstrated the possibility of implementing this scenario of destruction of structural elements with a sudden removal of a vertical bracing element. Experimental and numerical investigations carried out by Fedorova et al. [8] for models of three-story flat frames showed that in the scenario of removing one of the columns, additional loading of the preserved eccentrically compressed columns in adjacent spans can lead to destruction of concrete along inclined sections at the junction nodes of the girders. The formation of an inclined crack in such areas requires taking into account the change in the conjugation conditions at the nodes when modeling the reinforced concrete frames of buildings using the bar and plate analogy.

Grudev [9] noted that in the cases when all the parameters determining the process of deformation of structural system elements in the considered emergency design situation are known (stress–strain diagrams, type, and arrow of initial deflection, etc.), the calculation for progressive collapse in a nonlinear setting (physical, geometric,

---

S. Savin (✉)

Moscow State University of Civil Engineering, Moscow, Russian Federation

e-mail: [savinsyu@mgsu.ru](mailto:savinsyu@mgsu.ru)



genetic nonlinearity, etc.) can be considered as deterministic, and deformation and destruction of structures—as a stable process. With regard to reinforced concrete eccentrically compressed rods, the solution to the problem of nonlinear deformation of such structural members is presented, for example, in the paper of Radaykin [10]. Such a situation is possible when designing the reconstruction of buildings and structures, when the geometric parameters of structures, strength, and deformability of materials can be established as a result of the survey. However, in practice, the values of a number of parameters, as a rule, cannot be unambiguously established in advance, which requires variations of the design models for various emergency design situations in order to identify the most disadvantageous among them. In this regard, from an engineering point of view, it is justified for eccentrically compressed members with small eccentricities to calculate the buckling mode when one member of the frame is removed. It should also be noted that the solution of the deformation problem by step-iterative methods in many cases, especially when a small number of steps are used, into which the load is divided, will shift towards the solution by the method of secant elastic moduli. In this case, the final deformed state for the increment of the last step of the load is determined taking into account the secant moduli of deformations in the section of the stress–strain diagram. Thus, the ability to evaluate the behavior of a structural system under infinitesimal perturbations, which, for concrete, may also be associated with structural heterogeneity, is significantly hampered.

In this regard, attention should be paid to a number of analytical and numerical solutions to the problem of the bearing capacity of eccentrically compressed reinforced concrete elements under dynamic loading, taking into account the simultaneous manifestation of factors of long-term force and environmental resistance, obtained using the theory of stability. In particular, in the paper of Tamrazyan [5] an analytical solution to the problem of stability of a nonlinearly deformable reinforced concrete bar was proposed. Taking this solution into account, in the work [11] an analytical model was proposed for taking into account the influence of disruption of adhesion of reinforcement and concrete in corrosively damaged areas. An analytical solution and a numerical analysis of the stability of elements in the structure of the building frame, taking into account the influence of the system, are given in the work of Kolchunov, Savin [12], which shows a significant decrease in the bearing capacity and a change in the nature of deformation and destruction of elements during corrosion damage to concrete. In the development of these studies in the paper of Kolchunov, Fedorova, Savin [13] an incremental model was proposed to take into account external disturbances for stability. In the paper [14], this model was implemented to structural analysis of reinforced concrete eccentrically compressed members. The results of structural analysis were compared with deformation calculation based on the step-iterative method. The results obtained in this work have demonstrated the effectiveness of the proposed approach as applied to elements loaded with small eccentricities at the values of flexibility that require taking into account the deformed state of the elements.

All of the above works were devoted to the solution of important, but still particular problems, while a general approach to their solution has not yet been developed,

there are no universal criteria that could be used to assess the special limiting state of eccentrically compressed elements reinforced concrete frames of structures in case of sudden. In this regard, the purpose of the study was to formulate criteria for a special state for eccentrically compressed reinforced concrete elements of load-bearing systems of structures, taking into account factors and to formulate a general algorithm for computational analysis. This paper presents an algorithm for calculating the buckling mode of reinforced concrete eccentrically compressed bar members of building frames, taking into account the nonlinear nature of their deformation, and also gives suggestions on the criteria for the special limiting state of the structural members under consideration.

## 2 Methods

### 2.1 Stability of Rod Elements Under Degrading of Restraint Conditions

Let us use the stability equation for a bar element proposed in [15]:

$$\frac{d^4 \bar{w}}{d\xi^4} + k^2 \frac{d^2 \bar{w}}{d\xi^2} = 0, \quad (1)$$

where

$$\xi = \frac{x}{l}, \quad \bar{w} = \frac{w}{l}, \quad k^2 = \frac{Nl^2}{B_{\text{red}}}. \quad (2)$$

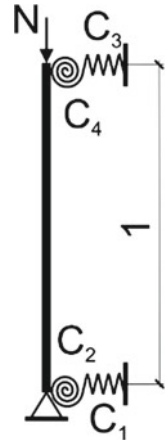
In expression (2)  $B_{\text{red}}$  = the flexural stiffness of the reduced cross-section of the reinforced concrete element, determined taking into account the loading mode and the presence of corrosion damage;  $x$  = the coordinate measured along the undeformed axis of the bar from the pinching point;  $w = w(x)$  is the deviation of the bar axis from the undeformed state;  $l$  is the length of the bar element;  $N$  = axial force.

If the ends of the bar are resiliently fixed against lateral displacements and turns (Fig. 1), then forces acting in the support sections of the element (in a dimensionless form) take the form:

$$\begin{aligned} \bar{Q} &= -C_i \bar{w} + k^2 \bar{w}' = -\bar{w}''', \\ \bar{M} &= -C_j \bar{w}' = -\bar{w}'', \end{aligned} \quad (3)$$

Here,  $C_i, C_j$  are the values of the compliance of the bar support anchors for lateral displacement and rotation, respectively.

**Fig. 1** A design scheme of a bar member



Substituting the solution to Eq. (1) by the method of initial parameters for  $\xi = 1$  into (3), we obtain a system of two linear homogeneous equations with two unknown variables:

$$A_1 \bar{w}_0 + A_2 \bar{w}'_0 = 0,$$

$$A_3 \bar{w}_0 + A_4 \bar{w}'_0 = 0. \quad (4)$$

Here,

$$A_1 = C_3 - C_1 + C_1 C_3 \left( \frac{1}{k^2} - \frac{\sin k}{k^3} \right),$$

$$A_2 = -C_1 C_4 \frac{1 - \cos k}{k} - C_1 \frac{\sin k}{k},$$

$$A_3 = -C_2 C_3 \frac{1 - \cos k}{k^2} - C_3 \frac{\sin k}{k},$$

$$A_4 = -(C_2 C_4 - k^2) \frac{\sin k}{k} + \cos k (C_4 - C_2).$$

Equating to zero the determinant composed of the coefficients at unknowns of the system of equations (4), we find the parameter of the critical force  $k$  for a compressed rod element at arbitrary values of the parameters  $C_i, C_j$ .

However, as applied to the entire building frame, the deformation process can be accompanied by partial unloading of individual compressed rods due to the redistribution of efforts by floor and roof structures to other vertical supporting structures. To take into account this effect, it is necessary to consider not a single rod, but the entire

rod system, taking into account the elastic conditions of conjugation at the nodes. Based on the computational analysis of the rod system of the reinforced concrete frame of the building, such combinations of the values of the parameters  $C_{i,cr}$ ,  $C_{j,cr}$  can be found, at which its buckling occurs under the given parameters of impacts.

## 2.2 Modeling Static-Dynamic Behavior of Reinforced Concrete

As a deformation rheological model of the static-dynamic resistance of reinforced concrete in this work, it is proposed to use a model consisting of two series-connected elements: a quasi-elastic element, which corresponds to the secant modulus of elasticity  $E_{sec,0}$ , calculated taking into account creep deformations, and an elastic-viscous element, represented by the Kelvin-Voigt model [4, 16]. Taking into account the adopted model, the physical relations for the stage of dynamic additional loading of the system take the form:

$$\Delta\varepsilon = \frac{\Delta\sigma}{E_{sec,0}}(1 - e^{-\omega t}), \quad \omega = \frac{E_{sec,0}}{K}, \quad (5)$$

where  $E_{sec,0}$  = secant modulus of elasticity for the stage of normal operation,  $K$  = modulus of viscous behavior of an element,  $t$  = time of dynamic reloading of load-bearing elements of a structural system during its sudden structural restructuring,  $\Delta\sigma$  and  $\Delta\varepsilon$  are increment of stresses and relative deformations in the section of a structural element during its dynamic loading.

The dynamic tangential modulus of concrete deformation for calculating eccentrically compressed elements with their dynamic additional loading, taking into account (4), can be determined from the expression:

$$E_{t,d}(y) = \frac{E_{t,1}}{(1 - e^{-\omega t})},$$

where  $E_{t,1} = d\sigma/d\varepsilon = E_0 - 2H_1 \varepsilon$  is tangent modulus for the deformed state preceding dynamic loading.

## 2.3 Consideration of Concrete Degradation Due to Corrosion

In order to take into account long-term processes of corrosion damage to structural elements in contact with an aggressive medium, in this work it is proposed to use the phenomenological model of the environmental resistance of concrete proposed by Bondarenko [17, 18].

In this case, taking into account the decrease in the strength and deformation characteristics of concrete to the depth of advancement of the front of corrosion damage during clogging of pores can be carried out by multiplying the modulus of concrete deformation by the function of corrosion damage  $K(z, t, \eta)$ , which can be written by analogy with [17] as

$$K(z, t, \eta) = \sum_{i=0}^{i=2} a_i z^i, \quad (6)$$

where  $z \in [h/2 - \delta(t); h/2]$  is the coordinate of an arbitrary point in the part of the section damaged by corrosion;  $a_i$ —parameters of the function of corrosion damage, determined empirically;  $\eta = \sigma/R_{b,n}$  is the ratio of the current stress level in compressed concrete to its design compressive strength;  $t$  = time of contact of the structure with an aggressive environment.

Separating the remaining part of the section and the part of the section damaged by corrosion processes, taking into account (5), the flexural stiffness of a rectangular section of an eccentrically compressed reinforced concrete element is determined from the following expression:

$$B_x = \int_{-\frac{h}{2}}^{\frac{h}{2} - \delta(t, \eta)} E_t(y) \cdot y^2 dy \int_{-\frac{b}{2}}^{\frac{b}{2}} x dx + \int_{\frac{h}{2} - \delta(t, \eta)}^{\frac{h}{2}} E_t(y) \cdot K(y, t, \eta) \cdot y^2 dy \int_{-\frac{b}{2}}^{\frac{b}{2}} x dx.$$

Since the determination of the value of advancement of the front of corrosion damage deep into the section of a structure for real structural systems under conditions of a variable value of the parameter  $\eta$  in time and a decrease in the value of the calculated resistance to compression  $R_{b,n}$  for fibers damaged by corrosion is a rather difficult problem, for solving applied problems in the first approximation, we can take  $\eta = 0.6$ , which corresponds to the boundary of the first and second sections of the three-line diagram of concrete state according to Code of RF SP 63.13330.2018, the thermodynamic and physicochemical factors of the environmental resistance are assumed constant, and the time intervals  $t$  are fixed.

Taking into account the calculated dependences presented in Sect. 2.2 of this article, as well as in this section, as criteria for the special limiting state of eccentrically compressed elements, the critical value of the reduced stiffness of the section  $B_{\text{red,cr}}$  and the critical time of the environmental resistance (interaction with an aggressive medium)  $t_{\text{cr}}$ , according to the outflow of which the sudden removal of one of the load-bearing elements of the system leads to the destruction of the considered eccentrically compressed reinforced concrete element.

### 3 Results and Discussion

#### 3.1 An Algorithm for Calculation of a Buckling Mode

The sequence of calculating the stability of the deformed shape of reinforced concrete eccentrically compressed elements of the frame of buildings with a sudden removal of one of the load-bearing elements of the structural system, taking into account the analytical expressions presented in the work to take into account the loading mode and environmental factors, consists of the following stages:

- a finite element model of the building frame is created using nonlinear finite elements;
- the stages of installation (dismantling) of the bearing elements of the model are set, as well as the sequence of application of constant and long-term loads and the generalized force that occurs at the place of the removed element in the secondary design scheme of the building;
- the calculation of the building frame is performed by the step method or by the method of variable parameters of elasticity (the secant method);
- the stiffness matrix of the model obtained at the last step of the calculation for constant and long-term loads is used for the subsequent linear calculation for a special effect caused by the sudden removal of the structural element of the structural system.

Thus, the calculation of the stability of nonlinearly deformable elements of the reinforced concrete frame of a building under a special emergency impact is reduced to a linear calculation of the stability of a fragment of the frame of a building with stiffness stepwise variable along the length of structural elements calculated by tangential modules. The value of the critical force obtained as a result of such a calculation should be compared with the forces in the corresponding structural elements obtained as a result of the deformation calculation for dynamic additional loading caused by a sudden emergency failure of one of the load-bearing elements of the structural system. The stability of the structural system is ensured if the condition is satisfied:

$$N_{cr,dyn} > N_{dyn},$$

where  $N_{cr,dyn}$  = critical force causing buckling of the system, the stiffness of which is determined on the basis of its deformation calculation for a particular emergency action,  $N_{dyn}$  = dynamic force in an element of the structural system under consideration.

In order to identify the most dangerous elements of a structural system from the point of view of buckling, one can use the energy criteria determined by the work of the nodal bending moments and shear forces  $A$  ( $M$ ,  $Q$ ) during bending [19]. The structural element of the building frame, which is losing stability, corresponds to the largest negative work of nodal bending moments and shear forces in absolute value:

$$A_i(M, Q) < 0.$$

When dividing a structural element into a number of finite elements (when calculating by FEM), this criterion can also be used to identify the sections of structural elements of the building frame that are most sensitive to loss of stability.

### 3.2 Numerical Analysis of a Scale Model of a RC Frame with Slender Columns

In order to illustrate the presented algorithm for calculating the shape stability of a nonlinearly deformable bar bearing, consider a scale model of a reinforced concrete frame from [20]. The geometrical dimensions and the scheme of reinforcement of the experimental structure of the reinforced concrete frame are shown in Fig. 2. Materials: concrete of compressive strength class B25, for which the standard compressive strength is  $R_{b,n} = 18.5$  MPa, the initial modulus of elasticity  $E_0 = 30,000$  MPa. Reinforcement of racks and crossbars is made with space frames with longitudinal reinforcement of class B500 ( $R_{s,n} = 500$  MPa) and transverse reinforcement A300 ( $R_{s,n} = 300$  MPa). The columns of the second floor of the experimental model have flexibility in the undeformed state  $\mu \dots l/h = 1.2 \dots 940/50 = 22.6$ , where  $\mu = 1.2$  is the coefficient of the calculated length for rods with pliable termination at the ends.

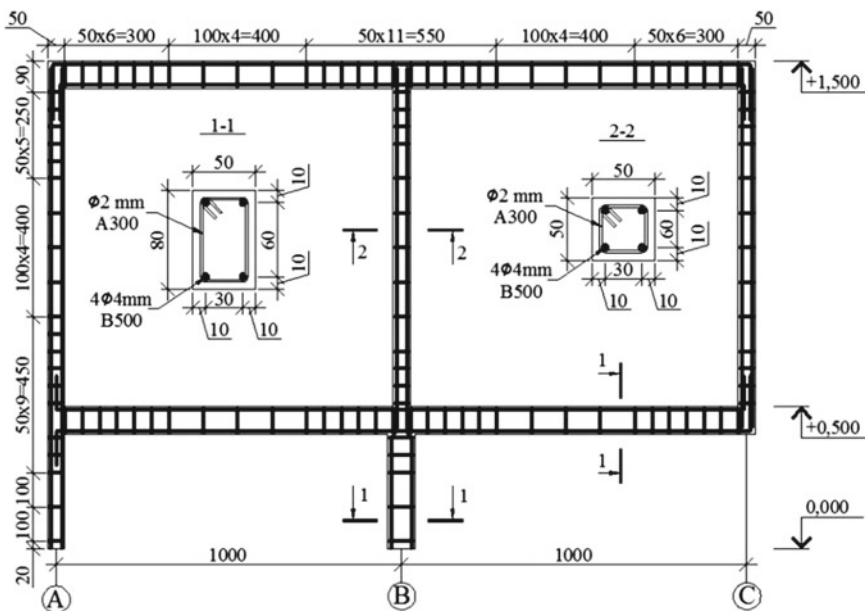
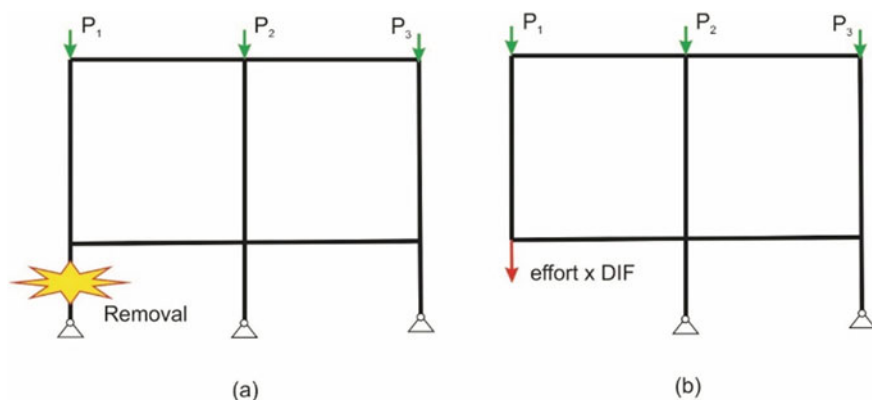


Fig. 2 Scale model of the reinforced concrete frame



**Fig. 3** Design model of reinforced concrete frame at outer column removal scenario: primary design scheme “ $n$ ” (a); secondary design scheme “ $n - 1$ ” (b)

At the stage of normal operation, concentrated forces  $P_1 = 4$  kN,  $P_2 = 20$  kN,  $P_3 = 16$  kN were applied to the upper frame nodes (Fig. 3a). The dynamic effect of the instantaneous removal of the leftmost frame post at time  $t = T/4$ , where  $T$  is the period of forced oscillations of the considered “ $n - 1$ ” rod system, was modeled by static application of a longitudinal force  $P = 4$  kN to the frame node at the place of the removed post, directed downward (Fig. 3b). Additionally, the calculation of the deformed state of the frame model at the time  $t = T/8$  was performed, at which the reaction is zeroed in the node at the place of the remote post.

As a result of calculating the stability of the deformed state of the frame using the proposed algorithm for the time  $t = T/8$ , the safety factor for stability  $k = 0.98$  was obtained, indicating a change in the equilibrium state of the considered bar system (Fig. 4). The most sensitive to the loss of stability were the elements of the rightmost pillar of the second floor of the frame, adjacent to the crossbars.

To assess the result obtained, a nonlinear deformation calculation of the reinforced concrete frame under consideration was performed using a 3D model, in which the concrete matrix and longitudinal reinforcement were modeled by 8-node volumetric finite elements, taking into account physical nonlinearity based on exponential approximation of the deformation diagrams of concrete and steel. The cross-sectional dimensions of prismatic 8-node FE simulating reinforcing bars were selected to be equivalent in area to reinforcing bars according to Fig. 2. The results of the calculation performed using the 3D model are presented in the form of normal stress patterns in concrete and reinforcement in Fig. 5.

The results obtained agree with the result of calculating the stability of the deformed state of the frame: in the end sections of the vertical supporting element of the 2D frame, which are most sensitive to buckling according to the results of the corresponding calculation, the values of normal stresses close to the standard resistance of concrete were obtained in the 3D model.



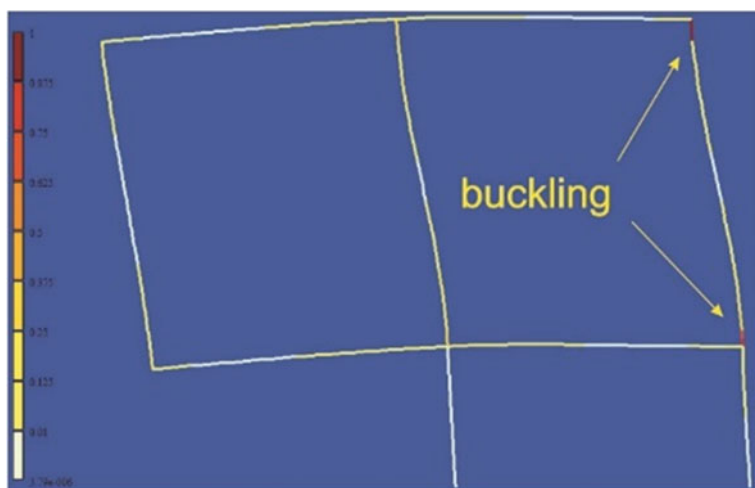


**Fig. 4** Results of numerical analysis of the stability of the deformed state of the frame at the time  $t = T/8$  from the beginning of the emergency impact

## 4 Conclusions

The paper presents design dependencies for assessing the bearing capacity of eccentrically compressed rod reinforced concrete elements of building frames under special influences caused by the sudden removal of one of the load-bearing elements of the structural system.

It is proposed to consider the critical force  $N < N_{cr}$  or other parameters derived from it (critical stiffness, critical time of environmental resistance, critical values of the flexibility of nodal restraints) as criteria for a special limiting state associated with the loss of shape stability for individual elements of building frames. At the same time, in accordance with codes, for example, clause B.9 of Code of RF SP 63.13330.2018 “Concrete and reinforced concrete structures”, the stability margin must be double or more to ensure structural safety.

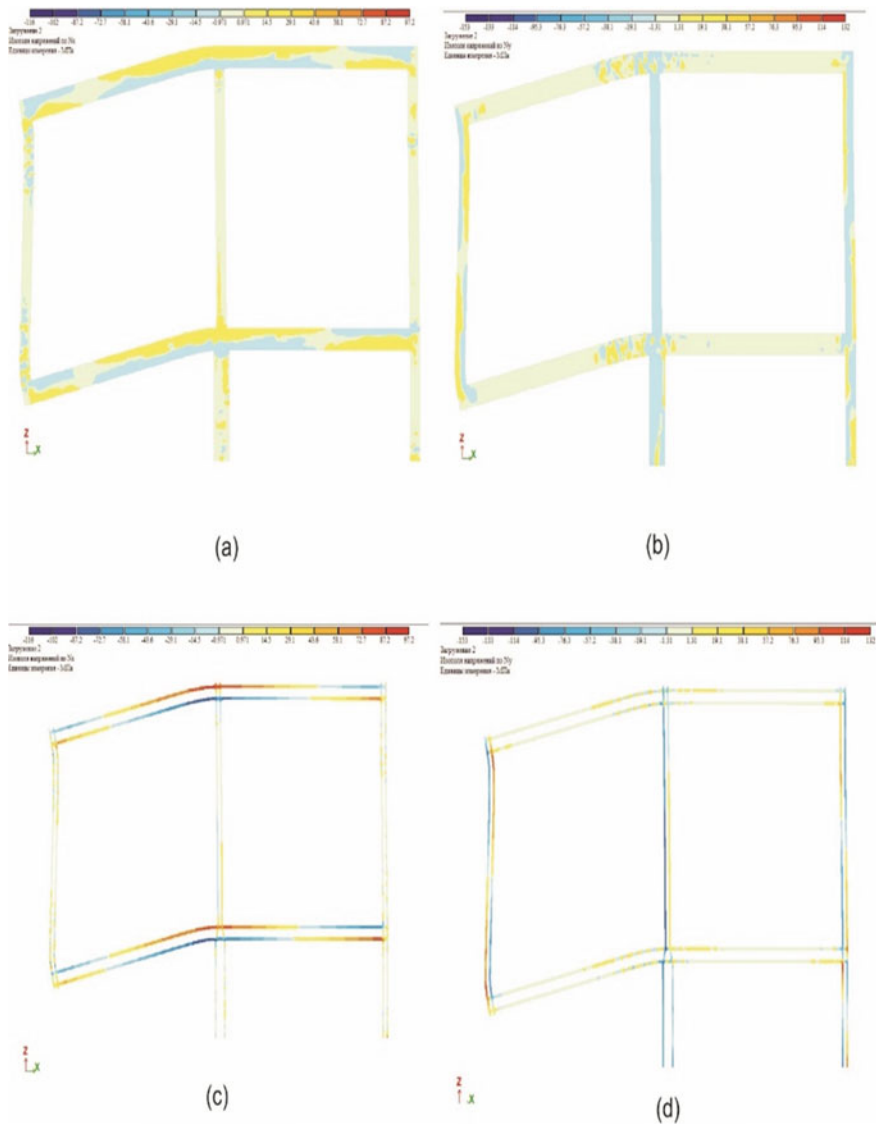


**Fig. 5** Normal stresses in the elements of a reinforced concrete frame at time  $t = T/4$ :  $\sigma_x$  (a) and  $\sigma_y$  (b) in concrete;  $\sigma_x$  (c) and  $\sigma_y$  (d) in steel reinforcement

## References

1. Golyshev, A.B., Kolchunov, V.I.: *The Resistance of Reinforced Concrete*. Osnova, Kiev (2009)
2. BS EN 1992-1-1: Eurocode 2: Design of Concrete Structures—Part 1-1 : General Rules and Rules for Buildings. Br. Stand. Inst. (2004)
3. Ulitsky, I.I.: *Structural Analysis of Reinforced Concrete Bars Taking into Account Long-Term Processes*. Budivel'nik, Kiev (1967)
4. Kolchunov, V.I., Klueva, N.V., Androsova, N.B., Bukhtiyarova, A.S.: *Survivability of Buildings and Structures Under Beyond Design Basis Impacts*. ASV Publishing, Moscow (2014)
5. Tamrazyan, A.G.: Dynamic Stability of the Compressed Reinforced Concrete Element as Viscoelastic Bar. *Vestn. MGSU.*, pp. 193–196 (2011)
6. Kolchunov, V.I., Fedorova, N.V., Savin, S.Y., Kovalev, V.V., Iliushchenko, T.A.: Failure simulation of a RC multi-storey building frame with prestressed girders. *Mag. Civ. Eng.* **92**, 155–162 (2019). <https://doi.org/10.18720/MCE.92.13>
7. Kolchunov, V.I., Prasolov, N.O., Kozharinova, L.V.: Experimental and Theoretical Research on Survivability of Reinforced Concrete Frames in the Moment of Individual Element Buckling. *Vestn. MGSU.*, pp. 109–115 (2011)
8. Fedorova, N.V., Tuyen, V.N., Yakovenko, I.A.: Strength Criterion for a Plane Stress Reinforced Concrete Element Under a Special action. *Vestn. MGSU.*, pp. 1513–1522 (2020). <https://doi.org/10.22227/1997-0935.2020.11.1513-1522>
9. Grudev, I.D.: *Bearing Capacity of Compressed Structural Elements*. MGSU Publishing, Moscow (2012)
10. Radaikin, O.V.: Strength of reinforced concrete elements of a rectangular profile under oblique out-of-center compression using a nonlinear deformation model. *Build. Reconstr.* **87**, 31–39 (2020). <https://doi.org/10.33979/2073-7416-2020-87-1-31-39>
11. Tamrazyan, A.G., Popov, D.S., Ubysz, A.: To the dynamically loaded reinforced-concrete elements' calculation in the absence of adhesion between concrete and reinforcement. *IOP Conf. Ser. Mater. Sci. Eng.* **913**, 022012 (2020). <https://doi.org/10.1088/1757-899X/913/2/022012>
12. Kolchunov, V.I., Savin, S.Y.: Survivability criteria for reinforced concrete frame at loss of stability. *Mag. Civ. Eng.* **80**, 73–80 (2018). <https://doi.org/10.18720/MCE.80.7>
13. Fedorova, N.V., Savin, S.Y., Kolchunov, V.I.: Affecting of the long-term deformation to the stability of RC frame-bracing structural systems under special accidental impacts. *IOP Conf. Ser. Mater. Sci. Eng.* **753**, 032005 (2020). <https://doi.org/10.1088/1757-899X/753/3/032005>
14. Savin, S.Y.: Deformation criteria for special limit state of rc frame bar elements in compression. *Build. Reconstr.* **91**, 59–69 (2020). <https://doi.org/10.33979/2073-7416-2020-91-5-59-69>
15. Gordon, V.A., Kolchunov, V.I.: To the calculation for the stability of an evolutionarily damaged reinforced concrete element with “degrading” support conditions. *Struct. Mech. Anal. Constr.* 33–38 (2006)
16. Geniyev, G.A., Kisyuk, V.N., Tyupin, G.: *Theory of Plasticity of Concrete and Reinforced Concrete*. Stroyizdat, Moscow (1974)
17. Bondarenko, V.M., Klyueva, N.V.: On the analysis of structures that change a design diagram due to corrosion damages. *News High. Educ. Instit. Constr.* 4–12 (2008)
18. Bondarenko, V.M.: Accounting for energy and corrosion dissipation of power resistance when assessing the stability of building structures. *Struct. Mech. Anal. Constr.* **235**, 51–57 (2011)
19. Alexandrov, A.V., Travush, V.I., Matveev, A.V.: On the calculation of rod structures for stability. *Ind. Civ. Eng.* 16–19 (2002)
20. Savin, S.Y., Kolchunov, V.I., Korenkov, P.A.: Experimental research methodology for the deformation of RC frame under instantaneous loss of column. *IOP Conf. Ser. Mater. Sci. Eng.* **962**, 022054 (2020). <https://doi.org/10.1088/1757-899X/962/2/022054>

# Problems of Accounting for External Reinforcement in the Nonlinear Calculation of Normal Cross Sections of Bent Reinforced Concrete Elements



O. A. Simakov  and D. V. Fuchizhi

The experience of using external reinforcement based on carbon fibers to strengthen reinforced concrete structures shows the high reliability of this system. It should be noted that over the past 15 years, the calculation method has undergone a number of significant changes, while the overall reliability coefficient of this method has decreased on average (a number of criteria have been introduced that determine the amount of reduction in the calculated value of the strength of external reinforcement). At the same time, according to the results of experimental studies, the difference between the experimental data and the results of calculations does not fall below 20%. This margin is justified due to a sufficiently large number of not sufficiently studied issues and developed calculation methods. First of all, this applies to taking into account changes in stiffness in statically undetectable systems when reinforcing reinforced concrete structures with external reinforcement.

Based on the results of the analysis of the methodology for accounting for the nonlinear operation of structures [1–20], a conclusion is made about the importance of accounting for the redistribution of forces in the structure. The experimentally calculated dependence is shown in Fig. 1 [2].

Taking this dependence, the analysis is carried out for the 5-span scheme of the beam floor. At the same time, the issue of only strengthening the beams in the span and separately above the supports is considered.

The general view of the calculation scheme is shown in Fig. 2.

General characteristics of the scheme:

- 5 spans of 6 m on  $x$  and  $y$ ;
- nodal supports with a step of  $6 \times 6$  m;
- the cross section of the plate is 200 mm, the beams are  $400 \times 600$ ;
- concrete B25 (strength 14.5 MPa);

---

O. A. Simakov (✉) · D. V. Fuchizhi  
Moscow State University of Civil Engineering, Yaroslavskoye Shosse, 26, Moscow 129337,  
Russia  
e-mail: [simakovoa@mgsu.ru](mailto:simakovoa@mgsu.ru)

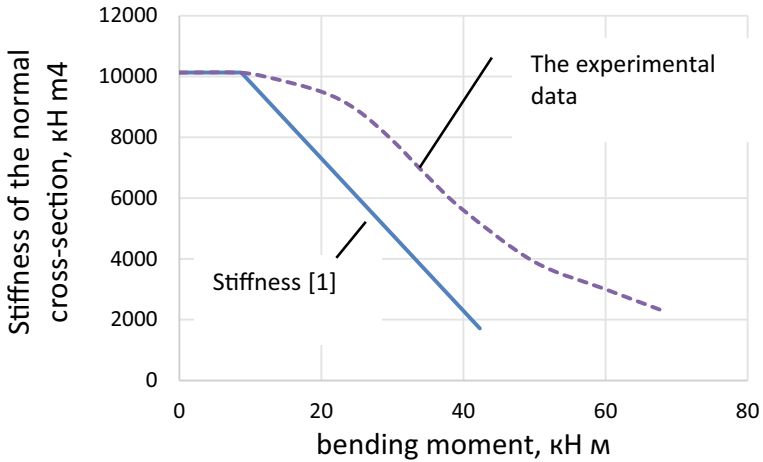


**Fig. 1** Graph of stiffness changes for the normal section of a reinforced concrete element

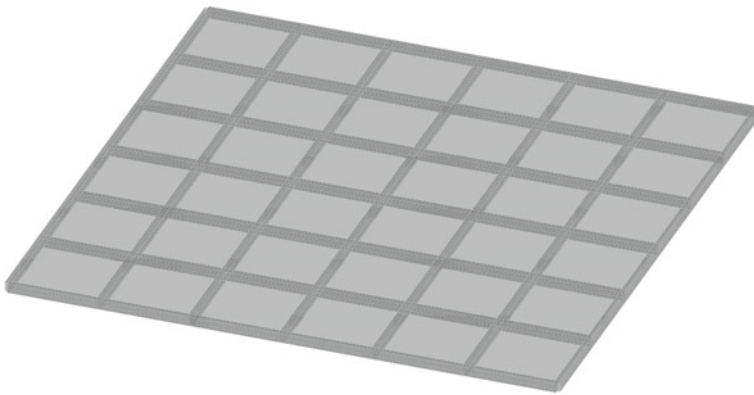


**Fig. 2** General view of the calculation scheme

- reinforcement A500S 3 $\phi$ 12;
- for the element with reinforcement, reinforcement with external reinforcement with carbon tape (strength 245 GPa).

In general, the following type of reinforcement scheme was adopted:

- reinforcement of beams along the lower face in the span of 2 layers of carbon tape with a density of 530  $\text{g}/\text{m}^2$  (thickness 0.294 mm);
- reinforcement of the support zones with carbon tapes in 1 layer.

External reinforcement parameters:

- Modulus of elasticity 245 Gpa;

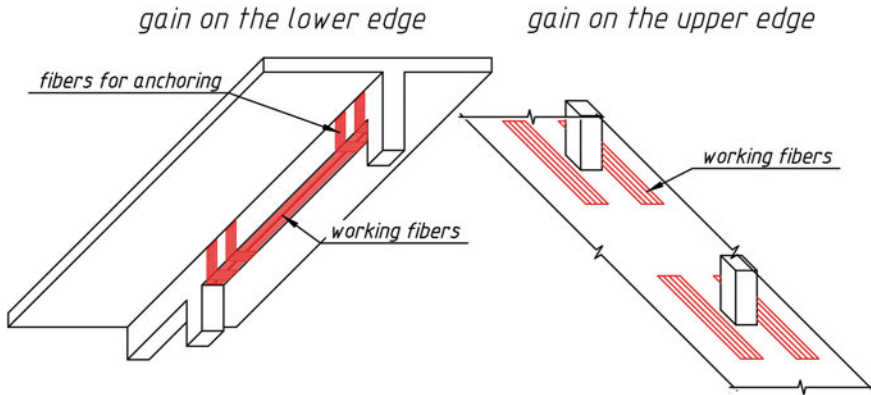


**Fig. 3** The amplification of overlapping

- The ultimate tensile strength of 3.6 Gpa.

The general scheme of reinforcement of structures is shown in Fig. 3.

The calculation is based on two dependences of the bending stiffness:

- proposed in [1];
- based on the experimental data given to the cross section under consideration.

In general, the method [1] suggests using the reduced moment of inertia according to the formula (1) and (2)

$$I_{red} = I_b + \alpha \cdot I_s + \alpha \cdot I'_s + \alpha_f \cdot I_f \tag{1}$$

$$I_{red} = \frac{bx^3}{12} + bx\left(\frac{x}{2}\right)^2 + \alpha \cdot A_s(x - a')^2 + \alpha \cdot A'_s(x - a)^2 + \alpha_f \cdot A_f(h - x)^2 \tag{2}$$

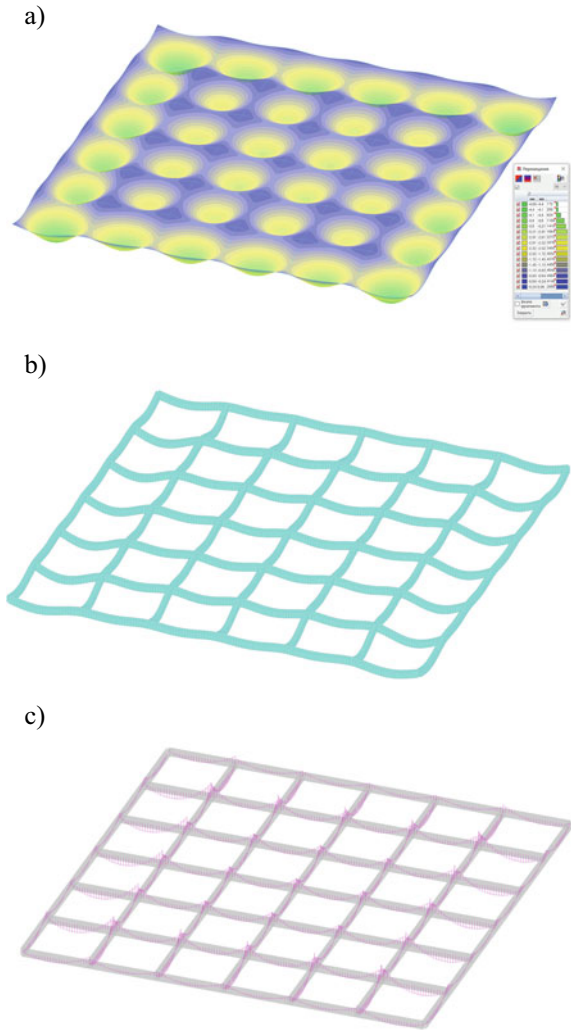
$$\alpha = \frac{E_s}{E_b}, \quad \alpha_f = \frac{E_f}{E_b}$$

The given method has the following provisions that cause reasonable criticism:

- it is based on a theory that does not take into account the significant creep deformations of the binder layer (the adhesive layer of the external reinforcement). At the same time, these deformations were noted in almost all experiments conducted for the earlier period of curing of the binder;
- the uneven distribution of forces in discrete steel reinforcement and external reinforcement is not taken into account.

As a result of calculations of the scheme presented in Figs. 4 and 5, the force isofields are obtained. First of all, the analysis is carried out on the isoples of bending

**Fig. 4** Diagram of the calculation results. **a** Vertical deformations of the plate, **b** vertical deformations of the beams, **c** diagrams of bending moments along the beams



moments—the main criterion for calculating the strength of normal cross sections of bent elements.

Figure 4 shows fragments of bending moments in spans 1–3 for different stiffness variants with the same load value.

After analyzing the data obtained, we can conclude that the difference in the obtained values is within 15%.

At the same time, by adjusting the height of the cross section of the beams, the range of changes in the values of bending moments expands and is 5–20% for this design scheme.

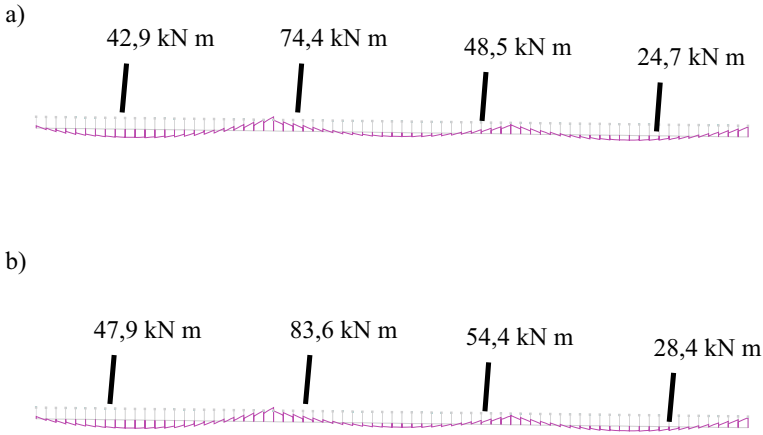


**Fig. 5** Diagrams of bending moments in floor beams. **a** The stiffness is calculated according to [1]; **b** the stiffness is assumed according to experimental data

The method [1] implies taking into account the initial deformations of the structure through the bending moment  $M_0$  from the load acting on the structure. The relative deformations of reinforcement and concrete are determined by the formulas:

$$\varepsilon_s^0 = \frac{M_0}{E_{b1} I_{red}} (h_0 - x_0)$$

$$\varepsilon_b^0 = \frac{M_0}{E_{b1} I_{red}} x_0$$

As well as limiting the boundary of the compressed concrete zone:

$$\xi_{R,f} = \frac{\omega}{1 + \frac{\varepsilon_{f,ult} + \varepsilon_b^0}{\varepsilon_s^0}}$$

If we take into account the absence of complete removal of the load when strengthening the structure, the range of changes in the value of bending moments is reduced to 2–10%.

To be applied at the regulatory level, the method [1] implies significant coefficients of the load-bearing capacity margin:

- the reliability coefficient for the composite material  $\gamma_f$ . For calculations for the first group of limit states, 1.2 is assumed for carbon composites;
- coefficient of the working conditions of the external reinforcement element, depending on the material and type of fibers  $\gamma_{f1}$ . For composite materials based on carbon fibers, it is accepted from 0.8 (woven materials that work in aggressive environments) to 0.95 (laminates that work in indoor areas);



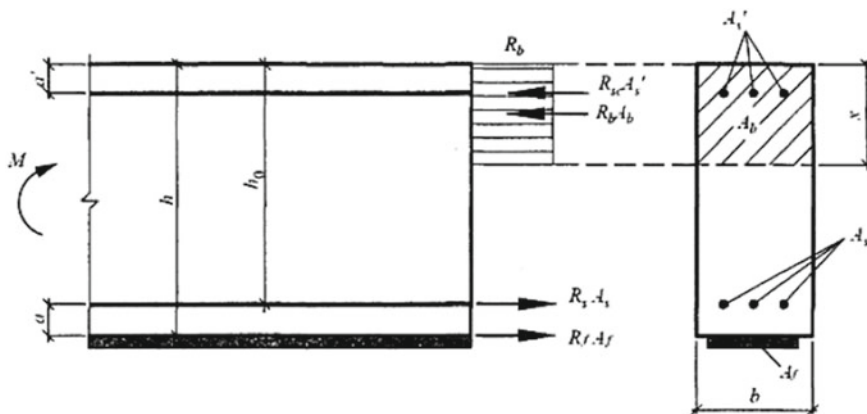


Fig. 6 Calculation scheme of the normal cross section of the bent element

- the coefficient of working conditions, taking into account the adhesion/adhesion of the reinforcement element with the base material  $\gamma_{f2}$ . The coefficient depends on the strength of the concrete base, the maximum relative deformations of the external reinforcement, as well as the stiffness of the reinforcement element. In general, the formula has the form:

$$\gamma_{f2} = \frac{1}{2.5\epsilon_{f,ult}} \sqrt{\frac{R_b}{nE_f t_f}} \leq 0.9$$

The equation of the calculated value of the tensile resistance of the external reinforcement, which is taken into account in the calculations, is determined by the formula:

$$R_f = \frac{\gamma_{f1}\gamma_{f2}R_{f,n}}{\gamma_f}$$

And the limiting bending moment perceived by the reinforced external reinforcement section is determined by the formula:

$$M_{ult} = R_b b x (h_0 - 0.5x) + R_{sc} A_s' (h_0 - a') + R_f A_f a$$

In accordance with the calculation scheme in Fig. 6.

Thus, the generalized reliability coefficient of the normal sections of bending elements is more than 1.3. Drawing an analogy with the limits of time, perceived a normal section of bendable element, vychisleny by the method of [1] and obtained experimental data it is possible to allocate the following:

- the current methods of calculating the normal cross sections reinforced by external reinforcement do not take into account a number of factors that determine the

actual operation of the structure. These simplifications are fully compensated by the stock coefficients (for some cases, they have too large values);

- the calculated bending moment has a value more than 20% lower than the value of the bending moment according to experimental studies.

Based on this analysis of the methodology [1] included in the current regulatory documents, as well as the numerical calculations of the bending moments for the stiffness values of the bent elements reinforced by external reinforcement, we can draw the following conclusions:

1. When determining the forces in statically indeterminate reinforced concrete structures, it is mandatory to take into account the redistribution of bending moments as a result of changes in the stiffness of the section. External reinforcement based on carbon fibers contributes a significant component to the value of the stiffness of the normal cross section. At the same time, the value obtained on the basis of analytical calculations according to the standards in force in the Russian Federation does not correspond to the actual values.
2. Before developing a methodology for accounting for changes in the stiffness of reinforced concrete sections, taking into account external reinforcement, it is recommended to introduce increasing coefficients for forces determined by various nonlinear methods. The value of the coefficients is planned to be determined in the future work.
3. Real value accounting effects stiffness enhanced external reinforcement of normal section bending element based on a portion of the load during the work on strengthening is in the range of 2–10%;
4. The method of calculating the normal cross sections of the bent elements, taking into account the external reinforcement, adopted in the regulatory documents, shows a real margin of reliability of more than 20%;
5. Taking into account the above factors, it is possible to state the possibility of applying the methods [1, 5] for the calculation of reinforced concrete statically indeterminate structures of civil buildings;
6. For the purpose of a more reliable analysis of the stress–strain state of the reinforced structure, it is permissible to use existing methods for reducing the rigidity of the reinforced element. In this case, the error will be in the range of up to 30%. What is compensated by the total reserves of the system (at the level of different reliability coefficients).

## References

1. Mukhamediev, T.A., Kuzevanov, D.V.: Calculation of the strength of normal sections of reinforced concrete structures reinforced with composite materials. *Concr. Reinf. Concr.* **6**, 20–24 (2013)
2. Simakov, O.A., Fujii, D.V.: Account Physical Nonlinearity in Bendable Reinforced Concrete Elements in the Amplification Systems of External Reinforcement, the Collection of Reports

- of Scientific-Technical Conference on the Results of Scientific Research Works of Students of the Institute of Construction and Architecture, our UNIVERSITY, Moscow, Publishing House, MISI–MGSU Publishing House (2020)
3. Casadei, P., Nanni, A., Galati, N., Ibell, T., Denton, S.: Moment redistribution in continuous CFRP strengthened concrete members: experimental results. In: International Conference Composites in Construction—CCC2003, Cosenza, Italy, pp. 307–312, 16–19 Sept 2003
  4. Cohn, M.Z., Lounis, Z.: Moment redistribution in structural concrete codes. *Can. J. Civil Eng.* **18**(1), 97–108 (1991)
  5. Mukhamediev T.A.: Rules for Designing Reinforcement of Reinforced Concrete Structures with Composite Materials, № 3 (2013)
  6. CEB-FIP: Ductility of Reinforced Concrete Structures. Synthesis Report and Individual Contribution, Bulletin 242 (May, 1998)
  7. Ashour, A.F., El-Refai, S.A., Garrity, S.W.: Flexural strengthening of RC continuous beam using CFRP laminates. *Cem. Concr. Compos.* **26**, 765–777 (2004)
  8. Garden, H.N., Hollaway, L.C.: An experimental study of the influence of plate end anchorage of carbon fibre composite plates used to strengthen reinforced concrete beams. *Compos. Struct.* **42**, 175–188 (1998)
  9. Swamy, R.N., Mukhopadhyaya, P.: Debonding of carbon fibre reinforced polymer plate from concrete beams. *Proc. Inst. Civil Eng. Struct. Buildings* **134**, 301–317 (1999)
  10. Arduini, M., Nanni, A., Di Tommaso, A., Focacci, F.: Shear response of continuous RC beams strengthened with carbon FRP sheets. Non-metallic (FRP) reinforcement for concrete structures. In: Proceedings of Third International Symposium (FRPRCS-3), Sapporo, Japan, October, vol. 1, pp. 459–466 (1997)
  11. Tamrazyan A.G., Fedorova N.V.: Ocenka nadezhnosti zhelezobetonnykh konstrukcij, usilennyh ugleplastikovym vneshnim armirovaniem. *Izvestiya vysshih uchebnyh zavedenij. Tekhnologiya tekstil'noj promyshlennosti* **6**(366), 226–231 (2016)
  12. ACI 440.2R-17.: Guide for the Design and Construction of Externally Bonded FRP Systems for Strengthening Concrete Structures
  13. Breveglieri, M., Barros, J.A., Dalfré, G.M., Aprile, A.: A parametric study on the effectiveness of the NSM technique for the flexural strengthening of continuous RC slabs. *Compos. Part B Eng.* **43**(4), 1970–1987 (2012)
  14. Silva, P.F., Ibell, T.J.: Evaluation of moment distribution in continuous fibre-reinforced polymer strengthened concrete beams. *ACI Struct. J.* **105**(6), 729–739 (2008)
  15. Lou, T., Lopes, S.M., Lopes, A.V.: Neutral axis depth and moment redistribution in FRP and steel reinforced concrete continuous beams. *Compos. Part B Eng.* **70**, 44–52 (2015)
  16. Tajaddini, A.: Investigation of moment redistribution in FRP-strengthened slabs and T-beams. Ph.D. thesis, University of Bath, UK (2015)
  17. Tajaddini, A., et al.: Quantifying Moment Redistribution in FRP-Strengthened RC Beams. *Structures & Buildings*, 20–24 May 2016
  18. Darby, A., Tajaddini, A., Ibell, T., Evernden, M., Silva, P.: The effect of FRP strengthening on moment redistribution in RC members. *ACI Struct. J.* (2018)
  19. Spadea, G., Bencardino, F., Swamy, R.N.: Structural behaviour of composite RC beams with externally bonded CFRP. *J. Compos. Construct. ASCE* **132**–137 (1998)
  20. Oehlers, D.J., Ju, G., Liu, I.S.T., Seracino, R.: Moment redistribution in continuous plated RC flexural members. Pt. 1. Neutral axis depth approach and tests. *Eng. Struct.* **26**, 2197–2207 (2004)

# Traditional Measurements in Experiments on Determination of Mechanical Properties Materials and Nuances for Composites



Alexander Anatolyevich Treshchev 

## 1 Traditional Methods of Testing Analysis of Tubular Samples

Traditionally, when covering the methods of experimental identification of the properties of structural materials, the reader is convinced of the universality of data on the loading of thin-walled cylindrical shells, that is, tubular samples. Such tests served as a universal method for testing the proposed postulates in the development of deformation models of structural materials.

The design of the prototypes is widely known and adopted by the type of cylindrical shell with end sections convenient for fixing in the standard grips of the stand [1–3]. This ensures reliably adjustable loading of the cylindrical part of the tube with a longitudinal force  $N$ , a uniform internal pressure  $q$ , and a torsional moment  $M$ . The tube dimensions are accepted according to the standards [1–3]. Testing and processing of the data obtained assume a uniform flow of stresses along the thickness of the tube, and this makes it easy to calculate the stresses. The coordinate system is oriented so that the  $x_1$  axis is the forming shell, the  $x_2$  axis is the guide, and the  $x_3$  axis is the radius. Then the components of the stress tensor on the calculated part of the tube are calculated as follows:

$$\begin{aligned}\sigma_{11} &= \frac{N}{\pi h_0 d_0}; & \sigma_{22} &= \frac{d_0 q}{2h_0}; \\ \tau_{12} &= \frac{2M}{\pi h_0 d_0^2}; & \sigma_{33} &= \tau_{23} = \tau_{13} = 0,\end{aligned}\quad (1)$$

where  $d_0$ —the initial size of the diameter of the middle surface of the tube;  $h_0$ —the initial size of the wall thickness of the shell.

---

A. A. Treshchev (✉)  
Tula State University, Tula 300012, Russia

The values of stresses (1) on the design area of the shell, calculated according to the results of the test of the tubes, are called controlled [1–3]. Varying the parameters of the force loading makes it possible to obtain the expected values of the resulting stresses. It is proved [1–15] that homogeneous stress states are realized as simply as possible in the cross sections of thin tubes, among which it is possible to partially change the independent stress parameters at the discretion of the researcher. The change in the stress ratio due to the regulation of force influences makes it possible to trace a wide range of changes in the stress phases.

By controlling the force loads and calculating the stresses from them (1), we obtain natural invariants of the deviator plane:

$$\begin{aligned}\sigma &= \frac{\sigma_{11} + \sigma_{22}}{3}; \quad 4,5\tau^2 = \sigma_{11}^2 - \sigma_{11}\sigma_{22} + \sigma_{22}^2 + 3\tau_{12}^2; \\ \tau^3 \cos 3\varphi &= -\sqrt{2}\sigma(\sigma_{11} - \sigma)(\sigma_{22} - \sigma),\end{aligned}\quad (2)$$

where  $\cos 3\varphi = \frac{\sqrt{2}\det S_{ij}}{\tau^3}$ —the phase invariant;  $S_{ij} = \sigma_{ij} - \sigma\delta_{ig}$ —the deviator stress.

Experimental studies of the mechanics of materials are usually carried out according to simplified test programs: **q**-experiments; **M**-experiments; **N**-experiments. In addition, combined studies are carried out: **q~M**-experiments; **N~M**-experiments; **N~q**-experiments; **N~M~q**-experiments. In the program **N**-experiments one is a non-zero longitudinal stress, and therefore, will receive

$$\begin{aligned}\sigma_{11} &= \frac{N}{\pi h_0 d_0} = t; \quad \sigma_{22} = \tau_{12} = 0; \quad \sigma = \frac{t}{3}; \\ \tau &= \frac{\sqrt{2}|t|}{3}; \quad \cos 3\varphi = \text{sign}(t).\end{aligned}\quad (3)$$

The **q**-experiments program gives non-zero stress  $\sigma_{22}$ :

$$\begin{aligned}\sigma_{11} = \tau_{12} &= 0; \quad \sigma_{22} = \frac{d_0 q}{2h_0} = p; \quad \sigma = \frac{p}{3}; \\ \tau &= \frac{\sqrt{2}|p|}{3}; \quad \cos 3\varphi = \text{sign}(p).\end{aligned}\quad (4)$$

The **M**-experiments program gives non-zero stress  $\tau_{12}$ :

$$\begin{aligned}\sigma_{11} = \sigma_{22} &= 0; \quad \tau_{12} = \frac{2M}{\pi h_0 d_0^2} = \tau_0; \quad \sigma = 0; \\ \tau &= \frac{\sqrt{2}}{3\tau_0}; \quad \cos 3\varphi = 0.\end{aligned}\quad (5)$$

For combined **N~q**-experiments, the values are valid:

$$\begin{aligned} \sigma_{11} &= \frac{N}{\pi h_0 d_0} = t; & \sigma_{22} &= \frac{d_0 q}{2h_0} = p; & \tau_{12} &= 0; & \sigma &= \frac{t+p}{3}; \\ 4,5\tau^2 &= t^2 - tp + p^2; & 3\tau^3 \cos 3\varphi &= -\sqrt{2}(t+p)(2t-p)(2p-t). \end{aligned} \quad (6)$$

In the experiments  $N\sim q$ , if  $p = 0$  and is accepted  $t > 0$ , then  $\varphi = 0$ , and if  $p > 0$  and for  $t = kp$  at  $k = -1$ , we have  $\sigma = 0$ ,  $\tau = \sqrt{\frac{2}{3}p}$ ,  $\varphi = \frac{\pi}{6}$ , which occurs with a pure shift. If we accept  $k = 1$ , we get  $\sigma = \frac{2p}{3}$ ,  $\tau = \frac{\sqrt{2}p}{3}$ ,  $\cos 3\varphi = -1$ . Hence, it can be seen that even in  $N\sim q$ -experiments, it is possible to study the entire interval of the existence of the stress phase.

Achieving the state of the cylindrical shell close to uniform in the process of axial compression may not be realized due to possible bulging of the wall, which will violate the experimental program. In this regard, experimental studies need to be carried out using combined experiments that implement different stress phases even for classical materials, including those caused by torsion of tubes by moments  $M$ .

In the considered experiments, along with the calculation of stresses and phases, measurements are always performed that allow us to calculate deformations and their invariants. When processing the results, the uniformity of deformations in the thickness of the shell is postulated. There are no difficulties in measuring the longitudinal, transverse, and shear strain ( $e_{11}$ ,  $e_{22}$ ,  $2e_{12} = \gamma_{12}$ ) of tubular samples. Some understatement remains when determining strains along the thickness of the tube wall  $e_{33}$ . The reason for this lies in the small base, when the accuracy of thickness measurements during deformation is significantly reduced, and therefore most experimental works [1–15] operate with  $e_{33}$  for the hypothetical law. Often, the law of linear volume change is adopted, that is

$$e_{33} = -(e_{11} + e_{22}) + \frac{\sigma_{11} + \sigma_{22}}{3K}, \quad (7)$$

where  $K = \frac{E}{3(1-2\nu)}$ —volumetric modulus of elasticity;  $E$ ,  $\nu$ —Young’s modulus and Poisson’s ratio, traditionally calculated from uniaxial experiments with core samples.

Having established from experimental data the strain  $e_{11}$ ,  $e_{22}$ ,  $2e_{12} = \gamma_{12}$  and having accepted their conditions (7) values  $e_{33}$ , taking into account that  $e_{13} = e_{23}$ , we obtain natural invariants of strain:

$$\mathfrak{I} = \frac{\gamma}{2}; \mathfrak{I}^3 \cos 3\beta = \sqrt{2} \begin{vmatrix} e_{11} - e & e_{12} & 0 \\ e_{12} & e_{22} - e & 0 \\ 0 & 0 & e_{33} - e \end{vmatrix}; 3e = \frac{\sigma_{11} - \sigma_{22}}{3K}; \quad (8)$$

$$e = \frac{(e_{11} + e_{22} + e_{33})}{3}; 9\mathfrak{I}^2 = (e_{11} - e_{22})^2 + (e_{22} - e_{33})^2 + (e_{33} - e_{11})^2 + 6e_{12}^2,$$

where  $\beta$ —phase of strain.

Confirmation of the known deformation laws is characterized by the establishment of a connection  $\tau$  with  $\gamma$  and  $\varphi$  with  $\beta$  under various combinations of stresses

and strain developing in the walls of tubular samples. In particular, for a classical material such as low-carbon steel, the hypothesis of the coincidence of stress and strain phases is satisfactorily confirmed, and at the extreme points of uniaxial tension and compression there is an absolute coincidence of them. This hypothesis seems to be very rough for composites (nonmetals). In the case of adopting the linear law volume deformation, zeroing the phase difference, the adoption of collinearity of the principal axes of the stress and strain states must be unambiguous when the octahedral shear stress and shear for the different phases. In this case, the compressive stress is formulated as the sum of the principal stresses on the variation of main strains, or to write down an inverse as a sum of products of strain variation of stress:

$$\delta U = \delta W = \sigma_k \delta e_k = e_k \delta \sigma_k. \quad (9)$$

The connection of principal stresses and deformations with universal invariants makes it possible to transform variation (9) to the form:

$$\delta U = \delta W = (\sigma + \sqrt{2} \tau \cos \varphi_k) \delta(e + \sqrt{2} \vartheta \cos \beta_k) = (e + \sqrt{2} \vartheta \cos \beta_k) \delta(\sigma + \sqrt{2} \tau \cos \varphi_k). \quad (10)$$

Decryption of variations leads to dependencies:

$$\delta U = 3\sigma \delta e + 3\tau [\cos(\varphi - \beta) \delta \vartheta + \sin(\varphi - \beta) \vartheta \delta \beta] = \delta W = 3e \delta \sigma + 3\vartheta [\cos(\varphi - \beta) \delta \tau - \sin(\varphi - \beta) \tau \delta \varphi]. \quad (11)$$

If the hypothesis of phase coincidence is valid, the variations (11) are reduced to the form:

$$\delta U = 3\sigma \delta e + 3\tau \delta \vartheta; \quad \delta W = 3e \delta \sigma + 3\vartheta \delta \tau, \quad (12)$$

for the existence of elastic potentials

$$\frac{\partial \sigma}{\partial \vartheta} = \frac{\partial \tau}{\partial e} \quad \text{and} \quad \frac{\partial \vartheta}{\partial \sigma} = \frac{\partial e}{\partial \tau}$$

the conditions and for the linear law of volumetric strain

$$\sigma = 3K e, \quad (13)$$

requires the manifestation of a connection  $\tau$  only with  $\vartheta$ , that is

$$\tau = 2G\vartheta = G\gamma. \quad (14)$$

## 2 Features of the Method of Testing Tubular Samples for Composites

These arguments are quite contradictory for the experimental analysis of structures, the stiffness parameters of which vary depending on the type of stress or strain states. Among such materials, composite materials are often found, polymerized, fiber-reinforced, and granular. Such materials do not obey the hypotheses of the disjointedness of the volume law from shear deformation and the equality of stress and strain phases, and this contradicts the fundamental equations (13), (14), while  $\omega = \varphi - \beta \neq 0$  [1–3]. Thus, planning and conducting mechanical tests of tubular samples for any series of  $N\sim M\sim q$ -experiments requires special care. When carrying out measurements in  $M$ -experiments, along with the determination of shear strain  $2e_{12} = \gamma_{12}$ , it is necessary to calculate strain  $e_{11}$ , that are absent in classical mechanics, and other experiments are required in the complex aspect. The essence of the contradiction between the classical data on the SSC of tubular samples becomes obvious when loading thin-walled cylindrical shells made of materials with a dependence of physical and mechanical properties on the type of stress state being realized.

In [16–20], the universality of the determining relations for these materials in the form of two forms of the strain potential is demonstrated:

$$\begin{aligned} W = & 0,5[(A + B\alpha_1)\sigma_1^2 + (A + B\alpha_2)\sigma_2^2 + (A + B\alpha_3)\sigma_3^2] \\ & + [C + E\alpha_3 + D(\alpha_1 + \alpha_2)]\sigma_1\sigma_2 + [C + E\alpha_1 + D(\alpha_2 + \alpha_3)]\sigma_2\sigma_3 \\ & + [C + E\alpha_2 + D(\alpha_1 + \alpha_3)]\sigma_1\sigma_3; \end{aligned} \quad (15)$$

$$W = (\tilde{b}_1 + \tilde{b}_3\xi)\sigma^2 + (\tilde{b}_2 + \tilde{b}_4\xi + \tilde{b}_5\eta \cos 3\varphi)\tau^2, \quad (16)$$

where

$$\alpha_k = \frac{\sigma_k}{S}; \quad S = \sqrt{\alpha_k \sigma_k}; \quad \cos \psi = \xi = \frac{\sigma}{S_0}; \quad \sin \psi = \eta = \frac{\tau}{S_0}; \quad S_0 = \sqrt{\sigma^2 + \tau^2};$$

$$S_0 = \frac{S}{\sqrt{3}}; \quad \alpha_1 + \alpha_2 + \alpha_3 = \sqrt{3}\xi; \quad \alpha_k \alpha_k \alpha_k = \frac{3\xi^3 + 9\xi\eta^2 + 1,5\sqrt{2}\eta^3 \cos 3\varphi}{\sqrt{3}};$$

$$\cos 3\varphi = \frac{\sqrt{2} \det(S_{ij})}{\tau^3}; \quad S_{ij} = \sigma_{ij} - \delta_{ij}\sigma; \quad \tilde{b}_1 = 1,5(A + 2C); \quad \tilde{b}_2 = 1,5(A - C);$$

$$\tilde{b}_3 = \frac{1,5(B + 4D + 2E)}{\sqrt{3}}; \quad \tilde{b}_4 = \frac{4,5(B - E)}{\sqrt{3}}; \quad \tilde{b}_5 = \frac{0,75(B - 2D + 2E)\sqrt{2}}{\sqrt{3}};$$

$$A = 0,5\left(\frac{1}{E^+} + \frac{1}{E^-}\right); \quad B = 0,5\left(\frac{1}{E^+} - \frac{1}{E^-}\right); \quad C = -0,5\left(\frac{v^+}{E^+} + \frac{v^-}{E^-}\right);$$



$$E = 0,25\sqrt{3}\left(\frac{1-2v^+}{E^+} - \frac{1-2v^-}{E^-}\right) - 0,25\left(\frac{1-4v^+}{E^+} - \frac{1-4v^-}{E^-}\right);$$

$$D = -0,5\left(\frac{v^+}{E^+} - \frac{v^-}{E^-}\right);$$

$E^\pm, v^\pm$ —elastic modulus and Poisson's ratio under uniaxial tension and compression.

The connection of stress and strain tensors resulting from the potential  $W$  is established by the Castigliano formulas:

$$e_{ij} = \frac{1}{3}\left\{2\left[\tilde{b}_1 + \tilde{b}_3\xi(1 + 0,5\eta^2)\right] + \frac{(\tilde{b}_4\eta^2 + 1,5\sqrt{2}\tilde{b}_5)\eta^2}{\xi} - \tilde{b}_5\eta^3 \cos 3\varphi\right\}\sigma\delta_{ij}$$

$$+ \frac{1}{3}\left\{2(\tilde{b}_2 + \tilde{b}_4\xi + \tilde{b}_5\eta \cos 3\varphi) - (\tilde{b}_3\xi^2 + \tilde{b}_4\eta^2)\xi\right.$$

$$\left. - \tilde{b}_5(3 - \eta\xi^2) \cos 3\varphi + 3\sqrt{2}\tilde{b}_5\mu_{ij}\right\}S_{ij}, \quad (17)$$

where  $\mu_{ij} = \frac{\lambda_{ij}}{S_{ij}}$ ;  $\lambda_{ij} = \frac{\Delta_{ij}}{S_0}$ ;  $\Delta_{ij}$ —minor for the component  $S_{ij}$ .

Generalized deformation laws for structural materials follow from the equations of states (17):

$$e = \frac{\sigma}{3K_0} + \frac{\tau}{3D_0}; \quad \vartheta = \sqrt{1 + tg^2\omega}\left(\frac{\tau}{2G_0} + \frac{\sigma}{3D_0}\right);$$

$$tg\omega = \frac{3\tilde{b}_5\eta \sin 3\varphi}{\frac{3\eta}{2G_0} + \frac{\xi}{D_0}}, \quad (18)$$

which do not correspond to, but rather refute, Eqs. (13), (14), which are immutable for classical mechanics. In the entry (18), there is a parameter  $K_0$ ,  $G_0$ , and  $D_0$  called generalized «modules» of volume strain, shape change (shift), and dilation (these are not constants, but nonlinear functions that depend on the type of stress state):

$$K_0 = \frac{1}{\left[2\tilde{b}_1 + \tilde{b}_3\xi(2 + \eta^2) - \tilde{b}_5\eta^3 \cos 3\varphi\right]}; \quad D_0 = \frac{1}{\tilde{b}_4\eta^3};$$

$$2G_0 = \frac{3}{2\tilde{b}_2 + \xi^3(2\tilde{b}_4 - \tilde{b}_3) + \tilde{b}_5\eta^3(2 + \xi^2) \cos 3\varphi}. \quad (19)$$

Considering a circular cylindrical shell with thin walls made of composite material, the location of each point in the middle-curved surface is usually determined

by Gauss coordinates  $\Gamma_1$ ,  $\Gamma_2$ , and  $\Gamma_3$ . Taking the shell length  $l$ , radius of curvature  $R$ , wall thickness  $h$ , subjected to pure torsion and the labeling of the axial displacement of the middle surface through  $u$ , the district—through and move along the radius  $w$ , we present the parameters of the Lamé and the main curvature to the form:  $\tilde{A} = 1$ ;  $\tilde{B} = R$ ;  $k_1 = 0$ ;  $k_2 = R^{-1}$ , where  $R$ —is the radius of the middle surface of the shell.

Let's replace the coordinates of the shell surface as follows:  $x_1 = \Gamma_1$ ,  $x_2 = \Gamma_2$ ,  $x_3 = \Gamma_3$ . It is obvious that the coordinate  $x_1$  is directed along the generatrix,  $x_2$ —along the guide, and  $x_3$ —along the radius of curvature of the surface from the center. We assume one end section of the shell with  $x_1 = 0$  a rigidly pinched, and the second—with  $x_1 = l$  a loaded torque with a uniformly distributed shear force intensity  $S = h\tau_0$  (pure torsion of the sample in  $\mathbf{M}$ -experiments), where  $\tau_0$ —uniform tangential stresses over the thickness of the section at  $x_1 = l$ . In this case, it is quite clear that both cylindrical surfaces of the shell are in an unloaded state. Such states correspond to a flat generalized stress state. Therefore, zero values of stresses  $\sigma_{33} = \tau_{13} = \tau_{23} = 0$  with characteristic boundary conditions are obvious:  $u = 0, v = 0$  at  $x_1 = 0$ ;  $\sigma_{11} = 0, \tau_{12} = \tau_0$  at  $x_1 = l$ . For axisymmetric loading of a shell, different from zero voltage to depend only on the coordinates  $x_1$ . The fundamental equilibrium equations [1] in the accepted coordinate system are as follows:

$$\sigma_{11,1} = 0; \quad \tau_{12,1} = 0; \quad \frac{\sigma_{22}}{R} = 0. \quad (20)$$

The elementary solution of equations (20) under the corresponding boundary conditions is reduced to the form:

$$\sigma_{11} = 0; \quad \sigma_{22} = 0; \quad \tau_{12} = \tau_0. \quad (21)$$

Equation (21) completely characterize the stress state of the shell, and the constitutional equations (17) are transformed to the form:

$$e_{11} = (1,5B - D)\alpha_{12}^2\sqrt{2}\tau_{12}; \quad e_{22} = (1,5B - D)\alpha_{12}^2\sqrt{2}\tau_{12}; \quad e_{12} = (A - C)\tau_{12}, \quad (22)$$

or, given (21):

$$e_{11} = \frac{(1,5B - D)\sqrt{2}\tau_0}{2}; \quad e_{22} = \frac{(1,5B - D)\sqrt{2}\tau_0}{2}; \quad e_{12} = (A - C)\tau_0, \quad (23)$$

The selected coordinate system leads to dependencies

$$e_{11} = u_{,1}; \quad e_{22} = \frac{w}{R}; \quad e_{12} = 0,5v_{,1}, \quad (24)$$

where  $u(x_1)$ ,  $v(x_1)$ ,  $w(x_1)$ —longitudinal, circumferential, and normal displacements are averaged.

Taking the equalities of expressions (22) and (23), we come to a system of equations in displacements:

$$u_{,1} = \frac{(1,5B - D)\sqrt{2}\tau_0}{2}; \quad \frac{w}{R} = \frac{(1,5B - D)\sqrt{2}\tau_0}{2}; \quad v_{,1} = 2(A - C)\tau_0. \quad (25)$$

The solution of equations (25) in combination with boundary conditions is reduced to the dependencies:

$$u = \frac{(1,5B - D)\sqrt{2}\tau_0 x_1}{2}; \quad v = 2(A - C)\tau_0 x_1; \quad w = \frac{(1,5B - D)\sqrt{2}\tau_0 R}{2}, \quad (26)$$

or

$$\begin{aligned} u &= \frac{\left[ \frac{(3+2v^+)}{E^+} - \frac{(3+2v^-)}{E^-} \right] \sqrt{2}\tau_0 x_1}{8}; \\ v &= \left[ \frac{(1+v^+)}{E^+} + \frac{(1+v^-)}{E^-} \right] \tau_0 x_1; \\ w &= \frac{\left[ \frac{(3+2v^+)}{E^+} - \frac{(3+2v^-)}{E^-} \right] \sqrt{2}\tau_0 R}{8}. \end{aligned} \quad (27)$$

The above decisions show that unlike classical methods of experimental determination of deformations of  $M$ -experiments for composite materials is the need to measure not only the angle of torsion and circumferential displacement  $v$ , but also other displacements  $u$  and  $w$  (27), missing in steel shells. If we take the special case when the characteristics of the shell materials are reduced to the classical ones  $E^+ = E^- = E$ ,  $v^+ = v^- = v$ , then the displacements will be equal:

$$u = w = 0; \quad v = \frac{2(1+v)}{E}\tau_0 x_1. \quad (28)$$

Analyzing Eqs. (27) and (28), it is possible to establish qualitative differences between the calculated and experimentally obtained characteristics of the SSC of shells associated with taking into account the different resistance of composites. As can be seen from Eq. (20), with a nature different resistance of the material ( $E^+ > E^-$  or  $E^+ < E^-$ ) the shell in the case of free torsion lengthens or shortens, increasing or decreasing the diameter, which confirms the differences in the quality patterns of its SSC. In addition, the pure torsion of the shell leads to a change in the volume:

$$e = \frac{\sqrt{2}\tau_0\tilde{b}_4}{3\sqrt{3}}$$

and this is not observed in experiments with samples made of materials such as steel [1–3].

Table 1 summarizes the calculated data for a cylindrical shell with a pure torsion when  $E^+ = E, E^- = 2E, v^+ = 0,1, v^- = 0,2$  and at  $E^+ = E, E^- = 0,5E, v^+ = 0,2, v^- = 0,1$  as well as at  $E^- = 3,4E, v^+ = v^- = 0,2$ , and at  $E^+ = E, E^- = 0,294E, v^+ = v^- = 0,2$  («T»). Comparative characteristics can be given in the table of calculated results, which follow from the different-module theory of S.A. Ambartsumyan («A») [21], as well as classical solutions for  $E = E^+$  («K<sup>+</sup>»),  $E = E^-$  («K<sup>-</sup>») and  $\frac{1}{E} = 0,5(\frac{1}{E^+} + \frac{1}{E^-})$  («KO») [1]. The considered example demonstrates the error of the classical theory of elasticity for displacements  $\frac{vE}{\tau_0x_1}$  at  $\frac{E^-}{E^+} = 2$  or  $\frac{E^-}{E^+} = 0,5$ , which reaches 29,4% and depends on the values  $E^-, E^+, v^+, v^-$ , so that with an increase in  $\frac{E^-}{E^+}$  or  $\frac{E^+}{E^-}$  this error increases to 54,5% (at  $\frac{E^-}{E^+} = 3,4$  or  $\frac{E^-}{E^+} = 0,294$ ). The difference in the calculated results for the displacements  $\frac{uE}{\tau_0x_1}$  and  $\frac{wE}{\tau_0R}$  in the models «T» and «A» is 6%, and for  $\frac{vE}{\tau_0x_1}$  the complete coincidence is observed.

The considered example demonstrates the error of the classical theory of elasticity for displacements  $\frac{vE}{\tau_0x_1}$  at  $\frac{E^-}{E^+} = 2$  or  $\frac{E^-}{E^+} = 0,5$ , which reaches 29,4% and depends on the values  $E^-, E^+, v^+, v^-$ , so that with an increase in  $\frac{E^-}{E^+}$  or  $\frac{E^+}{E^-}$  this error increases

**Table 1** The results of the calculation of the shell to the pure torsion

Solution option	$v^-$	$v^+$	$\frac{E^-}{E^+}$	$\frac{uE}{\tau_0x_1}$	$\frac{vE}{\tau_0x_1}$	$\frac{wE}{\tau_0R}$
K <sup>+</sup>	0,2	0,1	2,0	0	2,2	0
KO				0	1,7	0
K <sup>-</sup>				0	1,2	0
T			2,0	0,265165	1,7	0,265165
A			2,0	0,25	1,7	0,25
K <sup>+</sup>	0,1	0,2	0,5	0	2,4	0
KO				0	3,4	0
K <sup>-</sup>				0	4,4	0
T			0,5	-0,53033	3,4	-0,53033
A			0,5	-0,5	3,4	-0,5
K <sup>+</sup>	0,2	0,2	3,4	0	2,4	0
K <sup>-</sup>				0	0,706	0
K <sup>+</sup>			0,294	0	2,4	0
K <sup>-</sup>				0	8,163	0
T			3,4	0,424	1,553	0,424
T			0,294	-1,443	5,281	-1,443

to 54,5% (at  $\frac{E^-}{E^+} = 3,4$  or  $\frac{E^-}{E^+} = 0,294$ ). The difference in the calculated results for the displacements  $\frac{uE}{\tau_0 x_1}$  and  $\frac{wE}{\tau_0 R}$  in the models  $T$  and  $A$  is 6%, and for  $\frac{vE}{\tau_0 x_1}$  the complete coincidence is observed.

Another example of the fallacy of classical methods of testing tubular samples is a similar shell, but loaded according to the programs of  $N$ - $M$ -experiments. For these experimental programs, it is possible to imagine the SSC of a cylindrical shell with similar geometric characteristics: length  $l$ , radius of curvature  $R$ , wall thickness  $h$  and fixed at one end, and at the other—loaded with twisting load forces  $S = h\tau_0$  and tensile force  $N = ht$ .

The considered loading also applies to the plane generalized stress state at  $\sigma_{33} = \tau_{13} = \tau_{23} = 0$ . The accepted anchoring of the shell leads to boundary conditions of the form:

$$u = 0, v = 0 \text{ при } x_1 = 0; \quad \sigma_{11} = \frac{N}{h} = t, \tau_{12} = \tau_0 \text{ при } x_1 = l. \quad (29)$$

In this case, the resulting stresses depend on a single coordinate,  $x_1$  and therefore the equilibrium equations do not change and, taking into account the boundary conditions, they elementary lead to a solution for the stresses

$$\sigma_{11} = \frac{N}{h} = t; \quad \sigma_{22} = 0; \quad \tau_{12} = \tau_0. \quad (30)$$

Three equations (30) give the values of the parameters of the stress state of the shell. In this case, the equations of state (17) are transformed to the form

$$\begin{aligned} e_{11} &= [A + 0,5B(3 + \alpha_{11})\alpha_{11}^2]\sigma_{11} + (1,5B - D(1 + \alpha_{11}^2))\alpha_{12}\tau_{12}; \\ e_{22} &= C\sigma_{11} + (1,5B - D)\alpha_{12}\tau_{12}; \\ e_{12} &= [A - C + 0,5B\alpha_{11}^3 + (1,5B - D)(1 + \alpha_{11}^2)]\tau_{12}, \end{aligned} \quad (31)$$

or taking into account (30)

$$\begin{aligned} e_{11} &= \left[ A + 0,5B \frac{\left( 3\sqrt{t^2 + 2\tau_0^2} + t \right) t^2}{(t^2 + 2\tau_0^2)^{\frac{3}{2}}} \right] t + \frac{2(1,5B - D)\tau_0^2}{(t^2 + 2\tau_0^2)^{\frac{3}{2}}}; \\ e_{22} &= \frac{Ct + (1,5B - D)\tau_0^2}{t^2 + 2\tau_0^2}; \\ e_{12} &= \left[ \frac{A - C + 0,5Bt^3}{(t^2 + 2\tau_0^2)^{\frac{3}{2}}} + \frac{(1,5B - D)(t^2 + 3\tau_0^2)t}{(t^2 + 2\tau_0^2)^{\frac{3}{2}}} \right] \tau_0. \end{aligned} \quad (32)$$

Geometric relations have the form:

$$e_{11} = u_{,1}; \quad e_{22} = \frac{w}{R}; \quad e_{12} = 0, 5v_{,1}. \quad (33)$$

By establishing equalities between expressions (32) and (33), we arrive at a system of differential equations in displacements:

$$\begin{aligned} u_{,1} &= \left[ A + 0,5B \frac{\left(3\sqrt{t^2 + 2\tau_0^2} + t\right)t^2}{(t^2 + 2\tau_0^2)^{\frac{3}{2}}} \right] t + \frac{\frac{2(1,5B-D)\tau_0^2}{t^2 + \tau_0^2}}{(t^2 + 2\tau_0^2)^{\frac{3}{2}}}; \\ \frac{w}{R} &= \frac{Ct + (1,5B - D)\tau_0^2}{t^2 + 2\tau_0^2}; \\ v_{,1} &= 2 \left[ \frac{A - C + 0,5Bt^3}{(t^2 + 2\tau_0^2)^{\frac{3}{2}}} + \frac{(1,5B - D)(t^2 + 3\tau_0^2)t}{(t^2 + 2\tau_0^2)^{\frac{3}{2}}} \right] \tau_0. \end{aligned} \quad (34)$$

The solution of equations (34) with the use of boundary conditions (29) is reduced to the dependencies

$$\begin{aligned} u &= \left[ A + 0,5B \frac{\left(3\sqrt{t^2 + 2\tau_0^2} + t\right)t^2}{(t^2 + 2\tau_0^2)^{\frac{3}{2}}} \right] tx_1 + \frac{\frac{2x_1(1,5B-D)\tau_0^2}{t^2 + \tau_0^2}}{(t^2 + 2\tau_0^2)^{\frac{3}{2}}}; \\ w &= \frac{CRt + (1,5B - D)R\tau_0^2}{t^2 + 2\tau_0^2}; \\ v &= 2 \left[ \frac{A - C + 0,5Bt^3}{(t^2 + 2\tau_0^2)^{\frac{3}{2}}} + \frac{(1,5B - D)(t^2 + 3\tau_0^2)t}{(t^2 + 2\tau_0^2)^{\frac{3}{2}}} \right] \tau_0 x_1. \end{aligned} \quad (35)$$

By analogy with the previous example, taking the characteristics of the shell materials from the conditions  $E^+ = E^- = E$ ,  $v^+ = v^- = v$  (for the classical solution), we obtain the displacements as such

$$u = \frac{tx_1}{E}; \quad v = \frac{2(1 + \nu)}{E} \tau_0 x_1; \quad w = \frac{Rvt}{E}. \quad (36)$$

The above analysis shows that any test programs for composite tubular samples lead to the conclusion that the measured and calculated SSC parameters do not coincide with similar values obtained by classical approaches.

### 3 Conclusion

The examples discussed above confirm the inconsistency of traditional approaches to processing the obtained parameters and the execution of experimental studies of composite thin-walled tubular samples, or those made of materials with a granular structure. This requires a review of well-established hypotheses and methods of testing materials under complex SSC.

### References

1. Tolokonnikov, L.A.: *Mechanics of a Deformable Solid*. Higher School, Moscow (1979)
2. Bell, J.F.: *Experimental Foundations of Mechanics of Deformable Solids*. Part 1. Small Deformations. Nauka, Moscow (1984)
3. Bell, J.F.: *Experimental Foundations of Mechanics of Deformable Solids*. Part 2. Large Deformations. Nauka, Moscow (1984)
4. Berezin, A.V.: *Influence of Damages on Deformation and Strength Properties Characteristics of Solids*. Nauka, Moscow (1990)
5. Berezin, A.V., Stokov, V.I., Barabanov V.N.: *Deformability and Destruction Isotropic Graphite Materials*. In: *Construction Materials on the Carbon-Based*, vol. 11, pp. 102–110. Metallurgy, Moscow (1976)
6. Fridman, A.M.: Some features of methods for studying the strength of properties graphite in a flat stressed state. *Factory Lab.* **9**, 1137–1140 (1972)
7. Stokov, V.I., Barabanov, V.N.: Methods for studying the strength and deformation properties of graphite in a complex stress state. *Factory Lab.* **9**, 1141–1144 (1974)
8. Fridman, A.M., Anufriev, Yu.P., Barabanov, V.N.: Research of destruction carbon-graphite materials under complex stress conditions. *Probl. Strength* **1**, 52–55 (1973)
9. Jones, R.M.: Modeling nonlinear deformation of carbon-carbon composite materials. *AIAA J.* **18**(8), 995–1001 (1980)
10. Jones, R.M.: Stress-strain relations for materials with different moduli in tension and compression. *AIAA J.* **15**(1), 16–25 (1977)
11. Tasuji, M.E., Slate, F.O., Nilson, A.H.: Stress-strain response and fracture of concrete in biaxial loading. *ACI J.* **7**, 806–812 (1979)
12. El'suf'ev, S.A., Chebanov, V.M.: Studying the deformation of fluoroplast under the conditions of flat stress state. *Stud. Elast. Plast.* **8**, 209–213 (LSU, Leningrad) (1971)
13. Kalinka, Yu.A., Borovikova, S.M.: Investigation of physical and mechanical properties chaotically filled with fiberglass. *Mech. Polym.* **3**, 411–415 (1971)
14. Amelina, E.V.: On nonlinear deformation of carbon fiber plastics: experiment, model, calculation. *IVT SB RAS. Comput. Technol.* **20**(5), 27–52 (2015)
15. Kayumov, R.A., Lukankin, S.A., Paimushin, V.N., Kholmogorov, S.A.: Identification mechanical characteristics of fiber-reinforced composites. *Scientific notes Kazan University. Phys. Math. Sci.* **157**(4), 112–132 (2015)
16. Berezin, A.V.: On the laws of deformation of multi-modulus dilating media. *Probl. Mech. Eng. Autom.* **2**, 70–72 (2007)
17. Matchenko, N.M., Tolokonnikov, L.A., Treshchev, A.A.: Defining relations isotropic different resistant environments. Part 1. Quasilinear relations. *News Russian Academy of Sciences. Solid State Mech.* **1**, 73–78 (1995)
18. Matchenko, N.M., Tolokonnikov, L.A., Treshchev, A.A.: Defining relations isotropic different resistant environments. Part 2. Nonlinear relations. *News Russian Academy of Sciences. Solid State Mech.* **4**, 87–95 (1999)

19. Treshchev, A.A.: Theory of Deformation and Strength of Materials with Initial or Induced Sensitivity to the Type of Stress State. Defining features ratios. TulaSU, Tula (2016)
20. Treshchev, A.A., Bobryshev, A.A., Shafigullin, L.N.: Constitutional relations for isotropic materials allowing quasilinear approximation of the deformation law. IP Conf. Ser. Mater. Sci. Eng. **481**, 1–7 (2019) 012014
21. Ambartsumyan, S.A.: Multimodulus Elasticity Theory. Nauka, Moscow (1982)



# Numerical Study of Crack Formation and Strains Distribution During the Punching of Reinforced Concrete Slabs



Valery Borisovich Filatov  and Zulfat Shavkatovich Galyautdinov 

## 1 Introduction

The analysis of works on the study of the strength of reinforced concrete slabs under punching [1–6] showed that in all studies, the authors of the works carried out tests on samples with square columns. Experiments on punching slabs by columns of rectangular section [7–11] show a significant effect of the shape of the column section on the strength of a reinforced concrete slab during punching. The results of these studies are used in the calculations for punching in the European, American, Swiss design codes and some others. However, the issue cannot be considered solved and the influence of design parameters on the strength of slabs during punching is studied by many authors [12–14].

Russian design codes there are no recommendations on taking into account the aspect ratio of the column section for punching shear strength of the slab. Meanwhile, the lack of such recommendations, as shown by the results of experimental studies, can lead to a significant overestimation of the calculated estimate of the punching strength of slabs of a monolithic non-girder frame. This leads to a decrease in the mechanical safety of the buildings and structures being constructed.

To study the features of the operation of a monolithic floor slab during punching by columns of various sections, the authors tested four samples. The samples were a fragment of a monolithic reinforced concrete junction of a column and a floor slab of a non-girder frame. The view of one of the samples during the tests is shown in Fig. 1.

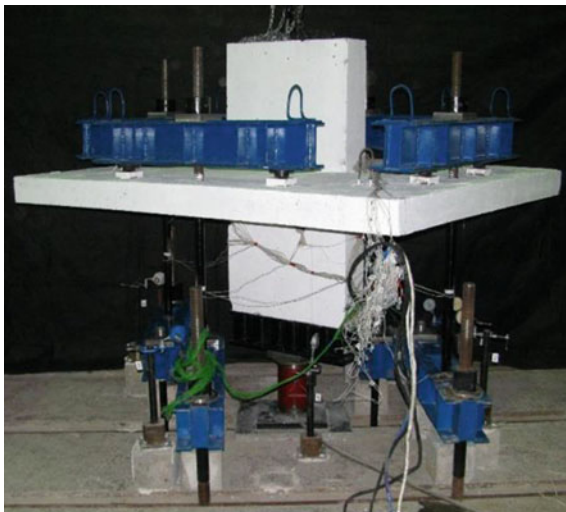
The variable parameter was the column cross-sectional shape. The four specimens have been tested:

- CMR-D—a column of round section with a diameter of 210 mm.
- CMR-I—a column of square section with a side size of 200 mm.

---

V. B. Filatov (✉) · Z. S. Galyautdinov  
Samara State Technical University, Molodogvardeyskay str. 194, 443001 Samara, Russian Federation

**Fig. 1** View of sample CMR-4 during testing



- CMR-2.5—a column of rectangular section of the size  $200 \times 500$  mm.
- CMR-4—a column of rectangular section of the size  $200 \times 800$  mm.

Some results of experimental data analysis are given in [15, 16].

For a deeper analysis of the experimental data, a numerical study was performed on finite element models in Simulia Abaqus. The finite element model is developed in a nonlinear formulation and takes into account the peculiarities of the operation of reinforced concrete structures: the formation and development of cracks, plastic deformations of concrete and the possibility of brittle failure. To describe the behavior of concrete at all stages of loading, the law of concrete deformation is used, taking into account plastic deformations.

Finite element modeling to study the stress-strain state of slabs during punching was effectively used by the authors [17–21].

## 2 Structure of Finite Element Model

Models of four samples were developed, corresponding to full-scale samples, the test results of which are given in [16]. The general view of the finite element model is shown in Fig. 2a. Since the model is symmetric, only a quarter of the samples were modeled, and the reactions of the discarded parts were modeled by imposing constraints. Steel plates on the top face of the slab were modeled, which transferred the load to the specimen slab by means of rods. On the lower node of the rods, a connection was superimposed that forbade movement along the vertical axis; thus, the fixation of the rod in the power floor was simulated. The samples were loaded with a monotonically increasing uniformly distributed load applied to the lower face

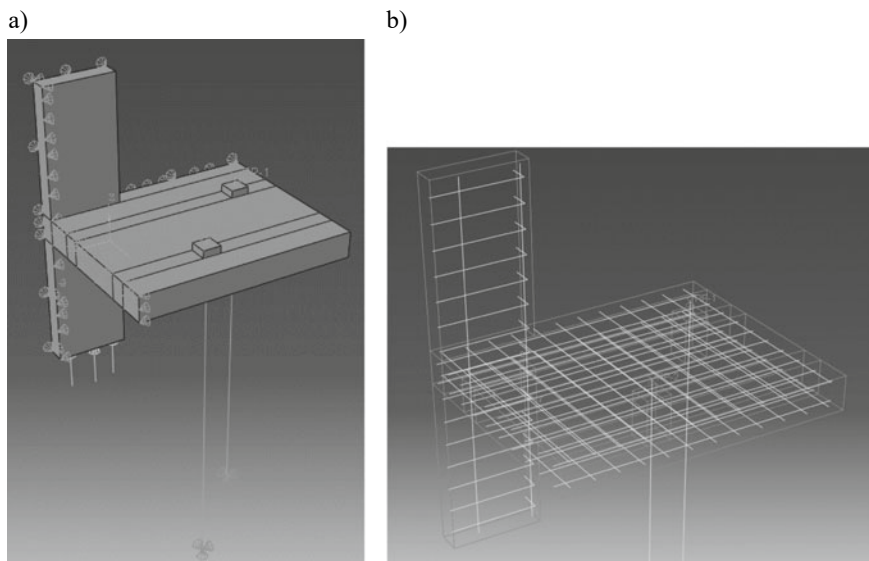


**Fig. 2** General view and reinforcement of the finite element model

of the column. The finite element mesh is adopted with a size of 7 mm in plan. The reinforcing bars of the upper and lower grids of the plate, the longitudinal and transverse reinforcement of the column, adopted in the finite element model are shown in Fig. 2b.

The slab reinforcement in perpendicular direction was located at different depths, differing by the value of the reinforcement bar diameter. The reinforcement was modeled by a finite element “beam”, that is, the bending work of the element was taken into account.

Table 1 shows the values of failure loads obtained in finite element modeling and in the experiment on test samples. The results in Table 1 show that the finite element model underestimates the strength of the samples with a uniform distribution of shear stresses (sample CMR-D). For samples with a small stress concentration in the column corners (samples CMR-1 and CMR-2.5), there is a satisfactory convergence of the results. For the CMR-4 sample with the greatest unevenness of shear stresses at the control perimeter, the finite element model slightly overestimates the strength

**Table 1** Comparison of the values of failure loads of finite element models and test samples

Samples	$P_{FEM}$ (kN)	$P_{test}$ (kN)	$P_{FEM}/P_{test}$
CMR-D	62	71	0.87
CMR-1	62	68	0.91
CMR-2.5	71	70	1.01
CMR-4	88	82	1.07

of the sample. This trend allows us to conclude that it is necessary to improve the strength criterion in finite element modeling.

### 3 Results and Discussion

The finite element model was verified by comparing it with the test results of test samples. Figure 3 shows the schemes of cracks on the tensioned side of the plate of the finite element model at different loading levels.

A comparison was made of the crack formation patterns on the tensioned edge of the slab, as well as the values of the deformations of the tensioned reinforcement and compressed concrete in the areas where the strain gauges were installed in the sample.

Note that at the initial stage of loading, radial cracks are formed in the sections of the plate near the column corners. Thus, the concentration of deformations near the corners of the column is observed not only on the compressed, but also on

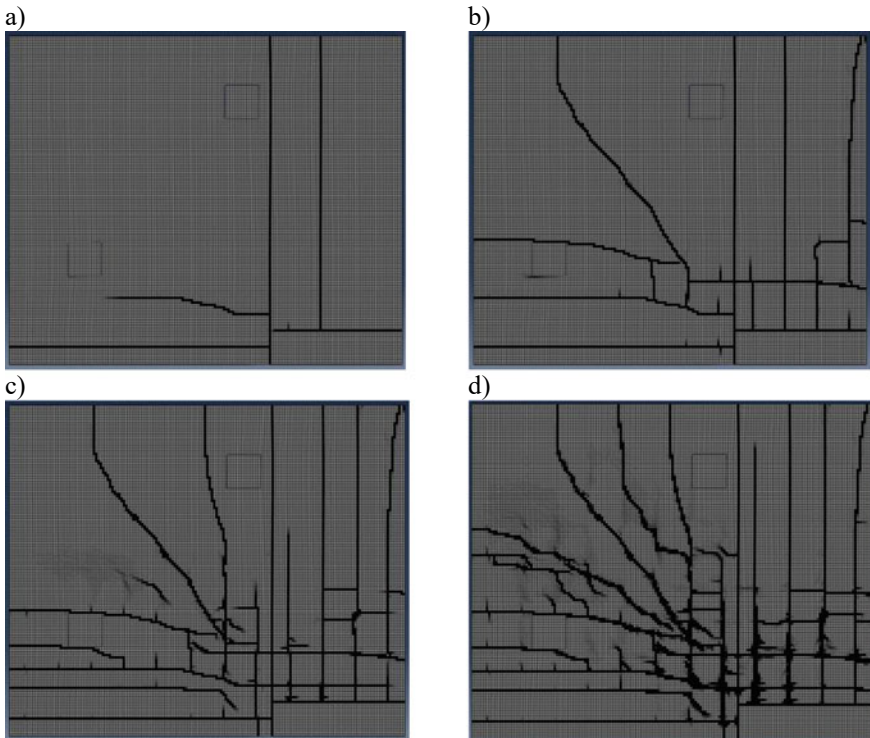


**Fig. 3** Crack patterns in the slab of the finite element model at load levels: **a**  $0.3 P_{ult}$ ; **b**  $0.5 P_{ult}$ ; **c**  $0.7 P_{ult}$ ; **d**  $0.9 P_{ult}$ .

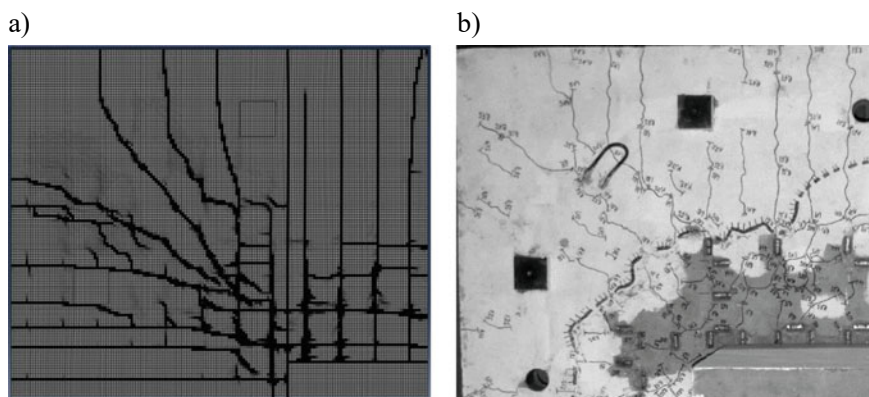


**Fig. 4** Crack patterns in the slab of the finite element model (a) and test sample CMR-4 (b)

the tensioned face of the slab. Note that the cracks width was limited to one finite element, that is, the cracks were not distributed over the entire tensioned face of concrete, which corresponds to the real work of concrete under tension, when the ultimate stresses are reached, a crack is formed and then the stress is “removed” from adjacent sections concrete.

Comparison of the schemes of cracks on the tensioned face of the finite element model (Fig. 4a) and the test sample CMR-4 (Fig. 4b) has been performed. It was noted that the crack patterns have the following similarities:

- radial cracks prevail;
- cracks in the tangential direction are mainly located near the corners and at the long side of the column;
- cracks are located above the reinforcement bars (with a step of 100 mm);
- highest concentration of cracks is localized in the area of slab adjacent to the column’s corner.

Figure 5a shows the graphs of concrete tangential strains on compressed side of the slab along the column’s long side for the finite element model and the full-scale sample.

Analysis of the graphs shows that near the column’s corner there is a significant increase in strains of the slab concrete, while at the middle of the column’s long side, there are practically no concrete strains. The specified feature of concrete deformation when punching a slab with a rectangular column has been repeatedly noted by the authors [10, 11, 13]. This is an essential remark, because the values of tangential strains prevail over radial ones and therefore, they make a significant contribution to the unevenness of the stress-strain state of concrete in the punching zone.

Figure 5b shows the graphs of concrete radial strains on compressed side of the slab along the column’s long side. It follows from the graphs that the radial strains of the slab increase near the corners of the column, but are generally more evenly distributed in this area. The distribution of radial and tangential deformations

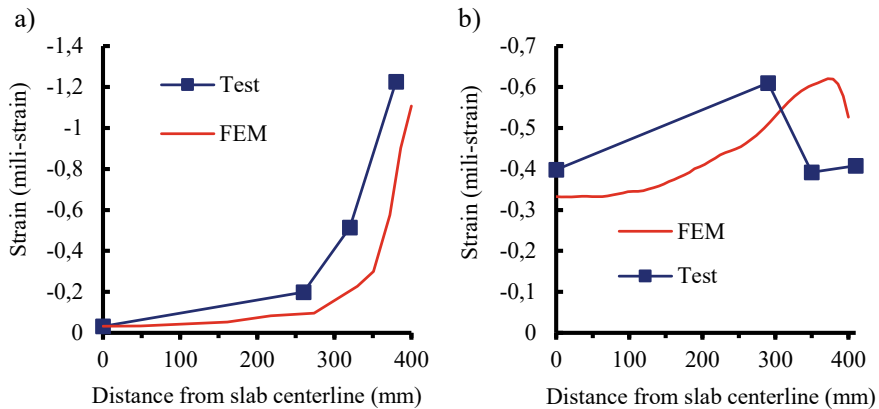


**Fig. 5** Graphs of tangential (a) and radial (b) strains of concrete sample SMR-4 at load level 0.7  $P_{ult}$ .

of concrete during punching was investigated by the authors [11]. The results of studying the distribution of shear stresses on the control perimeter by the method of finite element modeling are presented in [10]. In both cases, concentration of forces in the slab near the corners of column and their decrease along the long side of column were noted.

Note that graphs of tangential and radial strains of concrete compressed face of the slab for finite element model and full-scale sample have good convergence for a qualitative estimate. Evaluating the results from a quantitative point of view, it can be noted that the deformations of the concrete of the prototype exceed the values obtained in finite element modeling. This may be due to underestimation of tensile reinforcement deformations in the finite element model, which will be discussed below.

Figure 6 shows a comparison of deformations of tensile reinforcement for a finite element model and a full-scale sample. Note that the graphs have good convergence, which indicates the correctness of the developed finite element model. At the same time, it should be noted that the correspondence of the results for strain gauges No. 4 and No. 8 is somewhat worse than for No. 3. Apparently, this can be explained by the fact that strain gauges No. 4 and No. 8 are located near the corner of the column, where intense cracking is observed. The formation of cracks leads to a partial destruction of the bond between reinforcement and concrete, which was not taken into account in the finite element model. Debonding of reinforcement with concrete leads to a redistribution of tensile forces from concrete to reinforcement. In the finite element model, the bond of reinforcement to the concrete was considered as provided and the tensile force from concrete to reinforcement was not redistributed. As a result, deformation of the sample reinforcement slightly exceeds the values obtained in finite element modeling.

Strain gauge No. 3 is located at a distance of 1.5  $h_0$  from the column corner. This distance corresponds to the length of the effective control perimeter, which is

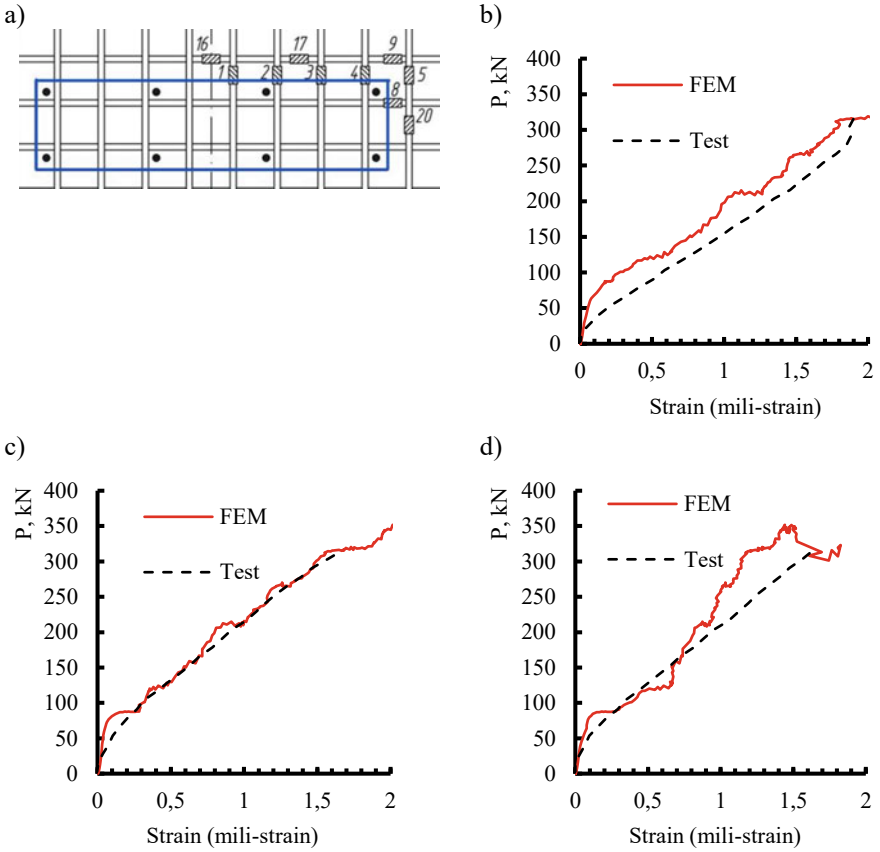


**Fig. 6** Strain gauge scheme (a); graph of strain gauge No. 8 (b); graph of strain gauge No. 3 (c); graph of strain gauge No. 4 (d)

taken into account when calculating punching shear according to the Model Code 2010 method. As test results of the sample show (Fig. 4b), the intensity of cracking decreases with distance from the corner of column. The concrete receives the tensile forces together with the reinforcement. This is most consistent with the nature of finite element model deformation and strain gauge No. 3 shows the best coincidence of the calculated and experimental values of reinforcement deformations.

The noted features of deformation of this finite element model will be taken into account for its subsequent correction and improvement.

## 4 Conclusion

1. The results of numerical experiments on finite element models showed a good convergence of the qualitative and quantitative picture of deformation with the results of experimental studies on test samples.
2. The results of the finite element experiment show that plate deformations are concentrated near the column's corners and decrease along the long side of rectangular column, which indicates an uneven distribution of internal forces along the length of the control perimeter. The same character of plate deformation is noted in the results of experimental studies on test samples. This fact is of significant importance, since the method of Russian design code assumes a uniform distribution of shearing forces along the length of control perimeter.
3. Comparison of the results of finite element modeling and experimental studies on test samples is a verification of the finite element model and allows the model to be used to study various design parameters that affect the strength of a reinforced concrete slab during punching.

## References

1. Tamrazyan, A.G., Zvonov, Y.N.: To assessing the reliability reinforced concrete flat slabs for punching under the action of concentrated force at high temperatures. *Ind. Civ. Eng.* **7**, 24–28 (2016)
2. Trekin, N.N., Pekin, D.A.: Hidden metal capitals of monolithic beamless slabs. *Ind. Civ. Eng.* **7**, 17–20 (2014)
3. Bolgov, A.N., Sokurov, A.Z.: Numerical modeling of punching flat slabs strengthened by shear reinforcement. In: *Concrete and Reinforced Concrete—Glance at Future*, pp. 139–149. MGSU, Moscow (2014)
4. Brooms, C.E.: Tangential strain theory for punching failure of flat slabs. *ACI Struct. J.* **113**, 95–104 (2016)
5. Muttoni, A.: Punching shear strength of reinforced concrete slabs without transverse reinforcement. *ACI Struct. J.* **105**, 440–450 (2008)
6. Guandalini, S., Burdet, O.L., Muttoni, A.: Punching tests of slabs with low reinforcement ratios. *ACI Struct. J.* **106**, 87–95 (2009)
7. Hawkins, N.M., Falssen, H.B., Hinojosa, R.C.: Influence of column rectangularity on the behaviour of flat plate structures. *ACI Spec. Publ. SP-30*, 127–146 (1971)
8. Al-Yousif, A.T., Regan, P.E.: Punching resistances of RC slabs supported by large and/or elongated columns. *Struct. Eng.* **81**, 30–34 (2003)
9. Teng, S., Cheong, H.K., Kuang, K.L., Geng, J.Z.: Punching shear strength of slabs with openings and supported on rectangular columns. *ACI Struct. J.* **101**, 678–687 (2004)
10. Sagaseta, J., Tassinari, L., Ruiz, M.F., Muttoni, A.: Punching of flat slabs supported on rectangular columns. *Eng. Struct.* **77**, 17–33 (2014)
11. Setiawan, A., Vollum, R.L., Macorini, L., Izzuddin, B.A.: Punching of RC slabs without transverse reinforcement supported on elongated columns. *Structures* **27**, 2048–2068 (2020)
12. Muttoni, A., Fernández Ruiz, M., Simões, J.T.: The theoretical principles of the critical shear crack theory for punching shear failures and derivation of consistent closed-form design expressions. *Struct. Concr.* **19**, 174–190 (2018)



13. Shu, J., Belletti, B., Muttoni, A., Scolari, M., Plos, M.: Internal force distribution in RC slabs subjected to punching shear. *Eng. Struct.* **153**, 766–781 (2017)
14. Pani, L., Stochino, F.: Punching of reinforced concrete slab without shear reinforcement: Standard models and new proposal. *Front. Struct. Civ. Eng.* **14**, 1196–1214 (2020)
15. Filatov, V.: Experimental investigation of stress-strain conditions in punching zone of flat slabs. *MATEC Web Conf.* **117**, 00045 (2017)
16. Filatov, V.B., Galyautdinov, Z.S.: Experimental research of punching shear strength on reinforced concrete test samples. *IOP Conf. Ser. Mater. Sci. Eng.* **451**, 012061 (2018)
17. Genikomsou, A.S., Polak, M.A.: Finite element analysis of punching shear of concrete slabs using damaged plasticity model in ABAQUS. *Eng. Struct.* **98**, 38–48 (2015)
18. Goh, C.Y.M., Hrynyk, T.D.: Numerical investigation of the punching resistance of reinforced concrete flat plates. *J. Struct. Eng.* **144**, 04018166 (2018)
19. Milligan, G.J., Polak, M.A., Zurell, C.: Finite element analysis of punching shear behaviour of concrete slabs supported on rectangular columns. *Eng. Struct.* **224**, 111189 (2020)
20. Sanabria, R.A., Oliveira, L.H.B., Trautwein, L.M., Almeida, L.C., Santos, A.C.: Aspects of finite element modeling of punching shear behavior of reinforced concrete flat slabs. *Lat. Am. J. Solids Struct.* **15** (2018)
21. Sarvaicova, S., Borzovic, V., Augustin, T.: The influence of a column shape cross-section on the punching capacity. In: Proceedings of the 13th International conference “Modern Building Materials, Structures and Techniques (MBMST 2019)”, pp. 455–462 (2019)

# **Reliability, Inspection and Monitoring of Buildings and Structures**

# Forecast Durability for Protective Penetrating Waterproof Coating



A. I. Bedov, A. I. Gabitov , I. G. Terekhov, and A. S. Salov 

The current level of construction materials production enables applying various materials. Mass and precast concrete, as well as reinforced concrete, are widely applied for installing substructures, foundations, both bearing and enclosing structures, while silicate and red bricks, gas-concrete and cellular blocks are commonly used in making external walls, enclosing structures and interior partitions.

Generally, the durability of structures made of the above materials depends on two points: secondary protection of construction materials and reliable waterproofing thereof.

The correct choice of technology for protecting construction materials and waterproofing structures is defined by a great number of points: kind of negative destructing effect, type of structure and construction materials it is made of, operating conditions and aesthetic and structural requirements.

This paper deals with finding a method for using innovative waterproof material and technologies to provide durability for hydraulic structures under construction, operation, repair and renovation thereof.

The proposed problem was being solved using the “Kalmatron” system including:

- “Kalmatron” protective waterproofing compound;
- “Kalmatron-Econom” waterproofing plastering;
- “Kalmatherm” protective thermal insulation composition.

---

A. I. Bedov

Federal Budget Educational Institution of Higher Education, Moscow State University of Civil Engineering (National Research University), Moscow, Russia  
e-mail: [gbk@mgsu.ru](mailto:gbk@mgsu.ru)

A. I. Gabitov · I. G. Terekhov · A. S. Salov (✉)

Federal Budget Educational Institution of Higher Education, Ufa State Petroleum Technological University, Ufa, Russia  
e-mail: [salov@list.ru](mailto:salov@list.ru)

A. I. Gabitov

e-mail: [azat7@ufanet.ru](mailto:azat7@ufanet.ru)

Application of this system provides for reliable waterproofing of concrete, brick and other structures, making high-strength waterproof coating protecting facilities against various natural and man-made aggressive environments, and recovering waterproofing and strength of the failed structures.

In the course of investigations, the efficiency of applying this system and possibilities thereof in providing reinforced concrete structures and items with high-performance properties was analyzed.

Experience in operating concrete and reinforced concrete structures and, that of buildings, facilities and technological systems made therefrom, accordingly, revealed that these objects are to be protected against the corrosion [1–4]. Moisture penetration is due to precipitation, steam condensation and water flow from wet ground layers towards the structures. Further structural changes in the structure materials, as well as freezing of the buildings and facilities elements, basically of footings and foundations thereof, result in destruction. Penetrating waterproof method was developed to overcome the above difficulties [5, 6].

The only document regulating the quality and characteristics of penetrating waterproofing (in Russia) is GOST 31357-2007 “Dry building mixes based on cement binder. General technical conditions”. In particular, it states the fact that “a material can be considered as a penetrating waterproofing, after treatment with which the water resistance of concrete increases by at least 2 steps” [GOST 31357-2007].

The proposed problem may be solved using the Kalmatron penetrating protective waterproofing compound. Application of this compound enables reliable waterproofing of concrete, brick and other structures, making high-strength waterproof coating protecting facilities against various natural and man-made aggressive environments, and recovering waterproofing and strength of the failed structures. Waterproofing efficiency is achieved due to a number of successive reactions occurring in time and inside the structure of the material to be protected between components within thereof found in Kalmatron compound solution. Poorly and slightly soluble new formations filling the capillaries, pores and microcracks displacing water therefrom are formed by these chemical reactions, which may also be applied for “self-healing” effect [7, 8].

Certain number of experiments were made to identify Kalmatron features using the procedure for mathematical design of experiments with a view to make a forecast durability model for “Kalmatron” waterproof coating depending on conditions and thickness thereof [9, 10].

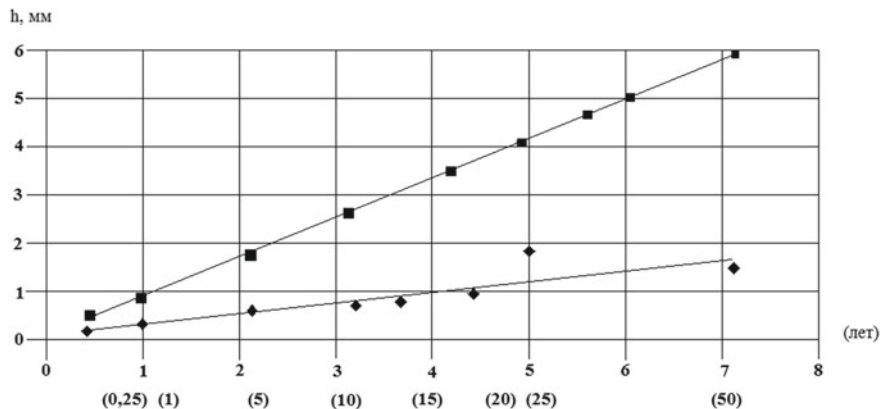
A four-factor experiment plan was made and 9 series of samples (prisms and cylinders) were prepared and mixture properties and composition were defined for testing in hydrochloric acid. Each series included 12 prisms (6 main and 6 check ones) and 6 cylinders (3 main and 3 check ones).

A four-factor experiment plan consisted of:

- selection and variation of factor items (Table 1);
- combination square plotting;
- definition of factor combinations.

**Table 1** Name and options of factor items

Item name	UOM	Item symbol	No. and option value		
Testing length	Months	<i>T</i>	1	2	3
Acid strength	RC (ph)	<i>K</i>	0.01(4)	0.05(3)	0.1(1)
Chemically active particles content of cement by weight		<i>A</i>	2	6	10
Cement content in dry mix by weight		<i>C</i>	30	40	50

**Fig. 1** Results of forecast durability of «Kalmatron» properties depending on conditions and thickness thereof

By mathematical transformations using design models of the procedure for mathematical design of experiments [11, 12], we got diagrams and analytical expressions of both partial and general dependences of the studied values of factors *T*, *K*, *A*, *C* (Table 1), thereby enabling to find values of the forecast durability of “Kalmatron” coating [13–15] depending on conditions and thickness thereof (Fig. 1).

Proceeding from the experiments the following results are obtained:

1. The use of the technique of mathematical planning of the experiment made it possible to obtain, with a minimum amount of testing, analytical dependencies that establish relationships between the studied parameters of the samples and the parameters (factors) of the tests.
2. The analysis of the obtained dependences enabled to reveal corrosion patterns of the aggressive hydrochloric acid affecting fine grain concrete protected by “Kalmatron” coating under variation of (*T*, *K*, *A*, *C*) factors.
3. The required thickness of the protective “Kalmatron” coating providing the durability of structures in this aggressive environment for 50 years is considered to be 1.5–6 mm after processing the results of testing the samples in hydrochloric acid with the strength of 0.01–0.1 rated consumption ( $\text{pH} = 1\text{--}4$ )

In conclusion, we would like to note that actual testing data may be practically applied at the design stage when determining the calculated thickness of the protective penetrating waterproof coating under construction or repair of concrete structures operating in an aggressive environment.

## References

1. Veselkov, D.Ye.: "Lakhta" waterproofing materials. *Constr. Mater.* 3, 20–21 (2001)
2. Valtsifer, I.V.: Efficiency in applying penetrating waterproofing compositions for concrete structures. In: Valtsifer, I.V., Astafiev, S.A., Sizneva, I.P., et al. (eds.) Proceedings of the I International Research to Practice Conference "Problems of Construction Operations and Property Management", pp. 209–212. Kuzbas State Technical University, Kemerovo (2010)
3. Zaykov, D.N.: New generation of Russian waterproofing materials. *Constr. Mater.* 12, 20–21 (2003)
4. Bedov, A.: CAD methods of structural solutions for reinforced concrete frame. In: Bedov, A., Salov, A., Gabitov, A. (eds.) XXI International Scientific Conference on Advances in Civil Engineering "Construction—The Formation of Living Environment" (FORM 2018), vol. 365, pp. 1–8. Moscow, Russian Federation (2018)
5. Kapustin, F.L.: Application of penetrating waterproofing to increase corrosion resistance of cement rock. In: Kapustin, F.L., Spiridonova, A.M., Pomazkin, Ye.P. (eds.) *Concrete Technology*. M.: Composite XXI c. No.3–4 (104–105), pp. 44–47 (2015)
6. Labunsky, A.V.: Waterproofing and corrosion protection for hydraulic facilities. In: Labunsky, A.V. (eds.) *Mechanization Constr.* 11, 22–24 (2006)
7. Latypov, V.M.: Current materials against corrosion and waterproofing of construction structures. In: Latypov, V.M., Lomakina, L.N., Latypova, T.V., Lutsyk, Ye.V. (eds.) *Handbook*. Ufa, p. 6 (2007)
8. Bedov, A.: Engineering solutions for heart efficient exterior walls in climatic condition of the Republic of Bashkortostan. Bedov, A., Gaysin, A., Gabitov, A., Salov, A. (eds.) *E3S Web of Conferences*, p. 02039 (2019)
9. Bedov, A.I.: Application of information modeling technologies at making process engineering documentation. In: Bedov, A.I., Gabitov, A.I., Salov, A.S., Gaisin, A.M. (eds.) *News of Higher Educational Institutions. Textile Industry Technology*. No. 4, pp. 148–153 (2019)
10. Gabitov, A.I.: CAD simulation for stress and strain behaviour of wall constructions made of hollow ceramic blocks. In: Gabitov, A.I., Gaisin, A.M., Salov, A.S. (eds.) *IOP Conference Series: Materials Science and Engineering*, vol 463, Issue 2, 31 December 2018, No 022041. International Multi-Conference on Industrial Engineering and Modern Technologies 2018; Vladivostok; Russian Federation; 2–4 October 2018; Code 144116
11. Bedov, A.I.: The usage of computer modeling to optimizing the cross-sections of reinforced concrete frame elements. Bedov, A.I., Gabitov, A.I., Salov, A.S., Gaisin, A.M., Khabibullina, L.I. (eds.) *Build. Reconstr.* (November–December) No. 6 (74), pp. 3–12 (2017)
12. Sakhibgareev, R.R.: Application of software package "Hector: design-engineer" in course and thesis engineering of construction-related engineering. In: Sakhibgareev, R.R., Terekhov, I.G., Salov, A.S. (eds.) *Educational Process in Higher Institution in Current Conditions*. Proceedings of the II Scientific Research Conference, pp. 39–41. USPTU, Ufa (2013)
13. Khairullin, V.A.: Method for calculating the social effect in the course of investment and construction process. Khairullin, V.A., Terekhov, I.G., Ogneva, A.S. (eds.) *Internet-Magazine "Knowledge Science"*, No.4 (17), p. 58 (2013)
14. Sinitsyn, D.A.: High strength concrete of new generation when erecting high-rise buildings in the Republic of Bashkortostan. In: Sinitsyn, D.A., Salov, A.S., Terekhov, I.G., Timofeev, A.A. (eds.) *Constr. Mater.* No. 6, pp. 8–12 (2020)

15. Nikiforov, A.P.: New and traditional sealing materials for construction and repair. Nikiforov, A.P. (ed.) *Construction Materials*, No.11, p. 19 (1996)
16. Vinnichenko, V., Gabitov, A., Salov, A., Gaisin, A., Kuznetsov, D.: The heat loss calculating methods of external walls in the buildings reconstruction. *MATEC Web of Conferences 7. 7th International Scientific Conference "Reliability and Durability of Railway Transport Engineering Structures and Buildings"* (Transbud 2018), vol. 230. Article number 02038 (2018)
17. Krot, A., Ryazanova, V., Gabitov, A., Salov, A., Rolnik, L.: Resource-saving technologies for advanced concrete in the Republic of Bashkortostan. *MATEC Web of Conferences 7. 7th International Scientific Conference "Reliability and Durability of Railway Transport Engineering Structures and Buildings"* (Transbud 2018), vol. 230. Article number 03009 (2018)
18. Bedov, A.I., Gabitov, A.I., Salov, A.S., Biktasheva, A.R.: Increase of energy performance of residential buildings with enclosing structures made of masonries with application of ceramic blocks. *J. Phys. Conf. Series.* **1425**(1), 012042 (2020)
19. Bedov, A.I., Gabitov, A.I., Gaisin, A.M., Salov, A.S., Chernova, A.R.: CAD technologies under thermal properties analysis of wall cladding of framed buildings. *IOP Conference Series: Materials Science and Engineering: Volume 465, 2018.VII International Symposium Actual Problems of Computational Simulation in Civil Engineering 1–8 July 2018, Novosibirsk, Russian Federation*, pp. 1–8 (2018)
20. Vinichenko, V., Gabitov, A.I., Salov, S.A., Gaisin, A.M., Kuznetsov, D.V.: The heat loss calculating methods of external walls in the buildings reconstruction. *MATEC Web of Conferences Volume 230 (2018) 7th International Scientific Conference "Reliability and Durability of Railway Transport Engineering Structures and Buildings"* (Transbud-2018) Kharkiv, Ukraine, November 14–16, pp. 1–6 (2018)

# The Use of Carbon Fiber Tapes as One of the Ways to Increase the Seismic Resistance of Gas-Silicate Walls



B. K. Dzhamuev  and E. S. Erizhokova

## 1 Introduction

The use of walls made of gas-silicate blocks in buildings and structures erected in the regions of Russia that are subject to seismic activity is limited due to the following reasons:

- masonry made of gas-silicate blocks, as well as brick, is considered as elastic (up to the set load level) or brittle material (above this level). Structures made of plastic material easily tolerate some significant overloads. When calculating such structures, the average intensity of the seismic impact can serve as the main one. Structures made of brittle materials, including lightweight concrete blocks, are very sensitive to the peaks of accidental overloads, which can be critical for these structures. Overload peaks are most dangerous for brittle materials since their elastic limit is close to the ultimate strength.
- use of, mainly, cement mortar for masonry walls made of gas-silicate blocks does not allow the requirements of Seismic Building Design Code [1] to the masonry, in terms of its resistance to seismic effects: value of the normative traction should be  $R_{tt} \geq 0.18$  MPa (for masonry of the I-th category) and  $0.18 \text{ MPa} \geq R_{tt} \geq 0.12$  MPa (for masonry of the II-th category).

When building walls made of gas-silicate blocks, the issues of increasing the strength and earthquake resistance of structures are solved by using high-strength materials, special masonry solutions, which significantly increase the solidity of masonry and reinforcement. Restoration of structures damaged by earthquakes is carried out by applying structural reinforcement methods: metal and reinforced concrete clips or external reinforcement based on the use of carbon fiber (fiber-reinforced polymer-FRP).

---

B. K. Dzhamuev (✉) · E. S. Erizhokova  
National Research Moscow State University of Civil Engineering, Moscow, Russia



At the Center for Earthquake Engineering Research (hereinafter CEER), CSRIBS named after V. A. Kucherenko under the direction of the Head of the laboratory of seismic Resistance of Structures, Ph.D. in Engineering, Associate Professor Granovskiy Arkadiy developed and implemented a comprehensive program of experimental investigations of strength and deformability of load-bearing structures (walls and columns), made of gas-silicate blocks, ceramic brick, and reinforced concrete, reinforced with FRP brand MBrace FIB CF («BASF»).

The purpose of the research is to evaluate the effectiveness of using carbon fiber fabric to increase the strength and rigidity of load-bearing and enclosing structures made of light concrete of buildings under construction in both conventional and earthquake-prone regions of the Russian Federation.

The tests were conducted in 2 stages:

- at the first stage, the behavior of walls under various schemes of their reinforcement FRP on the effect of the static load was studied: the wall is skewed in its plane;
- at the second stage, dynamic tests were carried out on the vibration platform of walls made of gas-silicate blocks with an opening made in full size. The tests were carried out on non-reinforced and reinforced FRP samples.

**Masonry and reinforcement material.** For laying the fragments of the walls of the prototypes, gas-silicate blocks were used, manufactured according to the YTONG technology by Xella-Aeroblock-Center CJSC, with a concrete class of B3.5 and a density of D500. The masonry of the walls was carried out on the adhesive solution of the brand “YTONG-economy”. FRP canvases of the MBrace FIB CF 230/4900.200g/5.100m brand were used to reinforce the walls.

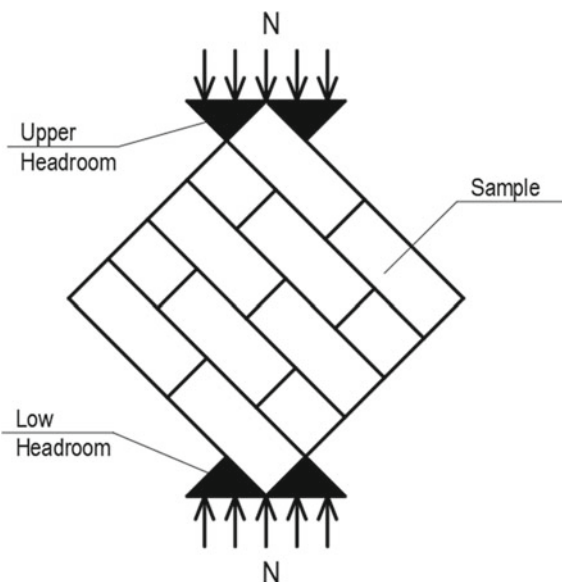
Fragments of walls without reinforcement were used as reference samples. In the prototypes of the I-th and III-th series, reinforcement with carbon fiber canvases was performed from 2 sides, in the samples of the II-th series only from one side. Figure 1 shows the test circuit of the prototypes. In all series, including reference one, 3 samples were tested.

## 2 Static Tests on the Skew

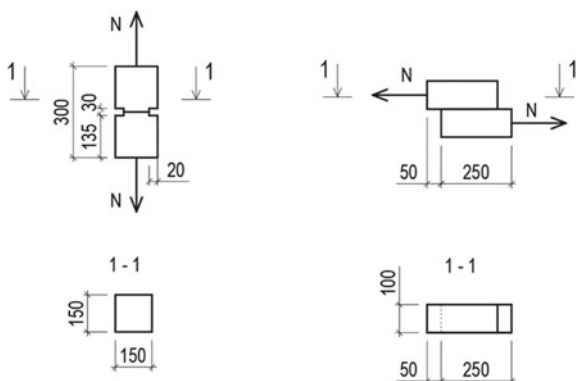
Preliminary tests (according to the scheme in Fig. 2) the cubes are glued together on an adhesive solution “YTONG-economy” tensile (normal grip) and cut (tangential grip) showed that the magnitude of the normal and tangential block chaining, respectively,  $R_{\text{tent}} = 0.2$  MPa and  $R_{\text{cut}} = 1.07$  MPa. To Seismic Building Design Code [1] for masonry walls of the 1-st category of the value of the temporary resistance to tension needs to be  $R_{\text{Bp}} \geq 0.18$  MPa. That is, the masonry of walls made of gas-silicate blocks “YTONG-economy” meets the requirements of the Seismic Building Design Code [1] for masonry walls of the 1-th category.

Table 1 shows the test results of the prototypes. The analysis of the test results of fragments of masonry walls made of YTONG gas-silicate blocks manufactured by

**Fig. 1** The scheme of the test prototypes



**Fig. 2** Scheme of samples for testing on the tensile (normal grip) and cut (tangential grip)



**Table 1** The results of static tests

Nº of series	Scheme of reinforcement	$N_{dest}$ (kN)	Limit of masonry strength on the cut $R_{cut}$ (MPa)	Relative strength (%)
Etalon	Nonreinforced	174.6	0.67	100
I	3 canvases on both sides	338.3	1.28	193
II	3 canvases on the one hand	260.8	0.99	148
III	1 canvas on both sides	206.3	0.79	134

Xella-Aeroblok-Center CJSC on the “YTONG-economy” brand adhesive solution reinforced with MBrace (BASF) carbon fiber allows us to note the following:

- the ultimate strength of the masonry when cut along an unbound seam, depending on the scheme of reinforcement with carbon fiber, is 1.34–1.93 times higher than the strength of the non-reinforced masonry;
- the adhesion of the carbon fiber to the gas-silicate blocks was ensured until the masonry was destroyed.

The third column shows the average values based on the test results of the 3 samples. The fourth column shows the value of the strength limit of the masonry when cutting along the bandaged section, which was determined by the formula:

$$R_{\text{cut}} = N_{\text{dest}} / (1.4 \cdot a \cdot d) \quad (1)$$

where

$R_{\text{cut}}$	limit of the strength of masonry on the not-tied masonry joint, MPa;
$N_{\text{dest}}$	the calculated value of the horizontal force, kN;
$a$	half the length of the sample, m;
$d$	thickness of the sample, m.

### 3 Dynamic Tests

At the second stage of the tests, the behavior of masonry walls made of gas-silicate blocks (without reinforcement and with carbon fiber reinforcement) under the influence of dynamic loads simulating seismic impacts with an intensity of 7–9 points, according to the MSK-64 scale, was studied.

Dynamic tests were performed on pre-compressed samples. The value of the minimum value, i.e., until the vertical load on the sample is completely removed.

**Methods of testing.** To excite the vibrations of a fragment of a wall with an opening, a test bench was used, the excitation of which is carried out using a vibro machine VID-12 fixed on a pendulum platform (Fig. 3). Due to the inertial force developed by the vibrating machine, a frequency spectrum of effects on the test bench and a certain level of the amplitude of the platform vibrations is provided. Based on the test results, the maximum amplitude of the platform vibrations when using the VID-12 is 150 mm, the frequency range is up to 75 Hz.

Recording and measurement of signals were carried out using a specialized measuring and computing complex MIC-036 (Fig. 4), designed for collecting, converting, registering, processing, transmitting, and presenting information received from sensors.

This MIC-036 complex additionally includes a laptop with a specialized package of application programs and peripherals necessary for the automated signal processing process, as well as for documenting the processing results.

**Fig. 3** Vibration machine  
VID-12



**Fig. 4** Measuring and  
computing complex  
MIC-036



To measure accelerations, vibration frequencies, and dynamic displacements, one-component sensors-accelerometers AT 1105-10 m are used (Fig. 5). The locations of the accelerometers are shown in Fig. 6.

At accelerations corresponding to 8 points and a compression level of  $0.2 \times N_{\text{dest}}$  the destruction of the reference sample occurred (Fig. 7).

At dynamic impacts corresponding to 9 points, the reinforced fracture pattern is of a minor nature: the rupture of the carbon fiber fabric and the appearance of cracks in the horizontal joints of the masonry (Fig. 8).

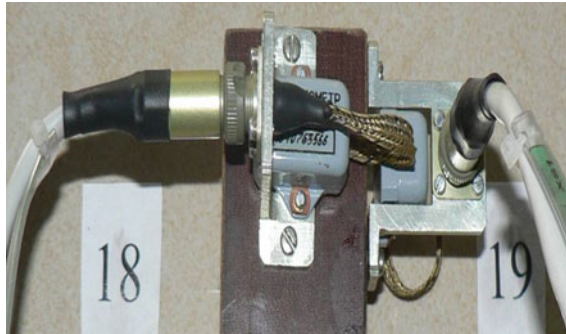
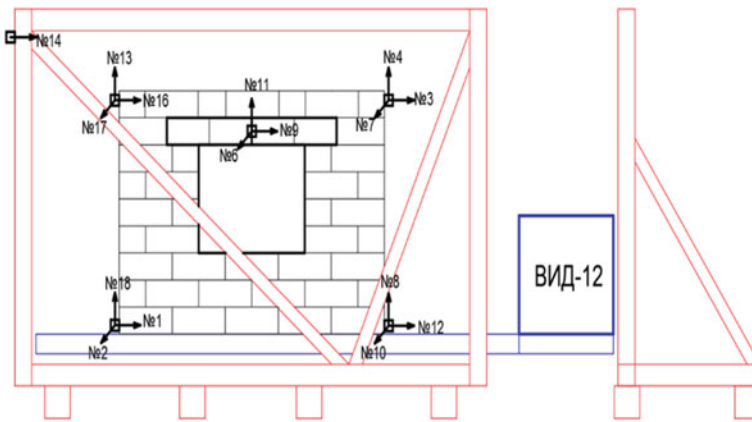
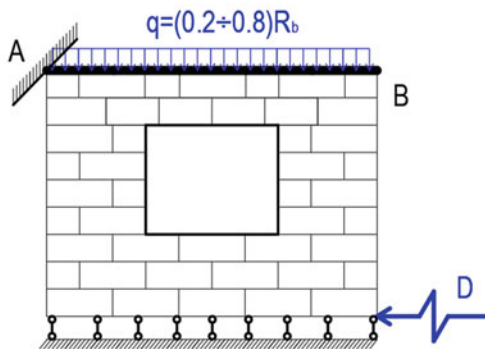


Fig. 5 Sensors-accelerometers AT 1105-10 m



(a)



(b)

Fig. 6 a The location of the accelerometers. b Conditional calculation scheme

**Fig. 7** General view of non-reinforced prototype wall after testing



**Fig. 8** General view of carbon-reinforced prototype wall after testing



## 4 Conclusions

1. Walls made of YTONG gas-silicate blocks based on “YTONG-economy” brand adhesive solution meet the requirements of Seismic Building Design Code [1] for masonry of the 1-th category, and can be recommended for use in earthquake-prone regions with appropriate design and design justification.
2. Increasing the strength and rigidity of the walls made of YTONG gas-silicate blocks due to the use of external reinforcement made of MBrace carbon fiber fabric (BASF) can be recommended both in the design of new structures and in the process of strengthening them.
3. The analysis of the results of numerous studies of the seismic resistance of walls made of gas-silicate blocks [2–20], as well as the results of these studies, allows us to recommend for use in earthquake-prone regions of the Russian

Federation walls made of gas-silicate blocks produced by Xella-Aeroblock-Center CJSC, made using YTONG technology on “YTONG-economy” brand adhesive solution, reinforced with carbon fiber.

## References

1. Seismic Building Design Code, Set of rules 14.13330.2014 «Construction in seismic regions»
2. Polyakov, S.V.: Clutch in Masonry. Stroizdat, Moscow (1959)
3. Polyakov, S.V.: Seismic Building Structures. Moscow (1969)
4. Korchinsky, I.L.: Seismic Construction. Higher School Publishing House, Moscow (1971)
5. Trumbovetsky, V.P.: On the use of cellular concrete in seismic construction. *Concr. Reinf. Concr.* **9**, 46 (1980)
6. Mochalov, A.L., Granovsky, A.V., Kostenko, A.N.: Strengthening of brick structures using elements of external reinforcement from carbon fiber. *Ind. Civil Constr.* **7**, 47–48 (2006)
7. Aprile, A., Benedetti, A., Steli, E., Mangoni, E.: Seismic risk mitigation of masonry structures by using FRP reinforcement. FRPRCS-8 University of Patras (2007)
8. Uddin, N., Fouad, F.H., Vaidya, U.K., Khotpal, A.K., Serrano-Perez, J.C.: Structural behavior of fiber-reinforced polymer-autoclaved aerated concrete panels. *Struct. J.* **6**, 722–730 (2007)
9. Raongjant, W., Jing, M.: The effects of diagonal web reinforcement on cyclic behavior of lightweight structural walls. *Struct. Concr.* **1**, 35–43 (2009)
10. Granovsky, A.V., Dzhamuev, B.K.: On the possibility of using walls from cellular concrete blocks in seismic regions. *J. Ind. Civil Eng.* **4**, 37–39 (2011)
11. Granovsky, A.V., Dzhamuev, B.K.: The use of external carbon fiber reinforcement to strengthen the walls of cellular concrete blocks. *J. Building Mater.* **7**, 68–69 (2011)
12. Tonkikh, G.P., Kabantsev, O.V., Granovsky, A.V., Simakov, O.A.: Experimental study of seismic retrofitting using externally bonded fiber reinforced polymers. *Bull. Tomsk State Univ. Archit. Civil Eng.* **6**(47), 57–69 (2014)
13. Granovsky, A.V., Kostenko, A.N., Dzhamuev, B.K.: Strength and deformability of masonry structures reinforced by cfrp under static and dynamic loads. International Conference on FRP Composites in Civil Engineering CICE 2014. Canada, Vancouver (2014)
14. Gasiev, A.A., Granovsky, A.V., Dzhamuev, B.K.: The effectiveness of use of the sheets from carbon-fibre fabric in brickwork of the buildings from different rock materials, constructed in earthquake zones. *J. Seismic Constr. Safety Struct.* **3**, 46–51 (2015)
15. Karpov, A.E., Kosareva, Y.E., Lukovenko, A.G., Lukovenko, G.A., Useinov, E.S.: Methods of seismic reinforcement of buildings with load-bearing masonry walls. *Bull. Sci. Creativity* **5**(5), 206–215 (2016)
16. Tonkikh, G.P., Osipov, P.V., Temiraliuly, G., Fedorov, S.K.: Experimental research of carbon fiber-reinforced masonry. *Bull. Tomsk State Univ. Archit. Civil Eng.* **2**(61), 98–111 (2017)
17. Granovsky, A.V., Dzhamuev, B.K., Osipov, P.V., Simakov, O.A.: Earthquake resistance of brick walls of buildings reinforced with composite materials. *J. Ind. Civil Eng.* **4**, 44–49 (2017)
18. Dzhamuev, B.K.: Using of carbon fiber fabric for reinforcement the walls of the aerated concrete blocks in buildings, constructed in seismic regions. VI International Scientific Conference (IPICSE-2018). Moscow, Russia (2018). [https://www.matec-conferences.org/articles/mateconf/pdf/2018/110/mateconf\\_ipicse2018\\_02041.pdf](https://www.matec-conferences.org/articles/mateconf/pdf/2018/110/mateconf_ipicse2018_02041.pdf)
19. Granovsky, A.V., Simakov, O.A., Dzhamuev, B.K.: The FRP and TRC strengthening of the masonry structures. XXII International Scientific Conference FORM-2019. Tashkent, Uzbekistan (2019)
20. Shokbarov, Y.M., Temiraliuly, G.: Effect of number of layers of composite material in the amplification samples masonry. *Kazakh Res. Inst. Constr. Archit.* **2**(11), 67–73 (2019)

# Migrating Corrosion Inhibitor (MCI) for Concrete Rebar and Its Inhibitory Efficiency



Sergei N. Leonovich , L. S. Karpushenkava , and S. A. Karpushenkov 

## 1 Introduction

In the repair and construction industry, the use of reinforcement corrosion inhibitors is becoming significantly important to increase the service life of existing reinforced concrete structures [1–4]. To date, many studies have shown [1, 5] that the destruction of reinforced concrete structures occurs due to a change in the composition of the pore liquid in the structure of old concrete due to the washing out of calcium hydroxide by water and aqueous solutions containing chlorides and other activators of corrosion of reinforcement. These processes lead to the intensification of corrosion of steel reinforcement inside reinforced concrete structures, corrosion products. Corrosion products of reinforcing steel have a larger volume than non-corroded metal. Therefore due to corrosion in places where metal and concrete come into contact, internal stresses arise, which lead to cracks and destruction of the concrete structure.

In the modern construction industry, steel reinforcement corrosion inhibitors are added to the mixing water during the construction phase during the manufacture of the concrete mix [1, 6–8]. This allows to significantly reduce the rate of corrosion processes of the metal rebar during the long-term operation of reinforced concrete structures for various purposes. For concrete structures that have been made of concrete without the addition of corrosion inhibitors, when repairing them, it is proposed to use compositions of migratory corrosion inhibitors (MCIs) [9–15]. When such solutions are applied to the surface of a cleaned concrete structure, their active components migrate through the pore space of concrete and are adsorbed on the reinforcement surface, preventing corrosion processes. Recently, in European countries, including the Republic of Belarus, there is a tendency to abandon the use of such traditional compounds like calcium and sodium nitrites as corrosion inhibitors.

---

S. N. Leonovich (✉)

Belarusian National Technical University, Nezavisimosti av. 65, Minsk, Belarus

L. S. Karpushenkava · S. A. Karpushenkov

Belarusian State University, Nezavisimosti av. 4, Minsk, Belarus



This is primarily due to their toxicity to humans and the environment, as in Germany and Sweden, such compounds are already banned in the manufacture and repair of reinforced concrete structures [1, 10, 11].

Amino compounds based on amino alcohols, amines, and amine salts are substances that can slow down the corrosion of steel reinforcement and migrate through the pore space of concrete [2, 6, 9, 10]. The treatment of reinforced concrete with compositions based on such components, according to the studies carried out to date, can increase the service life of concrete structures by an average of 30–40 years [2, 9]. Increasing the service life of reinforced concrete products is very beneficial economically, therefore, the search for new and optimization of existing compositions of migrating corrosion inhibitors of steel reinforcement is an important and urgent task.

This paper summarizes the results of many years of research on the creation and optimization of compositions of migrating corrosion inhibitors (MCIs) of reinforcement in concrete and the application of accelerated electrochemical methods for assessing the effectiveness of such compositions, carried out at the Faculty of Chemistry of BSU and at the Faculty of Civil Engineering of BNTU.

## 2 Experimental

### 2.1 Preparation of Inhibitor Solutions and Components

Corrosion inhibitor compositions were prepared by sequentially dissolving amino compounds, salts, and surfactants in water. When preparing solutions of inhibitors, the total concentration of all components in water was 30 wt%. For the produce of inhibitor compositions, we used the following components: monoethanolamine (MEA, Sigma-Aldrich,  $\text{NH}_2\text{CH}_2\text{CH}_2\text{OH}$ ,  $\geq 98.0\%$ ), diethanolamine (DEA, Sigma-Aldrich,  $\text{HN}(\text{CH}_2\text{CH}_2\text{OH})_2$ ,  $\geq 98.0\%$ ), dimethylaminoethanol (DMAE, Sigma-Aldrich,  $(\text{CH}_3)_2\text{NCH}_2\text{CH}_2\text{OH}$ ,  $\geq 99.5\%$ ), cyclohexylamine (Sigma-Aldrich,  $\text{C}_6\text{H}_{11}\text{NH}_2$ , 99.0%), sodium benzoate, potassium dihydrogen phosphate, a commercial wetting agent “Euroxide CDM” (YDS Chemicals, Cocamine Oxide, Activity  $\sim 30\%$ ), and distilled water.

### 2.2 Samples Production

Smooth and corrugated rods with a diameter of 6 and 10 mm made of carbon steel St3 (analog steel Q235 with a composition in mass%: 0.14–0.22 C, 0.15–0.3 Si, 0.4–0.65 Mn, up to 0.3 Ni, up to 0.3 Cr, up to 0.3 Cu, up to 0.05 S, up to 0.04 P, up to 0.08 As, up to 0.008 N and Fe balance) were used to study corrosion. The

metal samples were ground silicon carbide abrasive paper, rinsed in distilled water and ethanol, and dried in warm air.

All mortars used for casting samples were manufactured with ordinary Portland cement with water/cement/standard sand (STB 1168-99—Republic of Belarus) at a mass proportion of 0.5/1/3. The fresh mortar specimens were cured at 95% relative humidity (RH) for 28 days at  $20 \pm 2$  °C.

### 2.3 Corrosion and Migration Research

**Visual observation.** For visual observation and determination of migrating compositions action efficiency for corrosion of reinforcing steel, 3% sodium chloride solution was used with the addition of 2% inhibitor composition.

**Gravimetric research corrosion method.** The quantitative assessment of the protective ability ( $Z$ ) was determined by the gravimetric method in 3% sodium chloride solution without and with the addition of 2% inhibitor composition, according to GOST 9.506-87 for 10 days.

**Electrochemical corrosion research method.** The inhibitory effect of the developed compositions was assessed by analyzing the electrochemical data obtained by stationary anodic polarization measurements on reinforcing steel rods. Polarization curves were recorded using PI-50-1.1 potentiostat (Russia) in sodium chloride solutions at  $20 \pm 2$  °C. The potential sweep rate was 30 mV/min in the range from  $-1.5$  to  $+1.5$  V. In the study of the inhibiting effect of the inhibitor composition, the electrochemical method was used in two versions: in a 3% sodium chloride solution with the addition of an inhibitor composition and immersion of reinforcing steel into it, and when soaking concrete specimens containing rebar rod (after surface applied inhibitor composition of samples and aged for 14 days) in a 3% sodium chloride solution.

**Migration research.** An artificial (simulated) concrete pore solution (concrete extract solution) with the addition of 0.2% sodium chloride was used as a medium in the study of the migratory ability of the inhibitor composition. The solution itself is an aqueous extract isolated from the mass of a sand-cement mixture with water (sand/cement ratio = 3/1, water/cement = 0.5, pH = 12.5), prepared in accordance with the method [16].

### 3 Results and Discussion

#### 3.1 Preparation Corrosion Inhibitor Compositions

Studies [6, 10, 17–19] carried out by us earlier showed that monoethanolamine (MEA), diethanolamine (DEA), dimethylaminoethanol (DMAE), and cyclohexylamine (CHA) can be used as the main inhibiting components for concrete impregnation. These compounds do not react with the components of the cement stone, but at the same time, they dissolve in concrete pore solution, which promotes their migration to the steel reinforcement and adsorption on its surface with the formation of a passive layer. It was also found that the effectiveness of the inhibitor composition and its consumer properties can be improved by using additives of various natures to solutions of amino compounds. Thus, the use of sodium benzoate, which also exhibits inhibitory properties with respect to rebar, allows minimizing the pungent unpleasant odor characteristic of all amino compounds. The addition of a surfactant makes it possible to achieve better wettability of the surface of the concrete structure and its internal pores, which contributes to faster penetration of inhibitors through the concrete pore space. The addition of potassium dihydrogen phosphate to the solution of the amino compound leads to a chemical reaction of this additive with calcium hydroxide present in the concrete pore solution. During the reaction, insoluble calcium phosphate is formed and clogs the pores, creating an additional barrier for the migration of corrosion activators through the concrete pore space.

Traditionally [20], inhibitor aqueous solutions contain about 30% of active components. During the development and optimization of the corrosion inhibitor compositions, as well as in the study of the action of both individual inhibiting components and complex mixtures, the total concentration of all components was 30 mass %. It allows the most optimal comparison of the inhibitory effect of the formulations with each other, as well as with the already known formulations produced by Sika AG (Switzerland) or Cortec (USA).

#### 3.2 Optimization Corrosion Inhibitor Composition MCI

At the first stage of the work, the analysis of the inhibitory action of the components and their mixtures on the corrosion of reinforcing steel was assessed visually and electrochemically [18] in a 3% sodium chloride solution. Based on the data of our earlier studies [6, 10, 17–19], from a variety of amino compounds, we have identified the most promising ones in terms of inhibitory action and availability: MEA, DEA, DMAE, and CHA. In the same way, additional components of the compositions were selected: sodium benzoate and potassium dihydrogen phosphate. When interpreting the experimental results, not only the effect of additives on the inhibition of reinforcement corrosion was taken into account, but also the stability of the

final composition (during their storage, the formation of turbid solutions or precipitation was not observed, which leads to an undesirable change in the concentration of solutions) was considered.

The effectiveness of a wetting additive (surfactant) was assessed by the rate of absorption of two drops into the volume of a concrete sample (one drop of a composition without a wetting agent, and the second drop—a composition containing a wetting agent). Some surfactants, despite good wettability indicators, turned out to be unsuitable, since they violate the stability of the inhibitor composition itself (the appearance of turbidity, foaming, etc.). The most optimal wetting additive was the Euroxide CDM surfactant, the addition of which to the inhibitor composition in an amount of 0.5% increased the rate of droplet absorption (wetting) by 9–10 times compared to ordinary water [17].

The accelerated tests carried out by us [17, 20] of preliminary compositions with various ratios and combinations of components made it possible to determine the optimal inhibiting composition (MCI), containing (wt%): DEA—13, CHA—2, sodium benzoate—7.5, potassium dihydrogen phosphate—7.5, surfactant Euroxide CDM—0.5 and water balance. The protective ability ( $Z$ ) of the optimal inhibitor composition, determined in accordance with GOST 9.506-87 (Russia) in 3% sodium chloride solution for 10 days, was 97%. The appearance of a rebar with an inhibitor did not change (Fig. 1).

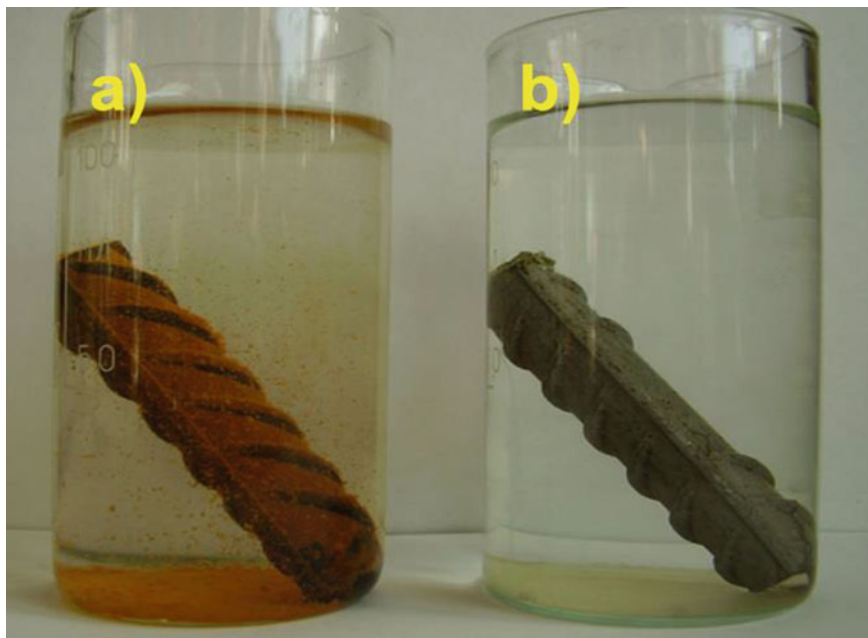


**Fig. 1** Photo of rebar samples in a 3% sodium chloride solution without (a) and with the addition of 2% MCI composition (b). Time of testing 10 days

### 3.3 Migration Research

The migrating ability of the components of the inhibitor composition through the pore structure of concrete was determined using a three-section electrochemical cell (Fig. 2), manufactured in accordance with the procedure presented in [21]. The medium in the electrochemical cell was an artificial concrete pore solution (concrete extract solution) with the addition of 0.2% sodium chloride.

An inhibiting composition was added to the left (Fig. 2a, section 1) part of the cell in an amount of 4% of the solution volume (120 ml), and electrodes (Fig. 2a, section 3) for electrochemical measurements were immersed in the right section (working-Fe (rebar), platinum—Pt, and reference electrode-saturated silver chloride Ag/KCl). Electrodes connected to the potentiostat to registered the change in the value of the flowing current depending on the applied voltage. The area of the working electrode (rebar) was 3 cm<sup>2</sup>, and the area of the concrete plate (Fig. 2a, section 2), which was in contact with the solution on both sides, was 20 cm<sup>2</sup> (from each side). In the course of the experiment, the components of the inhibitor composition diffused through the concrete plate (the thickness of the plate varied from 1 to 3 cm) and inhibited the corrosion of the rebar (working electrode) in the right vessel of the cell. The holding time for diffusion of the components of the inhibitor composition was 5 days [18].

The anode curves (Fig. 2b) show that the anode current has decreased by 1.5–2 times. This is due to the significant anodic inhibitory effect of the MCI composition. Therefore, the inhibiting components of the MCI composition can indeed migrate through the concrete plate and thereby reach the rebar surface inside the reinforced concrete construction. For comparison, a similar study was carried out for a commercial analog inhibitor composition “Sika FerroGard 903” (Sika AG, Switzerland). As seen from Fig. 2b, the anode curves for the compositions MCI and «Sika FerroGard

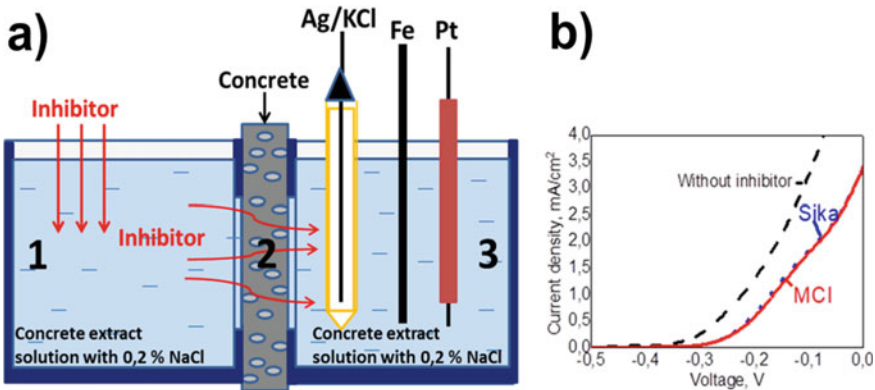


**Fig. 2** The schematic presentation of the three-section cell for migratory research of corrosion inhibitor compositions (a) and the view of anodic polarization curves (thickness of a concrete plate 1 cm) (b)

903» practically overlap each other. It confirms the equivalence of the properties MCI and «Sika FerroGard 903» in this experiment.

### 3.4 Electrochemical Corrosion Research

In this experiment, the effectiveness of the MCI composition was determined on model samples with rebar rods inside the concrete. According to STB 1168-99 (Belarus), cylindrical specimens (with a diameter of 7 cm and a height of 12 cm) with a rebar rod 1 cm in diameter inside concrete were made (Fig. 3a). The ends of the rebar rod were insulated with chemically resistant varnish. The area of the uncoated rebar surface inside the concrete sample was 30 cm<sup>2</sup>. After drying and hardening for 28 days, the surface of the concrete samples was cleaned before the appearance of the concrete pores. After cleaning the surface, certain samples were treated with inhibitor compositions (MCI and «Sika FerroGard 903»). Then samples were kept for 14 days so that the components of the inhibitor compositions reached the rebar surface inside the concrete sample. On the second day after treatment, the concrete samples were moistened with water. After the end of the saturation period, untreated concrete samples and treated with inhibitor compositions concrete samples were placed in 3% sodium chloride solution for 24 h for saturation, and then anodic polarization curves were registered (Fig. 3b) [18].

Figure 3b shows that after treatment of the samples with inhibitor compositions (MCI and «Sika FerroGard 903»), reinforcement corrosion slows down (shift of the anodic current curves towards the region of positive potentials). The anodic current density much decreases, both for the MCI composition and for the analog composition «Sika FerroGard 903». From the experimental data, it can be concluded

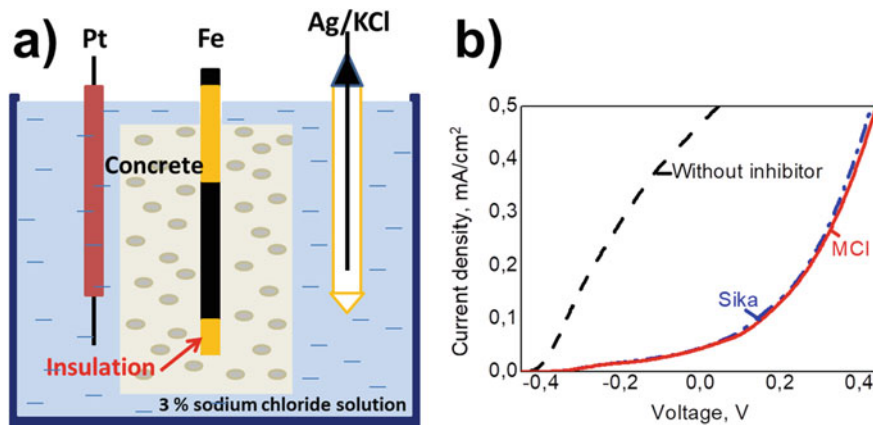


**Fig. 3** The schematic presentation of the electrochemical cell (a) for study the inhibiting ability of inhibitor compositions (a) and the view of anodic polarization curves (b)

that the inhibitor's compositions within 14 days migrated through a dense concrete layer about 3 cm thick and passivated the rebar surface.

## 4 Conclusions

Overall, the authors considered the possibility to obtain and optimize the composition containing migratory corrosion inhibitors for the treatment of reinforced concrete products and structures. The effectiveness of the composition was evaluated using accelerated electrochemical methods for studying the corrosion of reinforcement and the migration of inhibiting components through the structure of hardened concrete. It is shown that after the treatment of concrete structures with the developed MCI composition, the corrosion of reinforcing steel is suppressed even in the corrosive environment of sodium chloride. The effectiveness of the developed composition is additionally confirmed by comparative tests with the already known composition-analog of «Sika FerroGard 903».

## References

1. Gaidis, J.M.: Chemistry of corrosion inhibitors. *Cement Concr. Compos.* **26**(3), 181–189 (2004). [https://doi.org/10.1016/S0958-9465\(03\)00037-4](https://doi.org/10.1016/S0958-9465(03)00037-4)
2. Wombacher, F., Maeder, U., Marazzani, B.: Aminoalcohol based mixed corrosion inhibitors. *Cement Concr. Compos.* **26**(3), 209–216 (2004). [https://doi.org/10.1016/S0958-9465\(03\)00040-4](https://doi.org/10.1016/S0958-9465(03)00040-4)
3. Pan, C., Chen, N., He, J., Liu, S., Chen, K., Wang, P., Xu, P.: Effects of corrosion inhibitor and functional components on the electrochemical and mechanical properties of concrete subject to chloride environment. *Constr. Build. Mater.* **260**, 119724 (2020). <https://doi.org/10.1016/j.conbuildmat.2020.119724>
4. Stephenson, L.D., Lawrence, D., Kumar-Fnace, A.: Corrosion inhibitors for rebar in concrete-part 1. *Mater. Perform.* **49**(12), 50–53 (2010)
5. Peng, Y., Liu, L., Wang, S., Lin, Y., Sun, Y., Xia, R.: Effect of simulated pore solution on passivation characteristic of P110 steel. *J. Petrol. Sci. Eng.* **167**, 949–956 (2018). <https://doi.org/10.1016/j.petrol.2018.03.009>
6. Shchukin, G.L., Belanovich, A.L., Karpushenkov, S.A., Savenko, V.P., Radyukevich, P.I.: The inhibitory effect of the domestic anti-corrosion composition “MCI” on the corrosion of steel reinforcement. *Stroitel'naya nauka i tekhnika [Build. Sci. Tech.]* **6**, 55–58 (2008). (in Russian)
7. Ngala, V.T., Page, C.L., Page, M.M.: Investigations of an ethanolamine-based corrosion inhibitor system for surface treatment of reinforced concrete. *Mater. Corros.* **55**(7), 511–519 (2004). <https://doi.org/10.1002/maco.200303768>
8. Bellal, Y., Benganem, F., Keraghel, S.: A new corrosion inhibitor for steel rebar in concrete: synthesis, electrochemical and theoretical studies. *J. Mol. Struct.* **1225**, 129257 (2021). <https://doi.org/10.1016/j.molstruc.2020.129257>
9. Malik, A.U., Andijani, I., Al-Moaili, F., Ozair, G.: Studies on the performance of migratory corrosion inhibitors in protection of rebar concrete in Gulf seawater environment. *Cement Concr. Compos.* **26**(3), 235–242 (2004). [https://doi.org/10.1016/S0958-9465\(03\)00042-8](https://doi.org/10.1016/S0958-9465(03)00042-8)

10. Leonovich, S.N., Sviridov, D.V., Karpushenkov, S.A., Shchukin, G.L., Belanovich, A.L., Savenko, V.P., Gurinovich, V.Y.: Physical and mechanical properties of concrete and reinforcement corrosion in sodium chloride environment: the effect of amino alcohols. *Stroitel'nye Materialy* [Constr. Mater.] **1**, 34–36 (2012). (in Russian)
11. Jamil, H.E., Shri, A., Boulif, R., Bastos, C., Montemor, M.F., Ferreira, M.G.S.: Electrochemical behaviour of amino alcohol-based inhibitors used to control corrosion of reinforcing steel. *Electrochim. Acta* **49**(17–18), 2753–2760 (2004). <https://doi.org/10.1016/j.electacta.2004.01.041>
12. Holloway, L., Nairn, K., Forsyth, M.: Concentration monitoring and performance of a migratory corrosion inhibitor in steel-reinforced concrete. *Cem. Concr. Res.* **34**(8), 1435–1440 (2004). <https://doi.org/10.1016/j.cemconres.2004.01.019>
13. Morris, W., Vázquez, M.: A migrating corrosion inhibitor evaluated in concrete containing various contents of admixed chlorides. *Cem. Concr. Res.* **32**(2), 259–267 (2002). [https://doi.org/10.1016/S0008-8846\(01\)00669-X](https://doi.org/10.1016/S0008-8846(01)00669-X)
14. Prieto, M.I., Cobo, A., Rodríguez, A., González, M.N.: The efficiency of surface-applied corrosion inhibitors as a method for the repassivation of corroded reinforcement bars embedded in ladle furnace slag mortars. *Constr. Build. Mater.* **54**, 70–77 (2014). <https://doi.org/10.1016/j.conbuildmat.2013.12.014>
15. Fedrizzi, L., Azzolini, F., Bonora, P.L.: The use of migrating corrosion inhibitors to repair motorways' concrete structures contaminated by chlorides. *Cem. Concr. Res.* **35**(3), 551–561 (2005). <https://doi.org/10.1016/j.cemconres.2004.05.018>
16. Jamil, H.E., Montemor, M.F., Boulif, R., Shiri, A., Ferreira, M.G.S.: An electrochemical and analytical approach to the inhibition mechanism of an amino-alcohol-based corrosion inhibitor for reinforced concrete. *Electrochim. Acta* **48**(23), 3509–3518 (2003). [https://doi.org/10.1016/S0013-4686\(03\)00472-9](https://doi.org/10.1016/S0013-4686(03)00472-9)
17. Shchukin, G.L., Belanovich, A.L., Karpushenkov, S.A., Karpushenkava, L.S., Savenko, V.P., Radyukevich, P.I.: Composition of a corrosion inhibitor for impregnating reinforced concrete structures. BY Patent No. 16080 (2012). (in Russian)
18. Karpushenkov, S.A., Karpushenkava, L.S., Shchukin, G.L., Belanovich, A.L., Sviridov, D.V.: Electrochemical method for determination of efficiency of steel rebar inhibitors in concrete. *Sviridov Readings* **9**, 82–89 (2013). (in Russian)
19. Karpushenkov, S.A., Sviridov, D.V., Karpushenkava, L.S., Shchukin, G.L., Belanovich, A.L., Savenko, V.P.: Composition of a corrosion inhibitor for steel reinforcement in concrete. BY Patent No. 19469 (2015) (in Russian)
20. Marazzani, B., Burge, T.A.: Method for rehabilitative and/or protective corrosion-inhibition of reinforcing steel embedded in hardened concrete structure by means of surface-applied corrosion-inhibiting compositions. USA Patent No. 6712995 (2004)
21. Jamil, H.T., Shiriri, A., Boulif, R., Montemor, M.F., Ferreira, M.G.S.: Corrosion behaviour of reinforcing steel exposed to an amino alcohol based corrosion inhibitor. *Cement Concr. Compos.* **27**(6), 671–678 (2005). <https://doi.org/10.1016/j.cemconcomp.2004.09.019>



# Energy Efficiency and Sustainability of High-Rise Buildings and Structures



Lydia Ivanovna Malyanova  and Maria Alekseevna Sergeeva

## 1 Introduction

The relevance of this topic lies in the fact that construction is one of the main areas of human production activity. As a result of construction production, a completed construction product is created—a building or construction of a specific functional purpose, which is necessary for the functioning of society.

The interest in the construction of high-rise buildings stems primarily from economic considerations. From the investor's point of view, increasing the number of square meters on the foundation is beneficial, and therefore, the construction of high-rise buildings is advantageous. But it should be noted that the higher the building, the more expensive it is to operate.

## 2 Ways of Reducing

The construction of energy-efficient high-rise buildings is a way to reduce operating costs. Energy-efficient buildings are those that have been designed with a set of architectural and engineering measures that significantly reduce heating costs for these buildings compared to model buildings with the simultaneous improvement of the comfort of the microclimate in the premises [1].

---

L. I. Malyanova (✉)

Chuvash State University named after I.N. Ulyanov (ChuvSU), 15 Moskovskiy Prospekt, Cheboksary 428015, Russian Federation

Institute (branch) of Moscow Polytechnic University, Cheboksary, Russian Federation

M. A. Sergeeva

National Research Moscow State University of Civil Engineering (NRU MGSU), Moscow, Russian Federation

Each high-rise building is unique and cannot be built at the usual pace. The existing buildings have been under construction for a long period of time, and a large number of highly qualified specialists of different profiles have participated in their design. High-rise buildings are all the more in need of careful design. For example, the design and construction of the tallest building in Europe Commerzbank Tower, Frankfurt am Main, Germany, lasted eight years [2].

In the design of high-rise buildings, there is also the problem of material selection of the building structures. In the USA, steel is usually used as the main structural material, while in Europe, reinforced concrete is used. According to academician V. I. Travusz, Deputy Director of CRDIRPB named after Mezentsev, reinforced concrete constructions have three important advantages over the others: greater stability due to their high weight, oscillations shall be more rapidly attenuated in reinforced concrete constructions, reinforced concrete constructions of more fire-resistant [3].

The strength, stability, and spatial rigidity of high-rise buildings are ensured by the combined operation of horizontal (floor) and vertical (wall and frame) structures. Vertical and horizontal loads on the building are transferred through the floors to the vertical supporting structures and from them to the ground. The intensity, direction, and nature of the transfer of loads depend on the geometry of the vertical elements and their position in the plan.

Since horizontal loads, such as wind and seismic loads, are crucial in the design of high-rise buildings, vertical load-bearing structures must be sufficiently rigid to avoid undesirable deformations of the building. In order to increase rigidity in the longitudinal and transverse directions of the building, a system of horizontal communication is arranged. Horizontal loads through the overlaps are transmitted to vertical coupling structures. Horizontal loads are transmitted by means of joints, which move the forces perceptibly and are arranged between the vertical load-bearing structures and the overlaps.

The choice of vertical load-bearing structures, their combinations, and braces is the selection of the structural system of a building, the rigidity of which is determined by stiffness analysis and depends on many factors. The most important factor for the stability of a high-rise building is its resistance to wind loads that increase with height.

As an example, consider three unique high-rise buildings: Pearl River, Torre Major, and Taipei 101.

The Pearl River Tower is far from remarkable in terms of height. The original goal of the engineering team was to create a building with excess power generation that would supply itself with power and even sell this excess power to the local grid. The building was built with super-strong bolts and nuts. They are much better able to withstand seismic loads.

Wave-shaped facade is not just original design but also constructive necessity [4].

At technical levels, giant wind turbines have been installed vertically in special channels. This arrangement of windmills is more efficient. The engineers calculated that autonomous windmills would provide 15 times less energy than those installed in the building.

The strongest winds are blowing at a hundred meters high. Wind speeds will increase 2.5 times due to the structural features of the building. The facade of the skyscraper in the shape of a giant vertical wave is smoothly rounded in front of each canal with windmills. The air flows in the resulting giant slit will be directed with greater force, increasing the rotation of the huge turbine blades and potentiating the generation of megawatts of energy. Another positive feature of skyscraper holes is the reduction of the wind pressure on the building that all skyscrapers inevitably experience. The location of the building was also chosen by accident, and the facade of the house is oriented toward the winds blowing from the south of China.

The Torre Mayor (literally «Major Tower») is the tallest tower in 2003–2010 Latin American building. The Torre Mayor is of particular interest because the project uses a new approach to seismic absorption not previously used in high-rise construction [5]. The base of the tower is a square with an area of 80 m at the underground levels, and at the height of the 4th to 10th floors, it passes into a rectangle of 80 × 65 m. Above this level, the size of the building is reduced up to 48 × 36 m. Interfloor ceilings are a conjugation of a rectangle and a segment, which forms the convexity of the southern facade.

The main supporting structures of the building are mostly steel. The columns of the tower (up to the 35th floor in the core and up to the 30th of the perimeter) are taken into the reinforced concrete clip to give the frame more rigidity and bearing capacity, and also for the purpose of steel saving.

The foundation is a combined system of separate caissons and a solid slab. The constructors have built up a strength reserve to withstand the impact of the most powerful earthquake.

The shifting stability system of this project has been developed on the basis of a number of studies of alternative concepts of structural support. The effect, in this case, is achieved by the use of an ordinary «double» (sensitive to deviations) stability system under horizontal action in combination with an additional damping system (sensitive to the speed of oscillations) [6]. The result is a «triple» system, able to receive seismic energy of earthquake without damage to the structure. Such a system consists of the main superframes along the perimeter of the tower, connected to the perimeter structure, which perceives moments, and connected with the «pipe» in the core of the building. The bonds and composite columns of the nucleus attached by them form the main «spin ridge» of the building. The perimeter farms and the powerful superdiagonal system create a highly efficient tubular structure connected to the «spin ridge» and together with it counteracting seismic loads. The system is reinforced by a number of auxiliary viscous dampers which are oriented along north–south and east–west lines. This structural system includes auxiliary damping devices which, with high efficiency, eliminate seismic loads on both carrier and non-load elements (i.e., architectural and engineering). Additional damping of oscillations reduces the overall and local (interstorey) rocking of the tower.

The Torre Mayor was successfully tested of strength during the 7.6 magnitude earthquake in January 2003 without even having to evacuate the building.

The Taipei 101 is one of the most famous skyscrapers in the world, impressive not only for its grandeur, but also original, unlike any other architectural solution

[7]. This magnificent high-rise building is located in the unrecognized capital of the Republic of China, Taipei, and is named for its location and number of floors. The skyscraper is built in the heart of the typhoons and hurricanes that originate in the South China Sea, and the Taiwan region itself is located in an area where an active tectonic fracture is taking place. Earthquakes often occur here. Even the very fact of large-scale construction at this site has become a real challenge to nature.

The engineers' task was to design a skyscraper that was not very rigid at the same time to withstand strong winds and at the same time strong enough to prevent sideways displacement (lateral displacement). Low rigidity prevents damage to the structure at strong bending moments, while maintaining the high level of comfort of the tower's staff and visitors, as well as impermissible deformations, causing extra load on the glazing panel and non-load-bearing internal partition. To balance these opposing properties, the designers used 101 masses of technological innovations in the Taipei 101, ranging from an outer frame to a giant hanging ball called a damper, which does not allow the building to swing too much under hurricane winds [6]. The heart of the building is called a huge 700-ton ball, which corresponds to the weight of about two «Boeings». The huge pendulum is suspended on 16 steel cables. Under normal conditions, the oscillation amplitude of the ball is about 10 cm [8].

Stability was tested in 2002 when a 6.8 magnitude earthquake struck Taipei 101 on March 31. The survey showed that no damage was caused to the tower by the earthquake and construction resumed.

### 3 Conclusion

In conclusion, the population of the Earth is growing steadily, and so will the need for high-rise, high-performance, and sustainable buildings. The quality of the design of high-rise buildings is constantly increasing. Not only are building materials being improved, but also structural, technical, and engineering solutions are being developed. In the future, high-rise buildings will be even more striking and extraordinary on the outside and inside. All thanks to new architectural ideas and technological advances.

### References

1. Pilepenko, V.M., Danilevsky, L.N.: Construction of energy-efficient buildings. *Sci. Innov.* **6**, 22–24 (2010)
2. Tabuntachev, Y.A., Brodak, M.M., Shilkin, N.V.: *Energy Efficient Buildings*, pp. 100. AVOK-PRESS (2003)
3. Energy efficient high-rise building. Tax Reform: [https://studopedia.ru/1\\_468\\_energoeffektivnoe-visotnoe-zdanie.html](https://studopedia.ru/1_468_energoeffektivnoe-visotnoe-zdanie.html)
4. Baranina, A.A.: ECO-project pearl river tower. *Academy* **1**(52), 83–86 (2020)
5. Miller, F.P., Vandome, A.F., McBrewster, J.: *Alphascript Publishing*, p. 92 (2011)

6. Aragval, R.: Built. Unknown History of Known Buildings, p. 240. Bombora Publisher (2019)
7. The safest skyscraper in the world is Taipei 101. Tax Reform: <https://masterok.livejournal.com/355190.html>
8. The giant ball inside the skyscraper. Tax Reform: <https://yandex.ru/turbo/masterok.livejournal.com/s/2578051.html>

# Energy Survey of the Cogeneration Plant



A. S. Mozgova  and T. V. Shchennikova 

## 1 Introduction

The designed installed electrical capacity of the power plant (power unit) is 8 MW, the thermal capacity is at least 8 MW. The electric power is generated with eight gas-fired generating sets (GPUs). The main technical characteristics of the gas reciprocating engines are shown in Table 1.

The fuel used is natural gas.

Thermal power is generated by four power generating units through recuperation of heat coming from the high-temperature cooling circuit of the hot-gas reciprocating engine and the exhaust heat, for which each GPU is equipped with plate-type heat-exchangers and a waste-heat boiler [1–12].

The main technical characteristics of the heat recovery system equipment are shown in Table 2.

The waste-heat recovery system of the power generating unit includes two circuits from each of the four GPUs and grid water pipelines.

The first circuit of the waste-heat recovery system is the high-temperature cooling loop for the generator gas reciprocating engine. In the first circuit, heat extraction from the engine cooling jacket takes place. The second circuit of the GPU heat recovery system is formed with the engine exhaust gas recovery boiler, heat exchanger (heated side), grid plate-type heat-exchangers, piping system, and shut-off valves.

---

A. S. Mozgova (✉) · T. V. Shchennikova  
Chuvash State University, 15, Moskovskiy pr., Cheboksary, Chuvash Republic 428015, Russia

**Table 1** Main technical characteristics of gas reciprocating engines

Name	Nominal power (kW)	Motor	Frequency revolutions (RPM)	Generator voltage
Gas-fired generating set (GPU)	1750	Cummins QSV91G	1500	6.3 kV, 50 Hz

**Table 2** Main technical characteristics of the heat recovery system equipment

Name	Specifications	Number (pcs)	Note
Shell-and-tube heat recovery boiler	Nominal power 1054 kW	4	
GPU plate-type heat exchanger "Ridan"	696 kW, 109 plates	4	Heat transfer from the first to the second circuit
Plate-type heat exchanger in the heat supply unit "Ridan"	7000 kW, 217 plates	3	Heat transfer from the second circuit to the grid water
Pump in the heat supply unit GRUNDFOS NB 100-200/192	$Q = 301.7 \text{ m}^3/\text{h}$ , $H = 40.2 \text{ mH}_2\text{O}$ $N = 45 \text{ kW}$ , $n = 2970 \text{ rpm}$	2	

## 2 Methods

Thermal power generation in each circuit is defined using a formula, kcal/h [13–22]:

$$Q = G \cdot \rho \cdot c \cdot (t_1 - t_2), \quad (1)$$

where  $G$ —heating medium rate,  $\text{m}^3/\text{h}$ ;  $\rho$ —density of the heating medium,  $\text{kg}/\text{m}^3$ ,  $c$ —heat capacity of the heating medium,  $\text{kcal}/(\text{kg } ^\circ\text{C})$ ;  $t_1$ —heating medium temperature at the inlet to the heat exchanger or the recovery boiler,  $^\circ\text{C}$ ;  $t_2$ —heating medium temperature at the output from the heat exchanger or the recovery boiler,  $^\circ\text{C}$ .

Thermal power losses at the non-insulated pipeline section behind the recovery boiler to the heat-exchangers of the heat supply unit are defined according to Formula (1), where  $t_1$ —temperature of the heating medium at the beginning of the pipeline section,  $t_2$ —temperature of the heating medium at the end of the pipeline section,  $^\circ\text{C}$ .

Thermal power generated with one GPU is defined using a formula, kcal/h:

$$Q_{\text{GPU}} = Q_{II} + Q_{r-b} - Q_n,$$

where  $Q_{II}$ —thermal power generated with a GPU for the second circuit, kcal/h;  $Q_{r-b}$ —thermal power generated with a recovery boiler, kcal/h;  $Q_n$ —thermal power losses at the non-insulated pipeline section, kcal/h.

### 3 Results

Two power units were surveyed at 25% load mode: GPU No. 1 and No. 2. The measurements were taken at the outside temperature of  $-7$  °C. The indicators obtained through the instrumental survey of the GPU 1–2 recovery system are shown in Table 3.

Thermal power generated with the heat exchanger of GPU No. 2 for the second circuit:

$$Q_{II} = 71 \cdot 1066 \cdot 0.69 \cdot (56.9 - 51.7) = 271,559 \text{ kcal/h}$$

Thermal power generated with the recovery boiler:

$$Q_{r-b} = 71 \cdot 1061 \cdot 0.69 \cdot (66.4 - 56.9) = 493,723 \text{ kcal/h}$$

Losses of thermal power at the non-insulated pipeline section:

$$Q_n = 71 \cdot 1058 \cdot 0.69 \cdot (66.4 - 64.5) = 94,335 \text{ kcal/h}$$

Thermal power generated with GPU 2:

$$Q_{\text{GPU No.2}} = 271,559 + 493,723 - 94,335 = 670,946 \text{ kcal/h, or } 7,802 \text{ kW h}$$

At the time of the survey, thermal power was generated with GPU No.1, No.2, No.3 and No.4. The thermal power production at all the GPUs is about the same and equals in aggregate:

$$\begin{aligned} \sum Q &= (Q_{\text{GPU No.1}} + Q_{\text{GPU No.2}}) \cdot 2 = (648,546 + 670,946) \cdot 2 \\ &= 2,638,984 \text{ kcal/h, or } 30,686 \text{ kW h} \end{aligned}$$

The thermal power consumption to cover in-house needs of the power plant is:

$$Q_c = 23 \cdot 1068 \cdot 0.69 \cdot (51.8 - 51.0) = 13,560 \text{ kcal/h}$$

The delivery of thermal energy for heating the consumers is:

$$Q = \sum Q - Q_c = 2,638,984 - 13,560 = 2,625,424 \text{ kcal/h}$$



**Table 3** The indicators obtained through the instrumental survey of the GPU 1–2 recovery system

Name	Indicators GPU No. 1	Indicators GPU No. 2
Gas consumption (STCm <sup>3</sup> /h)	201.2	205.9
Electric power generation (kW h)	518.2	536.4
<b>First circuit</b>		
Coolant flow through the power generating unit (m <sup>3</sup> /h)	39.4	39.4
Coolant temperature at the inlet to the power generator heat exchanger (°C)	65.6	65.4
Coolant temperature at the outlet from the power generator heat exchanger (°C)	57.3	57.4
<b>Second circuit</b>		
Coolant flow through the power generator heat exchanger (m <sup>3</sup> /h)	68.0	71.0
Coolant temperature at the inlet to the power generator heat exchanger (°C)	51.7	51.7
Coolant temperature at the outlet from the power generator heat exchanger (°C)	57.3	56.9
<b>Recovery boiler</b>		
Coolant temperature at the inlet to the recovery boiler (°C)	57.3	56.9
Coolant temperature at the outlet from the recovery boiler (°C)	66.7	66.4
Coolant temperature at the end of the non-insulated section (°C)	64.7	64.5
Temperature and composition of the exhaust gases behind the power generator		
– exhaust gas temperature (°C)	544	546
– carbon dioxide CO <sub>2</sub> (%)	6.5	7.1
– oxygen O <sub>2</sub> (%)	9.2	8.6
– carbon monoxide CO (ppm)	847	843
– nitrogen oxide NO <sub>x</sub> (ppm)	163	1134
– excess air ratio $\alpha$	1.70	1.61
Temperature of exhaust gases behind the recovery boiler (°C)	84	86
<b>Heat supply unit</b>		

(continued)

The thermal power generation and delivery for heating the consumers in the heat supply unit from Heat exchangers No. 2 and No. 3 is determined through the formula:

$$\begin{aligned}
 Q &= Q_{\text{No.2}} + Q_{\text{No.3}} \text{ kcal/h} \\
 Q &= 271,000 \cdot 1 \cdot (49.1 - 44.4) + 263,000 \cdot 1 \cdot (49.4 - 44.4) \\
 &= 2,588,700 \text{ kcal/h, or } 2.59 \text{ Gcal/h.}
 \end{aligned}$$

Imbalance of the heat delivery for heating the consumers is:

**Table 3** (continued)

Name	Indicators GPU No. 1	Indicators GPU No. 2
Total flow of the cooling liquid (tosol) into the common secondary manifold at all the GPUs (m <sup>3</sup> /h)	300	300
Temperature of the cooling liquid (tosol) at the inlet to the common secondary manifold (°C)	64.6	64.6
Temperature of the cooling liquid (tosol) at the outlet from the common secondary manifold (°C)	51.9	51.9
Total flow of the coolant (water) into the common manifold of the consumers' network loop (m <sup>3</sup> /h)	534	534
Coolant (water) flow through Heat exchanger No. 2 (m <sup>3</sup> /h)	271	271
Coolant (water) temperature at the inlet to Heat exchanger No. 2 (°C)	44.4	44.4
Coolant (water) temperature at the outlet from Heat exchanger No. 2 (°C)	49.1	49.1
Temperature of the cooling liquid (tosol) at the inlet to Heat exchanger No. 2 (°C)	64.6	64.6
Temperature of the cooling liquid (tosol) at the outlet from Heat exchanger No. 2 (°C)	51.9	51.9
Coolant (water) flow through Heat exchanger No. 3 (m <sup>3</sup> /h)	263	263
Coolant (water) temperature at the inlet to Heat exchanger No. 3 (°C)	44.4	44.4
Coolant (water) temperature at the outlet from Heat exchanger No. 3 (°C)	49.4	49.4
Temperature of the cooling liquid (tosol) at the inlet to Heat exchanger No. 3 (°C)	64.6	64.6
Temperature of the cooling liquid (tosol) at the outlet from Heat exchanger No. 3 (°C)	51.9	51.9
Consumption of the cooling liquid (tosol) to cover in-house needs (m <sup>3</sup> /h)	23	23
Temperature of the cooling liquid (tosol) to heat the utilities (°C)	51.8	51.8
Temperature of the cooling liquid (tosol) from heating the utilities (°C)	51.0	51.0

$$2, 625, 424 - 2, 588, 700 = 36, 724 \text{ kcal/h, or } 1.4\%$$

The delivery of thermal energy for heating the consumers according to static instruments is 2.36 Gcal/h, the resulting value of the instrumental survey is 2.59 Gcal/h.

## 4 Discussion

The specific fuel consumption for electric power generation by GPU No. 1 (excluding thermal power generation) is:

$$b_s = \frac{B}{Q_{\text{GPU No.1}}} = \frac{201.2}{518.2} = 0.388 \text{ STCm}^3/\text{kW}$$

where  $B$ —natural gas flow,  $\text{STCm}^3/\text{h}$ ;  $Q_{\text{GPU No.1}}$ —electric power generation, kW h.

With the power plant running in a combined mode (both electric and thermal power generation), the specific fuel consumption for the electric and thermal power in GPU 1 is equal to:

$$b_s = \frac{B}{\sum Q_{\text{GPU No.1}}} = \frac{201.2}{518.2 + 754.1} = 0.158 \text{ STCm}^3/\text{kW}$$

where  $\sum Q_{\text{GPU No.1}}$ —generation of electric and thermal power, kW h,

- 518.2 kW h—electric power generated with GPU No. 1,
- 518.2 kW h—thermal power generated with GPU No. 1.

The aggregate electric and thermal power generated with GPU No. 1 amounts to  $518.2 + 754.1 = 1272.3$  kW h. In percentage correlation, the generated electric power made up 40.7%; the generated thermal power—59.3%.

The specific fuel consumption for electric power generation by GPU No. 2 (excluding thermal power generation) is:

$$b_s = \frac{B}{Q_{\text{GPU No.2}}} = \frac{205.9}{536.4} = 0.384 \text{ STCm}^3/\text{kW}$$

where  $Q_{\text{GPU No.2}}$ —generation of electric power, kW h,

With the power plant running in a combined mode (both electric and thermal power generation), the specific fuel consumption for the electric and thermal power in GPU 2 is equal to:

$$b_s = \frac{B}{\sum Q_{\text{GPU No.2}}} = \frac{205.9}{536.4 + 780.2} = 0.156 \text{ STCm}^3/\text{kW}$$

where  $\sum Q_{\text{GPU No.2}}$ —generation of electric and thermal power, kW h,

- 536.4 kW h—electric power generated with GPU No. 2,
- 780.2 kW h—thermal power generated with GPU No. 2.

## 5 Conclusions

With the power plants running in combined mode (both electric and thermal power generation), the specific fuel consumption for the electric and thermal power generation in GPU 1, 2, 3 and 4 is equal to:

$$b_s = \frac{\sum B}{\sum Q_{\text{GPU}}} = \frac{814.2}{(538.1 + 536.4 + 518.2 + 536.4) + 3068.6} = 0.157 \text{ STCm}^3/\text{kWh}$$

where  $\sum B$ —natural gas consumed with GPU 1, 2, 3 and 4, STCm<sup>3</sup>/h (predicted  $(201.2 + 205.9) \times 2 = 814.2$ );  $\sum Q_{\text{GPU}}$ —electric and thermal power generation in GPU 1, 2, 3 and 4, kWh,

- 538.1; 536.4; 518.2; 536.4 kWh—electric power yield,
- 306.6 kWh—thermal power yield.

## References

1. Mozgova, A.S.: Problems of thermal conductivity of closed pressure vessels. In: Salenko, S.D. (ed.) Sci. Ind. defense. Proc. XIX All-Russian Sci. Tech. Conf. vol. 4, pp. 63–65 (2018)
2. Nemirovsky, Y.V., Mozgova, A.S.: Problems of thermal conductivity for storage tanks of liquefied gases and oil products. J. Phys. Conf. Ser. **1128**, 012131 (2018). <https://doi.org/10.1088/1742-6596/1128/1/012131>
3. Nemirovsky, Y.V., Mozgova, A.S.: Thermal conductivity of gasholders during gas storage. J. Phys. Conf. Ser. **1565**, 012057 (2020). <https://doi.org/10.1088/1742-6596/1565/1/012057>
4. Nemirovsky, Y.V., Mozgova, A.S.: Problems of thermal conductivity of heat networks. Mater. XI All-Russian Sci. Tech. Conf. current issues Archit. Constr., pp. 9–15 (2018)
5. Mozgova, A., Shennikova, T.: Determination of the real energy efficiency of the inlet ventilation air heater and air curtain. IOP Conf. Ser. Mater. Sci. Eng. **890**, 012147 (2020). <https://doi.org/10.1088/1757-899X/890/1/012147>
6. Nemirovsky, Y.V., Mozgova, A.S.: Thermal conductivity of cylindrical tanks for backup fuel of boiler rooms. J. Phys. Conf. Ser. **1382**, 012139 (2019). <https://doi.org/10.1088/1742-6596/1382/1/012139>
7. Nemirovsky, Y.V., Mozgova, A.S.: Thermal conductivity of cylindrical tanks for backup fuel of boiler rooms. In: Journal of Physics: Conference Series. Institute of Physics Publishing (2019). <https://doi.org/10.1088/1742-6596/1382/1/012139>
8. Nemirovsky, Y.V., Mozgova, A.S.: Definition of thermal losses on the site of the layered pipeline of heat networks. Bull. Chuvash State Pedagog. Univ. named after I. YA. Yakovlev. Ser. Mech. a limit state № 2, pp. 23–32 (2017)
9. Nemirovsky, Y.V., Mozgova, A.S.: The thermal conductivity of the layered cylinder of finite dimensions. Mod. Quest. Contin. Mech. 2017 Collect. Artic. based Mater. Conf. (round table) with Int. Particip., pp. 60–64 (2017)
10. Nemirovsky, Y.V., Mozgova, A.S.: The thermal conductivity of a constructional element of the spacecraft in the form of the multilayered cylinder. Bull. Chuvash State Pedagog. Univ. named after I. YA. Yakovlev. Ser. Mech. a limit state № 1, pp. 49–54 (2017)
11. Nemirovsky, Y.V., Mozgova, A.S.: Two-dimensional steady-state heat conduction problem for heat networks. J. Phys. Conf. Ser. **1359**, 012138 (2019). <https://doi.org/10.1088/1742-6596/1359/1/012138>

12. Mozgova, A.S., Surikov, A.V: Energy inspection of boilers and heating networks. new Archit. Des. Build. Struct. Reconstr. Mater. III Int. (IX all-russian) Conf., pp. 474–480 (2016)
13. Kluczek, A., Olszewski, P.: Energy audits in industrial processes. J. Clean. Prod. 3437–3453 (2017). <https://doi.org/10.1016/j.jclepro.2016.10.123>
14. Kluczek, A., Olszewski, P.: Energy audits in industrial processes. J. Clean. Prod. **142**, 3437–3453 (2017). <https://doi.org/10.1016/j.jclepro.2016.10.123>
15. Alabugin, A.A., Aliukov, S.V., Osintsev, K.V.: Approximation methods for analysis and formation of mechanisms for regulating heat and mass transfer processes in heat equipment systems. Int. J. Heat Technol. **38**, 45–58 (2020). <https://doi.org/10.18280/ijht.380106>
16. Fresner, J., Morea, F., Krenn, C., Aranda Uson, J., Tomasi, F.: Energy efficiency in small and medium enterprises: lessons learned from 280 energy audits across Europe. J. Clean. Prod. **142**, 1650–1660 (2017). <https://doi.org/10.1016/j.jclepro.2016.11.126>
17. Makridou, G., Andriosopoulos, K., Doumpos, M., Zopounidis, C.: Measuring the efficiency of energy-intensive industries across European countries. Energy Policy **88**, 573–583 (2016). <https://doi.org/10.1016/j.enpol.2015.06.042>
18. Andersson, E., Arfwidsson, O., Bergstrand, V., Thollander, P.: A study of the comparability of energy audit program evaluations. J. Clean. Prod. **142**, 2133–2139 (2017). <https://doi.org/10.1016/j.jclepro.2016.11.070>
19. Anisimova, T.: Analysis of the reasons of the low interest of Russian enterprises in applying the energy management system. Procedia Econ. Financ. **23**, 111–117 (2015). [https://doi.org/10.1016/s2212-5671\(15\)00424-4](https://doi.org/10.1016/s2212-5671(15)00424-4)
20. Alabugin, A., Aliukov, S., Osintsev, K.: Management models of efficiency of development of resource and energy saving systems using methods of approximation of step functions. Lect. notes Eng. Comput. Sci. Ser. “Proceedings World Congr. Eng. 2017, WCE 2017”, pp. 102–106 (2017)
21. Borshcheniuk, V., Semeryanova, N., Filatova, U., Nikolaeva, D., Frolova, E.: Issues of implementing the state program of energy saving and energy efficiency. E3S Web Conf. **110**, 02080 (2019). <https://doi.org/10.1051/e3sconf/201911002080>
22. Cagno, E., Trianni, A.: Evaluating the barriers to specific industrial energy efficiency measures: an exploratory study in small and medium-sized enterprises. J. Clean. Prod. **82**, 70–83 (2014). <https://doi.org/10.1016/j.jclepro.2014.06.057>

# Analysis of Correlation of Monitoring Parameters of a Multi-storey Building for Determining Its Deformed State



Alexey N. Plotnikov , Sergey Andreevich Levin,  
Irina Sergeevna Gorbunova, Anastasia Georgievna Nikolaeva ,  
and Nadezhda Nikolaevna Arinina 

## 1 Introduction

The technical condition of multi-storey buildings, especially high-rise buildings, is largely determined by its deformations caused by the acting load of vertical and horizontal, uneven basement settlements and other factors. To ensure safety and reliability, it is necessary to carry out a continuous assessment of the state of structures throughout the entire service life [1–3].

The parameters of structural systems of reinforced concrete high-rise buildings, such as the ratio of the stiffness of interfloor floors and vertical elements, cores of stiffness and columns, the rigidity of the joints between these elements, differ from the design ones due to technological imperfections, the level of stresses in the elements, the development of shrinkage and force cracks [4].

The automatic monitoring system makes it possible at any time to receive information about the technical condition of structures and the building as a whole. As a result of scientific support of the object, a passport for monitoring the state of supporting structures is being developed, which includes a computer model of the object that is adequate to the current state of supporting structures, matrices of boundary values of integral characteristics corresponding to a violation of normal operation and a pre-emergency change in the state of supporting structures [5]. The data of the monitoring passport are used to form a matrix of settings for the SMIK software package.

The main information during monitoring can be obtained from the readings of the angles of rotation of the critical points recorded with the help of inclinometers. It is necessary to determine the location and number of critical monitoring points based on the analysis of the design model of the building.

---

A. N. Plotnikov (✉) · I. S. Gorbunova · A. G. Nikolaeva · N. N. Arinina  
Chuvash State University named after I.N. Ulyanov (ChuvSU), 15 Moskovskiy Prospekt,  
Cheboksary, Russian Federation

S. A. Levin  
LLC “SMIS-Expert”, 12 Kashirskoe highway, Moscow, Russian Federation

As a result of the ratio of the measured angles of rotation, it is necessary to draw a conclusion about the causes of excess deviations, which can be caused both by damage to the junction points of vertical structures with floors, and by loss of stability (bending during eccentric compression of reinforced concrete elements), as well as by turning the foundation.

## 2 Material and Research Methods

One of the challenges in designing a monitoring system is to reduce the number of sensors. It is impractical to supply each element of the building's structural frame with the entire list of sensors not only because of the increase in the cost of the system, but also because of the information redundancy of the received data stream. The readings of most of the sensors will either duplicate each other, or have a strong cross-correlation due to the spatial connectivity of the elements of the structural frame of the building, in which a change in the geometry or spatial position of one element will inevitably affect the state of others.

Strong correlation connectivity of the elements of a reinforced concrete building in a working condition within each floor and, accordingly, the mutual dependence of the deformation of the elements, allows you to minimize the number of controlled elements. To detect the accumulating deformations of the supporting frame, only the tilt angles of several key frame structures, measured by highly sensitive inclinometers, can be used as information parameters.

As an additional guideline for assessing the pre-emergency state of a building, we can consider the tendency in the development of deformation of the frame elements: the rate (and acceleration) of deformation changes and, accordingly, the predicted time for deformation to reach boundary values.

Supporting systems, especially multi-storey ones, have the property of genetic nonlinearity, including in the operation stage. As noted by Kabantsev [6], it is necessary to take into account the history of the closure of structures into the system. A real building is always different from its idealized design model. The stage of the initial operation of the building is important for setting monitoring parameters in a standard state.

Korgina [7] proposes to use a sample survey, spatial-coordinate measurements, finite element analysis of the stress-strain state of structures based on the measurement results.

An example of a static monitoring system is the system described in the work of Lazebnik [8]. When monitoring load-bearing structures of high-rise buildings, measurements of soil pressure, concrete deformation and forces in reinforcement bars are performed. The need to use this system was caused by the discrepancy between the calculated and actual values of settlements and rolls.

The concept of correlation is used to control the state of buildings and territories both in terms of deformation parameters and vibration frequencies, which is

described, in particular, in the works of Mordret et al. [9], Nakata et al. [10], Xiong H.-B., Cao J.-X., Zhang F.-L. [2244].

According to Snezhkova and Leonovich [11] structurally, in the automated monitoring system, two levels can be distinguished: technical, which includes the actual data collection system with sensor elements (sensors) and the decision-making level, the core of which is an algorithm for recognizing the approach of an emergency situation based on the aggregate of actual values of parameters obtained from sensors deformation of controlled elements. The inclinometer installation system should provide maximum information content, allowing the most probable changes in the geometry of the structural frame of the building to be recorded. From this point of view, the most effective installation sites for inclinometers are bearing columns in axes along the perimeter of the monolithic frame floor disks. For rectangular buildings, it is advisable to install inclinometers on corner columns. The paper introduces the need to establish correlations between deformations along the characteristic points of the building. The fact of deformation of the frame can be registered by the change in the inclination angles of the controlled columns, and a specific type of deformation—by the indicators of the correlation links of the inclination angles.

By analyzing correlations, the rigidity of both vertical and horizontal elements of the system, as well as their connections, can be estimated.

In the presented work, modeling of two types of buildings is carried out: frame and large-panel. The calculation was carried out in 2 modes of operation of the structure: the mode of the main operating period, the mode of special conditions of the operating period (according to 2 options).

The mode of the main operational period is a fully closed system of supporting structures, the geometric and stiffness parameters of which correspond to the design solution, i.e., the last stage of the erection mode. The exposure model is determined by the current regulations.

The modes of special conditions of the operational period, within which the stress-strain state (SSS) of the system of supporting structures under the action of special (emergency) loads is analyzed, correspond to the situation of deviation from the “normal” operating conditions of the building. In the first case, the values of wind effects in the design model were significantly increased, in the second case, the stiffness characteristics of individual structures in the body of the building on the first floor were changed. Structures for changing the stiffness characteristics were selected taking into account their maximum load (maximum emerging forces after calculation in the mode of the main operating period). As a rule, a special case of the operational period occurs after a certain period of normal operation of the building, within which the VAT of structures is formed, corresponding to the main operational period.

To clarify the question of whether there is a relationship between two values  $X$  and  $Y$ , it is necessary to determine whether there is a correspondence between large and small values of  $X$  with the corresponding values of  $Y$ , or such a relationship is not



found. The value of each element  $X_i$  and  $Y_i$  is determined by the magnitude and sign of the deviation from the arithmetic mean. If two quantities are related, then there is a correlation between them. The resulting measure of the relationship between  $X$  and  $Y$  was estimated by the Pearson correlation coefficient.

$$r_{xy} = \frac{\sum(d_x \cdot d_y)}{\sqrt{(\sum d_x^2 \cdot d_y^2)}} \quad (1)$$

Strong positive correlation is defined by the value  $r = 1$ . The term “strict” means that the values of one variable are uniquely determined by the values of another variable, and the term “positive” means that as the values of one variable increase, the values of the other variable also increase. An example of a strong correlation in the monitoring process is the correspondence between deformations and stresses with a constant stiffness of a member, or deformation of one element and deformation of another element (for example, two columns) with a constant stiffness of the entire supporting system.

Positive correlation corresponds to values of  $0 < r < 1$ . Positive correlation should be interpreted as follows: if the values of one variable increase, then the values of the other tend to increase. The closer the correlation coefficient is to 1, the stronger this tendency, and, conversely, as the correlation coefficient approaches zero, the tendency weakens.

The absence of correlation is determined by the value  $r = 0$ . A zero-correlation coefficient indicates that the values of the variables are not related to each other in any way.

Negative correlation corresponds to values of  $-1 < r < 0$ . If the values of one variable increase, then the values of the other tend to decrease. The closer the correlation coefficient is to  $-1$ , the stronger this tendency, and, conversely, as the correlation coefficient approaches zero, the tendency weakens. Strong negative, the correlation is determined by the value  $r = -1$ .

For building type 1—16-storey frame (Fig. 1a), the correlation between the angles of rotation of the corner columns within the tier was considered. For a building of the 2nd type—a 12-storey large-panel building (Fig. 1b), the deformations of its corner zones were compared. For frame (Fig. 2) and panel (Fig. 3) buildings, the placement of sensors was generally taken to be the same: in the center of stiffness and in the corner zones.

In the presented work, the correlation is determined by the adjacent columns of the frame building and the corners of the section of the panel building. The increment of the monitoring parameters simulated by the calculation is set by the difference between the stage of normal operation of buildings and scenarios of non-standard operation: a sharp increase in wind load and a decrease in rigidity as a result of damage to the lower tiers of load-bearing structures. The design models are implemented in a nonlinear setting for concrete.

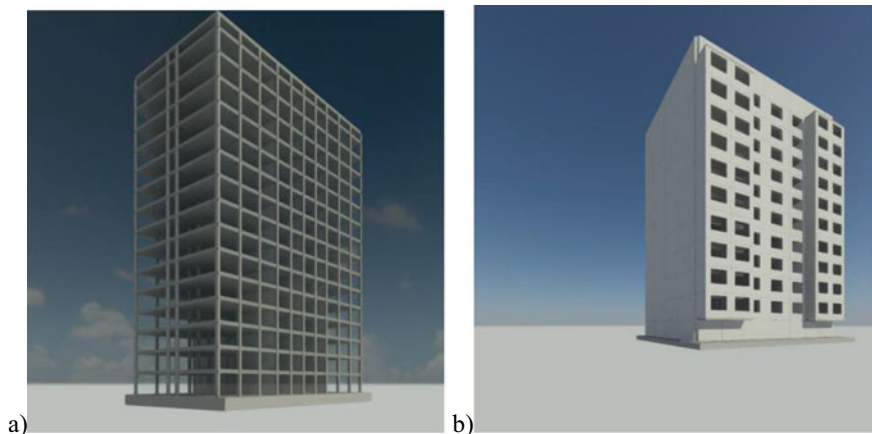


**Fig. 1** 16-storey frame building

### 3 Results and Problems

To obtain information on the most significant values—the angles of rotation of critical monitoring points when using inclinometers, deformation lines of the vertical axes of buildings were obtained. For a frame building, the data are presented in Figs. 4, 5 and 6. For panel—in Figs. 7, 8 and 9.

For all design situations, the increment of efforts and deformations is analyzed by stages: 1—normal operation, 2—increased wind load, by 1,7 times, 3—decrease in the rigidity of the lower tiers (by deflections by 1,4 times). Between these values, the average is determined, deviations from the average are determined for each scenario situation. As a result, the Pearson correlation coefficient is determined. An example of the analysis of ratios by correlation coefficients based on the obtained numerical data for a frame building is shown in Figs. 10 and 11.

Different situations are observed with the same influences. There is a positive correlation when the values of both compared variables increase (the deformations of adjacent columns are directed in the same direction). There is a negative correlation when the values of one variable increase, while the values of the other tend to decrease. The complex of these local situations as a whole gives a picture of the deformations of the building as a whole. In the case of the direction of the deformations of the columns in one direction, there is a general tilt of a part of the building, in the case of the direction of the deformations of the columns toward each other (negative correlation), there is an expectation of low stiffness of the floors in this zone. It is important to obtain such ratios for the height of the building, which will characterize the curvature of the vertical axis of the columns, its stress state. For a panel building, an example of analyzing the ratios by correlation coefficients based on the obtained numerical data is shown in Figs. 12 and 13.

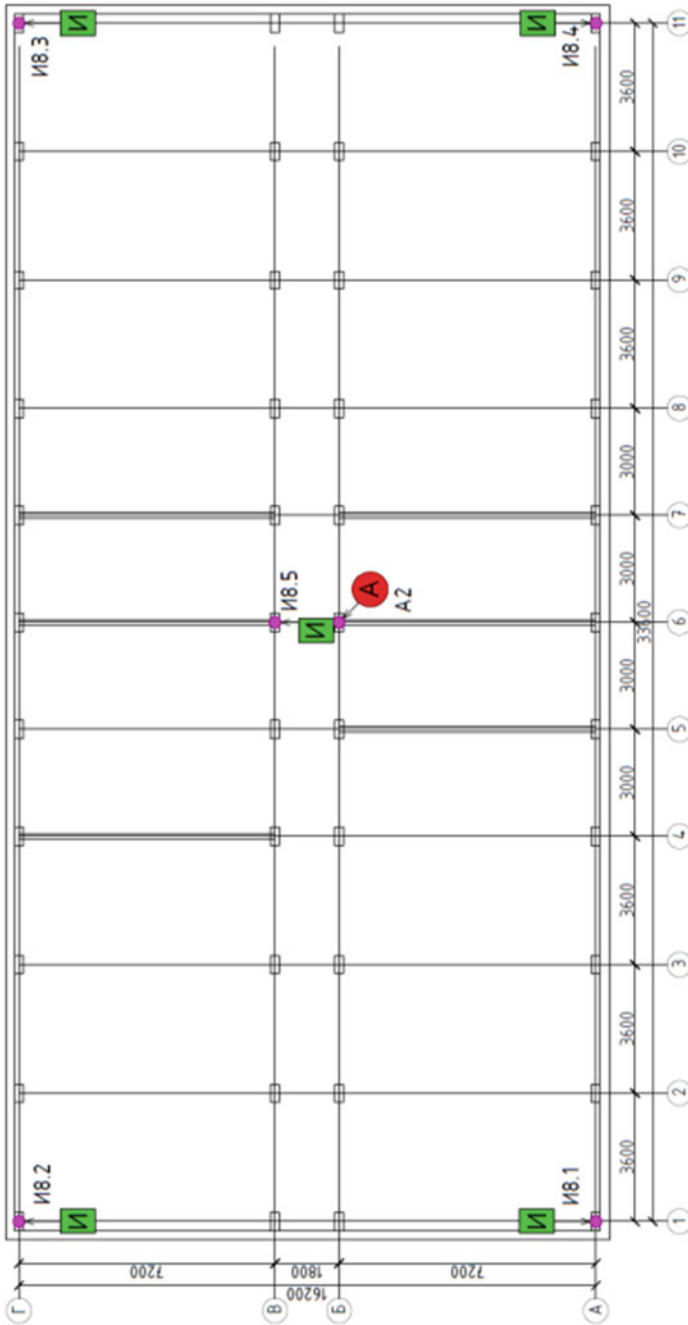


Fig. 2 Layout of monitoring sensors at elev. +16,240 frame building

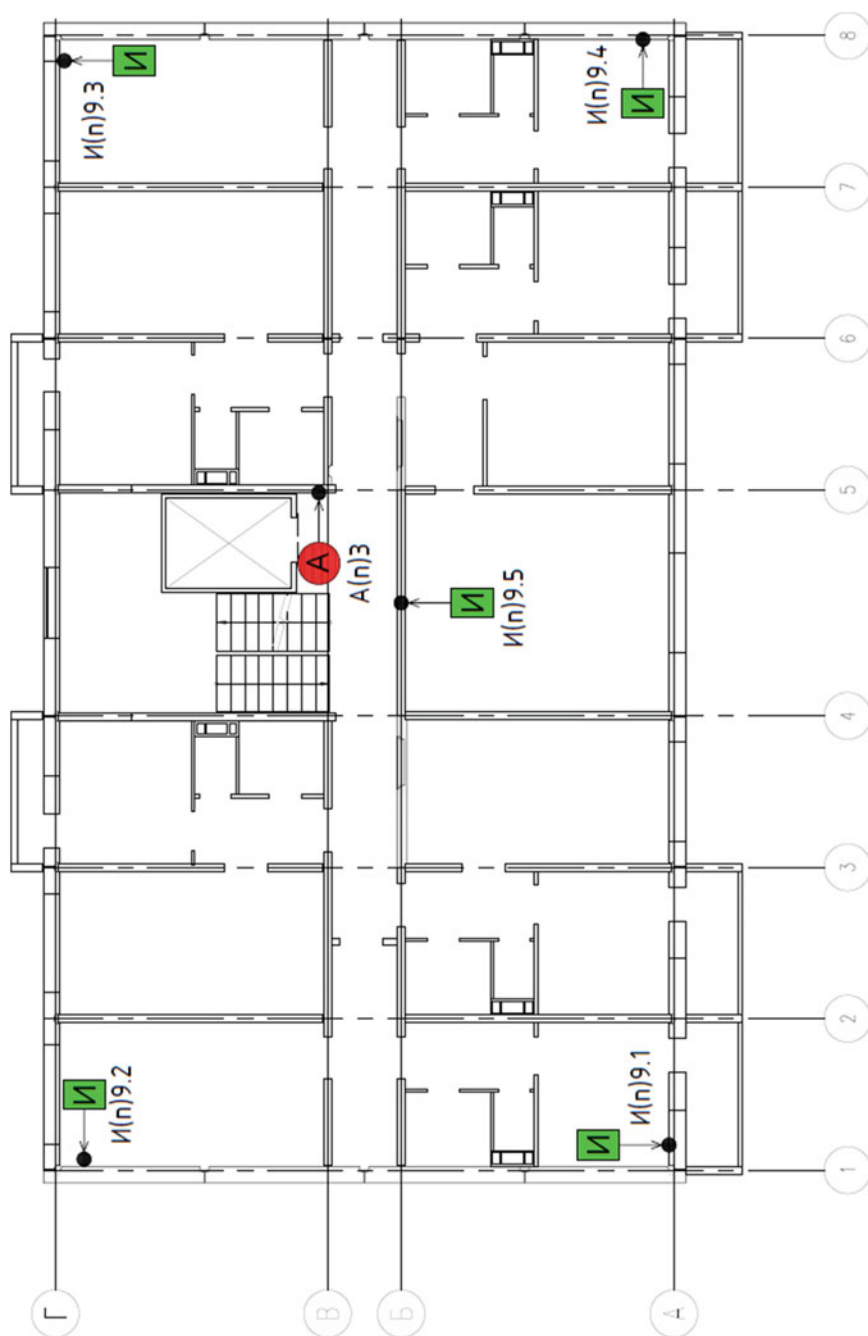


Fig. 3 Layout of monitoring sensors at elev. +21,440 panel building

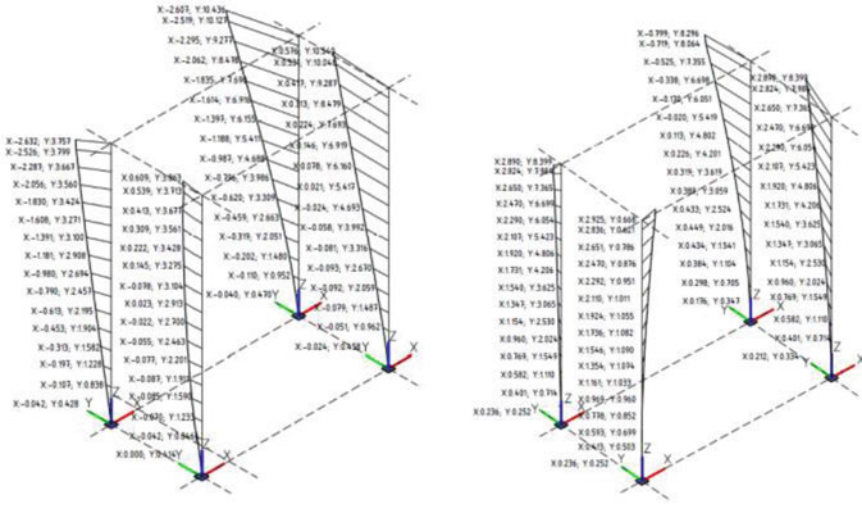


Fig. 4 Horizontal displacements of the corner columns of the building from wind load along Y and X (condition of normal operation)

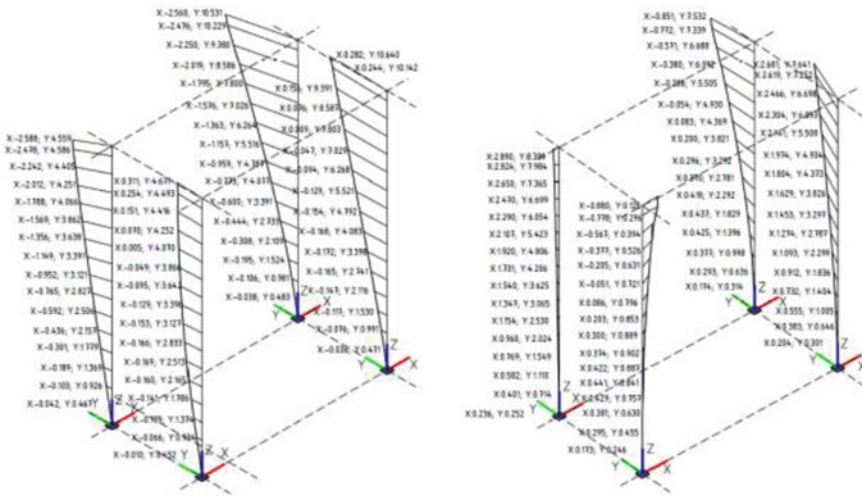
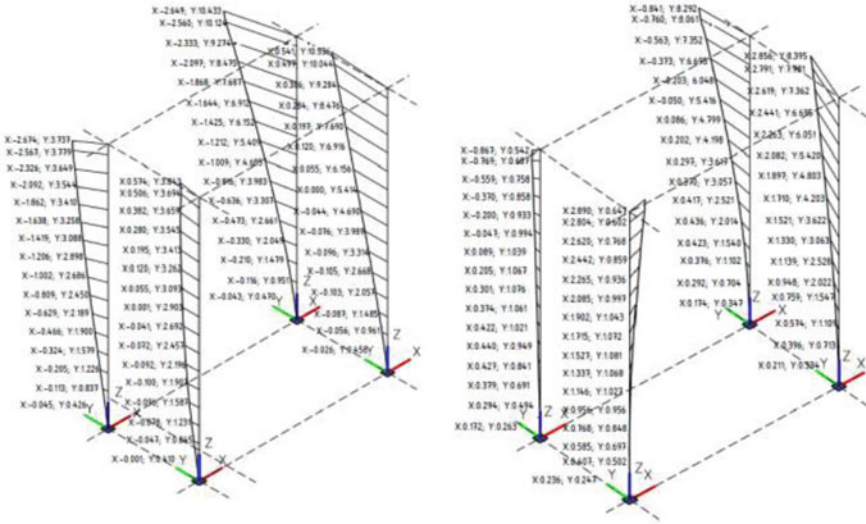
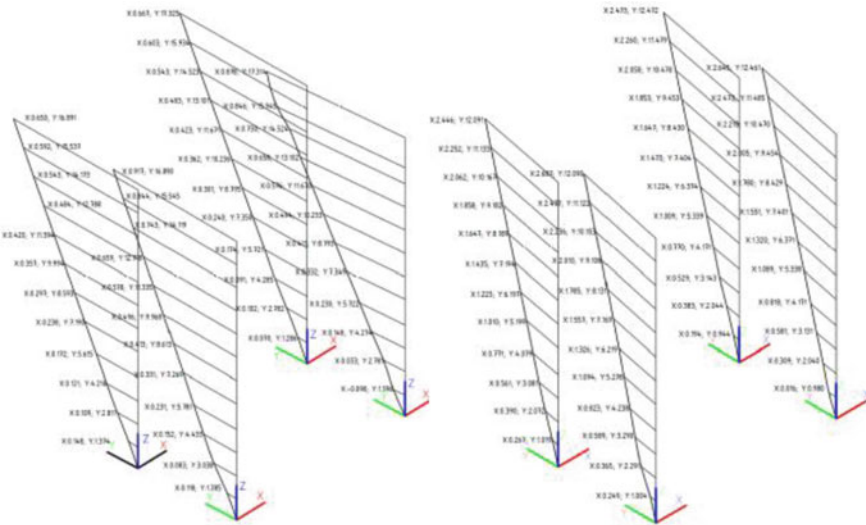


Fig. 5 Horizontal displacements of corner columns of the building from wind load along Y and X (condition of increased wind load)

A similar method based on the idea of correlating deformation parameters or displacement amplitudes measured by accelerometers is considered in [12]. In it, the translational amplitude-frequency modes “north–south”, “east–west” and torsional were graphically analyzed. Data were acquired in both the time domain and the frequency domain for each floor with the source at ground level. The wave impulse



**Fig. 6** Horizontal displacements of the corner columns of the building from wind load along Y and X (the condition for changing the stiffness of the structures of the 1st floor)



**Fig. 7** Horizontal displacements of the corner zones of a panel building from wind load along Y and X (condition of normal operation)

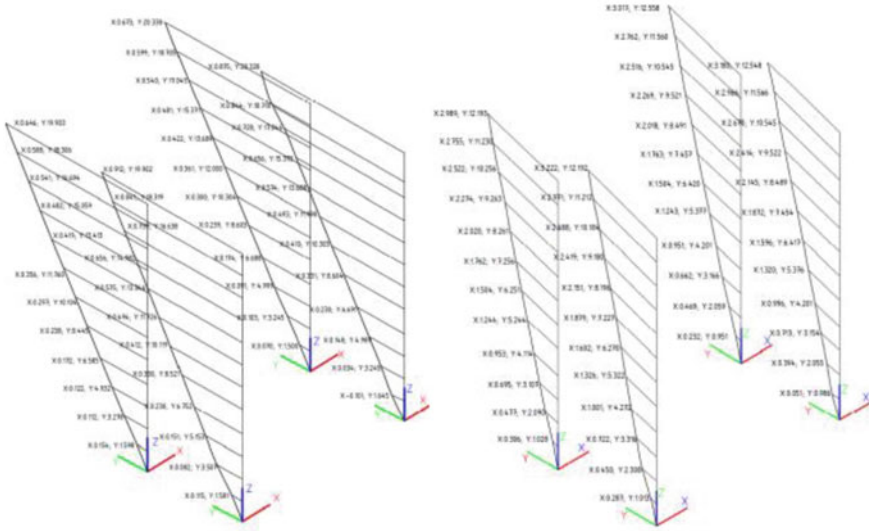


**Fig. 8** Horizontal displacements of the corner zones of a panel building from wind load along Y and X (condition of increased wind load)

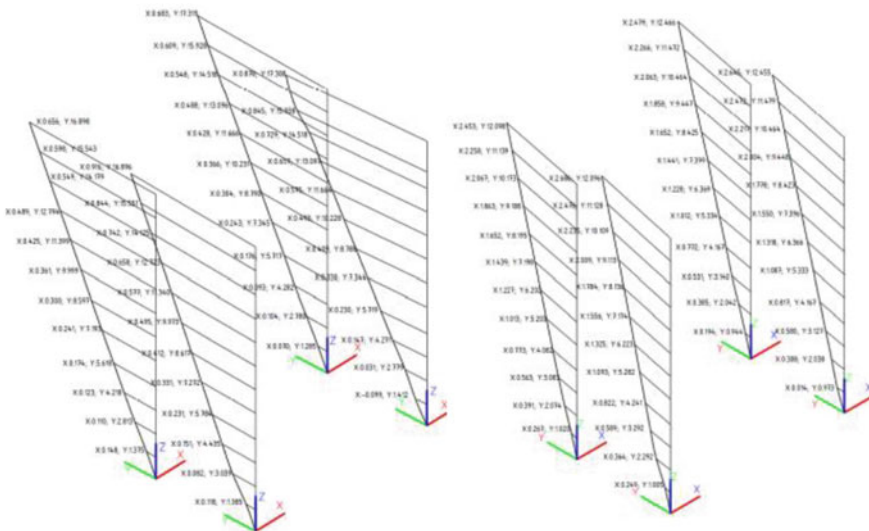


**Fig. 9** Horizontal displacements of the corner zones of a panel building from wind load along Y and X (the condition for changing the stiffness of the structures of the 1st floor)

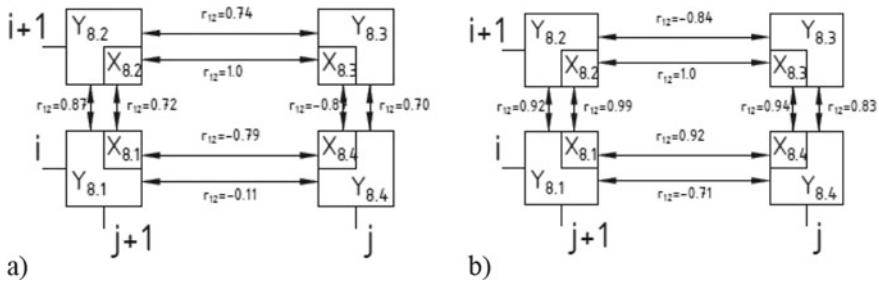


**Fig. 10** Scheme of the ratio of the correlation coefficients of the column tilt angles along the X and Y coordinate axes on the 8th floor of the frame building under the action of wind load along the Y axis (a), along the X axis (b)

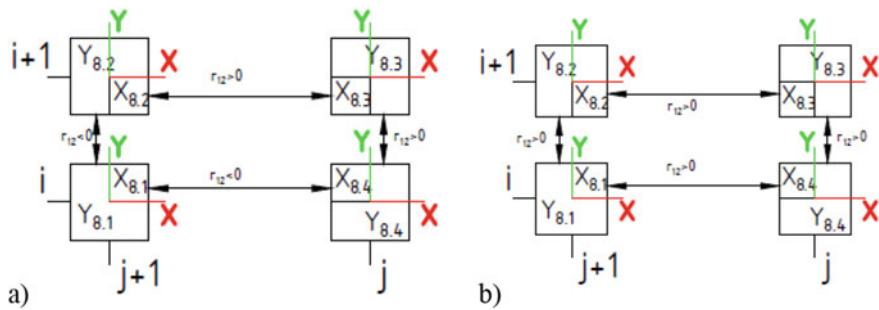


**Fig. 11** Scheme for analyzing the ratio of the correlation coefficients of the column tilt angles along the X and Y coordinate axes on the 8th floor of a frame building under the action of a wind load along the Y axis (a), along the X axis (b) using the example of the X coordinate direction

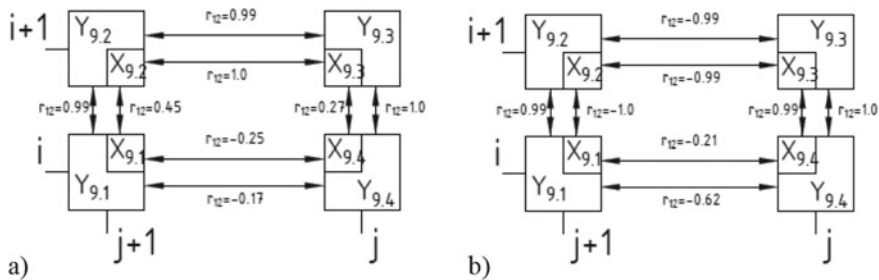


**Fig. 12** Scheme of the ratio of the correlation coefficients of the tilt angles of the intersection zones of the panels along the X and Y coordinate axes on the 9th floor of the panel building under the action of the wind load along the Y axis (a), along the X axis (b)



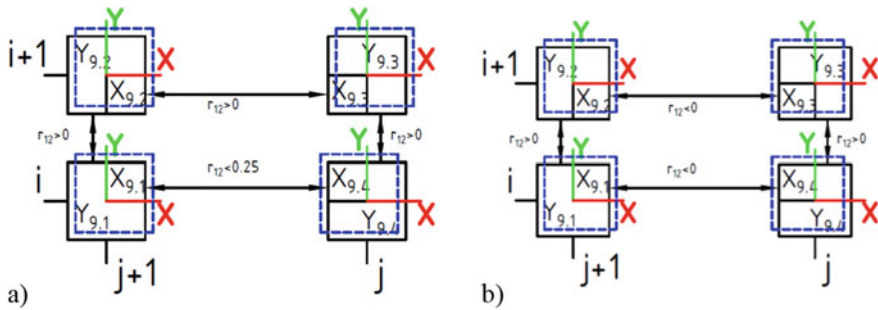


**Fig. 13** Scheme for analyzing the ratio of the correlation coefficients for the slope of the corner zones along the X and Y coordinate axes on the 9th floor of a panel building under the action of a wind load along the Y axis (a), along the X axis (b) using the example of the X coordinate direction

is clearly observed moving up and down the building at different speeds, depending on the type of vibration. The analysis uses the relative pulse velocities in different areas of the building. In this case, a drift of the fundamental mode frequency in one direction is observed, which indicates a change in the stiffness of the building.

The magnitude of the correlation coefficients, their sign depend on the stiffness ratio for the sections of the building. Overlapping discs have pliability of seams, this significantly reduces their rigidity in comparison with a solid monolithic overlap. This decrease can occur in individual areas [12–19]. A change in the pliability of the floor disks, which may also be due to cracks in monolithic floors, leads to a change in their effect on the redistribution of forces between vertical elements. The stiffer the disk and its interface with vertical elements, the smaller the difference in horizontal displacements it allows, the less negative correlation between the points of the floor supports, with absolutely hard disks, all points of vertical structures in the floor level would have the same horizontal displacements and the correlation would be close and positive.

## 4 Conclusion

For various types of buildings, it is necessary to develop schemes for the behavior of the building in case of violations of normal operation modes, abnormal effects and the state of the building. Building behavior diagrams should be linked to formalized deformation correlations, primarily of vertical structures. They are most informative about the behavior of the building as a whole. For buildings with a frame frame and panel multi-storey buildings, under extreme impacts, a decrease in the stiffness of the floors is characteristic, which is expressed by a negative correlation in the angles of rotation of the column points in the joints with the floors. This data is necessary for analyzing the situation in the automatic monitoring of buildings.

## References

1. Plotnikov, A.N., Ivanov, M.Y.: Monitoring system of high-rise buildings, determined from the nature of the curvature of the elastic line of vertical elements. *Constr. Sci. Educ.* **9**(4). Art. 3 (2019). <http://nso-journal.ru>. <https://doi.org/10.22227/2305-5502.2019.4.3>
2. Li, J., Hao, H.: A review of recent research advances on structural health monitoring in Western Australia. *Struct. Monit. Maintenance* **3**(1), 33–49 (2016). <https://doi.org/10.12989/smm.2016.3.1.033>
3. Quesada-Olmo, N., Jimenez-Martinez, M.J., Farjas-Abadia, M.: Real-time high-rise building monitoring system using global navigation satellite system technology. *Measurement* **123**, 115–124 (2018). <https://doi.org/10.1016/j.measurement.2018.03.054>
4. Plotnikov, A.N., Ivanov, M.Yu., Porfirieva, E.N.: Informativeness of monitoring systems for high-rise buildings from the principle of minimizing the number of sensors. *New in architecture, design of building structures and reconstruction: mat. IV Int. (X All-Russian) Conf. NASKR-2018*, pp. 267–277. Chuvash State University, Cheboksary (2018) (rus)
5. Nikolaeva, A.G.: Modeling of design schemes of panel buildings when calculating for progressive collapse. In: Nikolaeva, A.G., Ivanova, N.V., Gorbunova, I.S. (eds.) *Modern Problems of Continuum Mechanics—2019: Collection of Articles*. Art. Based on the Materials of the Conference from the International. Participation, pp. 128–134. Publishing House “Wednesday”, Cheboksary, (2019) (rus)
6. Kabantsev, O.V.: Method for calculating multi-storey buildings taking into account the process of changing the design scheme under different operating modes, pp. 43–51. *Vestnik MGSU*. No. 10 (2013) (rus)
7. Korgina, M.A.: Assessment of the stress-strain state of the bearing structures of buildings and structures during the monitoring of their technical condition. [Text]: dissertation. *Cand. tech. Sciences: 05.23.01/Mariya Andreevna Korgina*. M., 225 p (2008) (rus)
8. Lazebnik, G.E.: Monitoring of supporting structures of high-rise buildings [Text]. In: Lazebnik, G.Y., Kosheleva, N.N. (eds.) *Society of Geotechnics*, pp. 14–18 (2009) (rus)
9. Mordret, A., Sun, H., Prieto, G.A., Toksöz, M.N., Büyükoztürk, O.: Continuous monitoring of high-rise buildings using seismic interferometry. *Bull. Seismol. Soc. Am.* (2017)
10. Nakata, N., Snieder, R., Kuroda, S., Ito, S., Aizawa, T., Kunimi, T.: Monitoring a building using deconvolution interferometry. I: Earthquake-data analysis. *Bull. Seismol. Soc. Am.* **103**(3), 1662–1678 (2013)
11. Snezhkov, D.Y.: Monitoring of erected and operated reinforced concrete structures by non-destructive methods. In: Snezhkov, D.Y., Leonovich, S.N. (eds.) *Minsk: BNTU*, 331 p (2016) (rus)
12. Xiong, H.-B., Cao, J.-X., Zhang, F.-L.: Inclinometer-based method to monitor displacement of high-rise buildings. *Struct. Monit. Maintenance* **5**(1), 111–127 (2018)
13. Nikolaeva, A.G., Yakovleva, O.S.: Analysis of the effect of the loading sequence on the stress-strain state of the frame elements of multi-storey buildings. *Management of Assortment, Quality and Competitiveness in the Global Economy: Collection of articles of the VIII International Correspondence Scientific and Practical Conference (March 30, 2017)*, pp. 131–134. CHKI RUK, Cheboksary (2016) (rus)
14. Ivanova, N.V., Nikolaeva, A.G.: Influence of the percentage of reinforcement on the stress-strain state of the frame elements of multi-storey buildings in the calculation taking into account the construction. In: *Modern Issues of Continuum Mechanics 2017: Collection of Articles Based on the Conference (Round Table) with International Participation*, pp. 38–42. Chuvash Publishing House University, Cheboksary (2017) (rus)
15. Mustafin, M.G., Valkov, V.A., Kazantsev, A.I.: Monitoring of deformation processes in buildings and structures in metropolises. *Procedia Eng.* **189**, 729–736 (2017). <https://doi.org/10.1016/j.proeng.2017.05.115>
16. Yuan, K., Huib, Y., Chen, Z.: Effects of facade appurtenances on the local pressure of high-rise building. *J. Wind Eng. Ind. Aerodyn.* **178**, 26–37 (2018). <https://doi.org/10.1016/j.jweia.2018.05.004>

17. Li, J., Hao, H.: A review of recent research advances on structural health monitoring in Western Australi. *Struct. Monitor. Maintenance*. **3**(1), 33–49 (2016)
18. Lee, J.-J., Ho, H.-N., Lee, J.-H.: A vision-based dynamic rotational angle measurement system for large civil structures. *Sensors* **12**(6), 7326–7336 (2012)
19. Ivanov, M.Y., Plotnikov, A.N.: Monitoring system of high-rise buildings from the principle of minimizing the number of sensors. *Eng. Pers. Future Innov. Econ. Russ.* **5**, 25–28 (2019) (rus)

# Rigidity of Supporting Sections of High Building Bars and the Possibility of Its Monitoring by Inclinometers



Alexey N. Plotnikov and Mikhail Yurievich Ivanov

## 1 Introduction

Every year there is an expansion of construction production, the design solutions of high-rise buildings are being improved, which ensure safe life. It should be noted that the overall stability and spatial rigidity of a building depend not only on the mutual combination and location of structural elements, but also on the strength of the joints.

Modern high-rise buildings have a large mass, concentrated on a small part of the base surface, which significantly affects the deformations that occur during operation.

Various structural systems of high-rise buildings have common mathematical laws that affect various deformations.

Modern high-rise buildings are complex spatial systems consisting of various elements and joints, the parameters (stiffness, etc.) of which change during loading.

The ratio of the stiffness parameters of the vertical and horizontal bearing elements also affects the operation of the building as a whole [1]. In the process of operation, the state of buildings changes: the operability is limited and reliability decreases. In this regard, it becomes necessary to monitor the joints of vertical and horizontal load-bearing structural elements [2–11].

One such controlled parameter is the cross-sectional stiffness. In practice, the stiffness of the cross-sections of a multi-storey building can be monitored using inclinometers.

---

A. N. Plotnikov (✉) · M. Y. Ivanov  
Chuvash State University named after I.N. Ulyanov (ChuvSU), 15 Moskovskiy Prospekt,  
Cheboksary 428015, Russian Federation

## 2 Material and Research Methods

In many experimental studies, it was found that with an increase in the load and the development of nonlinear processes of the relationship “stress—deformation”, a redistribution of efforts occurs, which fully corresponds to the general theory of reinforced concrete [12, 13].

To calculate reinforced concrete structures under the action of any load and different stages of the stress-strain state (SSS) of the girder of different directions, continuous functions are required. At present, for the calculation of reinforced concrete structures, discontinuous functions are used, separately for each stage of SSS. The set of rules for the calculation of reinforced concrete structures SP 63.13330 proposes for stage II to define the shape of the compressive stress diagram as triangular, for stage III—as rectangular, and the element can be calculated at the same load using these two options. Diagrams of normal stresses by stages of loading are shown in Fig. 1.

Calculation of reinforced concrete girders with the formation and development of cracks (stage II) of stretched zones is reduced to determining the geometric parameters of the sections: the height of the compressed zone, the shoulder of a pair of forces in the section, as well as the proportion of plastic deformations in concrete. The deformation diagram is shown in Fig. 2.

Many works of authors like A. A. Gvozdev, V. I. Murashev, A. F. Loleit, S. M. Krylov, V. M. Bondarenko, N. I. Karpenko, A. G. Tamrazyan, E. N. Kodysh contributed to the development of the theory of calculation of reinforced concrete by limiting states. Thanks to computer calculation methods, it contributed to the consideration of nonlinear loads of structures by continuous functions [14].

Traditionally, the shoulder of a pair of forces  $z$  is found as the ratio of the static moment of the reduced area of the compressed zone of concrete relative to the tensioned reinforcement to the specified reduced area.

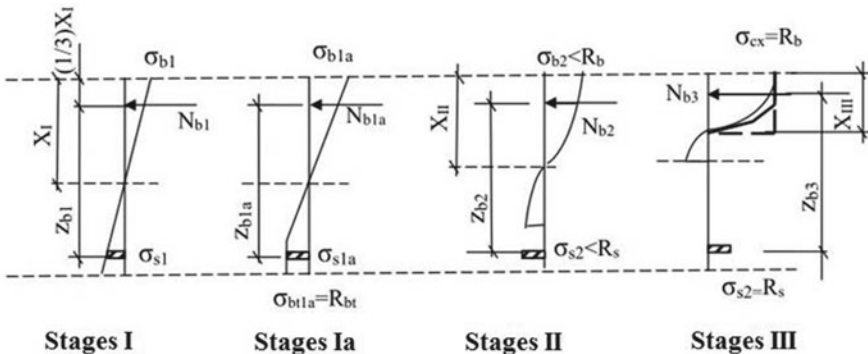
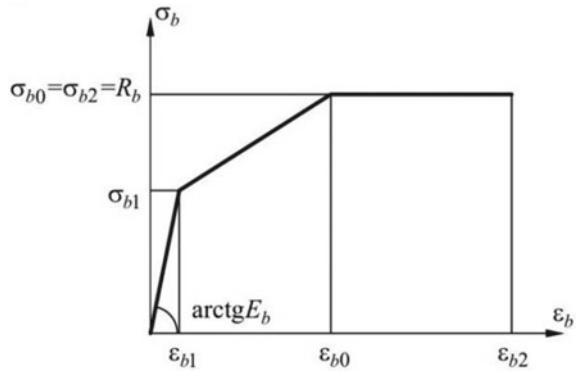


Fig. 1 Diagrams of normal stresses in a section of an element by stages of loading

**Fig. 2** Deformation diagram of concrete



According to the analysis of A. S. Zalesov, E. N. Kodysh L. L. Lemysh, I. K. Nikitin [15], a change in the relative height of the compressed zone  $\xi$  within 10–20% has an insignificant effect on the curvature of  $1/r$ , since at the same time, the shoulder of a pair of forces  $z$  in the section, deformation of concrete  $\epsilon_{bm}$  and reinforcement  $\epsilon_{sm}$  also changes, while the sum of deformations and curvature change little.

$$\frac{1}{r} = \frac{\epsilon_{bm} + \epsilon_{sm}}{r}. \tag{1}$$

Later, when returning to the hypothesis of flat sections in determining the width of crack opening and curvature of a bent element, based on the calculations of Kodysh et al. [15] and the normative document SP 63.13330.2018, the shoulder of a pair of forces began to be expressed as

$$z = h_0 - \frac{1}{3}x_m. \tag{2}$$

In the works of P. F. Drozdova, M. I. Dodonov notes that the change in the stiffness of the floor is usually considered [16, 17]:

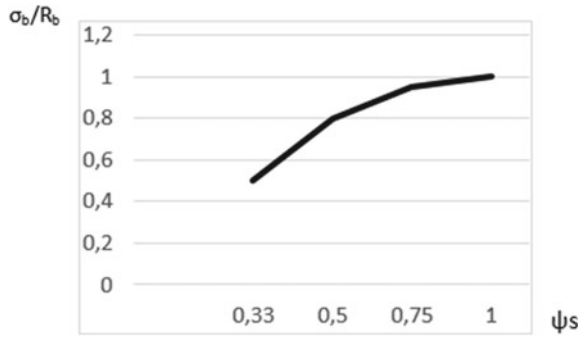
$$s = \frac{hl^3}{12\gamma B_u b} \tag{3}$$

The amount of change in stiffness  $B_u$  at the first stage of the stress-strain state of the girder structure is considered under the condition  $M_i < M_{cr}$ , as well as at the second stage when a crack is formed  $M_{cr} < M_i < M_u$ .

After the formation of cracks and their growth and an increase in the proportion of plastic deformations in the concrete of the compressed zone (decrease in the modulus of deformation), the flexural stiffness of the element is determined by the expression

$$D = E_{s,red} A_s z (h_0 - x_m) \tag{4}$$

**Fig. 3** The relationship between the stress level in concrete in the compressed zone and the coefficient of stress unevenness in tensile reinforcement (according to V. I. Murashev)



$$E_{s,\text{red}} = E_s/\psi_s \quad (5)$$

To implement the joining of solving problems for different stages of stress-strain state, we take a single center of rotation of the compressed zone of concrete relative to the center of gravity of the stretched reinforcement. The solution to the problem, basically, consists in finding the value of the displacement of the center of gravity of the diagram of the compressed zone when passing between stages of stress-strain state.

It is assumed that after the formation of cracks, at stage II, in addition to the forces in the section, the material parameter  $\psi_s$  changes from 0.4 to 1.0—the coefficient of non-uniformity of stresses along the length of the reinforcing bar between the cracks.

Inelastic deformations of concrete in the compressed zone are taken into account by the standard values of relative deformations during short-term and long-term loading of the structure according to SP 63.13330. After the formation of cracks in accordance with the three-line diagram of the work of compressed concrete, shown in Fig. 3.

$$E_{b1,\text{red}} = 0.6R_{bn}/\varepsilon_{b1} \quad (6)$$

At stage II, on average:

$$E_{b0,\text{red}} = R_{bn}/\varepsilon_{b0} \quad (7)$$

At stage III:

$$E_{b2,\text{red}} = R_{bn}/\varepsilon_{b2} \quad (8)$$

During the operation of high-rise buildings, various deformations occur, including a decrease in the bending moment in the supporting sections (decrease in rigidity) of reinforced concrete girders. Taking into account the formation of cracks and the development of a plastic hinge, the bending moment in the cross-section of the girder decreases to 30%.

### 3 Results and Problems

In work [18], a bending element was modeled with a reinforcement percentage of 1%, corresponding to structures of mass use at 3 stages of work.

At stage I, the height of the compressed zone and the shoulder of a pair of forces were determined using the SP 63.13330 method with a section height  $h = 350$  mm and a width  $b = 150$  mm, the shoulder of a pair of forces at stage I was  $z = 25.35$  cm.

At stage II, after the formation of cracks, the height of the compressed zone of concrete, depending on the magnitude of deformation according to the concrete diagram, and, accordingly, the level of load, the magnitude of stress unevenness along the length of the reinforcing bar (Fig. 1), which also depends on the level of the load, the shoulder of a pair of forces is determined equal to  $z = 25.77$  cm.

At stage III—destruction of a bent element, for the considered numerical example,  $z = 28.6$  cm.

The recently proposed method for calculating the ultimate deformations of concrete and reinforcement involves the use of a piecewise linear stress diagram of a compressed zone, which approximately describes a real nonlinear diagram.

In this case, taking into account the coefficient of completeness of the stress diagram

$$x = \frac{R_{sn}A_{sn}}{\omega R_{bn}b} \quad (9)$$

The value of the arm of the pair of forces determined at the stage of elastic work of concrete according to the given geometric characteristics can be corrected with an increase in the load on the coefficient.

$\beta = 1 - 1.13$ —with a short-term load,

$\beta = 1 - 1.17$ —with prolonged action of the load.

The amount of change in hardness  $B_u$  at stage I will be:

$$B_u = 2.5E_s A_s z (h_0 - x_{mI}) = 763.67E_s A_s \quad (10)$$

The amount of change in the hardness  $B_u$  at stage III will be:

$$B_u = 2.5E_s A_s z (h_0 - x_{mIII}) = 665.1E_s A_s \quad (11)$$

The rigidity of the girder structure at stage I will be:

$$D = EJ = 16078125000 \text{ H/CM}^2 \quad (12)$$

The moment of inertia of the cross-section of the girder will be:

$$J = \frac{bh^3}{12} = 53593.8 \text{ CM}^4 \quad (13)$$



The rigidity of the girder structure at stage III will be:

$$D = 63649600000 \text{ H/CM}^2 \quad (14)$$

Taking into account the formation of cracks and the development of a plastic hinge, there is a decrease in the bending moment in the supporting section of the girder, which reduces the rigidity of the supporting moment by up to 2.5 times.

The change in the stiffness of the girder connection can be traced using computer programs such as Lira-CAD, SCAD OFFICE.

Modeling of the work of reinforced concrete with cracks in them has not yet been implemented. To trace the change in stiffness, it is necessary to enter intermediate values of the elastic modulus in the support sections of the girder, which corresponds to a decrease in the reference moment to 30%.

In practice, the rigidity of the cross-sections of the cross-sections of a high-rise building can be tracked using inclinometers. Inclinometers are installed on columns through 1/4 of the building height [19, 20], measurements are made at the crossbar-column intersection. The deflection of the column from the vertical gives an increase in the deflection angle with a crack, which corresponds to a decrease in the rigidity of the cross-section of the girder. The total angle of rotation will be the sum of the parameters:

$$\varphi = \varphi_1 + \varphi_2 + \Delta\varphi \quad (15)$$

where  $\varphi_1$ —is the angle of rotation of the extreme column,  $\varphi_2$ —is the angle of rotation of the middle column,  $\Delta\varphi$ —is an additional angle of rotation that depends on the width of the crack opening in the structures.

For modeling the design model, the frame and frame-braced frames of a high-rise building were adopted. Changes in the support moment and the girder rotation angle were taken at the crossbar-column intersection nodes, at 6 points located through 1/4 of the building height. Deformations of systems during nonlinear concrete operation after cracking are shown in Fig. 4. The calculation results are summarized in Tables 1, 2 and 3, diagrams of comparison of the results are presented in Figs. 5, 6, 7 and 8.

In the sections where cracks are formed, a supporting finite element for reducing the stiffness is introduced, equal to the length of the crossbar bearing on a column 200 mm long. For these design solutions, the value of the elastic modulus in the support sections of the girder was taken, a value reduced by 1.25 and 2.5 times, which gives a decrease in the support rigidity during operation.

When the stiffness of the supporting finite element changes by 1.25 times:

- in the nodes of the crossbar connection to the column in the frame frame, the crossbar rotation angle will increase up to 1.02 times;
- in the nodes of the crossbar connection to the column in the frame-braced frame, the angle of the crossbar rotation will practically not change, it remains constant.

When changing the supporting finite element by 2.5 times:

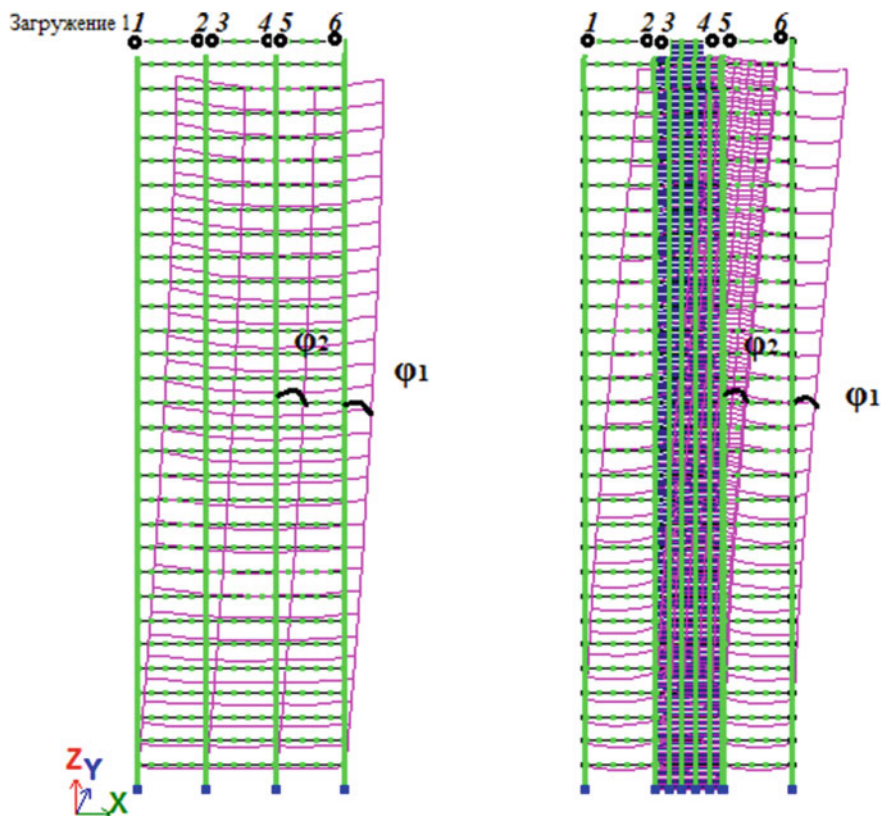


Fig. 4 Frame and frame-tie frames of the building

- in the nodes of the crossbar junction to the extreme column in the frame frame, the angle of the crossbar rotation will increase up to 1.12 times, at the junctions of the crossbar to the middle column—it will increase to 1.22 times;
- in the nodes of the crossbar connection to the column in the frame-braced frame, the angle of the crossbar rotation will practically not change, it remains constant.

Based on the results of the analysis of the results obtained, the angles of rotation were determined with a decrease in the supporting rigidity of the crossbar.

With a decrease in the supporting finite element by 2.5 times, the difference in the angle of rotation for the extreme columns was 46 angular sec, for middle columns—28 angular sec.

For the extreme columns, with a decrease in the supporting finite element by 1.25 times, the difference in the angle of rotation was 8 angular sec, for middle columns—5 angular sec.

**Table 1** Angles of rotation in the supporting sections of the frame girder

x/H	Mark	Angle of rotation $uY$ in the cross-section of the girder, rad * 1000					
		1	2	3	4	5	6
<b>Crossbar support stiffness unchanged</b>							
0	0	1.31183	0.310037	0.542432	0.340296	0.558201	0.066282
1/4	24.5	1.67247	0.752719	0.887259	0.11482	0.261187	-0.22968
1/2	52.5	1.81636	0.930448	1.00799	-0.11044	-0.014228	-0.59155
3/4	80.5	1.77686	0.947455	1.44988	-0.29346	-0.224767	-0.88502
1	105	2.52102	1.01407	1.10021	-0.61264	-0.510591	-1.92701
<b>Crossbar support stiffness reduced by 1.25 times</b>							
0	0	1.32852	0.283823	0.570767	0.312175	0.581687	0.043111
1/4	24.5	1.70545	0.742742	0.909091	0.091791	0.272822	-0.26462
1/2	52.5	1.85953	0.930889	1.0266	-0.13131	-0.012456	-0.63534
3/4	80.5	1.82563	0.953153	1.01618	-0.31320	-0.228513	-0.93340
1	105	2.56013	1.01646	1.12179	-0.63638	-0.510591	-1.96498
<b>Crossbar support stiffness reduced by 2.5 times</b>							
0	0	1.40864	0.161553	0.702691	0.179643	0.691752	-0.06809
1/4	24.5	1.86288	0.696669	1.0122	-0.01722	0.326696	0.114948
1/2	52.5	2.066	0.934783	1.11473	-0.23034	-0.005912	-0.84477
3/4	80.5	2.05937	0.982635	1.09878	-0.40698	-0.248613	-1.16521
1	105	2.74894	1.03211	1.22137	-0.74647	-0.517177	-2.1482

For the extreme columns, with a decrease in the supporting finite element by 2.5 times, the difference in the angle of rotation was 46 angular sec, for middle columns—28 angular sec.

Changes in the severity of the connection between the girder and the column in the support part can be traced using inclinometers, determining the displacements of vertical elements, and also taking into account the width of the crack opening, which give additional angles of rotation of horizontal structural elements. It is necessary to take into account the constructive solution of high-rise buildings, which determine the maximum angles of rotation of the structure, depending on the redistribution of forces depending on the deformations arising during operation.

## 4 Conclusion

The change in the stiffness of the cross-sections of the girder can be monitored using inclinometers located after 1/4 of the building height. Measurements are made at the crossbar-column intersections at both ends of the crossbar to control the integrity of the connection and their connection with each other.

**Table 2** Consolidated angle of rotation in the cross-section of the crossbar for the frame-braced frame

x/H	Mark	Angle of rotation $uY$ in the cross-section of the girder, rad * 1000					
		1	2	3	4	5	6
<b>Crossbar support stiffness unchanged</b>							
0	0	2.78553	-3.18363	0.105694	0.180775	3.04603	-2.92314
1/4	24.5	1.60516	-4.364	0.85779	0.886496	3.49498	-2.47418
1/2	52.5	0.715219	-5.25395	1.29528	1.32435	3.94529	-2.02388
3/4	80.5	0.241612	-5.72755	1.44988	1.47932	4.26215	-1.70701
1	105	0.113241	-5.85592	1.45224	1.51256	4.37061	-1.59855
<b>Crossbar support stiffness reduced by 1.25 times</b>							
0	0	2.78554	-3.18363	0.105722	0.180762	3.04602	-2.92314
1/4	24.5	1.60517	-4.36399	0.857837	0.886474	3.49496	-2.4742
1/2	52.5	0.71524	-5.25392	1.29534	1.32434	3.94525	-2.02392
3/4	80.5	0.24164	5.76109	1.45664	1.48606	4.28869	-1.68048
1	105	0.113271	-5.85589	1.4523	1.51256	4.37056	-1.59861
<b>Crossbar support stiffness reduced by 2.5 times</b>							
0	0	2.78555	-3.18361	0.105864	0.180689	3.046	-2.92316
1/4	24.5	1.60523	-4.36394	0.858064	0.886366	3.49485	-2.47432
1/2	52.5	0.71534	-5.25382	1.2956	1.32427	3.94505	-2.02411
3/4	80.5	0.241765	-5.7274	1.45021	1.47925	4.26186	-1.7073
1	105	0.113403	-5.85576	1.45257	1.51255	4.37031	-1.59886

By determining the displacements of vertical elements, as well as measuring the width of the crack opening, it is possible to trace the change in the support stiffness of horizontal elements (girders).

Depending on the design solution of a high-rise building, the boundary angles of rotation of the girder structure are determined, a further increase in the angles of rotation indicates a decrease in the support rigidity of the girder.

With the help of inclinometers, it becomes possible to trace the development of a plastic hinge, which reduces the rigidity of the structure in the bearing cross-section of the girder.

Using inclinometers located 1/4 of the height of the building, it is possible to track the state of not only vertical elements, but also horizontal ones, which gives a more "accurate picture" of the state of the building as a whole.

**Table 3** Consolidated angle of rotation in the cross-section of the girder to the frame and frame-braced frame at elev. 105 m

Frame frame							
x/H	Mark	Angle of rotation $uY$ in the cross-section of the girder, angle sec					
		1	2	3	4	5	6
<b>Crossbar support stiffness unchanged</b>							
1	105	528	209	226	126	105	397
<b>Crossbar support stiffness reduced by 1.25 times</b>							
1	105	529	210	231	131	106	405
<b>Crossbar support stiffness reduced by 2.5 times</b>							
1	105	567	212	252	154	107	443
Frame-braced frame							
x/H	Mark	Угол поворота $uY$ в опорном сечении ригеля, уг. сек					
		1	2	3	4	5	6
<b>Crossbar support stiffness unchanged</b>							
1	105	23	1207	299	312	901	330
<b>Crossbar support stiffness reduced by 1.25 times</b>							
1	105	23	1207	299	312	901	330
<b>Crossbar support stiffness reduced by 2.5 times</b>							
1	105	23	1207	299	312	901	330

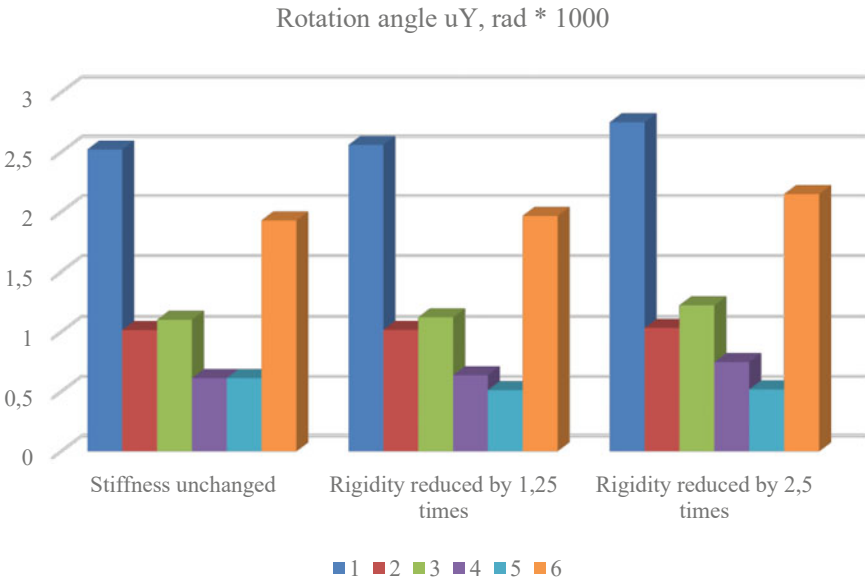


**Fig. 5** Diagram of the turning angles of the cross-section of the girder frame structure at elev. 105 m

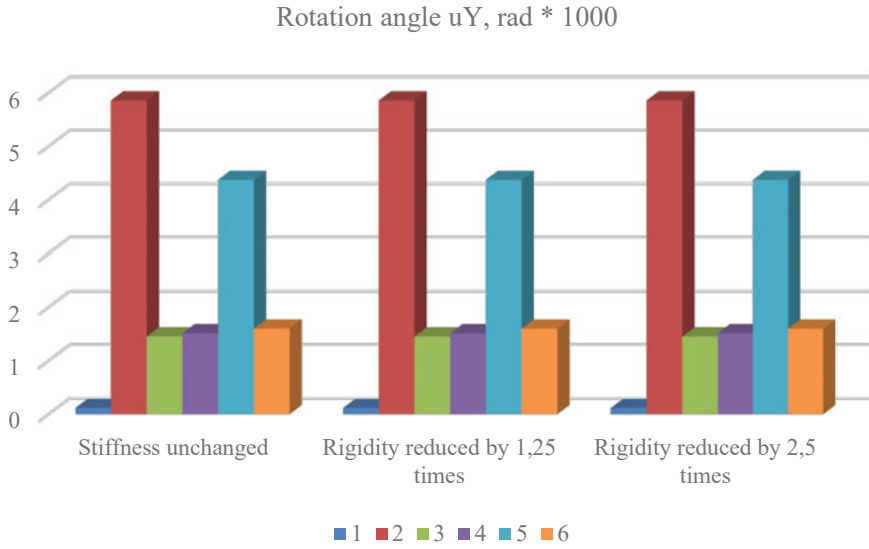


**Fig. 6** Diagram of the turning angles of the cross-section of the girder frame-braced structure at elev. 105 m

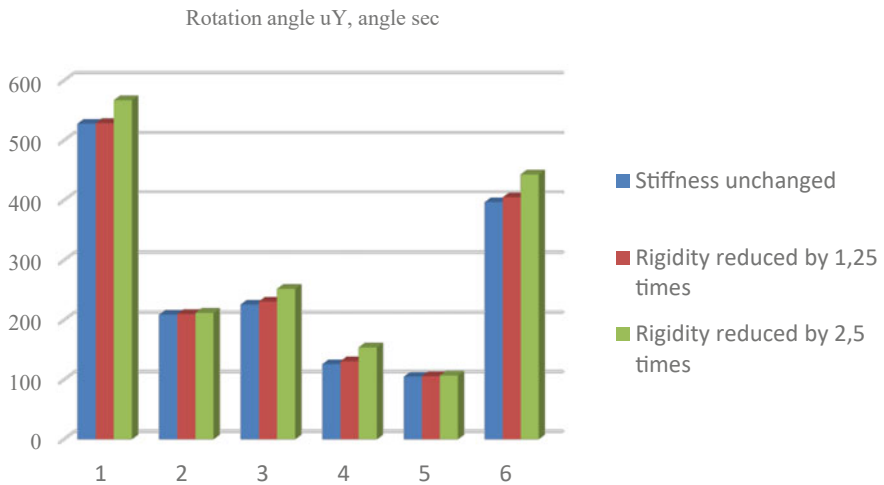


**Fig. 7** The summary diagram of the turning angles of the cross-section of the girder frame structure at elev. 105 m

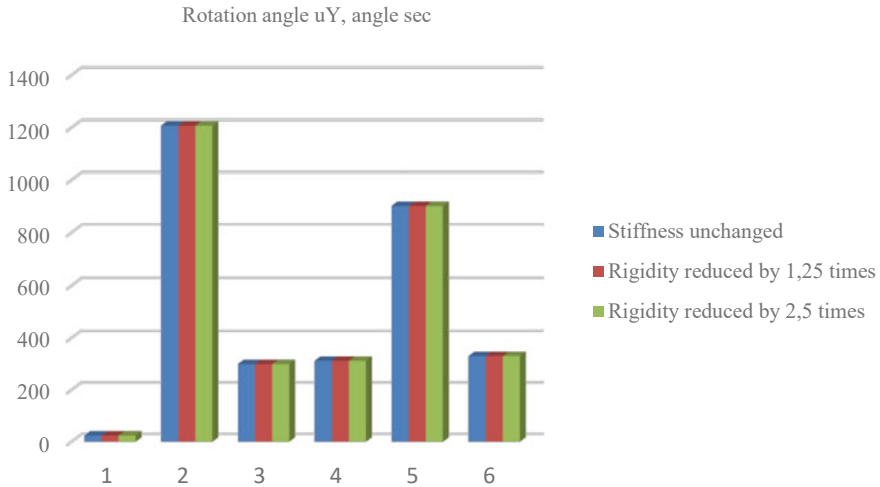


**Fig. 8** The summary diagram of the turning angles of the cross-section of the girder frame-braced structure at elev.105 m

## References

- Plotnikov, A.N., Ivanov, M.Y., Yakovleva, O.S.: Rigidity parameters of high-rise buildings and their determination during monitoring. *Bulletin of the Chuvash State Pedagogical University named after I.I. AND I. Yakovleva. Series: Limit State Mechanics. No. 1(43)*, pp. 55–65 (2020) (rus)
- Mustafin, M.G., Valkov, V.A., Kazantsev, A.I.: Monitoring of deformation processes in buildings and structures in metropolises. *Procedia Eng.* **189**, 729–736 (2017). <https://doi.org/10.1016/j.proeng.2017.05.115>
- Yuan, K., Huib, Y., Chen, Z.: Effects of facade appurtenances on the local pressure of high-rise building. *J. Wind Eng. Ind. Aerodyn.* **178**, 26–37 (2018). <https://doi.org/10.1016/j.jweia.2018.05.004>
- Li, J., Hao, H.: A review of recent research advances on structural health monitoring in Western Australi. *Struct. Monit. Mainten.* **3**(1), 33–49 (2016)
- Xiong, H.-B., Cao, J.-X., Zhang, F.-L.: Inclinometer-based method to monitor displacement of high-rise buildings. *Struct. Monit. Mainten.* **5**(1), 111–127 (2018)
- Lee, J.-J., Ho, H.-N., Lee, J.-H.: A vision-based dynamic rotational angle measurement system for large civil structures. *Sensors* **12**(6), 7326–7336 (2012)
- Ozbey, B., Erturk, V.B., Demir, H.V., Altintas, A., Kurc, O.A.: Wireless passive sensing system for displacement. Strain measurement in reinforced concrete members. *Sensors* **16**, 479–496 (2016)
- Eisenkrain, E.: Continuous monitoring of the movement of meridional cracks arising in the shells of cooling towers under the influence of external factors. *Constr. UniBuild. Struct.* **5**(32), 84–94 (2015) (rus)
- Belostotskiy, A.M., Akimov, P.A., Negrozov, O.A., Petryashev, N.O., Petryashev, S.O., Shcherbina, S.V., Kalichava, D.K., Kaitukov, T.B.: Adaptive finite element models in monitoring systems of buildings and structures. *Inzhenerno-stroitelnyj zhurnal* **2**(78), 169–178 (2018) (rus)
- Hong, K., Lee, J., Choi, S.W., Kim, Y., Park, H.S.: A strain-based load identification model for beams in building structures. *Sensors* **13**, 9909–9920 (2013)

11. Bulgakov, A., Shaykhutdinov, D., Gorbatenko, N., Akhmedov, S.: Application of full-scale experiments for structural study of high-rise buildings. *Procedia Eng.* **123**, 94–100 (2015)
12. Plotnikov, A.N.: Efforts of intersecting bending reinforced concrete elements with nonlinear changes in stiffness. “Loleyt Readings—150”. Modern methods for calculating reinforced concrete and stone structures by limiting states: a collection of reports of the International Scientific and Practical Conference dedicated to the 150th anniversary of the birth of the professor, the author of the method for calculating reinforced concrete structures by the stage of destruction, the founder of the Soviet scientific school of the theory of reinforced concrete, the founder and first head of the department of reinforced concrete structures of the Moscow Civil Engineering Institute (MISS) A.F. Loleita. M.: Publishing house MISSI-MGSU, pp. 346–350 (2018) (rus)
13. Golovin, N.G., Plotnikov, A.N.: Calculation of cross-ribbed floors taking into account physical nonlinearity. Concrete and reinforced concrete—a look into the future: scientific papers of the III All-Russian (II International) conference on concrete and reinforced concrete (Moscow, May 12–16, 2014): in 7 volumes. Vol. 1 ... Reinforced concrete theory. Reinforced concrete structures. Calculation and design. MGSU, Moscow, pp. 234–244 (2014) (rus)
14. Almazov, V.O., Klimov, A.N.: Comparison of the data of the monitoring system of high-rise buildings with the calculation in the program complex. Modern problems of calculation and design of reinforced concrete structures of multi-storey buildings: collection of articles report Int. scientific. conf., dedicated. To the 100th anniversary of the birth of P.F. Drozdov. Moscow: MGSU, pp. 38–44 (2013) (rus)
15. Kodysh, E.N., Nikitin, I.K., Trekin, N.N.: Calculation of reinforced concrete structures made of heavy concrete for strength, crack resistance and deformations: monograph. In: Kodysh, E.N., Nikitin, I.K., Trekin, N.N. M.: Publishing house of the Association of building universities, 352 p. (2010) (rus)
16. Drozdov, P.F.: Design and calculation of bearing systems of multi-storey buildings and their elements. M., Stroyizdat, 223 p. (1977) (rus)
17. Drozdov, P.F., Dodonov, M.I., et al.: Design and calculation of multistory civil buildings and their elements. M.: Stroyizdat, 351 p. (1986) (rus)
18. Plotnikov, A.N., Ivanova, N.V.: Shoulder of a pair of forces in the section of a reinforced concrete bending element at all stages of the stress state. In the collection: Modern issues of continuum mechanics—2019. Collection of articles based on the conference proceedings with international participation, pp. 52–60 (2019) (rus)
19. Plotnikov, A.N., Ivanov, M.Yu.: Monitoring system of high-rise buildings, determined from the nature of the curvature of the elastic line of vertical elements. *Constr. Sci. Educ.* **9**(4), 1–37 (2019) (rus)
20. Ivanov, M.Y., Plotnikov, A.N.: Monitoring system of high-rise buildings from the principle of minimizing the number of sensors. *Eng. Pers. Future Innov. Econ. Russ.* **5**, 25–28 (2019) (rus)



# The Issues of Reliability of Microclimate Creation Systems



N. G. Rusinova and N. A. Fedorov

One of the main systems for creating microclimate parameters is the ventilation system. The air-handling plant delivers air of a certain quality and quantity [1]. The quality of ventilation systems can be estimated by various groups of criteria [2]. With regard to engineering practice, a list of quality indicators is used, which forms three main groups of parameters. The first group comprises technical parameters, including system performance, efficiency of performance, and system resistance. The second group includes economic indicators and the level of energy efficiency. The third group is composed of functional parameters, namely the reliability of operation and characteristics of electrical, explosion, fire safety. The main functional parameter for an evaluation of the quality of the complex technical systems is their reliability. The reliability index permits an assessment of the system operation at any time after the start of its exploitation. The reliability of ventilation systems is a complex property, which in turn is characterized by such important indicators as the probability of failure-free operation, durability, maintainability, and persistence.

To calculate the reliability of systems in operation, the main reliability parameters are determined: the probability of failure-free operation, the failure rate, the probability of failure.

Two options are compared in the work. In the first version, a system with air-conditioning is considered, while in the second version, a ventilation system without cooling the supply air is.

To determine the reliability of ventilation systems, it is adopted that the system consists of series-connected elements (subsystems). The probability of failure-free operation is calculated as the product of the probabilities of individual elements (subsystems) by the formula (1):

$$P_{1-n} = P_1 \times P_2 \times P_2 \times P_3 \dots P_n \quad (1)$$

---

N. G. Rusinova (✉) · N. A. Fedorov  
Chuvash State University named after I. N. Ulyanov', Cheboksary, Russia

where

$P_{1-n}$  the probability of failure-free system of  $n$  elements;  
 $P_1, P_2 \dots P_n$  the probability of failure-free operation of  $i$ -th element.

The probability of failure-free operation of one element is calculated by the formula (2)

$$P = \exp(-\lambda t) \quad (2)$$

where

$\lambda$  the failure rate of  $i$ -th element;  
 $t$  the period of operation, for preliminary calculations 10,000 h are adopted.

The failure rate  $\lambda$  is taken from the reference literature [3]. In the systems, elements were taken into account according to the interrogatories, which are given by the customer.

The probability of failure ( $Q$ ) of individual elements and the system as a whole is calculated by the formula (3):

$$Q_{(i)} = 1 - P_{(i)} \quad (3)$$

The working draft (Version 1) for removing generated heat by the equipment of transformer substation at their load, taking into account the overload capability and the maximum design ambient temperature, establishes:

- supply and exhaust ventilation system ( $P1$ ) for Switchgear and control gear room No. 2 with low-voltage switchgear (cooler block is not provided in the description of the project document), with a total air flow rate on inflows of 15,270 m<sup>3</sup>/h, for the exhaust air of 6100 m<sup>3</sup>/h (with 100% load redundancy);
- supply and exhaust ventilation system ( $P2$ ) for room No. 3 of the FC zone, with a total air flow rate on inflows of 11,880 m<sup>3</sup>/h, for the exhaust air of 5940 m<sup>3</sup>/h (with 100% load redundancy).
- an autonomous precision air conditioner with the remote condenser for room No. 3, in the amount of 3 units, with the air power of 21,000 m<sup>3</sup>/h, an apparent refrigerating capacity of 83.2 kW of each air conditioner.

The supply and exhaust systems (rooms No. 2, No. 3) provide for an excess of inflow over the exhaust, to create a slight overpressure in the premises, taking into account the assimilation of excess heat from operating equipment and solar radiation, to ensure the temperature in the service area of electrical equipment (up to 2 m from the level floor), not exceeding a temperature of plus 35 °C. An autonomous precision

air conditioner with the remote condenser for room No. 3 is designed to maintain the temperature of the air not higher than the maximum permissible temperature according to the technical specifications for electrical equipment while operating in heat-stressed electrical rooms.

**Version 1.** The calculation of the reliability of the ventilation and air-conditioning system (Tables 1 and 2).

**Version 2.** The calculation of the reliability of the ventilation system (Tables 3 and 4).

**Table 1** The probability of failure-free operation for low-voltage switchgear and control gear room

No.	Element name	Failure rate $\lambda$ , 1/h	Probability of failure, $Q$	Probability of failure-free operation, $P$
Low-voltage switchgear and control gear room				
1	Inlet valve	0.0000034	0.03343	0.96657
2	Mechanical filter	0.0000003	0.003	0.997
3	Heater	0.0000007	0.00698	0.99302
4	Ventilator	0.0000024	0.02371	0.97629
5	Electric motor	0.00000524	0.05105	0.94895
6	Compressor	0.00001	0.09516	0.90484
7	Condenser	0.0000001	0.001	0.999
8	Evaporator	0.000015	0.13929	0.86071
9	Flow controller	0.00000355	0.03488	0.96512
110	Ventilator	0.0000024	0.02371	0.97629

**Table 2** The probability of failure-free operation of the system elements for the rooms with FC

No.	Element name	Failure rate $\lambda$ , 1/h	Probability of failure, $Q$	Probability of failure-free operation, $P$
The zone of FC				
1	Air valve	0.0000034	0.033428	0.966572
2	Air valve	0.0000034	0.033428	0.966572
3	Air valve	0.0000034	0.033428	0.966572
4	Mechanical filter	0.0000003	0.002996	0.997004
5	Heater	0.0000007	0.006976	0.993024
6	Ventilator	0.0000024	0.023714	0.976286
7	Electric motor	0.00000524	0.051051	0.948949
8	Ventilator	0.0000024	0.023714	0.976286
9	Electric motor	0.00000524	0.051051	0.948949
10	Air valve	0.0000034	0.033428	0.966572
11	Mechanical filter	0.0000003	0.002996	0.997004
12	Condenser	0.0000001	0.001	0.999
13	Compressor	0.00001	0.095163	0.904837
14	Evaporator	0.000015	0.139292	0.860708
15	Flow controller	0.00000355	0.034877	0.965123
16	Ventilator	0.0000024	0.023714	0.976286

**Table 3** The probability of failure-free operation of the system elements for low-voltage switchgear and control gear room

Low-voltage switchgear and control gear room				
No.	Element name	Failure rate $\lambda$ , 1/ч	Probability of failure, $Q$	Probability of failure-free operation, $P$
495-U-201A				
1	Inlet valve	0.0000034	0.03343	0.96657
2	Mechanical filter	0.0000003	0.003	0.997
3	Heater	0.0000007	0.00698	0.99302
4	Ventilator	0.0000024	0.02371	0.97629
5	Electric motor	0.00000524	0.05105	0.94895
495-KX-211A				
6	Inlet valve	0.0000034	0.03343	0.96657
7	Ventilator	0.0000024	0.02371	0.97629
8	Electric motor	0.00000524	0.05105	0.94895

**Table 4** The probability of failure-free operation of the system elements for the rooms with a FC

The zone of FC				
No.	Element name	Failure rate $\lambda$ , $1/\tau$	Probability of failure, $Q$	Probability of failure-free operation, $P$
495-U-203A, 495-U-204				
1	Air valve	0.0000034	0.03343	0.96657
2	Mechanical filter	0.0000003	0.003	0.997
3	Heater	0.0000007	0.00698	0.99302
4	Ventilator	0.0000024	0.02371	0.97629
5	Electric motor	0.00000524	0.05105	0.94895
6	Air valve	0.0000034	0.03343	0.96657
7	Mechanical filter	0.0000003	0.003	0.997
8	Heater	0.0000007	0.00698	0.99302
9	Ventilator	0.0000024	0.02371	0.97629
10	Electric motor	0.00000524	0.05105	0.94895
495-KX-212A				
11	Air valve	0.0000034	0.03343	0.96657
12	Ventilator	0.0000024	0.02371	0.97629
13	Electric motor	0.00000524	0.05105	0.94895

**Table 5** Indicators of reliability of the systems of versions No. 1 and No. 2

Name of the attended room	Version 1		Version 2	
	Probability of failure-free operation $P_1$	Probability of failure $Q_1$	Probability of failure-free operation $P_2$	Probability of failure $Q_2$
Low-voltage switchgear and control gear room	0.65	0.35	0.79	0.21
The zone of FC	0.54	0.46	0.70	0.3

The results of calculating the probability of failure-free operation and the probability of failure for two versions with a series connection of system elements are summarized in Table 5.

## Conclusion

1. Ventilation of the transformer rooms provides the dissipation of heat they emit in such quantities that under their load, taking into account the overload capacitance and the maximum design ambient temperature, the heating of the transformers does not exceed the permissible maximum. Ventilation of the transformer rooms is made in a way that the temperature difference between the air leaving the room and entering it does not exceed 15 °C.

The PES rules regulate the arrangement of the ventilation system, which corresponds to the design solution [2, p. 4.2.104].

2. The distribution of the air flow for the assimilation of excess apparent heat is carried out by the general ventilation system. In this case, air removal is performed with the upper zone, and the inflow is carried out into the lower zone, which meets the requirements [4].
3. According to TU [5], the air exchange for equipment is designed for the maximum allowable temperature plus 40 °C. According to the instructions, the temperature in the equipment zone is not more than plus 35 °C, the draft stipulated a temperature of 40 °C, which corresponds to the technical specifications for the operation of equipment [6].
4. The calculation of the excess heat gains for the assimilation in Low-voltage switchgear and control gear room of 50 kW, in a room with a FC of 120 kW [5], is made on the basis of not exceeding the permissible temperature inside the room at the maximum outside temperature plus 30 °C. The calculated air exchange, presented on sheet 2 of the graphic part of the Project, corresponds to the calculation method.
5. The designed ventilation system (hereinafter version No. 2) has a lower probability of failures in comparison with other possible combined systems providing heat removal from the substation equipment. The reliability of the systems functioning according to the indicator “Probability of failure-free operation” ( $P$ ) is higher for the systems of version No. 2. The reliability of the systems functioning in terms of the “Probability of failure” ( $Q$ ) is lower for the systems of version No. 2.

At the same time, the design of combined ventilation systems (with an air-conditioning system) with 100% redundancy requires large areas of support spaces. A preliminary assessment of the size of the cooling installations for removing heat from equipment at a given heat release for rooms No. 2 and No. 3 (hereinafter version No. 1, of combined ventilation system), showed insufficient areas of support spaces No. 1 and No. 4.

## References

1. Afanas'eva, D.: Optimizatsiya raboty ventilyatsionnoi ustanovki na baze kinoteatra Sinema 5 [Optimization of ventilation unit through cinema "Sinema 5"]. In: Afanas'eva, D., Markova, E., Rusinova, N.G., Shchennikova, T.V. (eds.) Nauchnye tendentsii: voprosy tochnykh i tekhnicheskikh nauk [Scientific trends: issues of science and technology]: sbornik nauchnykh trudov po materialam XIV mezhdunarodnoi nauchnoi konferentsii [Proceedings of the 14th International Scientific Conference], pp. 27–32. Saint Petersburg, February 12 (2018)
2. Ushakov, I.A.: Kurs teorii nadezhnosti system [The Course on the System Reliability Theory]. Drofa Publ., Moscow, 239 p (2008)
3. Polushkin, V.I., Anisimov, S.M., Vasil'ev, V.F., Deryugin, V.V.: Ventilyatsiya: ucheb. posobie dlya stud. vyssh. ucheb. zavedenii [Ventilation: A Reference Book for University Students], 416 p. Izdatel'skii tsentr "AkademiYA" Publ., Moscow (2008)
4. Kolpachkov, V.I., Yashchura, A.I.: Proizvodstvennaya ehkspluatatsiya, tekhnicheskoe obsluzhivanie i remont ehnergeticheskogo oborudovaniya [Operation, Maintenance and Repair of Electrical Equipment], 440 p. Rybinskiy Dom pechati Publ., Rybinsk (1999)
5. Shilyaev, M.I.: Tipovye primery rascheta sistem otopleniya, ventilyatsii i konditsionirovaniya vozdukha [Typical Examples of Heating, Ventilation and Air-Conditioning Systems Calculation] Shilyaev, M.I., Khromova, E.M., Doroshenko, Y.N. (eds.), 288 p. Tomsk, Tom. gos. arkhitekt.-stroitel'stvo Publ. (2012). ISBN 978-5-93057-478-4
6. Strakhova, N.A., Zhuravlev, V.P.: Nadezhnost' kak kriterii vybora sistem zashchity vozdukhnoy sredy [Reliability as a criterion for selecting air protection systems]. Izv. akad. prom. ehkologii [News of the Academy of Industrial Ecology], pp. 64–67. APEH Publ., Moscow, no.1 (1998)

**Geotechnics, Foundations, Construction  
Technology, Innovations in Construction  
Education**



# Tamped Slotted Foundations



Alexey Glushkov , Vyacheslav Glushkov , and Ilya Glushkov 

In modern conditions, there is a tendency to increase the loads on the soil foundations of buildings and structures [1–3]. In this case, one of the ways to increase the bearing capacity and reduce deformation of the base is to use tamped sleeper foundations. The joint deformation of the “tamped sleeper foundation—soil basis” system, taking into account the redistribution of efforts during the application of the load, has not been studied [4]. The absence of normative documents on the calculation of tamped sleeper foundations taking into account the formation of an “arch effect” in the soil foundation is noted [5–7].

Experimental studies of joint intermittent-sleeper foundations with a base were carried out by V. N. Golubkov and Yu. F. Tugaenko. As a result of the studies carried out, it was found that deformation zones are formed under the sole of the sleeper foundations [8, 9]. The volume  $V_a$  and depth  $H_a$  of the active deformation zone of the base under the sole of the sleeper foundations are less than under equivalent foundations with a solid base (Fig. 1) [10, 11].

To exclude the mutual adjacent sleepers foundations, optimal distances between individual sleepers have been established, a separate deformation zone is formed under each foundation (Fig. 1a). With an increase in the load, independent deformation zones are combined into a common deformation zone (Fig. 1b).

Improving the design of the sleeper foundation—giving it the shape of a tamped wedge, made it possible to significantly improve the conditions for joint operation of the tamped sleeper foundation with the base. A tamped pit is made in natural soil using a metal inventory punch, immersed in a percussion way using a diesel hammer. The tamped pits are located across the axis of the building with a step between the axes of adjacent sleeper foundations (Fig. 2).

---

A. Glushkov (✉) · V. Glushkov  
Volga State University of Technology, Panfilov str. 17, 424000 Yoshkar-Ola, Russia

I. Glushkov  
Perm National Research Polytechnic University, Perm, Russia

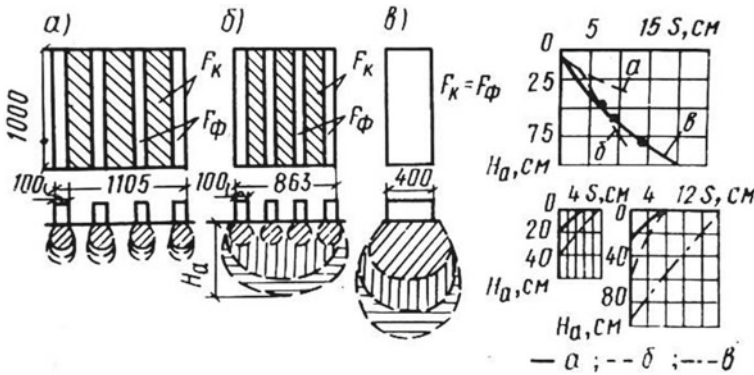


**Fig. 1** Experimental data on the development of deformation zones of the base with sleeper and solid foundations: **a** no mutual influence; **b** in the presence of mutual influence; **c** solid foundation

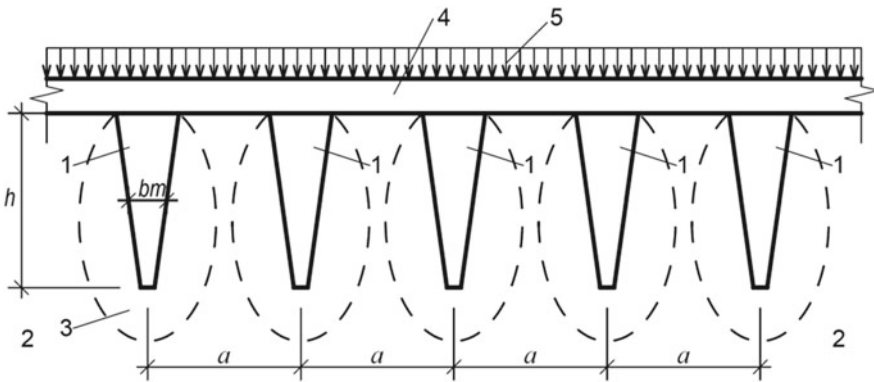


**Fig. 2** Strip tamped sleeper foundation: 1—tamped foundation, 2—soil basis, 3—compacted zone, 4—monolithic reinforced concrete grillage (rand-beam), 5—distributed load

In the design position, the tamped sleeper foundations work in the spacer according to the wedge principle [12].

When tamping the foundation pit, a compacted zone with increased strength and deformation characteristics is created around the side edges and the edge of the tamped foundation (Fig. 2).

The tamping process is accompanied by soil compaction with the formation of a compacted zone around the side walls and below the plane of the metal punch tip, associated with the creation of a new soil structure and a decrease in the value of the porosity coefficient  $e$ .

When the pit is tamped, a compacted zone is formed, having the shape of an ellipse, within which the density of the soil increases, the strength and deformation properties improve. The control of soil density at the base when constructing a shallow

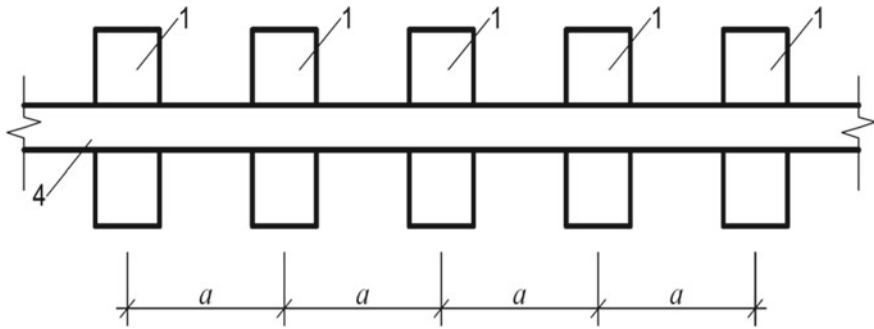


**Fig. 3** Strip tamped sleeper foundation (top view)

foundation is determined by the calculated resistance of the soil to the penetration of the micropenetrometer tip into it.

The thickness of the compacted layer under a separate foundation in a tamped pit is  $(1.6-2.2)b_m$  below the plane of the tip, the width of the compacted zone is  $(2.2-2.6)b_m$ , respectively, where  $b_m$  is the diameter of the tamped pit on average in depth section. The density of compacted soil at a depth of 20–30 cm from the bottom of the tamped pit is  $\rho_d = 1.70-1.75 \text{ g/cm}^3$  with a moisture degree of compacted soil  $S_r = 0.6-0.7$ , and  $\rho_d > 1.75 \text{ g/cm}^3$  at  $S_r < 0.6$ .

In the compacted massif, after tamping the pits at the base, the specific adhesion of the soil  $c$  increases by 5–7 times, the deformation modulus  $E_0$  increases by 2–5 times [13]. The depth at which the density of dry soil reaches a value usually equal to  $\rho_d = 1.60 \text{ g/cm}^3$  is taken as the lower boundary of the compacted zone.

After concreting the tamped pits along the axis of the building, a monolithic reinforced concrete grillage (rand-beam) is made, to which the load from the overlying structures of the building is transferred. Under the action of the load on the foundation, the load is transferred through the monolithic reinforced concrete grillage to the tamped sleeper foundation, first to the compacted area, and then to the soils of natural constitution (Figs. 2 and 3).

The tamped sleeper foundation works as follows. At step  $a > 3b_m$ , independent deformation zones develop at the base of the tamped sleeper foundation. Precipitation is due to the operation of a separate tamped foundation (Fig. 8). To optimize the value of  $a$  (the distance between the axes of tamped sleeper foundations), finite element calculations were performed using the Plaxis geotechnical complex (spatial elastoplastic problem) with simultaneous consideration of the strength and deformation properties of the foundation. The condition of the limit equilibrium of Mohr–Coulomb was taken as the condition of fluidity in solving the problem. The design scheme of the foundation took into account the formation of a compaction zone during tamping of the pit (Fig. 4).

The soil's own weight was taken into account in the form of initial stresses, the deformed state of the foundation was determined only from the external load on

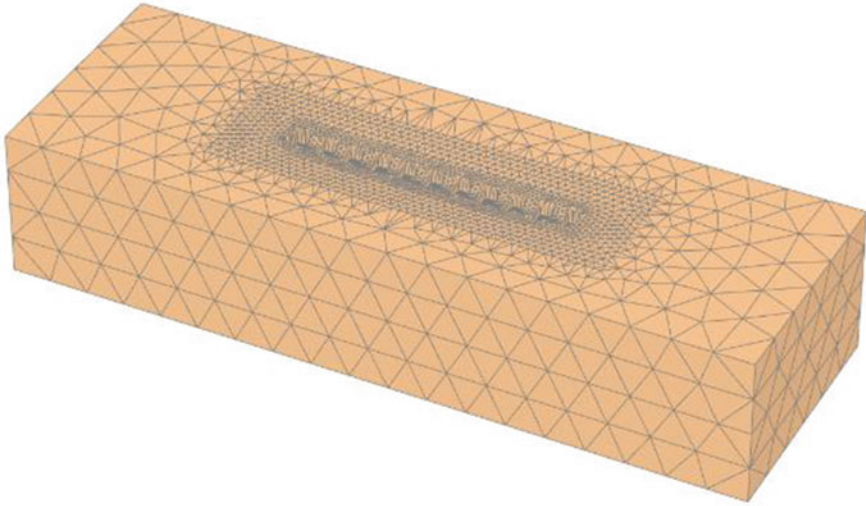


**Fig. 4** Design scheme of the finite element method (spatial elastoplastic problem)

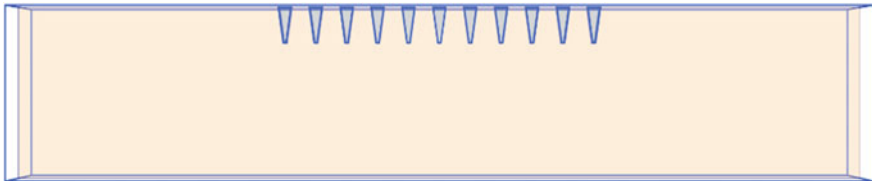


**Fig. 5** The interaction of the strip tamped sleeper foundation with base

the foundation. The calculated area of the base was taken as  $60.0 \times 20.0 \times 12.0$  m (Figs. 4 and 5) [14–16].

The results of theoretical studies of the bearing capacity of tamped sleeper foundations are shown in Figs. 6, 7 and 8.

In the design position, tamped sleeper foundations work in a thrust manner according to the principle of a wedge located at the base. In order to prevent deformation zones from affecting the settlement and bearing capacity of the foundation, an optimal pitch between the axes of individual foundations is proposed. With a small step  $a$ , mutually influencing deformation zones develop, leading to an increase in settlement and a decrease in the bearing capacity of the tamped sleeper foundation. With an increase in the step  $a > 3bm$ , the volume of the deformation zone is formed at the base of each tamped foundation, the mutual influence of the foundations decreases and the settlements decrease (Figs. 7 and 8) [17–21].

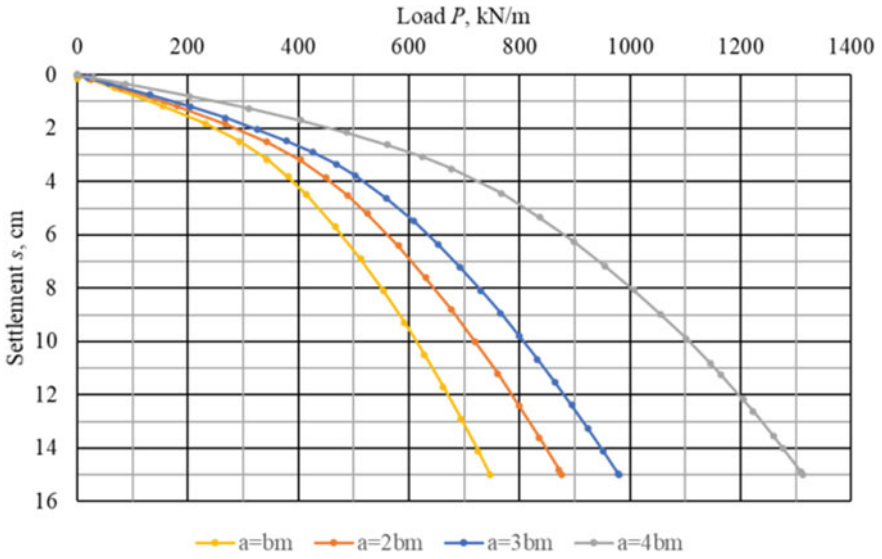


Fig. 6 Dependence of settlement on load  $s = f(P)$  of tamped sleeper foundation at step  $a = bm, a = 2bm, a = 3bm, a = 4bm$

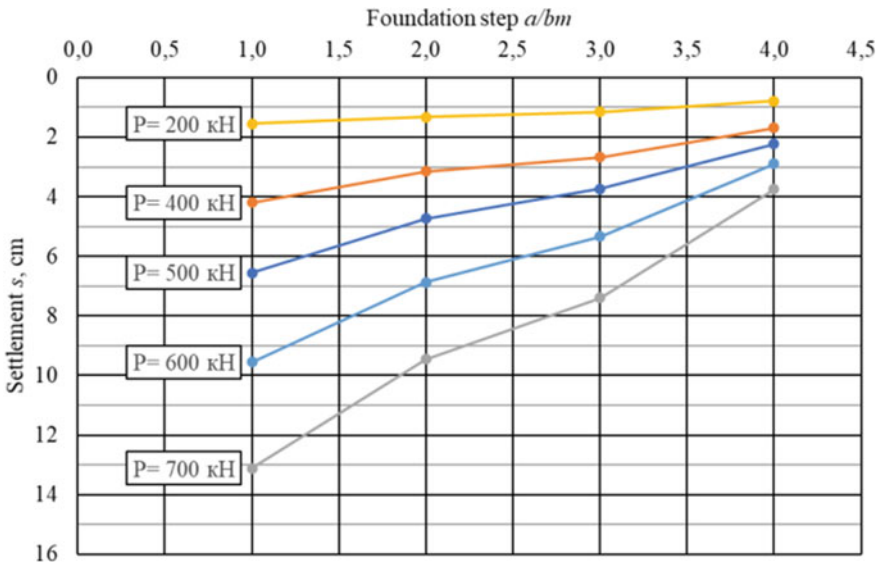
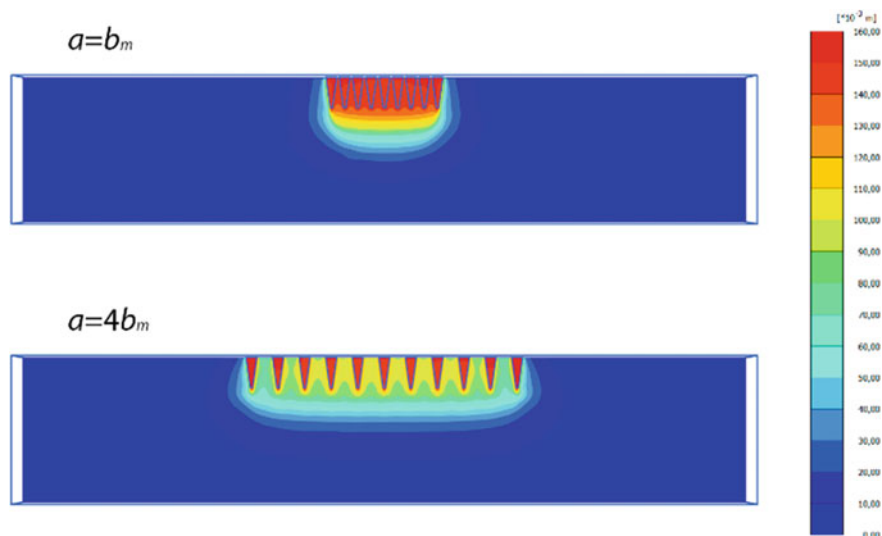


Fig. 7 Dependence settlements from step  $s = f(a/bm)$  of tamped sleeper foundation



**Fig. 8** Isolines of vertical displacements  $u_z$  at the base tamped sleeper foundation with  $a = bm$  and  $a = 4bm$

The use of tamped sleeper foundations makes it possible to reduce the material consumption of the zero cycle by 1.5–2.0 times, and to reduce the volume of excavation and formwork. The specific bearing capacity of foundations in tamped pits is 820–1100 kN/m<sup>3</sup>—significantly higher than traditional foundations.

The use of solutions of nonlinear soil mechanics makes it possible to assess the stress-strain state of the bases of tamped foundations in a wide range of load changes up to the limit. For practical application, an engineering method has been proposed that makes it possible to determine the optimal step of a tamped sleeper foundation, taking into account the strength and deformation properties of the soil.

## References

1. Bartolomey, A.A., Omelchak, I.M., Yushkov, B.S.: Principles of Pile Foundation Settlement Prediction. Stroyizdat, Moscow (1994)
2. Krutov, V.I., Sorochan, E.A., Kovalev, V.A.: Shallow Foundations (2009)
3. Mangushev, R.A., Gotman, A.L., Znamenskij, V.V., Ponomarev, A.B.: Piles and Pile Foundations. ASV, Moscow (2018)
4. Bartolomey, L., Glushkov, A., Glushkov, V.: Effective structures of tamped foundations of frame buildings. In: MATEC Web of Conferences (2016)
5. Code of rules 22.13330.2016. Soil bases of buildings and structures, Moscow
6. Code of rules 24.13330.2011. Pile foundations, Moscow
7. Sorochan, E.A.: Foundations of Industrial Buildings, Moscow (1986)
8. Golubkov, V.N., Tugaenko, Y.F., Kolesnikov, L.I., Kokorzchickij, K.M.: Sleeper and Wedge-Shaped Sleeper Scoring Foundations, Kiev (1976)

9. Golubkov, V.N.: *New Foundations in Odessa*, Odessa (1976)
10. Fidarov, M.I.: *Design and Construction of Intermittent Foundations*, Moscow (1986)
11. Kumara, J.J., Kimitoshi, H.: Deformation characteristics of fresh and fouled ballasts subjected to tamping maintenance. In: *Soils and Foundations*, pp. 652–663 (2016)
12. Verruijt, A.: *Offshore Soil Mechanics*. Delft University of Technology, Delft (2006)
13. Ponomaryov, A.B., Sazonova, S.A.: The use of express method for determining the modulus of deformation of fill soil. In: *Challenges and Innovations in Geotechnics—Proceedings of the 8th Asian Young Geotechnical Engineers Conference, 8AYGEC 2016* (CRC Press/Balkema, 2016), pp. 283–86 (2016)
14. Alfano, G., Crisfield, M.A.: Finite element interface models for the delamination analysis of laminated composites: mechanical and computational issues. In: *International Journal for Numerical Methods in Engineering*, pp. 1701–36 (2001)
15. Chou, Y.-C., Hsiung, Y.-M.: A normalized equation of axially loaded piles in elasto-plastic soil. *J. GeoEng.* **4**, 1–7 (2009)
16. Durcker, D.C., Prager, W.: Soil mechanics and plastic analysis or limit design. *Q. Appl. Math.* **2**, 157–65 (1952)
17. Mangushev, R.A., Boyarintsev, A.V., Rusetskiy, A.A.: Comparative calculation of the excavation pit enclosure types by the method of sheet pile walls and rigidity. In: *Bull. Civil Eng.* **1**, 75–82 (2018)
18. Ter-Martirosyan, A., Sidorov, V., Almakaeva, A.: Determining the interfaces parameters for geotechnical modelling. In: *E3S Web of Conferences*, EDP Sciences, (2019)
19. Vlasov, A.N., Volkov-Bogorodskij, D.B., Znamenskij, V.V., Mnushkin, M.G.: Finite element simulation of geomechanics and geophysics. In: *Vestnik Moscovskogo Gosudarstvennogo Stroitel'nogo Universiteta*, vol. 2, pp. 52–65 (2012)
20. Vlasov, A.N., Volkov-Bogorodskij, D.B., Znamenskij, V.V., Mnushkin, M.G.: Numerical simulation of construction of buildings with deep foundations in dense urban. *PNRPU Bull. Constr. Archit.* **2**, 170–79 (2014)
21. Tugaenko, Y.F., Kushchak, S.I.: Deformations in the bases of sleeper foundations. In: *Soil Mechanics and Foundation Engineering*, pp. 42–45 (1986)

# More About the Possibilities of the ERT Injection Piles



N. S. Sokolov 

The electro-discharge technology, having a number of technical and technological advantages [1–16], is widely used in geotechnical practice for the construction of EDT drilling piles in piling fields, piles for reinforcement of bases and foundations, fixing of foundations, slopes, when constructing nagels, etc. The technological advantage of this system is the explosive conversion of electrical energy into mechanical energy. The invention makes it possible to convert electrical energy into mechanical energy. The electro-hydraulic shock energy density reaches  $150 \text{ J/m}^3$  in a very short time (fraction of microseconds). The electro-hydraulic impact on the ground of the borehole wall filled with fine-grained concrete corresponds to a static load of up to 200.0 kPa. As a result of these high pressures and temperatures, a cavity is formed in the ground by gravitational forces, which are filled with fine-grained concrete. In this way there is an increase on a specific section on the height of the EDT-pile. This enlargement is further called «thrust bearing» [13–16]. In this way an additional support is created, which statically works together with the EDT-pile on the lower surface of the expansion and increases the load capacity of the EDT-pile on the ground. The geometrical parameters of the shape of the expansion in the first approximation can be taken as a sphere. The parameters of the sphere, such as diameter and height  $h$ , depend on electro-hydraulic impact energy, porosity, humidity and the type of soil to be treated. The diameter of the increase  $D$  can be determined by the size of the maximum decrease of the level of fine-grained concrete in the well, as geo-technics say, by «losses». It should be noted, of course, that the values of

---

N. S. Sokolov (✉)

Chuvash State University named after I.N. Ulyanov, prosp. Moskovsky, 15, Cheboksary 428015, Russian Federation

NPF FORST, ul. Kalinina, 109a, Cheboksary 428000, Russian Federation



«the losses» during electro-hydraulic treatment (that is why the level of fine-grained concrete should always be kept on the ground surface) and vary considerably over time. «The losses» in time before the start of concrete hardening can be from several cm to several meters. First of all, such large decreases are related to the specificity of the soil as a porous material. These vertical movements of fine concrete are further increased by electroosmotic absorption of cement milk into its soil structure.

It should be said that with the maximum intake of cement milk to the soil pores, the carrying capacity of the EDT-pile would be increased many times over by the strength of the soil mass, such as the specific adhesion and the angle of internal friction, to work with a matchmaker. However, this process is hindered by the fact that, when fine-grained concrete is mixed and electrohydraulically treated, it is magnetized, which contributes to the formation of cement colloids. At the same time, they are many times larger than soil pores. Unfortunately, there is no technology that prevents the lumping of cement milk. This is only possible by demagnetizing water bipolars in concrete.

Another aspect that needs to be addressed is the possible increase in carrying capacity of the bases reinforced by drilling piles. There was a consensus among designers that the larger the diameter of the drilling pile, the larger its carrying capacity in the ground. Yes, it is. In our opinion, the criterion for assessing the load capacity of the  $F_d$  on the ground should not be the diameter and length of the pile, but the «load capacity on the ground», i.e. the load capacity of one cubic metre of the drilling pile, as well as the «calculation unit load» i.e. the design load per cubic metre of the drilling pile. In this approach, by analyzing the results of the load-carrying capacity calculations for EDT welds and drilling piles of different diameters, it can be concluded that as the diameter of the drilling piles increases, the load-carrying capacity decreases, approaching some asymptote. At the same time, the most optimal by specific characteristics are «micropiles», i.e., EDT-piles made with electro-discharge technologies. This is illustrated by the calculations in Table 1 and Fig. 1.

**Table 1** The calculation of the best performance of piles

Nº	Pile type	Position	Effective load (kN)	Assumed load	Note	Pile volume (m <sup>3</sup> )	Specific load capacity (kN/m <sup>3</sup> )	Specific design load (kN/m <sup>3</sup> )	
1	2	3	4	5	6	7	8	9	
1	Bored pile Ø600 A = 0.28 m <sup>2</sup>	1	2330.0	1665.0	Uncased-pedestal pile	5.6	416.0	297.3	
		2	2300.0	1640.0		5.6	410.7	293.0	
		3	2465.0	1760.0		5.6	440.2	314.3	
2	Bored pile Ø800 A = 0.50 m <sup>2</sup>	1	3760.0	2685.0	Uncased-pedestal pile	10.0	376.0	268.5	
		2	3725.0	2660.0		10.0	372.5	266.0	
		3	3935.0	2810.0		10.0	393.5	281.0	
3	Bored pile Ø1000 A = 0.79 m <sup>2</sup>	1	5540.0	3960.0		15.7	352.9	252.2	
		2	5500.0	3930.0		15.7	350.3	250.3	
		3	5770.0	4120.0		15.7	367.5	263.4	
5	Bored pile Ø2000 A = 6.28 m <sup>2</sup>	1	19,400.0	13,860.0		Uncased-pedestal pile	125.6	154.4	110.3
		2	19,850.0	14,180.0			125.6	158.0	112.9
		3	19,860.0	14,200.0			125.6	158.2	113.0
6	Screw injection EDT-piles Ø350 A = 0.10 m <sup>2</sup>	4	1515.0	1080.0	EDT drilling pile without enlargement		2.0	757.5	540.0
		5	1680.0	1200.0	EDT drilling with enlarged toe base		2.0	840.0	600.0
		6	1880.0	1340.0	EDT drilling with enlarged toe base and along the pile shaft		2.0	940.0	670.0
		7	1930.0	1380.0	EDT drilling pile with enlarged toe base and two enlargement along the pile shaft		2.0	965.0	690.0

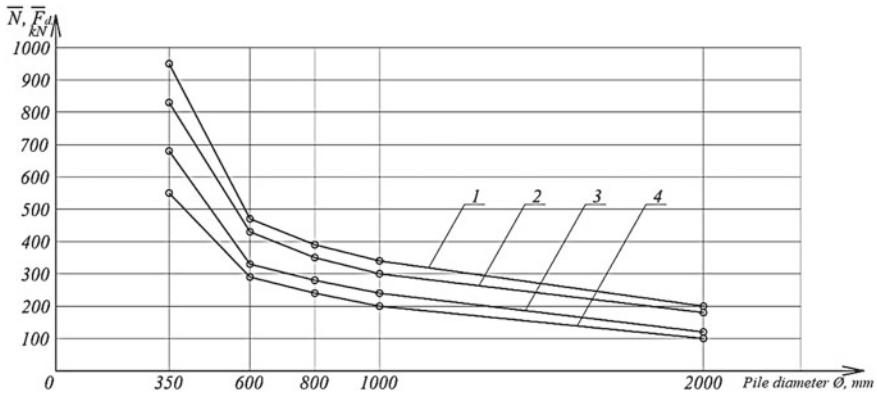


**Fig. 1** Dependency diagrams  $f(\phi, \bar{N})$  and  $f(\phi, \bar{F}_d)$ :  $\bar{F}_d$ —specific load capacity (kN);  $\bar{N}$ —specific design load (kN); 1, 2—diagrams  $f(\phi, \bar{F}_d)$ ; 3, 4—diagrams  $f(\phi, \bar{N})$ . Note 350—EDT-pile diameter (mm); 600, 800, 1000, 2000—diameter of drilling piles (mm)

## References

1. Cai, F., Ugai, K.: Numerical analysis of the stability of a slope reinforced with piles (2000). *Soils Found.* **40**, 73–84 (2011)
2. Hassiotis, S., Chamcau, J.L., Gunaratne, M.: Design method for stabilization of slopes with piles. *J. Geotech. Geoenviron. Eng. ASCE* **123**(4), 314–323 (1997)
3. Lee, J.H., Salgado, R.: Determination of pile base resistance in sands. *J. Geotech. Geoenviron. Eng.* **125**(8), 673–683 (1999)
4. Mandolini, A., Russo, G., Veggiani, C.: Pile foundations: experimental investigations, analysis and design. *Ground Eng.* **38**(9), 34–38 (2005)
5. Ilichev, V.A., Mangushev, R.A., Nikiforova, N.S.: Underground exploration experience. Experience of development of Russian Megacities Underground Space. *Soil Mech. Found. Eng.* **2**, 17–20 (2012)
6. Ulickij, V.M., Shashkin, A.G., Shashkin, K.G.: Geotechnical Support of Urban Development, p. 551. *Georeconstruction Publ.*, St. Petersburg (2010)
7. Ilichev, V.A., Konovalov, P.A., Nikiforova, N.S., Bulgakov, L.A.: Deformations of the retaining structures upon deep excavations in Moscow. In: *Proceedings of Fifth International Conference on Case Histories in Geotechnical Engineering*, pp. 5–24, April 3–17. New York (2004)
8. Ilichev, V.A., Nikiforova, N.S., Koreneva, E.B.: Computing the evaluation of deformations of the buildings located near deep foundation trenches. In: *Proceedings of the XVIth European Conference on Soil Mechanics and Geotechnical Engineering*. Madrid, Spain, 24–27th Sep 2007 «Geo-technical Engineering in urban Environments, vol. 2, pp. 581–585 (2007)
9. Nikiforova, N.S., Vnukov, D.A.: Geotechnical cut-off diaphragms for built-up area protection in urban underground development. The pros, of the 7th International Symposium on Geotechnical Aspects of Underground Construction in Soft Ground, 16–18 May 2011, tc28 IS Roma, AGI, 2011, № 157NIK (2011)
10. Nikiforova N.S., Vnukov D.A.: The use of cut off of different types as a protection measure for existing buildings at the nearby underground pipelines installation. *Proc. of Int. Geotech. Conf. dedicated to the Year of Russia in Kazakhstan*. Almaty, Kazakhstan, 23–25 September 2004. Pp. 338–342.
11. Petrukhin, V.P., Shuljatjev, O.A., Mozgacheva, O.A.: Effect of geotechnical work on settlement of surrounding buildings at underground construction. In: *Proceedings of the 13th European Conference on Soil Mechanics and Geotechnical Engineering*. Prague (2003)

12. Triantafyllidis, Th., Schafer, R.: Impact of diaphragm wall construction on the stress state in soft ground and serviceability of adjacent foundations. In: Proceedings of the 14th European Conference on Soil Mechanics and Geotechnical Engineering, pp. 683–688, Madrid, Spain, 22–27 Sep 2007
13. Sokolov, N.S.: Ground anchor produced by electric discharge technology, as reinforced concrete structure. Key Eng. Mater. Scopus. 76–81 (2018)
14. Sokolov, N.S.: Use of the piles of effective type in geotechnical construction. Key Eng. Mater. 70–74 (2018)
15. Sokolov, N.S.: One of geotechnological technologies for ensuring the stability of the boiler of the pit. Key Eng. Mater (Scopus). 56–69 (2018)
16. Sokolov, N.S.: Regulated injection pile-electric discharge technology with multiple pile enlargements posed as an underground reinforced concrete structure with a controlled load capacity. In: 18th International Multidisciplinary Scientific GeoConference SGEM 2018. Web of Science, pp. 601–608

# Optimum Type of Depth Constructions in Insulated Soils



N. S. Sokolov 

## 1 Introduction

The construction of structures on structurally unstable bases requires that designers, geotechnicians and builders take a special approach to the assignment of the type of deep construction. The most sought-after in modern geotechnical construction are piles submerged in ready-made soil or drilling piles [1–6]. Studies [7–15] have shown that they are best served by a specific load-bearing capacity of  $\bar{q}$ , which characterizes the load-bearing capacity of a pile per unit of volume:

$$\bar{q} = \frac{F_d}{V} \quad (1)$$

or a specific design load  $\bar{q}'$  describing the design load per unit volume:

$$\bar{q}' = \frac{N}{V} \quad (2)$$

According to this indicator, EDT drilling piles lead the whole line of drilling piles.

This article examines the case of the construction of multi-storey housing on the basis of first type slumping soil.

The engineering and geological structure of the construction site is characterized by the spread of the quaternary cover of various genesis (tIV, dII-IV, prIII, pdI-III) with a capacity up to 15.2 m on the Upper Permian sandstone-clay rocks of the Tatar stage (P3t). A summary of the engineering and geological section to the depth of 25.0 m (abs. el. 116.9 m) is given in Table 1.

---

N. S. Sokolov (✉)

Chuvash State University Named After I.N. Ulyanov, prosp. Moskovsky, 15, Cheboksary 428015, Russian Federation

OOO NPF FORST, ul. Kalinina, 109a, Cheboksary 428000, Russian Federation

**Table.1** Summary geotechnical cross-section to a depth of 25.0 m

Stratigraphic index	№ IGE	Description	Manner of occurrence	Thickness (m)
tIV	1	Man-made soils: brown, ground with soil and rare inclusion of building material (sand, rubble), semi-solid and refractory	Local	0.5–1.2
dIII-IV	2	The loam is heavy, brown, with an adhesion of aleuritic dust on cracks, with rare humus separations, mainly semi-solid, plots up to tight consistency	Areal	0.6–2.0
prIII	3	The loam is light, going into soup, brown, yellowish, macroscopic, filthy blurred, hard consistency	Areal	2.6–10.4
prIII	4	The loam is light, brown, yellowish brown, obscure layered, locally scattered, loosely scaled, preferably thick-faced, with patches up to soft-plastic	Local at the sites 1, 3	0.8–7.5
pdIII –III	5	The loam is light, greyish, grey, greenish, with nests of humus and cuttings, in the sole—often sandy, with the inclusion of crushed bedrock up to 5%, thick plastic consistency	Areal, in the soles of the forest swallows	1.1–5.3
P3t	6	The sand is polymictic, with a variety of grains: from dusty to medium size, green-grey, brown, tobacco-brown, clay, with thin layers of clay, aleurite, sandstone with a capacity of 5–20 cm, in degree of humidity—low-humidity, below GL—saturated with water	Areal	5.1–14.4
P3t	7	The clay is light, reddish-brown, red, aleuritic, sandy, less often gelatinous, permanganic on the cracks, mostly solid	Lensoid and sheetlike	Penetrated thickness 0.2–3.0

A detailed lithological description of the rocks is provided in the geological-lithological columns, and the deposit conditions in the geotechnical cross-section. Figure 1 shows a characteristic geotechnical cross-section.

The hydrogeological conditions of the area are characterized by the natural favourable conditions for drainage, which are facilitated by sufficient slopes of the surface for run-off and the adjacent sheep and beam network. This groundwater level (GL) does not affect the conditions of construction and exploitation. For the period of exploration (October 2017), the groundwater is located at a depth of between 16.8 and 22.6 m, in the range of 121.1–122.7 m. The aquifer is shallow. The GL is associated with the Upper Permian sandy formations of P2t. The steady state level is consistent with what's coming. The power of the horizon comes from infiltration of precipitation, and in the future from leaks from water-carrying communications. The unloading takes place generally to the north, towards the Volga River and the Shupashkarka River, as well as in the nearest ravines and beams adjacent to the site from the north-west and south, which are the right tributaries of

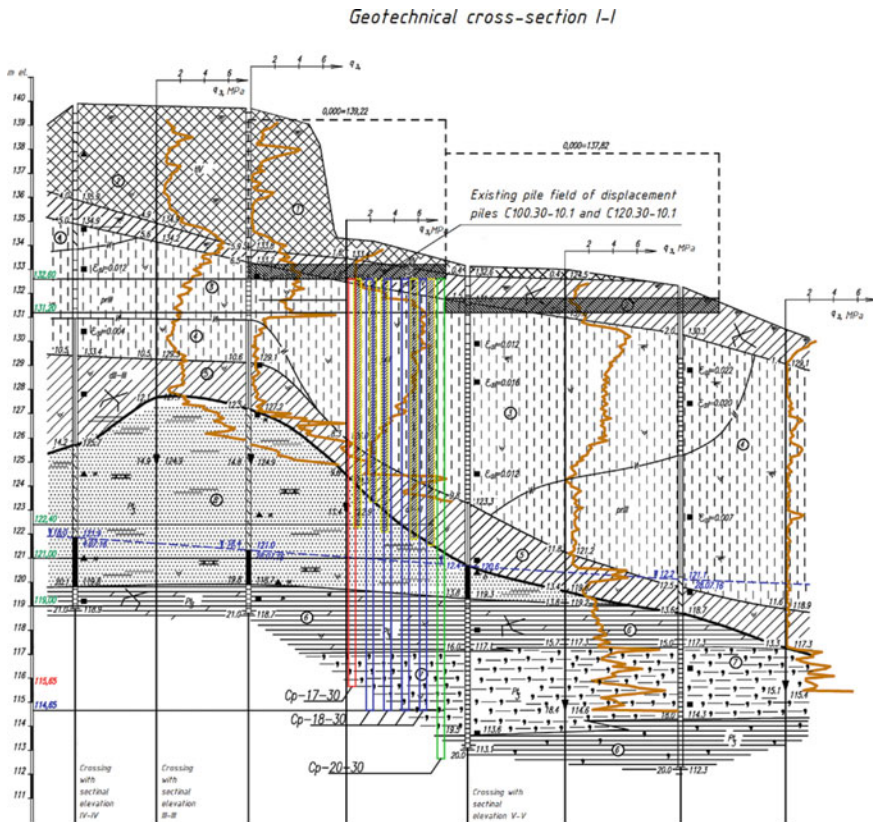


Fig. 1 Geotechnical cross-section with reference to screw injection piles

**Table.2** Specific resistance values ( $q_s$ , MPa) averaged for the selected EGE

№ EGE	Values $q_3$ (MPa)				Standard values for soil characteristics from the SP 11-105-97 «Engineering geological site investigations for construction»		
	Number of definitions	From	To	Characteristic	$E_0$ (MPa)	$c$ (kPa)	$\varphi$ (°)
2	91	0.1	2.4	0.9	6	17	19
3	471	0.5	8.8	3.0	21	23	21
4	195	0.1	3.0	0.7	5	14	16
5	149	0.4	4.1	1.4	10	19	20
6	338	3.1	19.5	8.6	24	–	32
7	167	1.1	8.3	2.6	18	38	19

the Shupashkarka River. In the future, after the development of a neighbourhood, the area is potentially flooded due to planned civil construction as well as the widespread use of welded foundations (barrage effect). Technological flooding will develop in the form of separate lenses and domes around emergency leaks from water-carrying communications. According to the site's geoenvironmental and lithological features and laboratory test data, 7 engineering geological elements (EGE) have been identified: EGE-1—man-made soil: semi-solid and refractory clay (tIV); EGE-2—loam heavy semi-solid and refractory (dIII-IV); EGE-3—loam light, converting to soup, forest-like, solid consistency (pr III); EGE-4—Loam light, forest-like, thick plastic, to soft-plastic (pr III); EGE-5—loam lightweight, tight (pdII-III); EGE-6—sand of mixed grain, medium density, mostly low density, in the sole—to saturated water (P3t); EGE-7—clay of light, aleuritic, with frequent interlayers and lenses (up to 0.1 m) of aleurite, mainly solid consistency (P3t). In order to clarify the boundaries of the EGE, to assess their spatial homogeneity, to obtain the initial data for the calculation of possible piling foundations, static sounding was performed at 9 points to a depth of up to 19.5 m. Specific resistance values ( $q_3$ , MPa) averaged for the selected EGE are given in Table 2.

## 2 Methods and Materials

The soil characteristics obtained from static soundings correspond to the natural condition at the time of exploration. In order to justify the optimum type of inbred structures, rounded piles C 15.30-10.1 with a length of 15 m (but their immersion tests with a length of more than 15 m do not reach design points) and drilling piles EDT CP-17-30, CP-18-30 and CP-20-30 are used. According to geotechnical calculations,



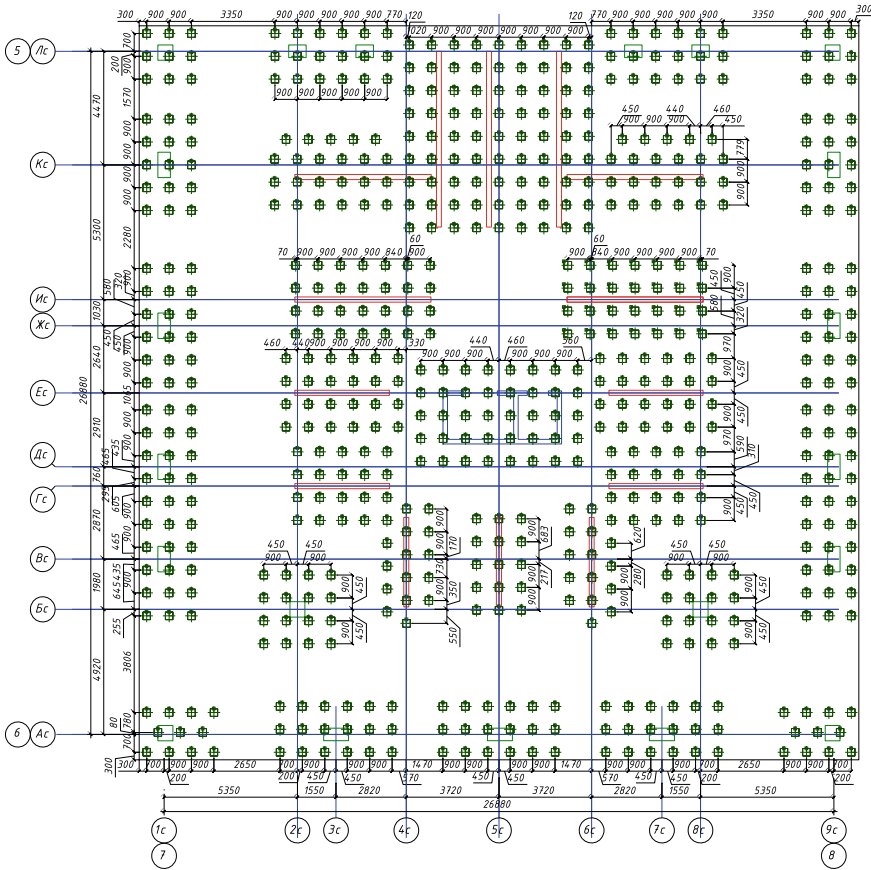
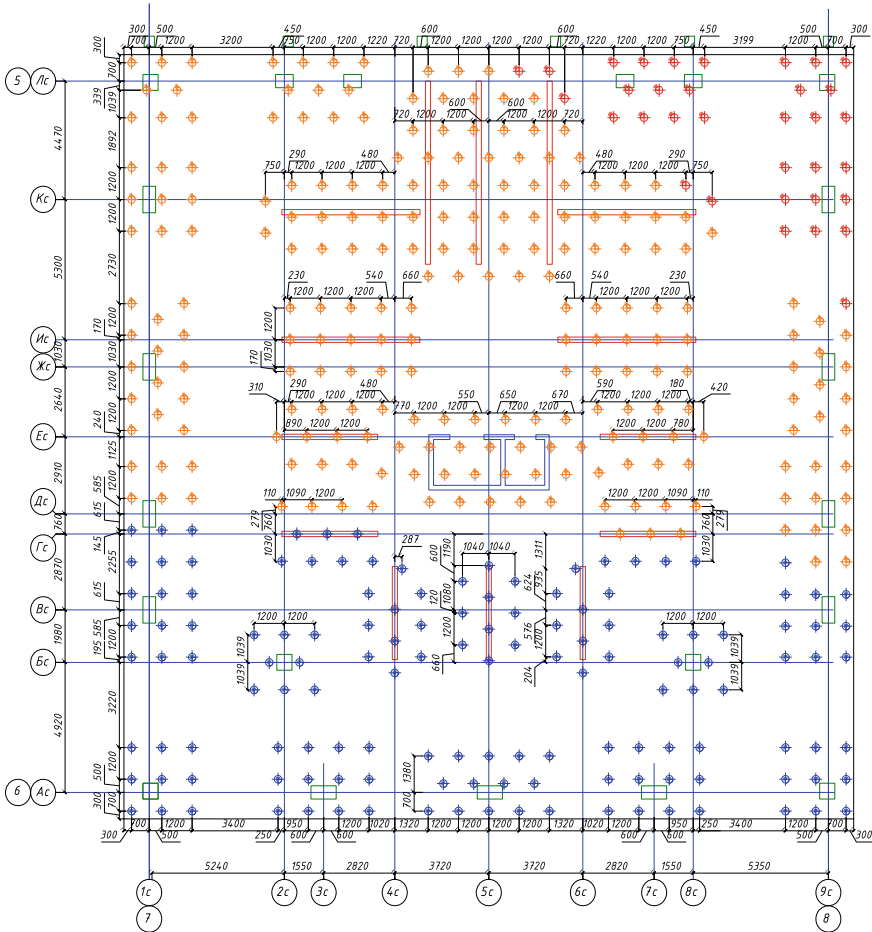


Fig. 2 Pile field of submersible piles C 15.30-10.1

644 piles are designed to be loaded with a total linear length of 9660.0 m (see Fig. 2) or 403 piles of EDT with a total linear length of 7120 m (see Fig. 3).

### 3 Results

According to techno-economic indicators, the cost of EDT piles was lower than the cost of piles. This is primarily due to the fact that both options have drilling activities. In the first variant, they are necessary for the installation of lead wells to facilitate the filling of piles, while in the second variant, drilling is a mandatory part of the production cycle. Therefore, the welding field from EDT drilling piles of length 17.0, 18.0 and 20.0 m has been accepted as a technically sound option and economically feasible option. At the facility the principle of interactive design «project—pilot



**Fig. 3** Welded field from EDT screw injection piles

site—real project» is used. Static tests have been carried out on two drilling pits for vertical compression load. The preparation of the foundation for the studies was carried out according to GOST 5686-2012 «Soils. Field test methods by piles» on the technology for the pre-soak soil around the test piles. It should be noted that in order to minimize negative friction and to increase the load capacity of piles, EDT pile № 101 is made with two extensions and pile № 25 with three extensions. In the studies [17–19] it is proved that the increase of the load-bearing capacity of the screw injection piles. Each contusion adds an increment of 20–30%.

The tests of two EDT piles № 101, 25 statically compressing increasing load were carried out according to GOST 5686-2012 «Soils. Field test methods by piles». The load stages were reported to the piles by the hydraulic jack IIC 200 Г160. The loading values were recorded by means of an exemplary gauge of 1000 kg/cm<sup>2</sup>

(105 kPa) at a cost of 20 kg/cm<sup>2</sup> (2000 kPa). Vertical movements of EDT screw injection piles were observed on two hourly-type indicators with an accuracy of 0.005 mm until the deformation was conditionally stabilized. The criterion for the conditional stabilization of deformation is the rate of precipitation of the pile on a given loading stage not exceeding 0.1 mm during the last observation hour. Based on the test results, the sediment is plotted according to load  $S = f(P)$  (see Fig. 4a, b), the sediment time curves for the individual load steps  $S = f(t)$ , and the test results tables.

The maximum resistance  $F_u$  from the vertical pressure load shall be taken as a load equal to or less than the precipitation determined by the formula:

$$S = \zeta \cdot S_{u,mt} \tag{3}$$

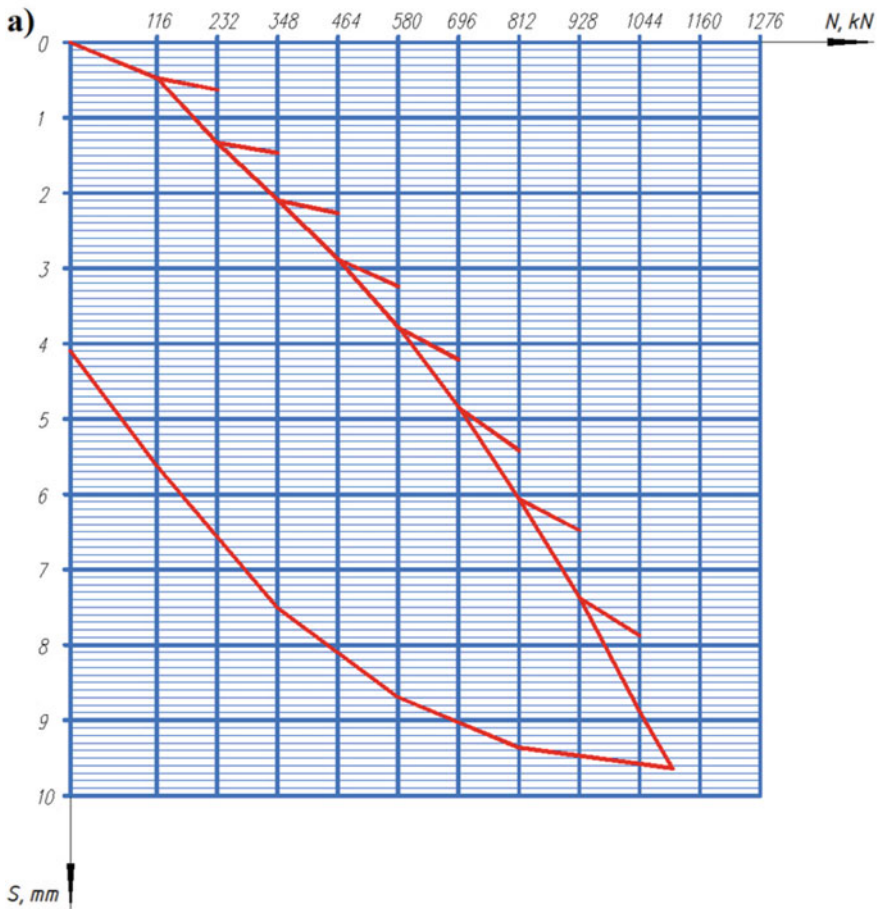


Fig. 4 Dependence diagrams of EDT pill settlement  $S$  to load  $N$ : **a** pile № 101; **b** pile № 25

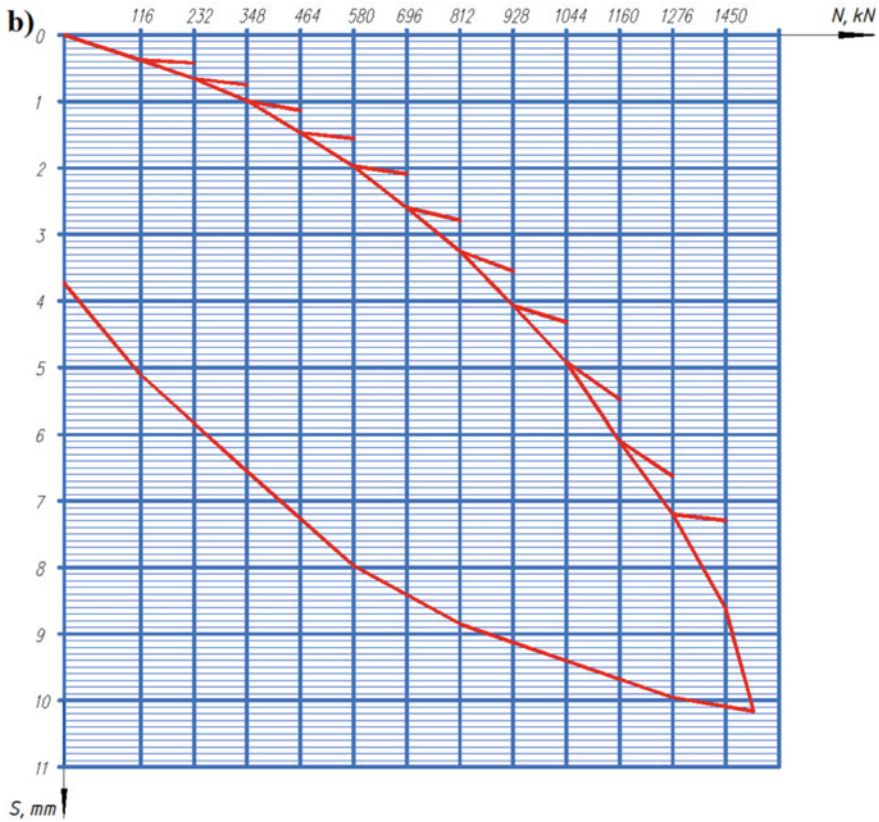


Fig. 4 (continued)

where  $S_{u,mt}$ —the limit value of the average sediment of the foundation of the planned building or building, set according to SP 22.3330.2011 «Soil bases of buildings and structures»;  $\zeta$ —the conversion factor from the limit value of the average sludge of the foundation of a building or structure  $S_{u,mt}$  to the sludge of a pile obtained in static tests with conditional stabilization (attenuation) of the draught equal to 0.2. In this case the design load on the pile should be determined by the formula:

$$N = \frac{F_d}{\gamma_k} \tag{4}$$

where  $\gamma_k$ —a safety factor of 1.2 in the static test of the piles on the vertical pressure load. Table 3 are the results of the research.

**Table.3** Results of studies on vertical depressing loads

Test pile	Name	Test pile № 101	Test pile № 25
Soils cut by piles		EGE-2 Loam Heavy Semi-solid Refractory EGE-3 Clay loaf is light Forestry, semi-solid consistency EGE-5 Loam lightweight, refractory EGE-8 Dust medium density sand EGE-6 Clay light aleuristic	EGE-2 Loam Heavy Semi-solid Refractory EGE-3 Clay loaf is light Forestry, semi-solid consistency EGE-5 Loam lightweight, refractory EGE-8 Dust medium density sand EGE-6 Clay light aleuristic
Soil under bottom end of pile		EGE-7 Alevrit clay, solid	EGE-7 Alevrit clay, solid
Research results	Maximum load (kN)	1044.0	1450.0
	Maximum load draught (mm)	9.640	10.16
	Load capacity (kN)	1044.0	1276.0
	Draught at load capacity (mm)	9.640	7.29
	Design load (kN)	870.0	1063.0
Design test load (kN)		900.0	900.0
Assumed load (kN)		600.0	600.0
% increase in load capacity $F_d$		45%	77%
Number of contusions along the pile shaft		2	3

## 4 Conclusion

In the difficult engineering geological conditions under consideration, in the presence of first type slumping soil, based on the cost-effective comparison of the two types of deep construction proved to be the most efficient EDT screw injection piles with multi-site extensions.

## References

1. Ilyichev, V.A., Mangushev, R.A., Nikiforova, N.S.: Experience of the development of the underground space of Russian megacities. *Soil Mech. Foundation Eng.* **2**, 17–20 (2012)
2. Ulitsky, V.M., Shashkin, A.G., Shashkin, K.G.: *Geotechnical support for urban development*. Sp.: Georeconstruction, p. 551 (2010)
3. Razpazovsky, D.E., Chepurnova, A.A.: Evaluation of the influence of the reinforcement of the foundations of buildings by the technology of jet cement on their draught. *Ind. Civil Eng.* **10**, 64–72 (2016)

4. Cai, F., Ugai, K.: Numerical analysis of the stability of a slope reinforced with piles (2000). *Soils Found.* **40**(1), 73–84 (2000)
5. Hassiotis, S., Chamcau, J.L., Gunaratne, M.: Design method for stabilization of slopes with piles. *J. Geotech. Geoenviron. Eng. ASCE* **123**(4), 314–323 (1997)
6. Lee, J.H., Salgado, R.: Deterrivation of pile base resistance in sands. *J. Geotech. Geoenviron. Eng.* **125**(8), 673–683 (1999)
7. Mandolini, A., Russo, G., Veggiani, C.: Pile foundations: experimental investigations, analysis and design. *Ground Eng.* **38**(9), 34–38 (2005)
8. Ilichev, V.A., Kononov, P.A., Nikiforova, N.S., Bulgakov, L.A.: Deformations of the retaining structures upon deep excavations in Moscow. In: *Proceedings of Fifth International Conference on Case Histories in Geotechnical Engineering*, 3–17 April. New York, pp. 5–24 (2004)
9. Ilyichev, V.A., Nikiforova, N.S., Koreneva, E.B.: Computing the evaluation of deformations of the buildings located near deep foundation trenches. In: *Proceedings of the XVth European Conference on Soil Mechanics and Geotechnical Engineering*. Madrid, Spain, 24–27th Sep 2007 «Geo-technical Engineering in urban Environments», vol. 2, pp. 581–585 (2007)
10. Nikiforova, N.S., Vnukov, D.A.: Geotechnical cut-off diaphragms for built-up area protection in urban underground development. In: *The Proceedings of the 7th International Symposium on Geotechnical Aspects of Underground Construction in Soft Ground*, 16–18 May 2011, tc28 IS Roma, AGI, 2011, № 157NIK (2011)
11. Nikiforova, N.S., Vnukov, D.A.: The use of cut off of different types as a protection measure for existing buildings at the nearby underground pipelines installation. In: *Proceedings of International Geotechnical Conference Dedicated to the Year of Russia in Kazakhstan*. Almaty, Kazakhstan, 23–25 Sep 2004, pp. 338–342
12. Petrukhin, V.P., Shuljatjev, O.A., Mozgacheva, O.A.: Effect of geotechnical work on settlement of surrounding buildings at underground construction. In: *Proceedings of the 13th European Conference on Soil Mechanics and Geotechnical Engineering*. Prague (2003)
13. Triantafyllidis, Th., Schafer, R.: Impact of diaphragm wall construction on the stress state in soft ground and serviceability of adjacent foundations. In: *Proceedings of the 14th European Conference on Soil Mechanics and Geotechnical Engineering*, Madrid, Spain, 22–27 Sep 2007, pp. 683–688
14. Ulitsky, V.M., Shashkin, A.G., Shashkin, K.G.: *Geotechnical Guide (guide to bases, foundations and underground structures)*. SPb., p. 284 (2012)
15. Sokolov, N.S.: One of the geotechnical technologies to strengthen the foundation base in constraint environment in the addition of 4 floors. In: *18th International Multidisciplinary Scientific GeoConference SGEM 2018*, pp. 513–522. Web of Science
16. Sokolov, N.S.: Ground anchor produced by electric discharge technology, as reinforced concrete structure. *Key Engineering Materials*. Scopus, pp. 76–81 (2018)
17. Sokolov, N.S.: Use of the piles of effective type in geotechnical construction. *Key Engineering Materials*, pp. 70–74 (2018)
18. Sokolov, N.S.: One of geotechnological technologies for ensuring the stability of the boiler of the pit. *Key Engineering Materials (Scopus)*, pp. 56–69 (2018)
19. Sokolov, N.S.: One of the approaches to the problem of increasing the load capacity of drilling piles. *Build. Mater.* **5**, 44–47 (2018)

# Optimum Type of Depth Reinforced Concrete Structures When Strengthening the Foundation of Industrial Buildings



Nikolay Sergeevich Sokolov , Svetlana Stanislavovna Viktorova , Galina Nikolaevna Alekseeva , Olga Pavlovna Terekhova , Lydia Ivanovna Malyanova , and Victor Vladimirovich Maguskin 

## 1 Introduction

Ensuring conditions for accident-free buildings management is fundamental to all phases of construction and operation. This is especially true for buildings under renovation as well as for buildings expected to increase the load above the design values.

Below we will consider the first example of strengthening the foundation base of a single-storey production building for the manufacture of passenger cars. The reconstructed building consists of a single-storey frame structure with reinforced concrete monolithic post footing, prefabricated reinforced concrete columns, and prefabricated building farms with spans of 24.0 m and 18.0 m. The production building has dimensions in plan (see Fig. 1a) in the axles  $\Gamma/\mathcal{K}$  and 3–23 of  $66.0 \times 120.0$  m with two bays of 24.0 m and one bay of 18.0 m. The bay between the columns along the alphabetical axes is 12.0 m. Two bridge cranes are operated in each bay. There are two cranes of 500 kN in bays  $\Gamma/\mathcal{A}$  and  $\mathcal{A}/E$ , and two cranes of 200 kN in bay  $E/\mathcal{K}$ .

## 2 Material and Research Methods

The problems with the building maintenance began in 2000. Distortions of craneways have been detected at the most unfavourable combinations of crane loads. The oscillations have cyclic pattern, i.e. the deformations are alternating in sign. High-precision geodetic observations of the foundation settlements of reinforced concrete columns confirmed high values of irregular deformations of up to 150 mm. The operation of

---

N. S. Sokolov (✉) · S. S. Viktorova · G. N. Alekseeva · O. P. Terekhova · L. I. Malyanova · V. V. Maguskin  
Chuvash State University named after I.N. Ulyanov (ChuvSU), 15 Moskovskiy Prospekt, Cheboksary 428015, Russian Federation

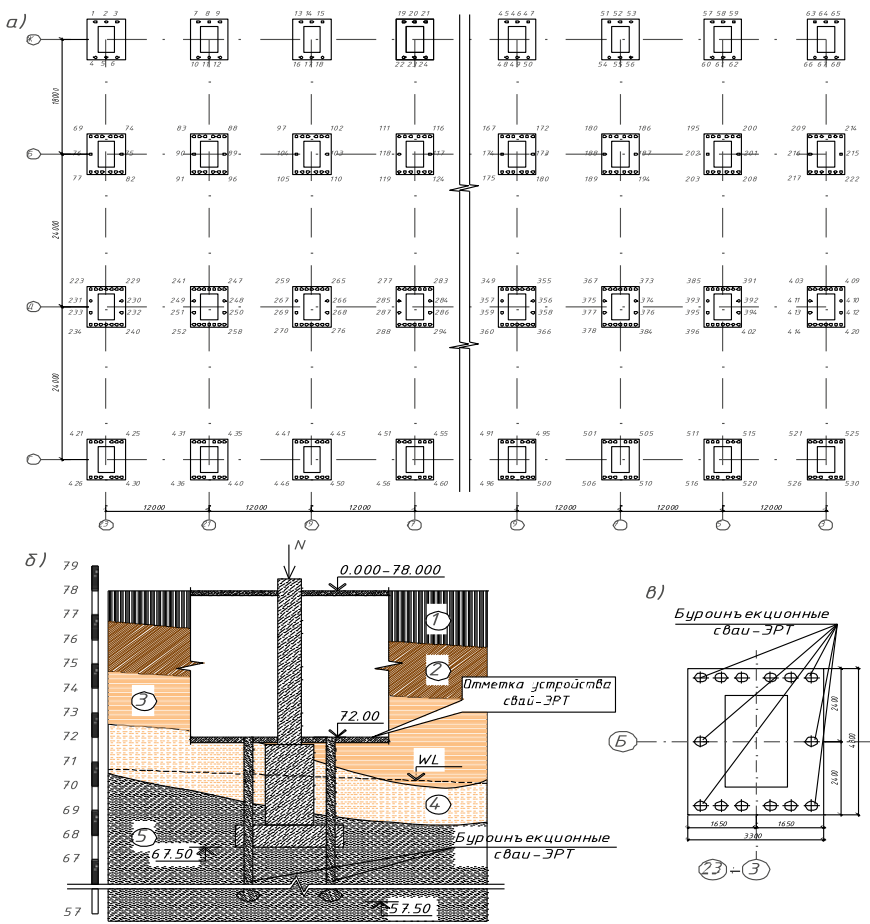


**Fig. 1** a EDT root piles plan; b basement section in the D/12 axes with reference to the geotechnical cross-section; c underpinning EDT root piles plan in axes B/5; 1—ground fill; 2—semi-hard loam; 3—sandy loam; 4—hard clay; 5—water-saturated fine sand

the cranes has become difficult at the sites with the highest differential foundation settlement.

This created a pre-emergency situation when the continued operation of the building became dangerous.

The Technical Commission headed by the chief architect of the plant is charged with urgently developing measures to prevent the pre-emergency situation on the site. It asked to the authors of this article ООО НПФ «ФОРСТ» (Research and Production Company FORST, LLC) to identify the causes of deformation and to work out measures to restore the operational reliability of the problematic production building.



It was decided to strengthen the foundation base with root piles, which are made according to the electric discharge technologies (EDT root piles) [1–6] with simultaneous geotechnical monitoring.

The geotechnical cross-section is represented from the surface by filled soil with a capacity of up to 2.0 m which clayey sand consistency of up to 5.5 m thickness is obtained below. A solid clay with a capacity of up to 2 m is then deposited. The underlying layer is a water-saturated medium-density fine sand.

An analysis of the geotechnical conditions suggested that the main cause of the foundation deformation was thixotropy of the carrier layer (the ability of the ground to dilute by mechanical action and to increase the viscosity while at rest). The sands are affected by this process. Mechanical effects are expressed as dynamic loads from bridge cranes, they usually operate unevenly. For example, when cranes are applied to the base on a specific axis, a dilution area emerges at that location, and on other axles where no crane loads are involved, the base is operated without an emergency.

Thus the foundations for the columns «sink» in turn, increasing the crests of the frame, which exacerbates the exploitation of the cranes. Once the dynamic action has ceased, the deformations of the foundations cease.

According to the instruction of the commission ООО НПФ «ФОРСТ» (Research and Production Company FORST, LLC) has developed a project to strengthen the foundation base with the help of EDT root piles. The piles of a diameter of 200 mm and a length of 12.0 m penetrate the lower stage of the post footing. The carrier layer of the pile bulb end is the water-saturated fine sand. The number of EDT root piles under different foundations is various. So there are 6 pieces on the axle «Ж», 14 pieces on the axle «Е», 18 pieces on the axle «Д», and 10 pieces on the axle «Г» (Fig. 1a). Figure 1b shows a geotechnical cross-section with a vertical snap of the foundations, and Fig. 1c shows a fragment of the underpinning EDT root piles plan.

The delivery of output to strengthen the foundations with the help of EDT root piles has made it possible for the bridge crane and the entire reinforced concrete frame of the press corps to function smoothly.

Geotechnical monitoring of the base deformation of the foundations confirmed their absence after completion of the EDT root piles work.

A second example of the successful use of EDT root piles is the accident of the emergency of the forge-stamping shop (FSS) in the Cheboksary Aggregate Plant. Due to the effect of dynamic loads from 10 forge hammers the building was in a state of emergency. Strain cracks appeared on all the brick walls of the fence and tended to increase. The resulting irregular deformation of the framework led to faulty operation of the bridge cranes. In addition, the bearing surface size of the slabs as well as of the building farms and crane rail has been reduced to close to the emergency in some cases. In order to prevent an emergency situation the emergency commission under the capital construction management of the plant entrusted the ООО НПФ «ФОРСТ» (Research and Production Company FORST, LLC) with the development of emergency measures including: (1) survey of the technical condition of the emergency building; (2) development of measures to minimize the negative impact of vibrations caused by the impact of forge hammers on the workshop building

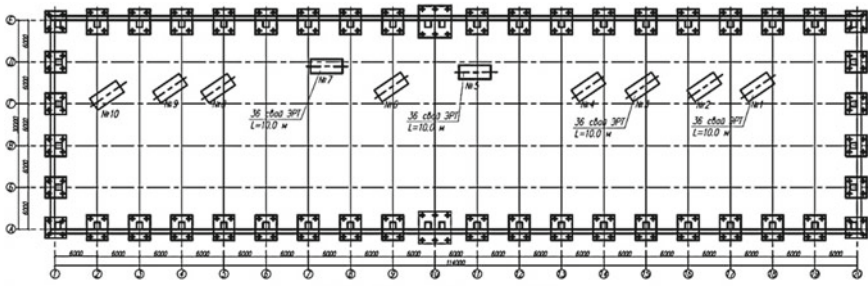


Рис. 4 План свайного поля из брызговичных свай ЗПТ

Fig. 2 Underpinning EDT root piles plan strengthening the bases of the foundations of the frame and the forge hammers 1, 3, 5, 7

and the adjacent buildings; (3) work to restore the operational safety of the FSS building.

The most rational and acceptable structure for strengthening the base of the foundations was adopted and used the EDT root pile, which is made according to the electric discharge technology. EDT pile has a number of advantages over root piles without compaction of well walls and auger piles including elevated load capacity values of approximately 1.5 to 1.8 times both on the ground and on the foundation body which presupposes the compact placement of them in the body of the reinforced foundation.

The emergency management plan includes strengthening the foundations of the frame and the 1, 3 forge hammers with the mass of the impact parts  $Q = 30$  kN and 5, 7 with the mass of the impact parts  $Q = 50$  kN. Figure 2 contains a plan to strengthen the foundations of the frame of the forge-stamping shop building and the hammers 1, 3, 5, 7.

The building of the forge-stamping shop in the Cheboksary Aggregate Plant with a frame structure has dimensions in plan in axles (A/E)/(1/20) – 30.0 × 114.0 m. The foundations of the building are monolithic reinforced concrete with a depth of 2.5 m. Columns are reinforced concrete two-member columns. Ceiling slab is reinforced concrete ribbed slabs on steel building farms. There are ten forge hammers in the workshop.

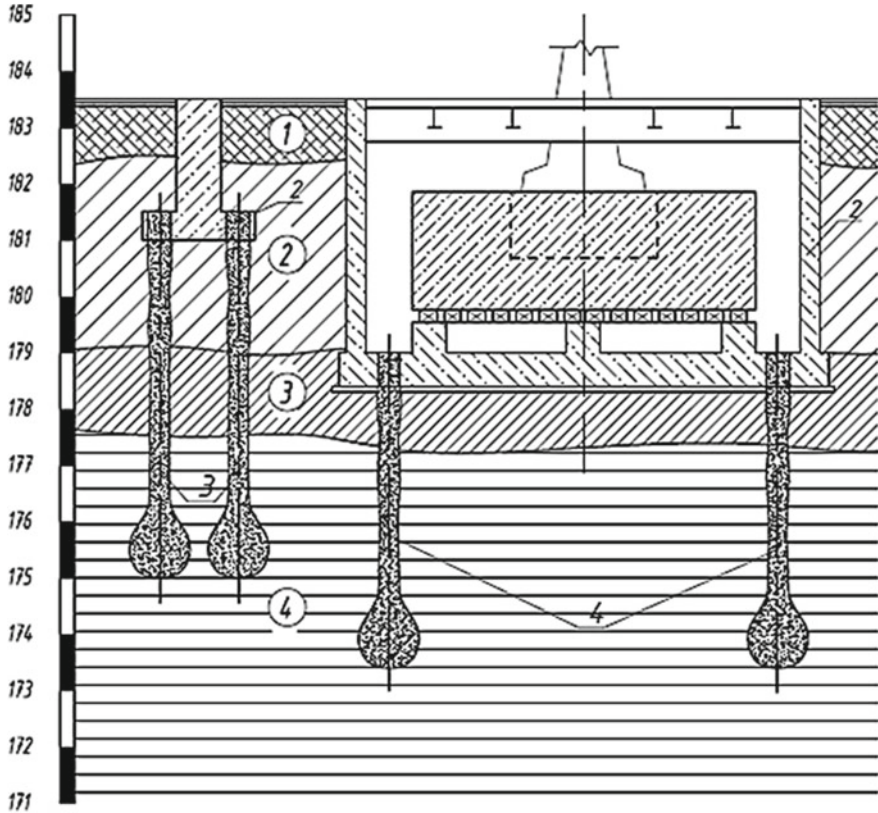
The geotechnical conditions of the construction site are represented from the surface by saturated soil with a capacity of up to 2.0 m, below there is a stiff loam capacity of 3.0–3.5 m. There is a soft-plastic loam below under which the stiff silty clay is found.

Table 1 shows the mechanical and physical properties of soils, and Fig. 3 shows the geotechnical cross-section with vertical anchoring of the foundations of the reinforced concrete frame of the building and the forge hammer 3.

The production of works on reinforcement of framework and hammers foundations was carried out by ООО НПП «ФОРСТ» (Research and Production Company FORST, LLC). Geotechnical monitoring was carried out during the period of the reconstruction and after the year.

**Table 1** Mechanical and physical properties of the soils

Layer number	Specific gravity, $\gamma$ (kN/m <sup>3</sup> )	Liquidity index, $I_L$ , fr. unit	Angle of internal friction, $\varphi$ (°)	Cohesion intercept, $C$ (kPa)	Total strain modulus, $E_0$ (kPa)
1	$R_0 = 100$ kPa				
2	18.5	0.45	27	40	6500
3	19.01	0.58	20	15	5400
4	21.0	0.15	32	45	12,500



**Fig. 3** The geotechnical cross-section: 1—frame building foundation; 2—forge hammer foundation; 3—EDT root piles strengthening the bases of the foundations of the frame; 4—EDT root piles strengthening the bases of the foundations of the forge hammers; The soil layer: 1—ground fill; 2—stiff loam; 3—soft-plastic loam; 4—stiff silty clay

In addition, research on the dynamic effect of the forge hammers on the base was organized [7].

The measurements were carried out in February 2002 in the hammer-room of the Cheboksary Aggregate Plant. Oscillations were recorded at hammers 1, 3, 5, 7 and 6 in axes 12–13. In addition, in some cases, the hammers 2, 4, 10 worked, which did not lead to significant changes at the measuring points. The choice of exposure sources and measuring points was determined by their proximity to the installation of a new hammer in the axes 16–17.

The research [7] confirmed that the EDT root piling field meets the requirements of p. 1.21 SNiP 2.02.05-87 «Dynamic Machinery». The static pressure under the sole of the conditional columns foundation is 240 kPa, which is less than the calculated resistance of the base ground of the 330 kPa. This indicates the permissibility of the existing vibrations in terms of the formation of additional sediments in the columns foundations.

Thus, the reinforcement of the foundations bases of the frame and forge hammers with the EDT root piles made it possible to eliminate the emergency situation of the forge-stamping shop building.

### 3 Conclusion

The article gives two successful examples of the use of EDM root piles to prevent critical (pre-accident) conditions in the structure of buildings. The use of EDT root piles strengthening the bases of the foundations has extended the lifespan of these buildings to avoid accidental operational conditions.

### References

1. Sokolov, N.S., Tavrín, V.Y., Abramushkin, V.A.: Patent of invention RU 2318961 C2. Discharge device for cast-in-place pile production. The Federal Service for Intellectual Property, Patents and Trademarks. The Official Bulletin no. 7 (2008)
2. Sokolov, N.S., Ryabinov, V.M., Tavrín, V.Y., Abramushkin, V.A.: Patent of invention RU 2318960 C2. Method for cast-in-place pile erection. The Federal Service for Intellectual Property, Patents and Trademarks. The Official Bulletin no. 7 (2008)
3. Sokolov, N.S., Tavrín, V.Y., Abramushkin, V.A.: Patent of invention RU 2250958 C2. Device for cast-in-place pile forming. The Federal Service for Intellectual Property, Patents and Trademarks. The Official Bulletin no. 12 (2005)
4. Sokolov, N.S., Tavrín, V.Y., Abramushkin, V.A.: Patent of invention RU 2250957 C2. Cast-in-place pile forming method. The Federal Service for Intellectual Property, Patents and Trademarks. The Official Bulletin no. 12 (2005)
5. Sokolov, N.S., Pichugin, Y.P.: Patent of invention RU 2282936 C1. Impulse currents generator. The Federal Service for Intellectual Property, Patents and Trademarks. Bulletin no. 24 (2006)
6. Sokolov, N.S., Jantimirov, H.A., Kuzmin, M.V., Sokolov, S.N., Sokolov, A.N.: Patent for useful model RU 161650 U1. Device for camouflage extensions of a stuffed structure in the ground.

- The Federal Service for Intellectual Property, Patents and Trademarks. The Official Bulletin no. 12 (2016)
7. Conclusion «Instrumental inspection of the FSS building and forecasting the vibrations of the projected foundation for a forging hammer 17KIII 5 t/s» at the Cheboksary Aggregate Plant». Research Institute of Foundations and Underground Structures. Moscow (2002)
  8. Sokolov, N.S., Ryabinov, V.M.: The method of calculation of the bearing capability the root piles. *Soil Mech. Found. Eng.* **1**, 10–13 (2005)
  9. Sokolov, N.S.: Metod of calculation the bearing capability the root piles taking into account «thrust bearings». Materials of the 8th All-Russian (the 2nd International) Conference on New in Architecture, Designing Construction and Renovation» (NADCR-2014), pp. 407–411. Cheboksary (2014) (In Russian)
  10. Sokolov, N.S., Viktorova, S.S., Fedorova, T.G.: Piles of the raised bearing capability. Materials of the 8th All-Russian (the 2nd International) Conference on New in Architecture, Designing Construction And Renovation» (NADCR-2014), pp. 411–415. Cheboksary (2014) (In Russian)
  11. Sokolov, N.S., Petrov, M.V., Ivanov, V.A.: Problems in calculating root piles made using electric discharge pile technology. Materials of the 8th All-Russian (The 2nd International) Conference on New in Architecture, Designing Construction and Renovation» (NADCR-2014), pp. 415–420. Cheboksary (2014) (In Russian)
  12. Sokolov, N.S., Sokolov, S.N., Sokolov, A.N.: Experience of the restoration of the damaged building of the Vvedenskiy Cathedral. *Cheboksary. Geotech.* **1**, 60–65 (2006)
  13. Sokolov, N.S., Ryabinov, V.M.: The efficiency of root piles with multi-position broadening using electrical-discharge technology. *Geotechnics* **2** (2016)
  14. Sokolov, N.S., Ryabinov, V.M.: Specific features of the construction and calculations of EDT root piles with multi-position broadening. *Geotechnique* **3**

# Deep Earth Anchor ERT



N. S. Sokolov  and P. Yu. Fedorov 

## 1 Introduction

A case in point is the geotechnical practice of constructing facilities on a landslide slope. Administratively, the survey area is located in the central part of the town Cheboksary on Gagarin Street, 35A. Geomorphologically, it is a gentle denudation-accumulative slope of the Kaibulka River, complicated by buried beams and a strongly fermented second- and higher-order riverbed with permanent streams. The absolute markings of the ground surface within the area vary from 129.1 to 137.5 m (by the estuaries of engineering and geological works). The relief is planned.

The geologo-lithological structure of the site is characterized by borehole columns 1–4, 9–11, 15, 17. (see Fig. 1).

The geologo-lithological structure of the site, based on the data of the Geological-Engineering Survey Report before the depth studied, is divided into 7 engineering geological elements (EGE) (see Fig. 2).

The hydrogeological conditions of the site to a depth of 23.0 m at the time of the exploration are characterized by the presence of several groundwater aquifers (GA). The first aquifer (GA) is free-flowing, associated with man-made formations, opened by all wells. Absolute groundwater level (GL) of hole № 9 is 128.5 m, hole № 1–135.7 m. Power supply of GL comes from leaks from water-carrying communications. The water-carrying soil is man-made and loamy (EGE 1, 2). The local water focus is the Upper Permian Clays (EGE 3); the Second Aquifer is associated with the native Upper Permian formations (Table 1).

---

N. S. Sokolov (✉) · P. Yu. Fedorov  
Chuvash State University named after I.N. Ulyanov, prosp. Moskovsky, 15, Cheboksary 428015,  
Russian Federation

N. S. Sokolov  
OOO NPF FORST, ul. Kalinina, 109a, Cheboksary 428000, Russian Federation

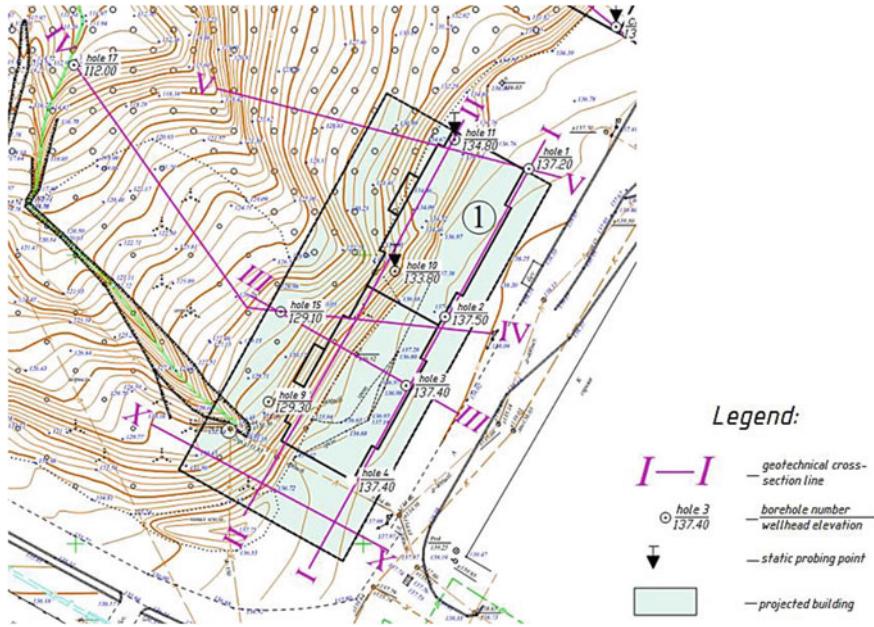


Fig. 1 Extracted from the master plan of the facility

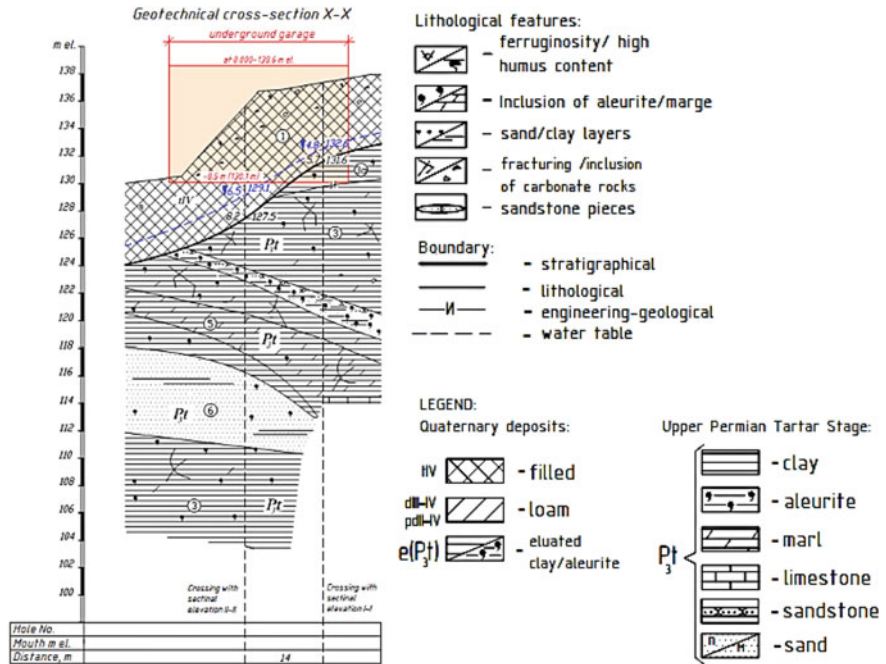


Fig. 2 Geotechnical cross-section of the construction site

**Table 1** Normative physico-mechanical characteristics of soils

EGE №	Soil type	$h, m$	$\gamma_I, (kN/m^3)$	$c_I (kPs)$	$\varphi_I, (^\circ)$	$k_{s,} (kN/m^3)$	$\lambda$	$E (MPa)$	$\nu$
1	Soft loam	8.6	19.6	16.0	11.0	2000	0.60	13.0	0.36
2	Stiff loam	4.0	19.6	11.0	12.0	4000	0.57	15.0	0.36
3	Stiff clay	2.2	19.9	29.0	20.0	4000	0.40	18.0	0.25
4	Bass clay	1.3	20.1	25.0	23.0	6000	0.52	22.0	0.34
3	Tough clay	2.5	19.9	29.0	20.0	4000	0.40	18.0	0.25
5	Semi-hard clay	20.0	21.3	26.0	24.0	6000	0.34	27.0	0.25

## 2 Methods and Materials

Engineered designs (see Fig. 3) are:

1. The special auxiliary restraint is a retaining wall consisting of fencing and anchoring structures.
2. The structures of the excavation fence in the area in question consist of 350 electrical discharge drilling piles (EDT piles [14-21]) fixed from a horizontal

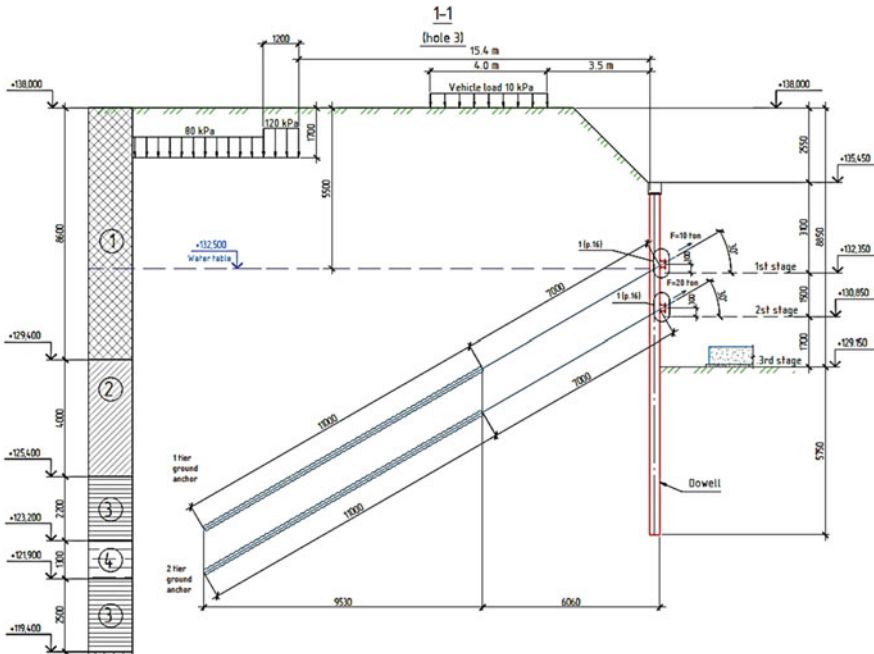


**Fig. 3** Construction of pit fencing using ground anchors



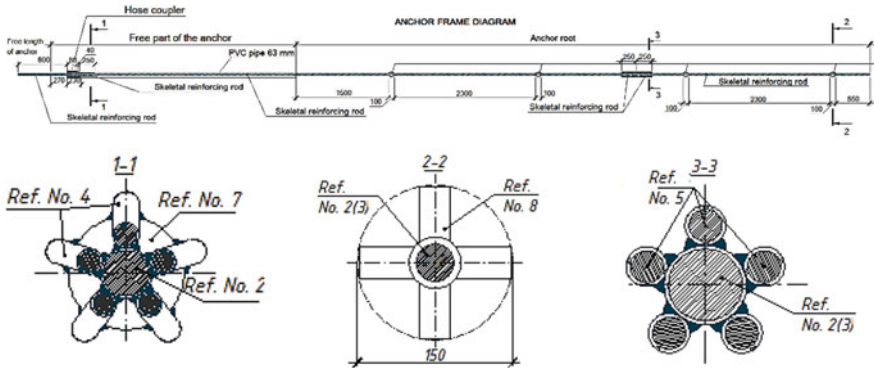


Fig. 4 Anchor frame diagram

deflection by ground EDT anchors of 18 and 17 m lengths, with an angle of 30°. The pitch of the ground anchors, as well as the distance from the bottom of the pit to the corresponding layer of anchors, are taken according to the plans specified in the draft.

3. Ground anchors (EDT anchors) are installed after the first stage of mining, according to the geotechnical cross-section specified in the project, and are pre-stressed elements with reinforced concrete roots obtained by electrically-discharged treatment of the soil wall (Figs. 3 and 4).

The strength of the elements of the retaining walls is calculated in the GeoWall software complex based on the Bloom-Lomeier method (the «elastic line» method).

### 3 Development Stages

The construction and operation of the structure of the ground anchors are carried out according to the following algorithm (Fig. 3). During the construction of the retaining wall, the following stage of ground development has been developed:

1. The first stage of the development of the soil involves the development of the soil up to the points indicated on the respective cuts; after the installation of the drop guard in the design position;
2. The ground anchors on the first level shall be carried out after the 1st stage of the ground development at +132.350 m;
3. The second stage of development involves excavation up to the absolute point (+130.850 m);
4. The third stage of development involves excavation up to the project bottom of the pit +129.150 m;
5. The development of the soil should be initiated only if the structural strength of the structure meets the requirements of the project;

6. Geotechnical monitoring of deformations of surrounding buildings is carried out prior to filling of the layers of the foundations during the construction of the superstructure;
7. The operation of ground anchors shall not be subject to dynamic or vibrational effects before the pits are filled;
8. Uniformly distributed loads per brow above those specified in the draft shall not be allowed to be exceeded.

The device for EDT drilling piles is composed of the following sequence:

1. Drilling of boreholes:
  - 1.1 The drilling of the screw is carried out according to the method statement (MS), the rig for drilling UBG-SG «Berkut» or analog.
  - 1.2 Boreholes shall be drilled from the working marks specified in the draft.
  - 1.3 The width of the ground berm shall be at least 18 m for the turning of drilling machines and for the mounting of anchor frames.
  - 1.4 During the drilling process, the depth of the ground shall be monitored: the soil characteristics of the base shall be determined from the soil residues on the elements of the drilling tool, and this fact shall be recorded in the well log book. The soil found in the well bottom is determined to correspond to the design values at the level of the anchor root.
  - 1.5 The lifting of the drilling tool shall be carried out only after it has been established that no pressure is reduced relative to the natural pressure of the ground in the well bottom.
2. Cementing of the underground well:
  - 2.1 The well shall be filled to the mouth through a concrete column having a diameter of at least 40 mm and lowered to the bottom by an upward ascending pipe (UAP). After reaching the bottom, the well must be washed with cement solution. Washing with cement solution continues until soil particles stop surfacing.
  - 2.2 The cement solution is prepared on the construction site immediately before it is injected into the well. For preparing and supplying the solution, pneumocressor PPN-500 (PPN-300) is used.
  - 2.3 The quantity of cement solution injected into the well is controlled against the design value and the volume of ground drained, and the amount of solution injected into the well must exceed the volume of ground drained.
3. Program for the electrical discharge treatment of a well filled with cement solution:
  - 3.1 The required energy storage capacity is not less than 50 kJ.
  - 3.2 The coaxial cable from GIT to the electrode system shall not be longer than 80 m, including the anchor length (TYPE-2 high-voltage cable 50 m, high-voltage low-induction (KVIM) high-voltage cable 30 m).

- 3.3 High-voltage electrical discharges are treated according to the length of the ground anchor root by a series of not less than 15 discharges at each level. The step of the levels is from 1.0 m.
  - 3.4 The calculated increase in the drilling diameter (150 mm) of the anchor root shall be increased to 200 mm and the level of the cement solution in the well shall be controlled before the start of the single-level treatment and after the completion of the treatment. The «failure» is a reduction in the level of the solution in the well for the last 5-bits not exceeding 10 mm. In order to establish the fact of «failure» the change of the level of solution in the well after each discharge or series of 5-bits is controlled.
  - 3.5 Control is exercised over the total amount of solution supplied to the well, including fractions above the volume of the spent well (volume of soil extracted from the well).
  - 3.6 As a result of the monitoring of the drop in the level of the cement solution in the test well or the volume of the added solution and seismic disturbances in the geotechnical element formation area, the program for treating the anchor root with electric shocks is adjusted.
4. Fitting the anchor frame:
    - 4.1 The anchor frame shall be lowered smoothly without jerks.
    - 4.2 The position of the reinforcement frame is controlled after it has been placed in the design position. The frame is secured against accidental immersion and deflection in the plan.
    - 4.3 The frame shall be cleared of inadvertent soil prior to installation.
5. The order of tension of the ground anchors consists of the following sequence:
    - 5.1 Prior to the start of work, all anchoring elements shall be installed on the intended tensile holder.
    - 5.2 Oblique washers are welded by electric arc welding directly on the construction site to the supporting plates (plates) of the steel distribution belt.
    - 5.3 The cubic strength of the cement stone of the anchor root shall be not less than 20 MPa. In order to control the strength set, 9 cubes of  $10 \times 10 \times 10$  cm are selected during the manufacture of the questionnaire and tested at the age of 3.7 (for internal use) and 10 days (for the report).
    - 5.4 The test load is assigned according to [1] equal to  $P_u = 1.2 * P_w$ . Control tests shall be carried out on each tenth anchor, starting with the load  $P_0 = 0.2 * P_u$ . The anchor shall be loaded with stages. Order of loading: First stage— $P_1$ ; Second stage— $P_2$ ; Third stage— $P_3$ ; Fourth stage— $P_4$ ; Fifth stage— $P_5$ ; Sixth stage— $P_6$ ; Seventh stage—test load  $P_u$ .  
 Each stage shall last at least 15 min until deformation of the EDT anchors has stabilized. Then the unloading is carried out to a value  $P_0$ , at which elastic and residual displacements are measured. The amount of movement is fixed at each step every 3 min. The last load stage is held to 30 min before the anchors are stabilized, then reduced to a value of  $P_0$ ,

the elastic and residual movements of the anchors are measured and the load is brought to the  $P_\delta$  value (blocking load), and the anchor is then fixed to the supporting structure.

- 5.5 If the test load is not reached during the control tests, the load of the last stabilized step (load capacity of the ground anchor) shall be taken as the test load followed by a calculation of the design load on the anchors, with a safety factor of 1.2. The project author adjusts the blocking load and the design solution accordingly.
  - 5.6 In the case of low absolute movements of the ground anchor (less than 20 mm), after the deformation has been stabilized, the test tests shall produce the anchor with steps equal to  $P_0 = 0.2 * P_u$ , which shall be conditionally stabilized at each new stage of deformation. At the same time, the strength of the material and the anchor attachments for super design loads must be ensured.
  - 5.7 The acceptance tests shall be carried out on every working anchor, with the exception of the anchors which have been bent over by the control test. The acceptance tests start with a load  $P_0$ , which records the initial reports of the movement of the anchor and brings it to a value  $P_u$ , holding it for 15 min, and measuring the movement of the anchor after 1, 3, 5, 7, 10 and 15 min, further reducing the load to a value  $P_0$ , by measuring the elastic movement of the anchors, the load to the blocking  $P_\delta$  is increased and the anchor is fixed to the structure.
  - 5.8 The load capacity and test loads of the intake anchors shall be defined as the minimum value of the test results from at least two nearest reference anchors.
6. Quality assurance for the manufacture of ground anchors includes:
- 6.1 The production of ground anchors shall be carried out by organizations with at least 5 years' experience in geotechnical work, where a quality assurance system has been established [2], which shall be confirmed by a certificate of conformity.
  - 6.2 In doing so, the manufacture should be certified as follows: (a) EDT drilling seams are to be planned-high; (b) Borehole diameter and depth to project; (c) Type of ground at the base of the anchor and its conformity with the project (in terms of residues on the elements of the drilling tool in the base); (d) Compaction of the ground in the base of the drilling tool; (e) Correspondence of the anchor frame to the project (length, diameter and class of the fixtures of the working rods, joints of the rods) and depth of the shell in the well; (f) the quality of the cement solution to be prepared (material consumption); (g) the difficulty of immersing the anchor frame under its own weight in the well (The free immersion of the reinforcing frame to the design mark indicates that there are no soil residues in the well and guarantees the integrity of the root stem); (h) the electrode immersion; the consumption of cement solution used in the production of ERT anchors: (1) During filling of the well; (2) During

- processing of the root on each horizon; (3) The total consumption of cement solution per well.
- 6.3 The strength of the cement solution shall be checked on the basis of [3] and [4] by taking samples of the cement solution at the place of manufacture and then by applying the normal conditions to meet the requirements of paragraph 2.3.2 [4].
  - 6.4 Covert work inspection reports shall be issued in accordance with the form specified in the updated SNiP 12-01-2004 «Organization of construction» [5], to be prepared for a completed process (questionnaire) performed by an independent implementing unit (integrated team) during shift.
  - 6.5 Further robots may not be performed in the absence of a formal certificate for hidden robots on completed EDT questionnaire production processes not certified by the technical supervision of the customer.
  - 6.6 The works shall be carried out in accordance with [6–12] and the method statement (MS).
  - 6.7 The quality of basic materials is determined by the requirements of the Town Planning Code and the Federal Law Technical Regulation, which must be confirmed by certificates of conformity, the State standard of the Russian Federation.

## 4 Conclusion

Complex engineering and geological conditions, combined with the rugged topography, unstable slopes are problematic areas for their construction development. For modern geotechnical construction of objects on them there is technical and technological potential for design and erection of objects of any complexity [13–17].

One of the techniques considered in the article for ensuring the stability of the mudslide slope is the confirmation that construction can be carried out under all engineering and geological conditions.

## References

1. VSN 506-88: Design and Installation of Soil Anchors. Minmontazhspestry USSR. Moscow (1989)
2. ISO 9001-2001: Quality management systems. Requirements. Gosstandart (2001)
3. GOST 18105-2012: Concretes. Rules for Control and Assessment of Strength. Standardinform. Moscow (2012)
4. GOST 10180-90: Concretes. Methods for Strength Determination Using Reference Specimens. Standardinform. Moscow (2006)
5. SNiP 12-01-2004 Organization of Construction. Russian Federation Gosstroy (2004)
6. SNiP 3.04.03-85 Corrosion Protection of Building Components and Structures. Gosstroy of the USSR (1985)
7. SNiP 3.03.01-87 Bearing and Enclosing Structures. Gosstroy of the USSR (1987)

8. SNiP 12-03-2001 Occupational safety in construction part one. General requirements. Russian Federation Gosstroy (2001)
9. SNiP 12-04-2002 Occupational Safety and Health in Construction—Part 2: Construction Technology. Russian Federation Gosstroy (2002)
10. TR 50-180-06 Technical recommendations for the design and construction of pile foundations carried out using discharge-pulse technology for high-rise buildings (piles-RHS). Government of the City of Moscow (2006)
11. Ilichev, V.A., Mangushev, R.A., Nikiforova, N.S.: Underground exploration experience. Experience of Development of Russian Megacities Underground Space. *Soil Mech. Found. Eng.* **2**, 17–20 (2012)
12. Ulickij, V.M., Shashkin, A.G., Shashkin, K.G.: Geotechnical Support of Urban Development, p. 551. *Georeconstruction Publ.*, St. Petersburg (2010)
13. Ter-Martirosyan, Z.G.: *Soil Mechanics*, p. 550. ASV, Moscow (2009)
14. Ulitsky, V.M., Shashkin, A.G., Shashkin, K.G.: Geotechnical Guide (guide to bases, foundations and underground structures). SPb., p. 284 (2012)
15. Sokolov, N.S., Sokolov, S.N.: The use of bored injection piles when fixing slopes. *Materials of the Fifth All-Russian Conference on New in Architecture, Design Construction Renovation (NADCR-2005)*, pp. 292–293. Publishing house of the Chuvash University, Cheboksary
16. Sokolov, N.S., Nikonorova, I.V.: Construction and territorial development of landslide slopes of the Cheboksary water reservoir. *Housing construction*. No. 9
17. Sokolov, N.S., Sokolov, S.N., Sokolov, A.N.: Fine-grained concrete as a structural building material for bore-injection piles-ERT. *Constr. Mater.* **5**, 16–20 (2017)

# Fibre-Reinforced Bored Electric Discharge Technology Pile as a Buried Reinforced Concrete Structure



P. Yu. Fedorov 

## 1 Introduction

Research in the field of construction, namely related to the construction of welded foundations with the use of fibre as a reinforcement element in the construction of foundations on weak soils, has been carried out by various institutions, in particular researchers from SPSUACE, OAO Fundamentproyekt, the Foundation Research Institute and underground facilities for them. N. M. Gersevanova, OAO TSNIIPromzdaniy, OOO NIIZhB, OAO SPbZNIiPI and others [1–19].

During the construction of welding foundations, studies were considered in connection with the solution of the problems of immersion of slaughtered piles up to the design marks. Problems with closures included premature breakage of heads, resulting in approximately 30% of reinforced concrete piles being below design levels when loaded into the heavy and medium ground, and more than 80% of piles had to cut their heads and barrels before the rostering device. In order to solve this problem, the above institutions have carried out studies aimed at the use of slaughtered piles made of a steel-fibreboard head and a reinforced concrete shaft, as well as piles made entirely of steel-fibreboard. The results of the tests were successful as welds made of steel-fibreboard were able to absorb significant impact energy and reduced dive time by 50%, improved welding capacity and welding productivity. As a result of the testing of the steel welds in the conditions of real construction, the researchers have established that they have a high impact resistance, providing for an unexposed dive up to the design marks and the possibility of eliminating the use of pile-doublers.

In a dense urban environment, the use of precast piles is not just unwelcome—in some cases, it is simply unacceptable. The impact dynamic and vibrational effects on the base of the construction may have the most unfortunate consequences for existing buildings, which fall within the area of influence of the new construction, up

---

P. Yu. Fedorov (✉)

Chuvash State University named after I.N. Ulyanov, prosp. Moskovsky, 15, Cheboksary, Russian Federation

to destruction. Therefore, when a newly built or refurbished building is built on low ground in cramped conditions, especially near old buildings or cultural heritage sites, the most relevant application of weld foundation technology with minimal negative or harmless impact on the base of the existing adjacent structure, namely drilling pile technology.

In view of the current relevance of drilling pile technology, as well as its extensive and widespread use, improvements are equally relevant, in particular the use of fibre as a reinforcement element.

The subject of the study is the development of technology for the manufacture of fully fibre-reinforced drilling piles, as well as the study of the operation of such piles in the ground.

The relevance of the fibre as a reinforcement element for drilling piles is that the technology will increase their load-bearing capacity by reinforcing the entire body of the foundation, increase the strength and crack resistance of the concrete. It will also shorten the construction time by eliminating traditional reinforcement with steel bars.

The scientific novelty of the research consists in the use of a fibre as a reinforcing element in the manufacture of a drilling pile, which includes the drilling of a well with a hollow screw with a drilling tool equipped with pipelines for supplying high-pressure water-cement solution with fibre, and in the creation of a variable cross section depending on the characteristics of the primer. The solution to the problem is achieved by forming an increased cross section in the areas of reduced mechanical properties of soils. As a consequence, positive results can be achieved.

## 2 Methods and Materials

The following tasks, divided into stages, were assigned to research and development of fibre-reinforced drilling piles:

Stage I: collection and analysis of the current regulatory framework, fibre-concrete research, dissertations on the subject, articles and projects; study of methods for calculating fibrous concrete structures, in particular, drilling pits; Preparation of the instrumentation and material base for research.

Stage II: study of varieties of fibre addition from different materials; determination of physical properties and parameters of certain fibres (steel, polypropylene, basalt, etc.); production of experimental cubes samples of concrete with different fibre additions for comparison and determination of their strength for compression, tensile, shear and other stresses; comparison of test results of samples with respect to strength, manufacturing process, cost-effectiveness; selection of the best fibre material from the research conducted.

Stage III: The production of experimental samples of drilling piles of concrete of a certain concrete grade and the most optimally selected fibre from all indicators, as well as drilling piles of concrete of the same brand with the application of a rod-reinforced frame; field testing of drill welds obtained; processing of test results;



comparison of test results of samples with respect to strength, manufacturing process, economy.

Following a comparison of the test results of the drilling seam samples, there are two possible scenarios: the first is that the load-bearing characteristics of the drilling piles reinforced with fibres and made of concrete of a specific concrete grade will be equal to or higher than the load-bearing capacity of the drilling piles reinforced by the traditional steel bar frame. In this case the research and development of the technology of reinforcing the drilling piles with fibrous reinforcement can be considered successful. The second variant of the event is that the carrying capacity of fibre-reinforced drilling piles will be lower than the carrying capacity of the piles reinforced by the traditional method. In such a case, it is planned to select the optimum concrete and fibre composition before achieving the load-capacity results at least as low as for rod-reinforced piles, while respecting not only the strength, but also the technological and economic performance of such piles.

The following is an example of an algorithm for selecting a fine-grained concrete mixture (FGCM) composition for manufacturing EDT piles.

### 3 Results and Discussion

One of the stages of construction design of the structures of the reinforced concrete shaft of the drilling EDT pile is the selection of the composition of the fine-grained concrete mixture (FGCM) according to GOST 7423-2010 «Fresh concrete. Specifications».

The FGCM selection algorithm is presented in the following sequence:

1. On the basis of the values of the design load capacity of the EDT pile  $F_d$ , the ground is assigned a class (grade) of concrete in terms of its compression strength. According to GOST 26633-91 «Heavy-weight and sand concretes. Specifications» the average strength of concrete is laid down at the coefficient of variation  $V = 13.5\%$ , security is not less than 95% of the assigned value. For example, at the design mark of fine concrete M400, the cubic strength should be  $R = 38.5 \text{ MPa}$  ( $392.5 \text{ kg/cm}^2$ ).
2. By GOST 7473-2010 «Fresh concrete. Specifications» concrete workability are selected according to the working capacity of the concrete mixture II and the mobility index (cone draught). For example, the symbol II4 refers to a cone draught of 20 cm.
3. The conditions of hardening are specified. On the base below the depth of freezing, the hardening conditions are natural. In geotechnical work at negative temperatures, either chemical hardening using sodium formation or electrical heating by heating wires is used. It should be noted that electric heating from work experience is not desirable. It is possible to create shrinkage cracks in the body of concrete as a result of a rapid strength set and, as a result, to remove the EDT pile part from the part of the concrete that is naturally hardened.

4. Components are selected for fine concrete: cement, small filling, concrete additives, water.
  - 4.1 Portland cement is generally shipped from the nearest cement plant. In Middle Volga region the cement production of OAO Mordovcement is used. According to GOST 31108-2003 «General structural Portland clinker cements. Specifications» controlled parameters are:
    - (a) compressive strength at 28 days  $R = 50$  MPa;
    - (b) the normal thickness of the cement test is 27%;
    - (c) timing: 2 h 35 min; end: 4 h 25 min;
    - (d) the true density  $\rho = 2.63$  g/cm<sup>3</sup>.
  - 4.2 Natural river sand according to GOST 8736-2014 «Sand for construction works. Specifications» with a model of size not exceeding  $M_k = 2.0$ . Determine the percentage of fractions larger than  $M_k \geq 2.0$  mm and the density of mineral particles  $\rho_s$ .
  - 4.3 4.3. Additives are used to increase concrete strength and mobility. For example, the additive EMBELIT 8-100—modifier of concrete on TU 5870-176-46854090-04, manufactured by OOO «Predpriyatiye Master Beton» (Moscow), is simultaneously a plasticizer and modifier.
  - 4.4 Water is also subject to special requirements according to GOST 23732-79 «Water for concrete and mortars. Specifications».
5. In the construction laboratory for assigned strength, mobility, usability, conditions of hardening according to GOST 27006-86 «Concrete. Rules of concrete composition» are planned:
  - 5.1 Cement water ratio, e.g. B/W = 0.51, where B is the mass of water;
  - 5.2 Mass ratio of materials, e.g. II:II = 1:2.1, where II is the mass of cement; II is the mass of sand;
  - 5.3 Additive content as % of cement mass, e.g. EMBELIT content 8–100 = 10;
  - 5.4 Material consumption per 1 m<sup>3</sup> of concrete mixture;

For example, cement—850 kg; sand—810 kg; EMBELIT 8-100—85 kg; water—465 kg.

In addition to the characteristics of the nominal composition of fine-grained concrete, the selection algorithm gives a section of the actual potential material consumption per 1 m<sup>3</sup> of concrete mixture.

6. The physico-mechanical properties of concrete required to validate composition selection in the object are: the average density of concrete in a series of samples measuring  $10 \times 10 \times 10$  cm,  $\rho$  [g/cm<sup>3</sup>] and the tensile strength at ages 7 and 28 d.

## 4 Conclusion

The application of fibre-reinforced drilling piling technology is possible for practical use after research.

The development of technology for the manufacture of fibre-reinforced drilling piles for the construction and reconstruction of cramped buildings on low ground in the immediate vicinity of existing buildings and structures is a pressing problem, because the distinctive feature of such piles is the absence of impact and vibration loading during their arrangement. In a dense urban environment, this method will minimize as much as possible the negative impact of a new construction or a reconstructed facility on existing buildings or structures adjacent to them.

In my view, the use of fibre as a reinforcement element will significantly improve the strength of drilling piles, giving them additional positive qualities such as cracking and water resistance. The fibre-reinforced drilling pile can become competitive due to the cheapness of the rod fittings as well as the high technological efficiency due to the shorter production time.

## References

1. Bogov, S.G., Zuev, S.S.: Experience of using jet technology for fixing weak soils during the reconstruction of a building on the street. Post office in St. Petersburg. Proceedings of the Scientific and Technical Conference SPbGASU, pp. 80–86 (2010)
2. Van Impe, V.F.: Deep foundations: trends and development prospects. *Reconstruction of Cities and Geotechnical Construction* **9**, 7–33 (2005)
3. Vasilyuk, L.V.: Vibration immersion of sheet piles near existing buildings in soil conditions of St. Petersburg. Engineering and geological surveys, design and construction of foundations, foundations and underground structures. C6. tr. All-Russian scientific and technical. conf. 1–3 February 2017, St. Petersburg, pp. 307–316
4. Voilokov, I.A.: The use of fiber in the manufacture of piles. *Eng. Constr. J.* **8**(10), 6–8 (2009)
5. Gavrilov, A.N., Gryaznova, E.M., Starkov, R.R.: Complex of exploration and research works for the design of new construction in conditions of dense urban development. *Soil Mech. Found.* **6**, 10–13 (2006)
6. Gursky, A.V.: Taking into account the effect of indentation of the sheet pile on the additional draft of neighboring buildings: Ph.D. diss. SPb., 133 p. (2016)
7. Dalmatov, B.I.: Soil mechanics, foundations and foundations: textbook for universities, p. 319. Stroyizdat, Moscow (1981)
8. Dyakonov, I.P.: Assessment of the bearing capacity of bored piles with an oversized tip. Engineering and geological surveys, design and construction of foundations, foundations and underground structures. Sat. tr. All-Russian scientific and technical. conf. 1–3 Feb 2017 SPb., pp. 316–322 (2017)
9. Sokolov, N.S., Sergey Ezhov, Svetlana Ezhova. Preserving the natural landscape on the construction site for sustainable ecosystem. *J. Appl. Eng. Sci.* **15**(4), 482. Skopus, 518–523 (2017)
10. Sokolov, N.S.: Electric impulse installation for the manufacture of bored injection piles. *Housing Constr.* **1–2**, 62–66 (2018)
11. Sokolov, N.S.: One of the approaches to the problem of increasing the load capacity of drilling piles. *Building Mater.* **5**, 44–47 (2018)

12. Sokolov, N.S.: Ground anchor produced by electric discharge technology, as reinforced concrete structure. *Key Eng. Mater.* Scopus 76–81 (2018)
13. Sokolov, N.S.: Use of the piles of effective type in geotechnical construction. *Scopus «Key Engineering Materials»*, pp. 70–74 (2018)
14. Sokolov, N.S.: One of geotechnological technologies for ensuring the stability of the boiler of the pit. *Scopus «Key Engineering Materials»*, pp. 56–69 (2018)
15. Sokolov, N.S.: Regulated injection pile-electric discharge technology with multiple pile enlargements posed as an underground reinforced concrete structure with a controlled load capacity. In: 18th International Multidisciplinary Scientific GeoConference SGEM 2018. *Web of Science*, pp. 601–608
16. Sokolov, N.S.: One of the geotechnical technologies to strengthen the foundation base in constraint environment in the addition of 4 floors. In: 18th International Multidisciplinary Scientific GeoConference SGEM 2018. *Web of Science*, pp. 513–522
17. Sokolov, N.S., Viktorova, S.S.: Method of aligning the turches of objects targe-sized foundations and increased loads on them. *Scopus «Key Engineering Materials»*, pp. 1–11 (2018)
18. Sokolov, N.S., Viktorova, S.S., Smirnova, G.M., Fedoseeva, I.P.: Drilling pile ERT as a buried reinforced concrete structure. *Constr. Mater.* **9**, 47–50 (2017)
19. Sokolov, N.S., Sokolov, S.N., Sokolov, A.N., Fedorov, P.Y.: The use of EDT bore injection piles as foundations of foundations with increased bearing capacity. *Ind. Civil Eng.* **9**, 66–70 (2017)

# Designing the Organization of Buildings and Structures Construction in Special Natural and Climatic Conditions



Vasily Filippovich Bogdanov , Alina Iosifovna Sokolova,  
and Irina Vladimirovna Petrova 

Project preparation is the development of a construction organization project (COP). The COP is a part of the design documentation of a building, structure, a lot has been written about the role of the COP, the requirements for its content and the tasks to improve the scientific and technical level, including in works [1–7] and many others. Unusual tasks are solved when designing a COP in special natural and climatic conditions. The list of conditions is extensive:

- soils are permafrost, subsidence, with karst inclusions, saline, heaving, peat, quicksand, technogenically polluted;
- northern regions, mountainous, high-mountainous, desert, semi-desert, with a particularly hot climate, seismic, as well as undeveloped, remote, inaccessible, sparsely populated;
- zones of water protection, resort, contaminated with radioactive elements;
- territories undermined, densely built-up.

There is no strict classification of complex conditions, however, they are divided into extreme natural and climatic and special engineering and geological [8, 9]. And in this case, a significant separation does not occur, geotechnical conditions are available in any natural and climatic conditions. In addition, construction on technologically contaminated territories, when building up was compacted, was not considered as construction in difficult conditions.

When building in special natural and climatic conditions, the COP takes into account the possibility of influencing the preparation, organization and implementation of construction by physical, geographical, and economic factors characteristic of these conditions. For example, for mountainous and high-mountainous regions “low

---

V. F. Bogdanov · A. I. Sokolova  
Chuvash State University named after I.N. Ulyanov (ChuvSU), 15 Moskovskiy Prospekt,  
Cheboksary 428015, Russian Federation

I. V. Petrova (✉)  
Institute (branch) of Moscow Polytechnic University, Cheboksary, Russian Federation

barometric pressure, which requires adherence to special adaptation modes of the work of builders; squally winds and increased lightning hazard; avalanche, mudflow, landslide and landslide phenomena; inaccessibility of the territory due to large slopes and elevation differences” [3].

It is more difficult, as the analysis of works [10–14, etc.] shows, to design and build in the northern construction and climatic zone, despite the extensive experience accumulated on the territory of the Russian Federation, covering the regions of the Far North, characterized by a long duration of time with low air temperatures, strong winds and snow drifts, low natural light; permafrost soils; remoteness of construction projects from industrially developed centers and bases of centralized material and technical supply; dependence of the delivery of material and technical resources on seasonal regimes on inland waterways and sea coastal (coastal) lines; limited local energy sources; the need to use special types of transport of northern design; increased susceptibility of ecological systems (tundra, the Arctic Ocean, etc.) to the impact of economic activities (hydrocarbon production, development of the Northern Sea Route) and their difficult recoverability, the need to eliminate waste that is not utilized in production; the complexity of organizing a construction site in swampy and flooded areas and organizing sanitary and domestic services for workers.

For most of the special conditions, TsNIIOMTP has developed guidelines, reference manuals to SNiP, guidelines, standards, and examples of COP [15–20], taking into account scientific and practical methods of organizing construction, including complete block, nodal and expeditionary rotational. That is, at the stage of development of the construction industry in Russia in the pre-market period (until 1991), through the efforts of research institutes, design institutes, and construction enterprises, many significant developments were carried out to improve the design business and design planning.

Land plots were and are allotted for construction, as a rule, unsuitable for other purposes (agricultural, environmental, recreational, etc.). Often they are built on slopes, in ravines, and on other irregularities, as well as in existing buildings, they begin to develop technogenically contaminated territories, which obliges construction industry specialists, especially designers, to solve complex design and construction issues and additionally take these features into account in the PIC.

At present, there is a noticeable tendency toward the compaction of buildings, especially in large cities and the development of underground space in the center and areas close to it. When compacting a building, a number of problems arise that must be taken into account when developing projects for organizing construction and production of work. They are:

- the limited size of the construction site forces the developer to obtain the consent of the owners of additional territories for their temporary use or to use the right of easement [21], additional territories are required for partial or complete placement of a household town, for closed warehouses and open storage of structures;
- the need to carry out a large amount of installation work “from wheels”;
- installation of tower cranes without crane runways, stationary with a large boom reach with a number of restrictions on the zones of influence of the mounting

mechanism, or place the crane inside the building, followed by dismantling in sections and sealing openings in the ceilings after the end of the work, or build without using a crane from monolithic reinforced concrete with the use of concrete pumps and small-scale mechanization, but the use of non-traditional non-standard technologies, as a rule, increases the cost of construction;

- the need to maintain the operational properties of existing buildings, preventing their deformations, which often requires the implementation of additional costly measures to strengthen the bases and foundations to prevent their slipping: the installation of sheet pile fences of the excavation, removed when necessary, fences from drill injection piles, leaving them in the ground, or the use of a “wall in the ground” structure, as well as temporary solutions such as the creation of artificial and natural buttresses, reinforcement of foundations with clips, freezing of soils, etc.;
- development of underground construction of infrastructure facilities and parking facilities for vehicles, etc.

The peculiarity of these factors is that for many of them there is no regulatory framework. Despite this, in the COP it is logical additionally to take into account the complexity of the organization of the construction site and the complexity of the organization of household supplies for workers, to give a list of measures to ensure the safety of existing buildings and structures.

The current period of development of the national economy is characterized by the presence of large technogenically contaminated territories. There are more of them due to various landfills, dumps from industrial waste, discharge of polluted effluents, and uncontrolled leaks from technological pipelines of industrial enterprises, but most of all due to various accidents and disasters. The complexity and inconsistency of the emerging situation with technogenic nature lie in the fact that many achievements of scientific and technological progress, providing means for solving material and social problems, bring new difficulties and dangers. For example, the development of chemical production gave rise to a toxic hazard, and a radiation hazard to the nuclear industry. The use of gas and hydrogen in different areas increases the threat of explosions. The increasing use of gas-liquid energy sources increases the risk of large-scale fire explosions. In contrast to destructive explosions, radiation and chemical damage have a long-term effect and the ability to spread in the post-accident period. That is, the possibilities of technogenic pollution are expanding. However, the territories under consideration in most cases have an established infrastructure and are attractive for construction due to the limited land resources and their increasing cost. Construction on technologically contaminated soils is an environmental protection, since, in the process of developing such territories, many issues of environmental safety and environmental protection are simultaneously resolved. To build on the ground they can be considered to replace or clean and sanitize or preserved, spending a lot of time. For example, cleaning a soil massif with a volume of 1500 m<sup>3</sup> from chlorine-containing hydrocarbons takes 3.5–4 months. The soil is cleaned to a level of 75–80% purity using microorganisms and ventilation in 5 months. All these actions increase the cost of construction, but at the same time

the safety of buildings and structures during their life cycle must be ensured [22]. In the considered conditions in the COP, it is necessary to additionally take into account the need to eliminate the technogenic contamination of the soil on the land allocated for construction, and if the conservation method is used, then to provide for the protection of the original natural soil, groundwater, and other areas with the device of reliable protective screens, other devices solutions.

The COP should contain specific measures for environmental protection, for example, for the northern regions, they should be developed for the conditions of the tundra of subarctic bogs. When developing the COP, it is necessary to take into account that in the territories where frozen soils are spread, the principles and methods of construction are determined by permafrost conditions. The latter change significantly as a result of the construction development of the territory. Permafrost conditions, favorable for the time of exploration, turn into unfavorable ones during the construction and operation of structures, which is accompanied by deformations of structures and a sharp complication and rise in the cost of their operation, and sometimes their complete destruction. Frozen rocks form where there were none before, and, conversely, thaw out where the permafrost conditions were sufficiently stable. As a result of the violation of natural conditions, ice formation, frost cracking, ice veins, thermokarst and thermal erosion, floods, landslides, collapses, landslides occur. The design of construction and the operation of buildings and structures should be carried out taking into account these conditions. These conditions must be taken into account when determining the general scheme and optimal methods for the widespread industrial development of large territories of the Far North. The COP of an industrial facility erected in frozen soil conditions should contain an overview of regional and specific forecasts of the possible transformation of the natural environment that may occur as a result of the project. In the conditions of the Arctic and Subarctic tundra, it is necessary to provide for a clear routing of transport communications with maximum restriction in the warm season of the movement of tractors and all-terrain vehicles, which causes serious damage to reindeer pastures. It should be taken into account, that the tracks of these machines tear the sod of the tundra cover, which leads to thawing of the frozen layer, the development of erosion and thermokarst, the formation of ravines and sinkhole lakes. The problem of nature conservation in these cases can be solved by fundamentally new types of vehicles, with low specific pressure on the ground, high traffic and carrying capacity, which do not violate the soil and vegetation cover. In the continental regions of the North, even in areas of the territory where frozen soils have a low temperature, considerable thickness and their thermal regime is sufficiently stable, the removal or compaction of peat-moss and snow covers, partial drainage of areas of the territory, dustiness, and gas contamination leads to the degradation of permafrost and cause permafrost aggression.

Not all the problems considered here are solved with the help of the COP, but it should contain [22] a list of requirements that should be taken into account in the working documentation developed on the basis of design documentation in connection with the adopted methods of erection of building structures and installation of equipment.



## References

1. Nosenko, I.Y.: POS i yego vliyaniye na smetnuyu stoimost'. I.YU. Nosenko, G.I. Arsen'yeva i dr. Sankt-Peterburg.: ZAO «INiK», 143 s (2002)
2. SN 47-74: Instruksiya po razrabotke proyektov organizatsii stroitel'stva i proyektov proizvodstva rabot: M., 50 s (1975)
3. SNiP 3.01.01-85: Organizatsiya stroitel'nogo proizvodstva. Gosstroy SSSR.-M.: TSITP Gosstroya SSSR, 56 s (1985)
4. SNiP 12-01-2004: Organizatsiya stroitel'stva. M., 30 s (2004)
5. MDS 12-81.2007: Metodicheskiye rekomendatsii po razrabotke i oformleniyu proyekta organizatsii stroitel'stva i proyekta proizvodstva rabot. TSNIOMTP Gosstroya SSSR. M., 10 s (2007)
6. Shreyber, K.A.: Tekhnologiya i organizatsiya remontno-stroitel'nogo proizvodstva. Nauch.izd. M.: Izd-vo ASV, 296 s (2008)
7. Petrova, I.V.: Proyekt'naya podgotovka organizatsii stroitel'stva: predmet, razvitiye i problemy. I.V. Petrova, V.F. Bogdanov, N.Z. Kiselev. Innovatsii v obrazovatel'nom protsesse sb. tr. nauch.-prakt. konf. –Vyp. 17.–Cheboksary: Politekh, s. 24–29 (2019)
8. Mustakimov, V.R.: Proektirovaniye zdaniy v osobykh prirodno-klimaticheskikh usloviyakh: uchebnoye posobiye. Tom 1/V.R. Mustakimov.–Kazan' : Izd-vo Kazansk. gos. arkhitekt.-stroit. un-ta, 239 s (2018)
9. Rukovodstvo po organizatsii stroitel'nogo proizvodstva v usloviyakh severnoy zony/TSNIOMTP Gosstroya SSSR.–Moskva: Stroyizdat, 108 s (1978)
10. Rogers, G.: Alaska Regional Population and Emploment. Collegs (1967)
11. Cold Weather Concreting: Journal of the American Concrete Institute, №5 (1978)
12. Blaha, B.: Concrete Helps Build Alaska Pipeline. Concrete Peoducts, №10 (1976)
13. Berezovskiy, B.I.: Stroitel'noye proizvodstvo v usloviyakh Severa.–L.: Stroyizdat, 108 s (1978)
14. Nazarova, L.G., Poluektov, V.Ye., Sorokin, A.A.: Proektirovaniye grazhdanskikh zdaniy dlya Kraynego Severa. Spravochnoye posobiye/ Pod red. L.G. Nazarovoy/L.: Stroyizdat, 216 s (1984)
15. Razrabotka proyektov organizatsii stroitel'stva i proyektov proizvodstva rabot dlya promyshlennogo stroitel'stva. TSNIOMTP.-M: Stroyizdat, 238 s (1990): il.–(Sprav.posobiye k SNiP)
16. Posobiye po razrabotke proyektov organizatsii stroitel'stva krupnykh promyshlennykh kompleksov s primeneniym uzlovogo metoda (k SNiP 3.01.01-85). PridneprovskiyPromstroyproyekt.-M.: Stroyizdat, 1989.-79 s. 17. Posobiye po razrabotke proyektov organizatsii stroitel'stva i proyektov proizvodstva rabot dlya zhilishchno-grazhdanskogo stroitel'stva (k SNiP 3.01.01-85). TSNIOMTP.-M.: Stroyizdat, 160 s (1989)
17. Posobiye po razrabotke proyektov organizatsii stroitel'stva i proyektov proizvodstva rabot dlya sel'skokhozyaystvennogo stroitel'stva (k SNiP 3.01.01-85). TSNIOMTP Gosstroya SSSR.-M.: Stroyizdat, 72 s (1988)
18. Metodicheskiy primer proyekta organizatsii stroitel'stva predpriyatiya khimicheskoy promyshlennosti. TSNIOMTP.-M.: Stroyizdat, 32 s (1983)
19. Etalon proyekta organizatsii zhilogo mikrorayona iz krupnopanel'nykh domov. M, Stroyizdat, 40 s (1973)
20. SP 48.13330.2011: Organizatsiya stroitel'stva. Aktualizirovannaya redaktsiya SNiP 12-01-2004
21. Tekhnicheskiy reglament o bezopasnosti zdaniy i sooruzheniy.-M.: Prospekt, 32 s (2011)
22. Postanovleniye Pravitel'stva Rossiyskoy Federatsii ot 16.02.2008 g.№87 «O sostave razdelov proyektnoy dokumentatsii i trebovaniyakh k ikh sodержaniyu»

# Overcoming Problems with Waste Water Treatment from Dense Emulsions in the Oil Refining Industry



E. M. Mikryukova  and E. V. Suvorova

## 1 Introduction

The petrochemical industry nowadays occupies one of the first places in the Russian economy. Unfortunately, the extraction, processing, transportation, and storage of oil and its derivatives often entail emissions of hydrocarbons into the environment that pollute it. Due to their high toxicity, according to UNESCO, petrochemical pollution is ranked among the ten most dangerous environmental pollutants [1]. At the moment, several million tons of oil sludge have already accumulated at the petrochemical plants. Oil refining waste is generated during wastewater treatment, in the water recycling system, drilling, oil preparation, and during tank cleaning. The demand for more advanced water purification technologies is growing and expanding every year due to the impact of environmental degradation on the economy [2].

## 2 Material and Research Methods

The petrochemical industry is responsible not only, directly, for the processing of substances produced from oil and natural gas, but also for the purification of technological effluents, which, during production, enter the sewage system, and also enter the environment, subsequently being washed away by storm water [3]. Hence an important task follows—to ensure the highest level of wastewater treatment through the use of modern technologies and the latest scientific developments.

Wastes sent for treatment include various impurities:

- dissolved organic compounds, including hydrocarbons;
- traces of heavy metals;

---

E. M. Mikryukova (✉) · E. V. Suvorova  
Kalashnikov Izhevsk State Technical University, Izhevsk, Russia

- dissolved mineral salts;
- chemical reagents used in production;
- oil particles in the form of an emulsion;
- sand.

Wastewater from petrochemical plants is highly toxic and can seriously damage the environment. Refinery effluent treatment is a complex process that requires appropriate step-by-step treatment, as by-products can be volatile, toxic, and even explosive. In addition, oily wastewater requires a combined approach to wastewater treatment to eliminate oils, oil films, organic substances, heavy metals, and salts [4].

The basic methods of wastewater treatment from oil and its derivatives are:

- mechanical;
- chemical;
- physical and chemical;
- biological.

## ***2.1 Mechanical Wastewater Treatment Method***

As an autonomous method, mechanical wastewater treatment is used in cases where the water treated in this way is suitable for the needs of the technological process or discharge into a natural reservoir without harming the environment [3, 5].

In other situations, this method is used as the first stage of wastewater treatment from oil and its derivatives. This cleaning technique allows you to separate 60–65% of suspended particles [6].

The most popular methods of mechanical wastewater treatment from oil products:

- sedimentation;
- centrifugal removal of water pollutants;
- filtration.

## ***2.2 Chemical Cleaning***

The idea of this method is the introduction into the treated wastewater of knowingly prepared chemical reagents that begin to interact with petrochemical pollution and oil products. The result of this chemical reaction is the precipitation of impurities. This is due to the oxidation of hydrocarbon components of oil and its derivatives [7].

## ***2.3 Physical and Chemical Cleaning Methods***

The main methods of physicochemical wastewater treatment include:

- coagulation;
- flotation;
- sorption.

The basis of coagulation is the rapid transformation of finely dispersed (particle size: 1–100  $\mu\text{m}$ ) and emulsified types of contaminants into larger particles, which further precipitate. Usually, this process is stimulated by special chemicals—coagulants [8].

Their action leads to the formation of flocs in the water, with a weak electrostatic positive charge. These flakes begin to interact with oil impurities, which are in a colloidal state, and also have a weak electrostatic charge. The coagulant electrostatically attracts oil impurities and as a result, under the action of gravity, they precipitate a loose structure to the bottom of the treatment tank. Then they are easily removed [9].

The flotation process, on the contrary, leads to the formation of a stable foam on the surface of the treated water, due to which harmful impurities of oil and its derivatives are captured and retained for a long time. This foam layer can also be easily separated from the treated waste water. The basis of the above-mentioned foam is a stable composition of air or gas bubbles with oil particles [10, 11].

Nevertheless, a high degree of purification of oil effluents can be achieved only after using the sorption method.

Physicochemical treatment methods define sorption as the absorption of harmful impurities from the water being purified by the adsorbent, including oil products.

Various materials with a porous structure can be used as sorbents:

- peat;
- coke;
- ash;
- silicate gel;
- various types of activated clays.

Experts believe that the most effective adsorbent materials are various types of activated carbon [12].

## ***2.4 Biological Wastewater Treatment***

At the moment, many experts agree that the biological method of wastewater treatment is one of the most promising areas in this area.

The essence of this method is based on the use of the decomposing ability of various microorganisms and the ability to absorb, break down and assimilate harmful impurities to purify water from oil and its derivatives.

In other words, oil and oil products are used by microorganisms in the process of their life as food sources. Thanks to biological methods of purification, oil product

impurities are oxidized and converted into absolutely safe products: carbon dioxide, ordinary water, nitrate and sulfate salts, and other harmless compounds [13].

The use of biological methods for purifying wastewater from impurities of oil and its derivatives involves the use of special aeration tanks and biological filters.

### 3 Results and Issues

#### 3.1 Using the Coalescence Process to Treat Refinery Wastewater

The most common equipment for the recovery of oil and oil products from wastewater are hydrocyclones, sedimentation tanks, oil traps, hydrophobic and hydrophilic filters, flotation devices, electrolyzers, filters with granular loading, we will consider in more detail the coalescence process (Fig. 1).

The basis of the processes of coalescence of emulsified oil products and fats on the filtering material are the processes of adhesion and wetting, which to some extent affect the processes of conventional filtration.

By coalescence, emulsions and dispersions are separated by means of interfacial tension between the hydrocarbon and aqueous phases. In the process of coalescence,

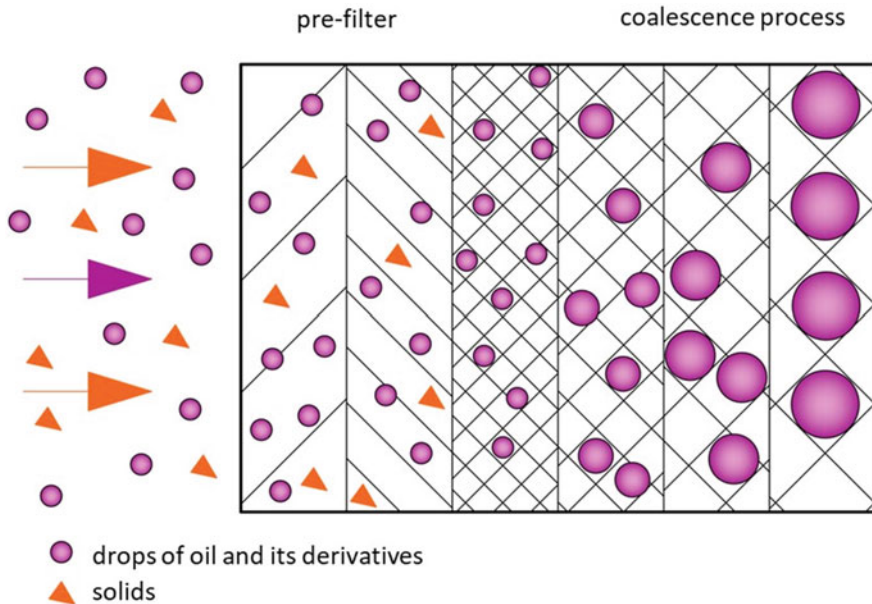


Fig. 1 Coalescence process

two drops of the same phase and identical composition come into contact with each other, forming one large drop and, thereby, decreasing their specific surface area (surface per unit volume) [14].

There are many types of coalescing media, from glass fibers with moderate characteristics to special polymeric membranes, which can provide excellent performance in the separation of dense emulsions, for example, with a certain content of surfactant compounds [15].

According to the structure of the material used, coalescing materials can be divided into the following main types:

- fibrous;
- knitted;
- porous;
- granular.

In the first case, fibrous materials are used mainly with a fleecy fiber surface.

In the second, weaving from polymer threads of a special porous structure, in some cases, composite materials are used, for example, polymer and steel threads. The role of porous materials can be rigid materials specially obtained by pressing or gluing polymers, and elastic materials such as polyurethane foams.

In granular, respectively, granular polymer or hydrophobized materials are used [16].

Let's consider in more detail the polymer membranes.

Membrane coalescence is a more efficient method than traditional separation methods. The membrane is a barrier between the two phases that selectively separates and restricts the transport of many chemicals.

Depending on the structure, membranes can be divided into four categories:

- homogeneous;
- heterogeneous;
- symmetrical;
- asymmetric.

Membranes can separate a solid or liquid, and can also carry a positive or negative charge, be neutral or bipolar [17].

As an effective method, membrane technology is one of the most commonly used methods for separating oil–water wastewater or emulsions. Compared to other types of treatment, the membrane coalescence method has higher efficiency, more stable waste water quality, and lower energy consumption. Depending on the separation and pore type, membranes can be divided into microfiltration (MF, pore size from 0.1 to 5  $\mu\text{m}$ ), ultrafiltration (UF, pore size range 0.01 to 0.1  $\mu\text{m}$ ), nanofiltration (NF, pore size range from 0.01 to 0.1  $\mu\text{m}$ ) and reverse osmosis (RO, pore size from 0.0001 to 0.001  $\mu\text{m}$ ) [18–20].

Coalescing membranes are polymer fibers that vary in diameter and surface finish depending on the application. The bonded structure of the fibers forms very small pores, which allow collecting drops of 0.2–50  $\mu$  in size and transforming them into a dispersion of larger drops with a diameter of 500–5000  $\mu$ . But due to the small pore

size of the fiber structure, solid particles must be removed from the liquid before it passes through the membrane [21].

The mechanism of membrane coalescence is determined by the following steps:

1. Removal of particulate matter from the pre-filter.
2. Adsorption of droplets on the membrane fibers.
3. The movement of droplets to the fibers of the membrane due to capture by the process flow.
4. Fusion of two tiny droplets to form a larger one, when the second droplet reaches the same intersection of the fibers.
5. Accumulation and release of larger droplets from fiber intersections and their entrainment by the process flow.
6. Repetition of steps 2 through 5 with gradually increasing droplets and larger pores in the fiber structure [17, 22, 23].

In accordance with the above mechanism, membrane coalescence is developed on an industrial scale, as a rule, with the following technological scheme: pre-filtration, coalescence and separation.

In most cases, pre-filtration takes place in a container with filter cartridges with a mesh size depending on the number and size of particles previously measured or estimated. The purpose of this step is to remove particulate matter that can increase the stability of the emulsion and thereby prevent clogging of the pores of the membrane in order to maintain its functionality for a long time.

While the pre-filtration takes place in a separate vessel, the fusion and separation takes place in the same equipment, but in separate compartments.

Regardless of the fact that separation is a formal step in the coalescence mechanism, it is necessary to achieve the main goal of coalescence, namely, the separation of two liquid phases.

A horizontal arrangement is most often used to separate hydrocarbons from the continuous aqueous phase. In this case, after coalescence, phase separation is achieved by settling the aqueous phase.

## 4 Conclusion

1. Membrane coalescence is a successful technology for the purification of wastewater from dense emulsions, contributing to the increase in the stability of the operation of petrochemical enterprises.
2. The coalescence method enlarges the droplets of water-insoluble liquids without unnecessary expensive elements and contributes to a significant increase in the degree of wastewater treatment.
3. The use of the coalescence process in wastewater treatment will significantly reduce the load on the main treatment facilities, increase their productivity and, thereby, significantly reduce harmful emissions into the environment.

4. Considering the polydispersity of oily effluents from industrial enterprises, it is not possible to use only one treatment method to obtain water of the required quality. In this regard, it is recommended to purify oily effluents in several stages, first getting rid of coarse emulsified particles, and then proceed to work with finely emulsified particles.

## References

1. The United Nations world Water Development Report, 2017: Wastewater: The Untapped Resource—UNESCO Digital Library. Accessed on 18 July 2019; Available online: <https://unesdoc.unesco.org/ark:/48223/pf0000247153>
2. Semenova, I.V.: Promyshlennaya ekologiya. Uchebnoe posobie dlya studentov vysshih uchebnyh zavedenij. -M.: Izdatel'skij centr «Akademiya». 2009. (Prirodnye i promyshlennye vody, s. 140–204. Energeticheskaya promyshlennost', s. 252–269. Gazoneftedobyvayushchij kompleks, s. 305–352. Neftepererabatyvayushchaya promyshlennost', s. 360–394. Neftekhimicheskaya promyshlennost', s. 394–410) (2009)
3. Sokovnina, O.V., Mikryukova, E.M.: Razrabotka lokal'nyh ochistnyh sooruzhenij poverhnostnogo stoka v g. Izhevsk Pervomajskogo rajona. V sbornike: Innovacionnye tekhnologii v sistemah vodosnabzheniya i vodootvedeniya. Sbornik statej po materialam Mezhdunarodnoj nauchno-prakticheskoj konferencii. FGBOU VO «CHuvashskij gosudarstvennyj universitet I.N. Ul'yanova». S. 105–110 (2019)
4. Ustinova, T.P., Titorenko, E.I., Artemenko, S.E.: i dr. Ob effektivnosti lokal'nyh ustanovok ochistki proizvodstvennyh stochnyh vod. Him. prom. -№ 2. S. 20–25 (2001)
5. Mikryukova, E.M., Sokovnina, O.V.: Podbor naibolee optimal'nogo nasosnogo oborudovaniya KNS dlya resheniya problemy livnevoj kanalizacii Pervomajskogo rajona g. Izhevsk. Intellektual'nye sistemy v proizvodstve, T. 16.№3. S. 22–27 (2018)
6. Adel'shin, A.B., Ivanov, I.N.: Osvetlenie stochnyh vod s primeneniem napornyh gidrociklonov. Neftegazopromyslovoe delo. -№ 8 (1976)
7. Yu, L., Han, M., He, F.: A review of treating oily wastewater. Arab. J. Chem. **10**, S1913–S1922 (2017). <https://doi.org/10.1016/j.arabjc.2013.07.020>
8. Investigation of the Electrocoagulation Treatment Technique for the Separation of Oil from Wastewater—SciAlert Responsive Version. Accessed on 22 July 2019
9. Getmancev, S.V., Nechaev, I.A., Gandurina, L.V.: Ochistka proizvodstvennyh stochnyh vod koagulyantami i flokulyantami. M.: AVS, 272 s (2008)
10. Rocha e Silva, F.C.P., Rocha e Silva, N.M.P., Luna, J.M., Rufino, R.D., Santos, V.A., Sarubbo, L.A.: Dissolved air flotation combined to biosurfactants: a clean and efficient alternative to treat industrial oily water. Rev. Environ. Sci. Biotechnol. **17**, 591–602 (2018). <https://doi.org/10.1007/s11157-018-9477-y>
11. Sylvester, N.D., Byeseda, J.J.: Oil/water separation by induced-air flotation. Soc. Pet. Eng. J. **20**, 579–590 (1980). <https://doi.org/10.2118/7886-PA>
12. Veprikova, E.V., Tereshchenko, E.A., Chesnokov, N.V., Shchipko, M.L., Kuznecov, B.N.: Osobnosti ochistki vody ot nefteproduktov s ispol'zovaniem neftyanyh sorbentov, fil'truyushchih materialov i aktivnyh uglej. Journal of Siberian Federal University, Chemistry. №3. R. 285–304 (2010)
13. SHvecov, V.N., Morozova, K.M., Nechaev, I.A., Pushnikov, M.Y.: Sovremennye tekhnologii biologicheskoy ochistki neftesoderzhashchih stochnyh vod. Vodosnabzhenie i sanitarnaya tekhnika. №3. S. 9–12 (2002)
14. Basu, S.: A study on effect of wetting on mechanism of coalescence. J. Colloid Interface Sci. **159**, 68 (1993)



15. Hu, S., Kintner, R.C.: The fall of single liquid drops through water, *AIChE J.* **42** (1955)
16. Urmitova, N.S., Abitov, R.N., Nizamova, A.H.: Koalesciruyushchie materialy, primenyaemye v nasadkah ustanovok ochistki neftesoderzhashchih stochnyh vod: sb. trudov III Mezhdunarodnoj nauchno-tehnicheskoy konferencii pamyati akademika RAN S. V. YAKovleva «YAKovlevskie chteniya»/NIU MGSU. Moskva, S. 912 (2017)
17. Abd El-Gawad, S.H.: Oil and Grease Removal from Industrial Wastewater Using New Utility Approach. Accessed on 17 Dec 2019
18. Fan, L., Yan, J., He, H., Deng, N., Zhao, Y., Kang, W., Cheng, B.: Electro-blown spun PS/PAN fibrous membrane for highly efficient oil/water separation. *Fibers Polym.* **18**, 1988–1994 (2017). <https://doi.org/10.1007/s12221-017-7429-8>
19. Zoubeik, M., Salama, A., Henni, A.: Investigation of oily wastewater filtration using polymeric membranes: experimental verification of the multicontinuum modeling approach. *Ind. Eng. Chem. Res.* **57**, 11452–11464 (2018). <https://doi.org/10.1021/acs.iecr.8b02529>
20. Zhu, Y., Wang, D., Jiang, L., Jin, J.: Recent progress in developing advanced membranes for emulsified oil/water separation. *NPG Asia Mater.* **6**, e101 (2014). <https://doi.org/10.1038/am.2014.23>
21. Sprow, F.B.: Drop size distribution in strongly coalescing agitated liquid-liquid systems. *AIChE J.* **13**, 995 (1967)
22. Kocherginsky, N.M., Tan, C.L., Lu, W.F.: Demulsification of water-in-oil emulsions via filtration through a hydrophilic polymer membrane. *J. Membr. Sci.* **220**, 117–128 (2003)
23. Membrane Microfiltration Market: Size, Trend, and Research Report. Accessed on 4 Nov 2019